

**Characterization of the interactions of the *Streptococcus pneumoniae* toxin,
Pneumolysin, with soluble molecules of the immune system**

Thesis submitted for the degree of
Doctor of Philosophy
At the University of Leicester

By
Bayan Hama Amin Faraj

Department of Infection, Immunity and Inflammation
University of Leicester

November 2017



Statement of originality

This accompanying thesis submitted for the degree of PhD entitled “Characterization of the interactions of the *Streptococcus pneumoniae* toxin, Pneumolysin, with soluble molecules of the immune system” is based on work conducted by the author in the Department of Infection, Immunity and Inflammation of the University of Leicester during the period between September 2013 and September 2017.

All the work recorded in this thesis is original unless otherwise acknowledged in the text or by references.

None of this work has been submitted for another degree in this or any other University.

Signed.....

Date.....

Characterization of the interactions of the *Streptococcus pneumoniae* toxin, Pneumolysin, with soluble molecules of the immune system

Bayan Hama Amin Faraj

Abstract

Pneumolysin (Ply) is a key virulence factor of the bacterium *Streptococcus pneumoniae* (Pneumococcus). Major functions include forming pores in mammalian cell membranes and activating the complement cascade to divert the host's immune system. The aim of this thesis was to investigate these processes at the molecular level to understand how Ply facilitates disease by the pneumococcus.

Previous studies have suggested that Ply interacts with various soluble molecules of the immune system, including L-ficolin and IgG. These interactions activate complement via the lectin and classical pathways, respectively. In this thesis I have demonstrated that Ply does not interact with either native serum L-ficolin or recombinant human L-ficolin produced in Chinese hamster ovary cells. The previous erroneous report probably arose as a result of contamination of Ply preparations with L-ficolin ligands. Investigation of binding between Ply and IgG showed that Ply binds to IgG2, IgG3 and IgG4 but not to IgG1. Binding is mediated through interactions between domains 1-3 of Ply and the Fab region of the IgGs.

An additional aim of this thesis was to investigate pore formation by Ply. The crystal structure of Ply, determined in our group, showed that Ply monomers in the crystal pack together similar to the way in which they are likely to assemble on the cell surface prior to pore formation. Based on the structure, a series of mutations were created to disrupt packing between Ply monomers during pre-pore and pore formation. The activities of two of the mutants, Asp205Arg and Asn339Arg were completely abolished and most of the mutants had greatly reduced activities compared to wild-type Ply indicating that these residues play important roles during pore formation. Interestingly, electron microscopy showed that Ply Asp205Arg forms chain like structures on membranes but cannot form circular pores or arcs. Thus although monomers still self-associated they could not kill cells. By contrast, Ply Asn339Arg, binds to the membrane but does not oligomerize.

In further work, crystal structures of the membrane-binding domain of Ply revealed conformational changes in a Trp rich-loop at the base of the toxin involved in membrane binding. These changes promote new packing interactions between Ply monomer thereby promoting oligomerization on the membrane.

Finally, I investigated the structural changes of the membrane by spectroscopic monitoring of optically trapped vesicles. The inelastic back-scattered light was monitored from a single liposome, held by optical tweezers and exposed to Ply. Ply binding increased the membrane fluidity due to a decrease in the short-range order of the lipid molecules in the bilayer. Analysis of a series of point mutants suggests that these changes are caused by association of Ply monomers during formation of the pre-pore, prior to insertion across the membrane.

Acknowledgements

First and foremost, I would like to thank God for giving me the opportunity to write this thesis without him, I can do nothing.

I would like to express my sincere gratitude to my both supervisors Prof. Russell Wallis and Prof. Peter Andrew for their continuous support of my PhD study, for their patience, motivation, and immense knowledge. Their guidance helped me in all the time.

My special thanks to

Dr. Umakhanth Venkatraman Girija, Dr. Christopher Michael Furze, Dr. Jamie Elton Marshall and Dr. Farah Badakshi for their help and support in the 218 laboratory. Dr. Andrew Hudson for providing the Raman Spectroscopy facilities in his lab in Chemistry Department at Leicester University.

Many thanks go to my cousin Dr. Chro Kamil Abdurrahman for her always support, with all my appreciation, I am grateful to Miss Natalie Susan Allcock, core of biotechnology services of Electron Microscopy Facility at Leicester University.

I would like to acknowledge and thank KRG-HCDP scholarship program human capacity development in Kurdistan for funding my scholarship.

A special word of thanks also goes to my family and specifically to my mum for her continuous support and encouragement.

Last but not least, I would like to thank all my siblings; I have been extremely fortunate in my life to have all of you who they showed me unconditional love and support.

Publication arising from this thesis

- 1- MARSHALL, J. E., FARAJ, B. H., GINGRAS, A. R., LONNEN, R., SHEIKH, M. A., EL-MEZGUELDI, M., MOODY, P. C., ANDREW, P. W. & WALLIS, R. 2015. The Crystal Structure of Pneumolysin at 2.0 Å Resolution Reveals the Molecular Packing of the Pre-pore Complex. *Sci Rep*, 5, 13293.

- 2- COLLARD, L., PEREZ-GUAITA, D., FARAJ, B. H. A., WOOD, B. R., WALLIS, R., ANDREW, P. W. & HUDSON, A. J. 2017. Light Scattering By Optically-Trapped Vesicles Affords Unprecedented Temporal Resolution Of Lipid-Raft Dynamics. *Sci Rep*, 7, 8589.

Table of contents

| | | |
|------------------------------------|---|----|
| Abstract | II | |
| Acknowledgements | III | |
| Table of contents | V | |
| List of figures | IX | |
| List of tables | XII | |
| List of abbreviations | XIII | |
| Chapter 1 | General introduction | 1 |
| 1.1 | Pneumococcus | 1 |
| 1.2 | Pneumococcal epidemiology | 1 |
| 1.3 | Pneumococcal diseases | 3 |
| 1.3.1 | Otitis media (OM) | 4 |
| 1.3.2 | Sinusitis and bronchitis..... | 4 |
| 1.3.3 | Pneumonia and septicaemia | 4 |
| 1.3.4 | Pneumococcal meningitis..... | 5 |
| 1.4 | Pneumococcus virulence factors..... | 5 |
| 1.4.1 | The Capsule | 6 |
| 1.4.2 | The cell wall | 7 |
| 1.4.3 | Autolysin A (LytA)..... | 7 |
| 1.4.4 | Neuraminidases or sialidases | 7 |
| 1.4.5 | Hyaluronidase (Hyl) | 8 |
| 1.4.6 | Immunoglobulin A1 protease (IgA1)..... | 8 |
| 1.4.7 | Pneumococcal iron acquisition and uptake transporters | 8 |
| 1.4.8 | Pneumococcal surface protein A (PspA)..... | 9 |
| 1.4.9 | Pneumococcal surface protein C (PspC) | 9 |
| 1.4.10 | Pneumococcal adhesion and virulence A (PavA) and enolase (Eno)..... | 9 |
| 1.4.11 | Sortases..... | 10 |
| 1.5 | Vaccines against the pneumococcus..... | 10 |
| 1.6 | Treatment of the pneumococcus infections | 12 |
| 1.7 | Ply..... | 13 |
| 1.8 | Overview mechanism of pore formation | 15 |
| 1.9 | Role of Ply in pathogenesis..... | 18 |
| 1.10 | The mammalian immune system..... | 19 |
| 1.10.1 | Complement system | 20 |
| 1.10.1.1 | Classical pathway (CP)..... | 22 |
| 1.10.1.2 | Lectin pathway (LP) | 23 |
| 1.10.1.3 | Alternative pathway (AP) | 25 |
| 1.10.1.4 | Terminal pathway (TP) | 25 |
| 1.11 | Ficolins | 25 |
| 1.11.1 | Human M-ficolin..... | 26 |
| 1.11.2 | Human H-ficolin | 26 |
| 1.11.3 | Human L-ficolin | 26 |
| 1.12 | Mouse ficolins..... | 28 |
| 1.12.1 | Ficolin-A..... | 28 |
| 1.12.2 | Ficolin-B..... | 28 |
| 1.13 | Genetics of ficolins..... | 29 |
| 1.13.1 | Structure of ficolins..... | 31 |
| 1.14 | Ficolins and disease | 31 |
| 1.15 | Humoral immunity..... | 32 |
| 1.15.1 | Antibody structure..... | 33 |

| | | |
|------------|---|----|
| 1.15.2 | Ig isotypes..... | 34 |
| 1.15.2.1 | Immunoglobulin G (IgG)..... | 34 |
| 1.15.2.1.1 | IgG1 | 35 |
| 1.15.2.1.2 | IgG2 | 35 |
| 1.15.2.1.3 | IgG3 | 36 |
| 1.15.2.1.4 | IgG4 | 36 |
| 1.15.2.2 | Immunoglobulin A (IgA) | 37 |
| 1.15.2.3 | Immunoglobulin E (IgE)..... | 38 |
| 1.15.2.4 | Immunoglobulin D (IgD) | 38 |
| 1.15.2.5 | Immunoglobulin M (IgM)..... | 38 |
| 1.16 | Biological membrane | 39 |
| 1.16.1 | Structure and biophysical properties of lipid bilayers..... | 41 |
| 1.16.1.1 | Lipid molecules | 41 |
| 1.16.1.1.1 | Phospholipids | 41 |
| 1.16.1.1.2 | Cholesterol | 41 |
| 1.16.1.2 | Liposomes as the membrane model | 42 |
| 1.16.2 | Bilayer melting temperatures (T_m)..... | 44 |
| 1.17 | Physical states of lipid bilayer | 45 |
| 1.18 | General aims of the thesis | 46 |
| Chapter 2 | Production and purification of Ply and Ply domains..... | 47 |
| 2.1 | Objectives..... | 47 |
| 2.2 | Materials and methods | 47 |
| 2.2.1 | Materials..... | 47 |
| 2.2.2 | Electrophoresis..... | 47 |
| 2.2.3 | Competent cells and transformation | 48 |
| 2.2.4 | Competent cell preparation by the rubidium chloride method | 48 |
| 2.2.5 | Sodium dodecyl-polyacrylamide gel electrophoresis (SDS-PAGE)..... | 48 |
| 2.2.6 | Expression and purification of full-length Ply | 49 |
| 2.2.7 | Cloning and amplification of PlyD1-3 by PCR..... | 52 |
| 2.2.8 | Small scale expression of PlyD1-3 | 53 |
| 2.2.9 | Large scale protein expression | 54 |
| 2.2.10 | Inclusion body preparation | 54 |
| 2.2.11 | Inclusion body solubilisation..... | 54 |
| 2.2.12 | Small scale refolding test..... | 54 |
| 2.2.13 | Large scale refolding of PlyD1-3..... | 55 |
| 2.2.14 | Cloning, expression and purification of PlyD4 | 55 |
| 2.2.15 | Expression and purification of PlyD4..... | 57 |
| 2.3 | Results | 57 |
| 2.3.1 | Expression and purification of full-length Ply | 57 |
| 2.3.2 | Cloning, expression and purification of PlyD1-3 | 60 |
| 2.3.3 | Cloning, expression and purification of PlyD4 | 66 |
| 2.4 | Discussion | 69 |
| Chapter 3 | Interaction of Ply with human L-ficolin and IgG isotypes | 71 |
| 3.1 | Introduction | 71 |
| 3.2 | Objectives..... | 72 |
| 3.3 | Materials and methods | 72 |
| 3.3.1 | Materials..... | 72 |
| 3.3.2 | PCR amplification of the L- ficolin cDNA..... | 73 |
| 3.3.3 | Cloning of full-length L-ficolin into pGEM-T easy vector | 73 |
| 3.3.4 | Cloning of full-length L-ficolin into pED4 | 74 |
| 3.3.5 | Expression vector pED4..... | 74 |
| 3.3.6 | Cell culture..... | 75 |
| 3.3.7 | DNA precipitation | 76 |
| 3.3.8 | Transfection of mammalian cells by the calcium phosphate method... 76 | 76 |

| | | |
|-----------|---|-----|
| 3.3.9 | Expression and purification of full-length L-ficolin..... | 76 |
| 3.3.10 | Cell storage | 77 |
| 3.3.11 | Cloning, expression and purification of the fibrinogen-like domain of L-ficolin | 78 |
| 3.3.11.1 | Amplification of the cDNA encoding the fibrinogen-like domain of L-ficolin... | 78 |
| 3.3.11.2 | Expression and purification of the fibrinogen-like domain of L-ficolin..... | 80 |
| 3.3.12 | ELISA binding between Ply and L-ficolin..... | 80 |
| 3.3.13 | ELISA binding between Ply and IgG isotypes..... | 81 |
| 3.3.14 | Inhibition assay | 81 |
| 3.3.15 | IgG4 digestion with IdeS enzyme | 81 |
| 3.4 | Results | 82 |
| 3.5 | Cloning, expression and purification of L-ficolin..... | 82 |
| 3.5.1 | PCR amplification of full-length L-ficolin..... | 82 |
| 3.5.2 | Production and purification of full-length L-ficolin..... | 84 |
| 3.6 | Cloning expression and purification of fibrinogen-like domain of L-ficolin | 85 |
| 3.6.1 | PCR amplification and cloning of fibrinogen-like domain of L-ficolin.. | 85 |
| 3.6.2 | Expression and purification of fibrinogen-like domain of L-ficolin..... | 87 |
| 3.6.3 | Analysis binding between recombinant Ply and L-ficolin | 90 |
| 3.7 | ELISA binding between Ply and IgG isotypes..... | 96 |
| 3.8 | ELISA binding between PlyD1-3 and PlyD4 with IgG isotypes..... | 98 |
| 3.9 | ELISA binding between Ply and Ply domains with IgG fragments | 100 |
| 3.10 | Digestion of IgG4 with IdeS enzyme | 103 |
| 3.11 | ELISA binding between monoclonal Fab and Fc with the Ply, PlyD1-3 and PlyD4 | 106 |
| 3.12 | ELISA binding between Ply D385N and IgG isotypes | 108 |
| 3.13 | Inhibition assay | 109 |
| 3.14 | Discussion..... | 111 |
| 3.14.1 | Binding between Ply and L-ficolin..... | 111 |
| 3.14.2 | Binding between Ply and IgG isotypes..... | 111 |
| Chapter 4 | Inhibition of Ply by disruption of intermolecular packing..... | 113 |
| 4.1 | Objectives..... | 113 |
| 4.2 | Materials and methods | 116 |
| 4.2.1 | Materials..... | 116 |
| 4.2.2 | Construction of Ply mutants by SOE-PCR..... | 116 |
| 4.2.3 | Mutations in the TMH1 and TMH2 region of Ply | 119 |
| 4.2.4 | Fluorescence spectroscopy..... | 119 |
| 4.2.5 | Stability of mutants..... | 120 |
| 4.2.6 | Preparation of liposomes | 120 |
| 4.2.7 | Fluorescence data collection with liposomes | 120 |
| 4.2.8 | Haemolytic assay | 121 |
| 4.2.9 | Transmission electron microscopy (TEM)..... | 121 |
| 4.2.10 | Preparation of liposomes with calcein..... | 121 |
| 4.2.11 | Calcein-leakage assay..... | 122 |
| 4.2.12 | PlyD1-3 crystallization and optimization | 122 |
| 4.2.13 | PlyD4 crystallization with sLeX..... | 122 |
| 4.2.14 | X-ray diffraction of PlyD1-3 and PlyD4 crystals | 123 |
| 4.2.15 | Crystallization theory..... | 124 |
| 4.2.16 | X-ray diffraction | 125 |
| 4.3 | Results..... | 127 |
| 4.3.1 | SOE-PCR construction of single mutant Ply..... | 127 |
| 4.3.2 | Mutations inTMH1 and TMH2 region of Ply..... | 129 |
| 4.3.3 | Cytolytic activities of Ply mutants..... | 130 |
| 4.3.4 | Stability measurement of mutants by Gdn-HCl denaturation..... | 133 |

| | | |
|--|---|-----|
| 4.3.5 | Liposome binding | 142 |
| 4.3.6 | Calcein leakage from liposomes in the presence of Ply | 148 |
| 4.3.7 | Pore formation of Ply on Chol-containing liposomes by EM | 151 |
| 4.3.8 | Crystallization of PlyD1-3 and D4..... | 154 |
| 4.3.9 | Discussion | 158 |
| Chapter 5 The conversion of monomers of Ply to pre-pore complexes | | |
| promotes microdomain formation in lipid bilayers | | 160 |
| 5.1 | Raman spectroscopic analysis of lipid bilayers..... | 160 |
| 5.1.1 | Raman spectroscopy | 160 |
| 5.1.2 | Lipid Raman spectra..... | 161 |
| 5.1.3 | Optical tweezers (OT) | 163 |
| 5.1.4 | Microfluidic device | 165 |
| 5.2 | Objectives..... | 166 |
| 5.3 | Materials and methods | 166 |
| 5.3.1 | Materials..... | 166 |
| 5.4 | Preparation of lipid vesicles (Liposomes)..... | 166 |
| 5.5 | Microfluidic laminar flow cell..... | 167 |
| 5.6 | Raman tweezers of a single liposome with the wild-type Ply and Ply mutants | 169 |
| 5.7 | Raman measurement and data collection | 170 |
| 5.8 | The OT setup..... | 171 |
| 5.9 | Raman data normalization..... | 172 |
| 5.10 | Results..... | 173 |
| 5.10.1 | Lipid vibrational spectroscopy..... | 173 |
| 5.10.2 | Observing structural changes in a single liposome by wild-type Ply..... | 174 |
| 5.10.3 | The influence of lipid composition on the changes observed in the bilayers following the addition of wild-type Ply..... | 176 |
| 5.10.4 | Raman spectra of liposome with the PlyD4..... | 180 |
| 5.10.5 | Monitoring membrane, structural change of the liposome with Ply Asp205Arg (D205R) and Asn339Arg (N339R) | 183 |
| 5.10.6 | Monitoring membrane, structural change of the liposome with mutant Ply Thr304Arg, Arg226Ala, Thr88Glu, and Lys268Ala, Val341Arg and Leu11Arg..... | 185 |
| 5.10.7 | Influence of locked mutant on the chemical structure of the membrane..... | 188 |
| 5.10.8 | Monitoring change of the lipid layer of a liposome membrane composed of ternary mixture of POPC/Chol /SM (1:1:1)..... | 190 |
| 5.11 | Discussion..... | 191 |
| 5.12 | General discussion | 193 |
| 5.12.1 | ELISA binding between Ply and human L-ficolin | 193 |
| 5.12.2 | ELISA binding between Ply and IgG isotypes..... | 193 |
| 5.12.3 | Ply binds to the Fab region of IgG via domains 1-3 | 193 |
| 5.12.4 | Structural based mutation in Ply to block pore formation..... | 194 |
| 5.12.5 | Raman spectral analysis of Ply on the lipid bilayer membrane | 194 |
| 5.13 | Future work | 195 |
| 5.13.1 | Mutation in PlyD1-3 residues | 195 |
| 5.13.2 | Disruption of Ply monomers | 195 |
| 5.13.3 | Raman spectroscopy and Ply..... | 195 |
| Appendixes | | 196 |
| References..... | | 207 |

List of figures

| | |
|--|----|
| Figure 1-1: Pneumococcal pathogenic routes of infection. | 3 |
| Figure 1-2: Schematic diagram of the pneumococcus virulence factors. | 6 |
| Figure 1-3: Ply crystal structure. | 15 |
| Figure 1-4: Two hypothesis models of pore formation by CDCs. | 16 |
| Figure 1-5: Mechanism of pore formation of CDCs family on the lipid bilayer. | 18 |
| Figure 1-6: Three pathways of the complement system: Classical, Lectin and Alternative pathways (CP, LP and AP). | 21 |
| Figure 1-7: Schematic representation of human C1q and human IgG showing how C1q binds to IgG on the pathogen surface. | 23 |
| Figure 1-8: Schematic representation of MBL-MASPs binding to a pathogen surface. | 24 |
| Figure 1-9: Schematic representation of human ficolin genes <i>FCN-1</i> , <i>FCN-2</i> and <i>FCN-3</i> | 30 |
| Figure 1-10: Schematic diagram of ficolin structure and domain organisation. | 31 |
| Figure 1-11: Schematic diagram of Ig structure. | 34 |
| Figure 1-12: Schematic representation of membrane lipid types. | 39 |
| Figure 1-13: Schematic representation of fluid-mosaic model of a biological membrane. | 40 |
| Figure 1-14: Cholesterol chemical structure. | 42 |
| Figure 1-15: Schematic view of a liposome vesicle and a lipid bilayer. | 43 |
| Figure 1-16: Chemical structure of DPPC, POPC, DOPC and DLPC. | 44 |
| Figure 1-17: Membrane phase transition with increasing temperature. | 45 |
| Figure 2-1: Vector map of pLEICS-07. | 50 |
| Figure 2-2: Ply amino acid residues. | 51 |
| Figure 2-3: Vector map of pLEICS-01. | 53 |
| Figure 2-4: Vector map of pLEICS-10. | 56 |
| Figure 2-5: SDS-PAGE showing Ply purification by affinity chromatography on Ni- Sephadex column. | 58 |
| Figure 2-6: Size exclusion chromatography of recombinant full-length Ply on a Superdex 200 16/60 column analysed on a 15% SDS-PAGE gel. | 59 |
| Figure 2-7: Agarose gel showing PCR of PlyD1-3 DNA fragments. | 60 |
| Figure 2-8: 15% SDS-PAGE of small-scale expression of PlyD1-3 in inclusion body. | 61 |
| Figure 2-9: Elution profile of the purified PlyD1-3 on Superdex 200 10/300 after refolding screens. | 63 |
| Figure 2-10: Purified refolded recombinant PlyD1-3 after analytical size exclusion chromatography assessed by SDS-PAGE. | 64 |
| Figure 2-11: 15% SDS-PAGE of PlyD1-3 after purification on Ni-Sephadex column and size exclusion chromatography profile of PlyD1-3 on Superdex 75 16/60 column. | 66 |
| Figure 2-12: SDS-PAGE of purified PlyD1-3 after gel filtration on Superdex 75 16/60. | 66 |
| Figure 2-13: 15% SDS-PAGE of purified PlyD4 tagged with MBP after affinity chromatography on amylose resin column. | 67 |
| Figure 2-14: Elution profile of PlyD4 after digestion with TEV protease on a Superdex 75 16/60 gel filtration column. | 68 |
| Figure 2-15: 15% SDS-PAGE of purified PlyD4 after digestion with TEV protease on Superdex 75 16/60 gel filtration. | 69 |
| Figure 3-1: Map of a pED4 expression vector. | 75 |
| Figure 3-2: Amino acids sequence of human L-ficolin. | 77 |

| | |
|---|-----|
| Figure 3-3: Map of the bacterial expression vector pET28 a. | 79 |
| Figure 3-4: 1% w/v agarose gel electrophoresis showing PCR steps to amplify cDNA of the L-ficolin. | 83 |
| Figure 3-5: A restriction digestion of L-ficolin cDNA in pGEM-T easy (A) and pED4 (B) with <i>PstI/EcoRI</i> enzymes. | 84 |
| Figure 3-6: 15% SDS-PAGE gel analysis of recombinant L-ficolin after chromatography on a GlcNac-Sepharose column. | 85 |
| Figure 3-7: A 1% agarose gel showing PCR amplification of the cDNA encoding fibrinogen-like domain of L-ficolin and restriction digestion of the resulting clones in pGEM-T easy vector. | 86 |
| Figure 3-8: A 1% agarose gel of <i>NcoI/EcoRI</i> restriction digestion of seven different fibrinogen-like domain clones in pET28a. | 87 |
| Figure 3-9: SDS-PAGE of the fibrinogen-like domain of L-ficolin. | 88 |
| Figure 3-10: Size exclusion chromatography of recombinant fibrinogen-like domain on a Superdex 75 16/60 column analysed on a 15% SDS-PAGE gel. | 89 |
| Figure 3-11: No binding between recombinant Ply and purified recombinant L-ficolin by ELISA. | 91 |
| Figure 3-12: L-ficolin binding to recombinant Ply using monoclonal anti L-ficolin antibody by ELISA. | 92 |
| Figure 3-13: ELISA binding of Ply with serum L-ficolin. | 95 |
| Figure 3-14: ELISA binding assay between Ply and IgG isotypes. | 97 |
| Figure 3-15: ELISA binding of Ply domains with IgG isotypes. | 99 |
| Figure 3-16: ELISA binding of Ply and Ply domains with IgG fragments. | 102 |
| Figure 3-17: Elution profile of an IgG4 digestion with IdeS enzyme on Superdex 200 16/60. | 104 |
| Figure 3-18: Analysis of digested IgG4 on SDS-PAGE. | 105 |
| Figure 3-19: ELISA binding of Ply and Ply domains with the monoclonal Fab and Fc of digested IgG4. | 107 |
| Figure 3-20: ELISA binding comparison of wild-type Ply and mutant PlyD385N with IgG isotypes. | 108 |
| Figure 3-21: Inhibition of binding of IgG, Fab and Fc to Ply. | 110 |
| Figure 3-22: Alignment of the IgG CH1 amino acid sequences. | 112 |
| Figure 4-1: Packing of monomers in the Ply crystal reveals the packing of the pre-pore complex. | 113 |
| Figure 4-2: Ply residues contribute in the intermolecular interaction. | 115 |
| Figure 4-3: Vector map of pLEICS-9. | 118 |
| Figure 4-4: Schematic diagram of protein crystallization phase. | 125 |
| Figure 4-5: X-ray diffraction. | 126 |
| Figure 4-6: The two-dimensional representation of the reflected X-ray from two crystal planes. | 127 |
| Figure 4-7: SOE-PCR to introduce the mutations D205R and K268A into Ply. | 128 |
| Figure 4-8: Ply amino acid residues forming TMH1 and TMH2. | 129 |
| Figure 4-9: Result of SOE-PCR showing the construction of the Ply Thr55Cys+Val163Cys (TMH1) and Ala262Cys+Trp278Cys (TMH2) mutants. | 130 |
| Figure 4-10: Haemolytic activities of wild-type Ply, mutants Ply and ply truncated fragments. | 132 |
| Figure 4-11: Fluorescence emission spectra of wild-type Ply and mutants in Gdn-HCl. | 139 |
| Figure 4-12: Unfolding of wild-type and mutant Plys in Gdn-HCl. | 141 |

| | |
|---|-----|
| Figure 4-13: Fluorescence emission spectra of wild-type Ply and mutants in the presence and absence of cholesterol containing liposomes. | 146 |
| Figure 4-14: Change in the $\lambda_{em\ max}$ of wild-type Ply and mutants in the presence and absence of liposomes. | 147 |
| Figure 4-15: Calcein release from liposomes by Ply. Calcein leakage was measured as a function of time. | 150 |
| Figure 4-16: Negative-stain EM of wild-type Ply, mutants Ply Thr304Arg, and PlyD4 with unilamellar liposome containing-Chol. | 152 |
| Figure 4-17: Negative-stain EM of Ply Asp205Arg, with the unilamellar liposome containing-Chol. | 153 |
| Figure 4-18: Negative-stain EM of Ply Asn339Arg, with the unilamellar liposome containing Chol. | 154 |
| Figure 4-19: PlyD4 crystal structure the Trp loop in the green structure is flip down. | 155 |
| Figure 4-20: Ply domain structure and the likely changes upon membrane binding. . | 156 |
| Figure 5-1: Rayleigh and Raman scattering. | 161 |
| Figure 5-2: The gradient force mechanism in OT. | 165 |
| Figure 5-3: Microfluidic device pattern. | 169 |
| Figure 5-4: Microfluidic device preparation. | 169 |
| Figure 5-5: Liposome manipulation between two different solutions including PBS and Ply by OT. | 170 |
| Figure 5-6: Schematic of Optical tweezers. | 171 |
| Figure 5-7: Representative Raman spectra of an-optimally trapped POPC/Chol liposome and POPC/Chol separately. | 174 |
| Figure 5-8: The Raman spectra profile of an-optimally trapped liposome (1:1 mole ratio POPC/Chol) with and without wild-type Ply. | 175 |
| Figure 5-9: Raman spectra profile of an-optimally trapped pure POPC liposome with and without wild-type Ply. | 176 |
| Figure 5-10: Comparison Raman spectra of an-optimally trapped single liposome with and without wild-type Ply in low/high concentration of cholesterol. | 179 |
| Figure 5-11: Comparison of Raman spectra of an-optimally trapped liposome with and without PlyD4. | 182 |
| Figure 5-12: Raman spectra profile of an-optimally trapped liposome (1:1 POPC/Chol) with mutant D205R and N339R. | 185 |
| Figure 5-13: Raman spectra profile of-an optimally trapped 1:1 POPC/Chol vesicle with mutant Lys268Ala, Arg226Ala, Val341Arg, Thr88Glu and Leu11Arg. | 187 |
| Figure 5-14: Comparison of Raman spectra for an-optimally trapped liposome POPC/Chol 1:1 ratio and POPC/Chol low ratio with mutant Thr304Arg. | 187 |
| Figure 5-15: Comparison of Raman spectra for an-optimally trapped liposome POPC/Chol high with and without Thr304Arg. | 188 |
| Figure 5-16: Raman spectra analysis of an-optimally trapped liposome with Ply locked mutants (Thr55Cys+Val163Cys and Ala262Cys+Trp278Cys). | 190 |
| Figure 5-17: Raman spectra profile of 1:1:1 POPC/Chol/SM liposome with wild- type Ply, PlyD4 and Ply mutant T304R. | 191 |
| Figure 5-18: Schematic represntaion of impacting Ply on the the membrane phase. | 192 |

List of tables

| | |
|---|-----|
| Table 1-1: The pneumococcus vaccine types, which are currently licensed. | 12 |
| Table 1-2: A schematic outline of three human ficolins (M-ficolin, L-ficolin and H-ficolin)..... | 29 |
| Table 1-3: Human IgG isotypes characteristic. | 37 |
| Table 2-1: Oligonucleotide primers to amplify PlyD1-3..... | 52 |
| Table 2-2: Oligonucleotide primer sets for amplify PlyD4. | 56 |
| Table 3-1: Sequence of oligonucleotides using in the cloning of the human L-ficolin.. | 73 |
| Table 3-2: Oligonucleotide sequences used to amplify the cDNA encoding the fibrinogen-like domain of L-ficolin. | 80 |
| Table 4-1: Mutagenic Primer sequences to make the single point mutants..... | 117 |
| Table 4-2: Primer sequences of the TMH1 and TMH2 mutants. | 119 |
| Table 4-3: Optimisation crystallisation condition for PlyD1-3. | 123 |
| Table 4-4: Cytolytic activity of wild-type Ply and Ply mutants. The haemolytic activity of single mutants and double mutants were carried out at different time. Therefore, the relative activity of wild-type Ply is different. | 133 |
| Table 4-6: Data collection and refinement statistics (Marshall et al., 2015). | 157 |

List of abbreviations

| | |
|---------------|--|
| Ap | Alternative pathway |
| Arg | Arginine |
| Asn | Asparagine |
| Asp | Aspartic acid |
| BSA | Bovine serum albumin |
| CAP | Community acquired pneumonia |
| cDNA | Complementary DNA |
| CHO | Chines Hamster Ovary |
| CP | Classical pathway |
| CRM197 | Cross reactive material 197 |
| DHFBS | Dialysed heat fetal bovine serum |
| DLPC | 1, 2-dilauroyl-sn-glycero-3-phosphate |
| DLS | Dynamic light scattering |
| DMS | Dimethyl sulfoxide |
| dNTP | Deoxynucleotide triphosphate |
| DOPC | 1, 2-dioleoyl-sn-glycero-3-phosphocholine |
| DPPC | Dipalmitoylphosphatidylcholine |
| DTT | Dithiothreitol |
| <i>E coli</i> | <i>Escherichia coli</i> |
| EDTA | Ethylene diamine tetra acetic acid |
| ELISA | Enzyme linked immunosorbent assay |
| Eno | Enolase |
| Gdn-HCl | Guanidine-HCl |
| GlcNAc | N-acetyl glucosamine |
| Glu | Glutamic acid |
| GSSH | Glutathione disulphide |
| His-tag | Histidine-tag |
| Hyl | Hyaluronidase |
| Ig | Immunoglobulin |
| IPD | Invasive pneumococcal diseases |
| IPTG | Isopropyl β -D-1-thiogalactopyranoside |
| LB | Luria-Bertani broth |
| Ld | Liquid disorder |
| Leu | Leucine |
| Lo | Liquid order |
| Lp | Lectin pathway |
| LUVs | Large unilamellar vesicles |
| Lys | Lysine |
| LytA | Autolysin A |
| MAC | Membrane attack complex |
| MASP | MBL associated serine proteases |
| MBL | Mannose binding lectin |
| MBP | Maltose binding protein |
| Met | Methionine |
| mIgD | Membrane IgD |
| mRNA | Messenger RNA |
| MSB | Maurice Shock Building |
| MTX | Methotrexate |

| | |
|------------------|--|
| OM | Otitis media |
| OME | Otitis media with effusion |
| OT | Optical tweezers |
| P/S | Penicillin/Streptomycin |
| PAGE | Polyacrylamide gel |
| PavA | Pneumococcal adhesion and virulence A |
| PBS | Phosphate buffer saline |
| PCR | Polymerase chain reaction |
| PCV | Pneumococcal conjugates vaccine |
| PDMS | Polydimethylsiloxane |
| Phe | Phenylalanine |
| Ply | Pneumolysin |
| PlyD1-3 | Pneumolysin domain 1-3 |
| PlyD4 | Pneumolysin domain4 |
| PNACL | Protein nucleic acid chemistry laboratory |
| pNNp | p-Nitrophenyl phosphate disodium salt |
| POPC | Palmitoyl-2-oleoylsen-glycero-3-phosphocholine |
| PPV | Pneumococcal polysaccharide vaccine |
| PS | Phosphatidylserine |
| PspC | Pneumococcal surface protein C |
| RBCs | Red blood cells |
| Re | Reynolds |
| rFR ⁺ | Fermi resonance |
| rpm | Round per minute |
| SDS | Sodium dodecyl sulphate |
| SEM | Standard error of the mean |
| sIgD | Secreted IgD |
| sLeX | Sialyl Lewis X |
| SOE-PCR | Splicing overlap extension PCR |
| TBE | Tris borate EDTA |
| TE | Trypsin EDTA |
| TEM | Transmission electron microscope |
| Thr | Threonine |
| T _m | Melting temperature |
| TMH 1, 2 | Transmembrane hairpin 1 and 2 |
| Trp | Tryptophan |
| Tyr | Tyrosin |

Chapter 1 General introduction

1.1 Pneumococcus

The Pneumococcus was discovered and isolated by the George Sternberg in 1880 and Louis Pasteur in 1881 (Flaumenhaft and Flaumenhaft, 1993). It is a Gram-positive bacterium and previously known as a *Diplococcus pneumoniae* (Stevens and Kaplan, 2000). The ecological niche of this bacterium is a part of the human nasopharyngeal flora where it exists asymptotically as a commensal (Kadioglu et al., 2008). Approximately 25% of the population carries the pneumococcus in their nasopharynx but it becomes a pathogen when it spreads from the nasopharynx to the lungs, blood and brain (Paterson and Orihuela, 2010). In addition, when the immune system is compromised it causes many serious diseases such as pneumonia, meningitis, bacteremia and otitis media (Kadioglu et al., 2008).

Pneumococci are arranged in a pair or in a chain of varying lengths in blood cultures and liquid media (AlonsoDeVelasco et al., 1995). Pneumococci are facultative anaerobes and catalase-negative bacteria. They produce a green zone of hemolysis around colonies on blood agar hence are classified as alpha-hemolytic (Obaro and Adegbola, 2002). Pneumococcal infections are associated with a high rate of mortality and morbidity globally (Song et al., 2013). This might be a result of its increasing antibiotic resistance. In developing countries, pneumococcal septicemia is a major cause of child mortality (Kadioglu et al., 2008). The pneumococcus represents the most common bacterial cause of community-acquired pneumonia (CAP) in both developed and developing countries (Feldman and Anderson, 2016). Moreover, it is the most important respiratory tract bacterial pathogen in the UK and is responsible for most episodes of CAP.

1.2 Pneumococcal epidemiology

Normal carriage of the pneumococcus is first evident at 2-3 years old. Carriage in children is higher than in adults with a <10 % decrease in the adult population (Henriques-Normark and Tuomanen, 2013). The first step of pneumococcal infection is the colonization of the nasopharynx. Infection can spread from person to person via droplets/aerosols. Transmission is immediate on contact with respiratory droplets from persons with existing pneumococcal illness or commonly, from persons who

asymptomatically carry pneumococci in their nasopharynx (Hartzell et al., 2003). The pneumococcus lives in the upper respiratory tract as a normal flora and it is found in 30-70% of preschool children (Nilsson and Laurell, 2001).

Tracking the global or local spread of pneumococci is commonly done by serotyping of the capsular polysaccharide (Henriques-Normark and Tuomanen, 2013). So far, at least 93-serotypes based on capsular polysaccharide structures are known in the pneumococcus (Henriques-Normark and Tuomanen, 2013, Drijkoningen and Rohde, 2014). Studies in the USA in the late 1990s showed that serotypes 4, 6B, 9V, 14, 18C, 19F and 23F account for 59% of invasive pneumococcal diseases (IPD) in adults and 87% in children, respectively (Feikin and Klugman, 2002). The same serotypes caused 61-81% of IPD in Europe (Rudan et al., 2008). Most cases of childhood pneumonia occur in developing countries, mostly in India, China, and Pakistan (Rudan et al., 2008). Some serotypes, such as serotype 1 and 7F, have a high invasive disease potential, whereas other types are mainly involved in carriage. Serotypes 3, 6B, and 19F have a lower invasive disease potential but were associated with the highest mortality rates in patients (Sandgren et al., 2004). The common serotypes in Germany associated with IPD are serotype 6A and 6B. After introduction of the conjugate vaccine section 1.5, infections by both serotypes were reduced among children and adults. However, serotype 6C and possibly 6D increased in adults (van der Linden et al., 2013). A recent study carried out from April 2013 to March 2015 revealed that the most widespread serotypes in Japan were serotypes 3, 19A, and 22F and these were the most common isolates among adult patients with IPD (Fukusumi et al., 2017). However, another study suggested that serotype 1 is one of the most common cause of pneumococcal disease worldwide (Cornick et al., 2017). Figure 1-1 displays the pneumococcal infection progression route from nasopharyngeal carriage to respiratory diseases including pneumonia and systemic diseases such as septicemia, meningitis, otitis media and sinusitis.

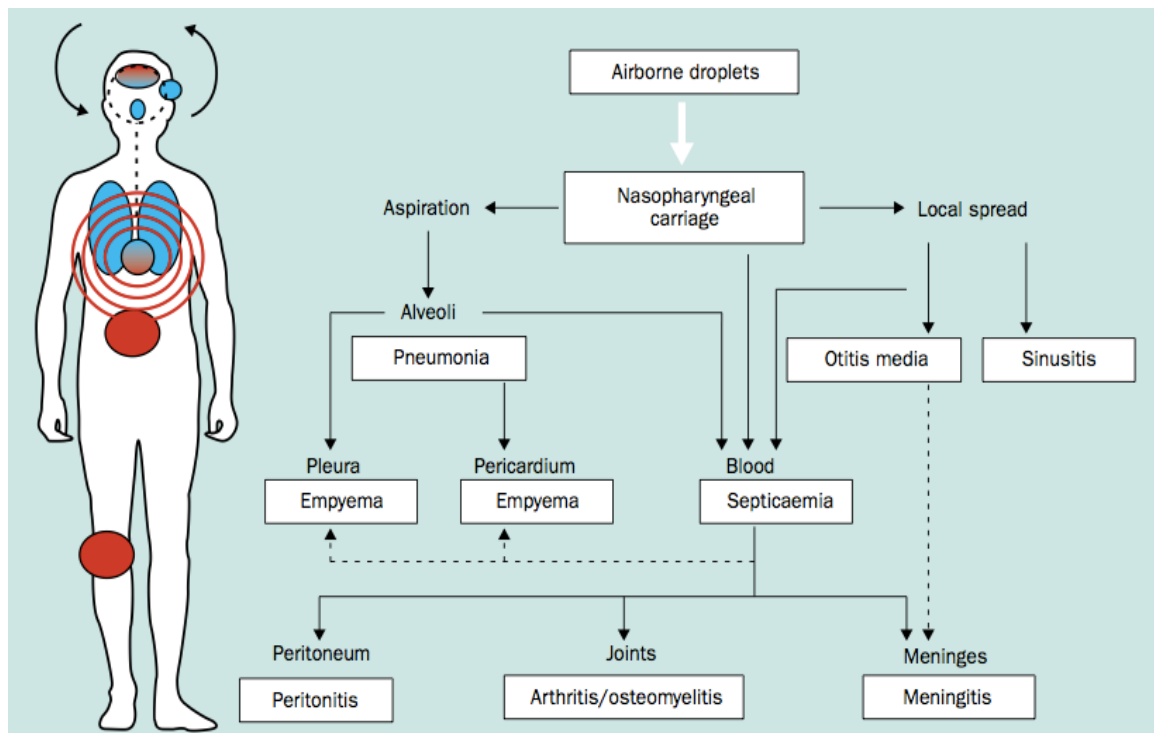


Figure 1-1: Pneumococcal pathogenic routes of infection.

Infection of organs is started through the airborne droplets displayed in blue and passed through to other organs include blood, brain and ears to cause septicaemia, meningitis, otitis media and sinusitis or by haematogenous route depicted in red. Image taken from (Bogaert et al., 2004).

1.3 Pneumococcal diseases

In young and elderly people the pneumococcal diseases represent a global health problem. Asymptomatic nasopharyngeal bacterial colonization can spread to the sterile parts of the body to cause pneumonia, sepsis, and middle ear infection (Li et al., 2016). Pneumococcal infection is divided into two types: invasive and noninvasive infections. Non-invasive disease occurs at mucosal surfaces of the respiratory tract, lung and middle ear in which the organism spreads directly from the nasopharynx. However, invasive diseases proceed by spreading of the bacteria to the sterile tissue. The pneumococcus is the major cause of pneumonia, septicemia and meningitis in children and annually more than a half million of them die from pneumococcal diseases (Ingels, 2015). According to epidemiological studies, approximately 1.6 million people die from IPD each year, 1 million of them are children aged <5 years, mainly from developing countries (O'Brien et al., 2009). Mortality is up to 10 times higher in some developing countries compared to developed countries (Lagos et al., 2002). In any population, the incidence of IPD is impacted by

different factors including the geographical location, season, prevalent serotype, age, and vaccination status of the population (Cilloniz and Torres, 2014).

1.3.1 Otitis media (OM)

Inflammation of the middle ear is a common disease of childhood (Ngo et al., 2016). OM is divided into two types: acute otitis media (AOM) which usually affects children under two years of age and may be caused by bacteria or viral infections (Qureishi et al., 2014) and OM with effusion (OME) which is a chronic inflammatory condition more common in children between 3 and 7 years old (Daniel, 2013). The pneumococcus causes AOM to give symptoms of earache and fever while the non-encapsulated *Haemophilus influenzae* causes AOM with conjunctivitis (Palmu et al., 2004). The pneumococcal conjugate vaccines PCV7 and PCV13 have decreased the incidence of IPD, but in the respect of the OM only modest success have been achieved (Shenoy and Orihuela, 2016).

1.3.2 Sinusitis and bronchitis

Sinusitis is an infection of the sinuses, which are cavities connecting the middle ear with the nasal cavity. Bronchitis is an infection of the airways leading from the trachea to the lungs (Noterman and Nurmio, 2016). Most cases of bronchitis are viral, but the pneumococcus and *Haemophilus influenzae* can cause chronic forms of bronchitis (O'Grady et al., 2013). It specifically occurs in children and adults. Patients with bronchitis may recover without antimicrobial treatment (Kristo et al., 2003).

1.3.3 Pneumonia and septicaemia

Pneumonia is an acute infection of lungs, where the alveoli fill with fluid and oxygen absorption is reduced. This disease affects approximately 450 million people each year (Rudan et al., 2008). Pneumonia is mostly caused by the pneumococcus and *Haemophilus influenzae* type b in unvaccinated children (O'Brien et al., 2009, Watt et al., 2009). In the UK, pneumococcal pneumonia is the most common cause of CAP in children under two years (Randle et al., 2011). Fortunately, CAP caused by the pneumococcus is now controlled because of the availability of effective vaccines. For example, paediatric heptavalent vaccines (PCVs) are effective in immunizing children (Principi and Esposito, 2016). A variety of microorganisms cause pneumonia including *Mycoplasma pneumoniae*, *Chlamydophila pneumoniae* and *Staphylococcus aureus* (Mandell, 2015). Pneumococcal septicaemia occurs when the pneumococcus infects the blood stream (Randle et al., 2011). Immunocompromised patients are particularly vulnerable (Iinuma

et al., 2007). The consequence of pneumococcal septicemia is that RBCs cannot properly transport oxygen efficiently to vital organs, and this can rapidly become life-threatening (File, 2003).

1.3.4 Pneumococcal meningitis

Meningitis is the inflammation of the meninges, the membrane surrounding the brain, which is a serious IPD (Randle et al., 2011). If bacterial meningitis is left untreated, it is almost always fatal and pneumococcal meningitis accounts for a significant proportion of meningitis deaths annually (Pollard et al., 2007). In the UK this disease is the second most common form of bacterial meningitis after meningococci in children over the age of one month (Randle et al., 2011). According to Levy *et al.* (Levy et al., 2014) bacterial meningitis by the pneumococcus is the most common cause of meningitis in children younger than two years. In Germany it has been reported that the mortality rate is ~7.5% among children (Imohl et al., 2015). Acute bacterial meningitis in Iran is being considered as a dangerous public health problem due to lack of the vaccination program against the meningeal etiology agent specifically pneumococci (Hourri et al., 2017). In 2000, following the use of PCV7, IPD decreased among both children and adults. However, the effect on pneumococcal meningitis was not clear (Hsu et al., 2009). Nevertheless, in Utah use of PCV7 was associated with a decrease in the incidence of pneumococcal meningitis of 72%, (Stockmann et al., 2013). Similarly, Bingen *et al.* observed a 68% decrease in PCV7 serotype pneumococcal meningitis and a 16% to 31% increase in non-PCV7 serotype disease (Bingen et al., 2008).

1.4 Pneumococcus virulence factors

The pneumococcus has a plethora of virulence factors, including the polysaccharide capsule, several surface-located proteins, and the toxin Ply (Kadioglu et al., 2008, Mitchell and Mitchell, 2010). Figure 1-2 below illustrates some of the virulence factors expressed by the pneumococcus.

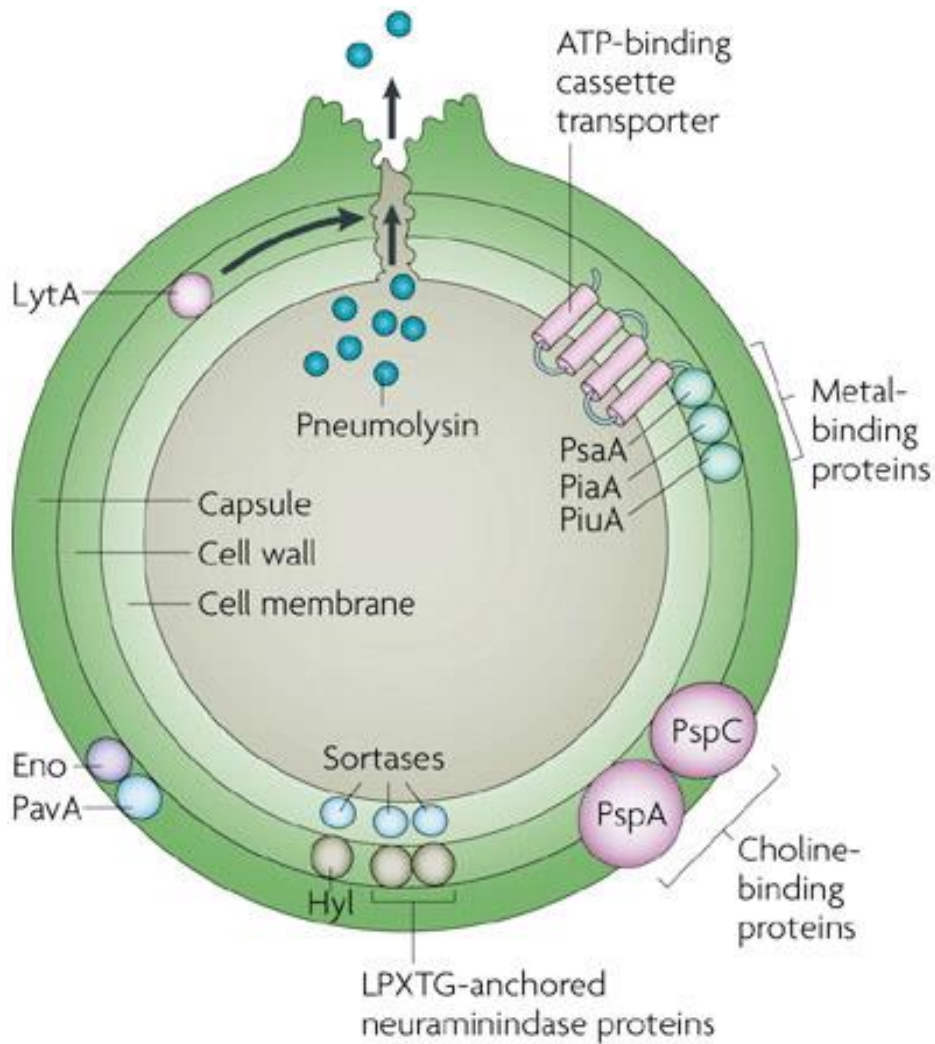


Figure 1-2: Schematic diagram of the pneumococcus virulence factors.

Virulence factors include the capsule, cell wall, choline-binding pneumococcal surface proteins A and C (PspA and PspC) the LPXTG-anchored neuraminidase, (Hyl), Ply, sortases, Eno, PavA and Lyt A (Kadioglu et al., 2008).

1.4.1 The Capsule

The polysaccharide capsule is a key virulence factor of the pneumococcus that promotes pneumococcal attachment to the nasopharyngeal epithelial surfaces and it plays a crucial role in protecting the pneumococcus from the host defenses by complement-dependent and-independent phagocytosis (Hyams et al., 2013). 93-pneumococcal serotypes have been identified, but only 20 serotypes are responsible for the majority of invasive diseases (Hausdorff et al., 2000). All pathogenic pneumococci express a capsular polysaccharide. In an animal model system, the presence of a capsule led to an increase in virulence by more than a million-fold (Zartler et al., 2009). The current pneumococcal vaccine target

is the capsule because the capsule is the principal virulence factor of the pneumococcus (Skov Sorensen et al., 2016).

1.4.2 The cell wall

Pneumococcal cell wall is a multi-molecular coat consisting of peptidoglycan, composed of N-acetyl glucosamine (GlcNAc) and N-acetyl muramic acid (MurNAc), which is covalently attached to teichoic acids (Bai et al., 2014). The cell wall provides two main functions include bacterial protection from phagocytosis and maintenance of cell shape (Bui et al., 2012). The pneumococcal cell wall strongly provokes inflammation due to the activation of a wide arrange of cytokines and enzymes (Tomasz and Saukkonen, 1989). The classical and alternative pathways of the complement system are activated by the pneumococcal cell wall via lipoteichoic acid components (Hummell et al., 1985).

1.4.3 Autolysin A (LytA)

The LytA is another virulence factor of the pneumococcus, which is involved in autolysis and in fratricidal penicillin induced lysis. LytA is mainly located intracellularly, but a small amount is attached to the extracellular cell wall (Mellroth et al., 2012). Structurally, LytA is a two-domain protein with an N-terminal acetylmuramoyl l-alanine amidase domain and a C-terminal choline-binding domain (Fernandez-Tornero et al., 2001). Mutation of LytA gene leads to a decrease in virulence compared to the wild-type pneumococcus (Hirst et al., 2008). LytA mediates lysis and release of Ply (Martner et al., 2008). In addition, release of LytA may lyse neighbouring non-competent pneumococcal cells in a fratricidal manner (Eldholm et al., 2009). The likely function of LytA is to release proteins involved in immune evasion or interference of the host immune response by the cell wall components (Martner et al., 2009).

1.4.4 Neuraminidases or sialidases

Neuraminidase or sialidases remove N-acetyl-neuraminic acid (sialic acid) from carbohydrates on host cells, which is a key carbohydrate source for the pneumococcus. In addition, it is a receptor for adhesion and invasion and promotes biofilm formation (McCombs and Kohler, 2016). Three types of neuraminidases are produced by the pneumococcus called Nan A, Nan B, and Nan C, which are ordered according to their contribution towards virulence (Xu et al., 2011, Walther et al., 2015). Nan A is the most highly expressed neuraminidase in all the pneumococcus strains and can hydrolyse α 2-3, α 2-6, and α 2-8 sialyllactose to release N-acetyl-neuraminic acid (Walther et al., 2015, Xu

et al., 2011, King et al., 2004). Nan B exists in most but not all the pneumococcus strains. Nan B deficient strains cannot colonize the nasopharynx or cause sepsis (Walther et al., 2015). Nan C only exists in 51% of strains (Gualdi et al., 2012, Smith et al., 2013). Nan A (~115 kDa), Nan B (~75 kDa), and Nan C (~82 kDa) each have an N-terminal signal sequence, followed by a lectin domain, and a catalytic domain. Nan A also has a C-terminal domain LXPTG motif that is used to attach to the cell wall (King et al., 2004).

1.4.5 Hyaluronidase (Hyl)

Hyl degrades hexosaminidic linkages of hyaluronan or hyaluronic acid and also cleaves other polysaccharide components such as chondroitin or chondroitin sulfates (Zwijnenburg et al., 2001, Hynes and Walton, 2000). The three dimensional structure of Hyl has been determined by X-ray crystallography. It is composed of an N-terminal catalytic domain and a C-terminal supportive β -domain connected by a short peptide linker (Akhtar and Bhakuni, 2003). It has been suggested that Hyl plays a major role in both colonization and invasion thus it is an important virulence factor, which exists in most clinical isolates of the pneumococcus (Feldman et al., 2007). However, another study showed that hyaluronidase did not contribute to virulence in a meningitis model of infection (Wellmer et al., 2002).

1.4.6 Immunoglobulin A1 protease (IgA1)

The *iga* gene encodes the IgA1 protease, a 200 kDa metalloprotease that cleaves the hinge region of human IgA1 at the bond between Pro-227 and Thr-228 (Wani et al., 1996). Cleavage impacts the protective function of IgA1 and inhibits the phagocytic killing of the pneumococcus (Janoff et al., 2014). IgA is the most common immunoglobulin on mucosal surfaces and IgA1 represents over 90% of total IgA. IgA2 comprises only 10% of IgA. Thus the IgA1 protease is a major virulence factor for colonization in the nasopharynx (Weiser et al., 2003, Janoff et al., 2014).

1.4.7 Pneumococcal iron acquisition and uptake transporters

The pneumococcus encounters iron scarcity in the human host. To provide an appropriate iron supply, the ATP binding cassette transporter Pia works to take up iron chelated by hydroxamate siderophore, via the membrane-anchored substrate-binding protein PiaA (Cheng et al., 2013). Piu A (~34 kDa), Pia A (~42 kDa) and Pit A (~37 kDa) are lipoprotein components of two pneumococcal iron ABC transporters (Whalan et al., 2005, Brown et al., 2002a). The three proteins are encoded by unlinked genes, *piu A*, *pia*

A and *pit A* (Brown et al., 2002a). Mutation in any one of the three loci results in a modest reduction in virulence, while mutation in two or three loci causes a more substantial reduction of growth in an iron-restricted environments (Janulczyk et al., 2003).

1.4.8 Pneumococcal surface protein A (PspA)

PspA is a surface exposed protein of the pneumococcus (Tu et al., 1999). The virulence role of PspA has been demonstrated in the pneumococcus strains in which the PspA genes deleted or inactivated. PspA mutant strains are cleared more quickly from the blood of nonimmunized mice than the wild-type strain (Haughney et al., 2013). PspA reduces the deposition of complement component C3b on the pneumococcus thereby preventing elimination of the pneumococcus by the complement system (Tu et al., 1999). A mutant strain that lacks PspA shows greater deposition of complement than the wild-type strain (Mukerji et al., 2012). PspA also inhibits the bactericidal activity of apolactoferrin, which is present on the mucosal surface during inflammation (Haughney et al., 2013).

1.4.9 Pneumococcal surface protein C (PspC)

PspC is found in all pneumococcal strains. It consists of a coiled-coil α helix, a proline-rich region and a choline-binding domain (Yother and Briles, 1992). PspC leads to adhesion and colonization on the nasopharynx of the pneumococcus. Mutations in PspC reduce the ability of the pneumococcus to colonize in the mouse model (Balachandran et al., 2002). The role of PspC in pneumococcal sepsis was investigated in a murine infection model by deleting the *pspC* gene of strain D39. When mutant strains were injected intravenously into mice, their survival rates increased significantly compared to the wild-type strain (Iannelli et al., 2004). PspC provides protection of the pneumococcus from the host immune system by binding of complement components including C4b binding protein (C4BP) and factor H. In this way, it inhibits the CP and the AP pathways of the complement system (Agarwal et al., 2012).

1.4.10 Pneumococcal adhesion and virulence A (PavA) and enolase (Eno)

PavA and Eno are present on the surface of the pneumococcus and bind to the extracellular matrix components fibronectin and plasminogen (Holmes et al., 2001, Bergmann et al., 2001). Fibronectin is a mammalian glycoprotein, which exist as both soluble and less soluble forms. The soluble form is localised in body fluids, including plasma, CSF and amniotic fluid, whereas the less soluble form is localised in the extracellular matrix and basement membrane (van der Flier et al., 1995). PavA present

on the pneumococcal outer cell surface binds fibronectin, either in the fluid phase or immobilized onto a surface. This interaction has also been postulated to assist adhesion of group A streptococci to epithelial cells (Holmes et al., 2001). Another study also reported that PavA is not only important for adhesion but also for invasion because PavA mutant strains were attenuated both in murine pulmonary models and in septicemia models of pneumococcal infection (Pracht et al., 2005). Eno is an anchorless surface protein of the pneumococcus and has previously been identified as a plasminogen binding protein (Kolberg et al., 2006). Pneumococci deficient in Eno are attenuated in a model of respiratory infection, which indicates that plasminogen binding plays a role in respiratory disease (Bergmann et al., 2001).

1.4.11 Sortases

Sortases are a family of enzymes present in Gram-positive bacteria (Ton-That et al., 1999). They are cysteine transpeptidases enzymes that provide the covalent attachment of substrate proteins to the cell walls of Gram-positive bacteria (Kang et al., 2011). They are classified into three types: Srt C-1, Srt C-2, and Srt C-3 previously known as Srt B, Srt C, and Srt D and are encoded by the *rfa* islet genes. Sortases are important for the assembly of a pilus and mediate cell wall localization (LeMieux et al., 2008). The pilus is a long filamentous protein fiber that projects from the cell surface. It plays a key role in pathogenesis through attachment to host cells, immune evasion and biofilm formation (Jacobitz et al., 2016).

1.5 Vaccines against the pneumococcus

Despite antibiotic treatment and vaccines, the burden of disease due to the pneumococcus remains high (Reynolds et al., 2014). Furthermore, the rapid emergence of antibiotic resistance in pneumococci highlights the need for effective vaccines. Two types of pneumococcal vaccine are currently available: pneumococcal polysaccharide vaccine (PPV) and pneumococcal conjugate vaccine (PCV) (Principi and Esposito, 2016). Pneumovax® 23 provides protection against 23 pneumococcal polysaccharides. It is composed of 23 purified polysaccharide antigens of pneumococcal serotypes 1, 2, 3, 4, 5, 6B, 7F, 8, 9N, 9V, 10A, 11A, 12F, 14, 15B, 17F, 18C, 19A, 19F, 20, 22F, 23F, 33F. Pneumovax® 23 was licensed in 1983 in the United States and replaced an earlier 14-valent formulation that was licensed in 1977 (Pilishvili and Bennett, 2015).

In the United States PPV23 is recommended for vaccination of children >2 years old with severe chronic underlying diseases associated with an increased risk of complications due to pneumococcal infection (Nuorti and Whitney, 2010). Nasopharyngeal carriage of the pneumococcus in children is reduced by PPV (Pilishvili and Bennett, 2015). A study performed in Taiwan suggested that the PPV23 is effective against pneumococcal infection in elderly adults over 75 years old. Vaccination in the previous year led a reduction of 60%, 76% and 90% of pneumonia hospitalization, of IPD, and of death from pneumonia respectively (Tsai et al., 2015). PPV23 induces antibodies primarily through T-cell independent mechanisms, and therefore induces a relatively weak immune response. Therefore, in children <2 years whose immune systems are immature, antibody responses to PPV is poor. T-cell independent antigens do not induce immunological memory. Furthermore, anti-PS antibodies have relatively low affinity for their carbohydrate antigens because switching from IgM to IgG does not occur even after repeat vaccinations. Taken together, the lack of memory has some vital consequences for vaccination and the antibodies rapidly decline in serum so revaccination is often required (Kayhty and Eskola, 1996). The second type of pneumococcal vaccine is the PCV which is composed of capsular polysaccharide covalently attached to a nontoxic version of *Corynebacterium diphtheriae* toxin (CRM197) carrier protein (Principi and Esposito, 2017). The first licensed PCV vaccine was PCV7, which was recommended for use in infants and young children with a 4 dose schedule in 2000 in the United States (Pilishvili and Bennett, 2015). Serotypes covered by PCV7, are serotype 4, 6B, 9V, 14, 18C, 19F, and 23F (Principi and Esposito, 2017). A study by Simonsen *et al.* has shown that PCV7 positively impacts on CAP in children and adults (Simonsen et al., 2011). PCV7 was also shown to be effective in Europe and was added to the national immunisation program in September 2006 in the United Kingdom (Elemraid et al., 2013). PCV7 vaccination was abandoned in 2010 worldwide and replaced by new vaccines including PCV10 and PCV13. Therefore, it became clear that there was a necessity for vaccines with further pneumococcal serotypes (Principi and Esposito, 2017). The covered serotypes for all pneumococcal vaccines are shown in (Table 1-1), PCV10 serotypes comprise 1, 4, 5, 6B, 7F, 9V, 14, 18C, 19F and 23F (Principi and Esposito, 2017). While PCV13 covers serotypes 1, 3, 4, 5, 6A, 6B, 7F, 9V, 14, 18C, 19A, 19F, 23F (Principi and Esposito, 2017). In PCV10, eight capsular polysaccharides are conjugated to a non-lipidated cell surface lipoprotein (protein D) of non-typeable *Haemophilus influenzae*, and two capsular polysaccharides are conjugated to tetanus or diphtheria toxoid. However, In PCV13, a

nontoxic mutant of diphtheria toxin is used with all serotypes conjugated to CRM197, (Principi and Esposito, 2017).

PCV10 and PCV13 are licensed to prevent IPD, CAP and OM in children from 6 weeks to 5 years of age. However, PCV13 has also been licensed for use in older subjects (Principi and Esposito, 2017). Conjugate vaccines provide improvement of the immune and memory response, permanent protection and protect newborns and children, reduce the bacterial carriage and provide immunity to a large group of animals (WHO). In addition, to polysaccharide and conjugate vaccines, a recent study suggested that a mutant Ply C428G and W433F denoted as PlyM2 provides effective protection against pneumococcal infection (Sun et al., 2015). The advantages of the latter approach is that Ply is universally expressed in virulent forms of the pneumococcus so it is not strain specific in contrast to the polysaccharide vaccines.

Table 1-1: The pneumococcus vaccine types, which are currently licensed.

| Pneumococcus vaccines | Serotypes covered | License year |
|------------------------------|---|---------------------|
| PPV23 (Pneumovax) | 1,2,3,4,5,6B, 7F, 8,9N, 9V, 10A, 11A, 12F, 14,15B, 1F, 18C, 19F, 19A, 20, 22F, 23F, 33F | 1983 |
| PCV7 (Prenvar®) | 4, 6B, 9V, 14, 18C, 19F, 23F | 2000 |
| PCV10 (Synflorix™) | PCV7 serotypes + 1, 5, 7F | 2009 |
| PCV13 (Prevenar™) | PCV10 serotypes +3, 6A, 19A | 2010 |

1.6 Treatment of the pneumococcus infections

The drug of choice to treat pneumococcal diseases is penicillin, which was introduced in 1943, and used continuously between the 1960s and 1990s (Chiou, 2006), However, in the mid-1970s, resistant strains of the pneumococcus were observed. Penicillin resistance is related to structurally modify penicillin-binding proteins of the pneumococcus (Van der Poll and Opal, 2009). Pneumococcal infections are widely treated with aminopenicillins and these are used as the first line antimicrobial drugs in the treatment of OM and CAP in many countries (File et al., 2004). CAP can be treated with β -lactams

or macrolides or fluoroquinolones alone or in combination (Caballero and Rello, 2011). Combination antibiotic therapy generally has a better outcome compared with monotherapy (Caballero and Rello, 2011). Additionally, resistance of the pneumococcus to penicillin is likely to be associated to the increase in use of β -lactams in the early 1990s and the expansion of resistant clones (Granizo et al., 2000, McGee et al., 2001). Several studies suggested that antibiotic resistance of the pneumococcus has been reduced by reducing antibiotic consumption (Low, 2005, Guillemot et al., 2005). However, other studies do not support this conclusion (Barkai et al., 2005, Belongia et al., 2001). In a recent study, the pneumococcus was recorded as the most frequently isolated pathogen from the middle ear in children with AOM and showed a high rate of resistance to penicillin, erythromycin, and clindamycin (Zielnik-Jurkiewicz and Bielicka, 2015). Widespread macrolide use, however, is associated with increased macrolide resistance pneumococcus (Malhotra-Kumar et al., 2007, Schroeder and Stephens, 2016). Corticosteroids are also used in the treatment of pneumococcal pneumonia (van de Beek et al., 2007). However, evidence is somewhat contradictory. For example, corticosteroids did not reduce the mortality rate in one study of hospitalized CAP patients. In contrast, the mortality rate was reduced by ~3% in another study (Siemieniuk et al., 2015).

1.7 Ply

Ply is a cholesterol-dependent cytolysin (CDC), which exists as water-soluble monomers or dimers, and oligomerizes on target membranes (Sonnen et al., 2014). It is a key virulence factor of the pneumococcus and forms pores in the membrane of mammalian cells (van Pee et al., 2016). All clinical isolates of the pneumococcus express Ply and it plays a key role during pneumococcal infection (Berry et al., 1989, Mitchell et al., 1997).

CDCs are secreted as soluble monomers by pathogenic bacteria. They bind to cholesterol-containing cell membranes, where they oligomerize to form circular pores with a diameter of approximately 30 nm. CDCs are produced by a variety of Gram-positive bacteria including *Streptococcus*, *Bacillus*, *Listeria*, and *Clostridium* (Dowd et al., 2012, Cassidy and O'Riordan, 2013). They have similar tertiary structures with 40-70% sequence identity and conserved pore-forming mechanisms (Tweten, 2005, Bhakdi et al., 1993, van Pee et al., 2016). Ply does not have a signal sequence present in many CDCs. Instead, it is released from the pneumococcus by autolysis mediated by LytA or via a non-autolytic mechanism that remains undefined (Price et al., 2012, AlonsoDeVelasco et al., 1995). Balachandran *et al.* found that Ply to be released in the absence of LytA, indicating an

autolysis-independent release of Ply (Balachandran et al., 2001). Price and Camilli suggested that Ply exists in the cell wall of the pneumococcus in agreement with the previous study of Balachandran that Ply can be released without depending on autolysis (Price and Camilli, 2009).

Ply consists of 471 amino acids residues with a molecular mass of ~53 KDa. It is composed of four domains; three contiguous domains (D1-3) and a fourth separate membrane binding domain (D4) (Figure 1-3) (Walker et al., 1987). Ply has an elongated shape. Circular dichroism revealed that Ply is structurally rich in β -sheet 36% and α -helices 11% (Morgan et al., 1993, van Pee et al., 2016, Lawrence et al., 2015). In three recent studies, the Ply was crystallized successfully and its structure determined by X-ray diffraction (Marshall et al., 2015, Lawrence et al., 2015, van Pee et al., 2016). PlyD2 provides the connection between the head D1 and the tail of the monomer D4. PlyD1 plays an important role in orienting the toxin in the membrane because of the high content of negatively charged residues on one face packing against positively charged residues on the other (Rossjohn et al., 1998). PlyD4 binds to the membrane of the host cell. A sequence of 11 amino acids (⁴²⁷ECTGLAWEWWR⁴³⁷) known as the Trp-rich loop is responsible for binding to cholesterol, its receptor in the membrane (Gilbert et al., 1999). A recent study suggested that Ply has another receptor: sialyl Lewis X (sLeX) present on many cells including the surface of the RBCs (Shewell et al., 2014). Nevertheless, Ply binds liposomes that lack sLeX, so unlike cholesterol this receptor is not essential.

PlyD1 has six β -strands and two α -helices. PlyD2 has three long β -strands that connect D1 to D4, while PlyD3 comprises a five-stranded antiparallel β -sheet surrounded by two three-helix bundles (transmembrane hairpins TMH1 and TMH2 or HB1 or HB2 helical bundles). PlyD4 is composed of a compact β -sandwich with two β -sheets, each with four β -strands. In contrast, to PlyD1-3, which is intertwined, PlyD4 is linked an independently folding unit linked via a glycine (Gly361) to PlyD2 (Van Pee et al., 2016).

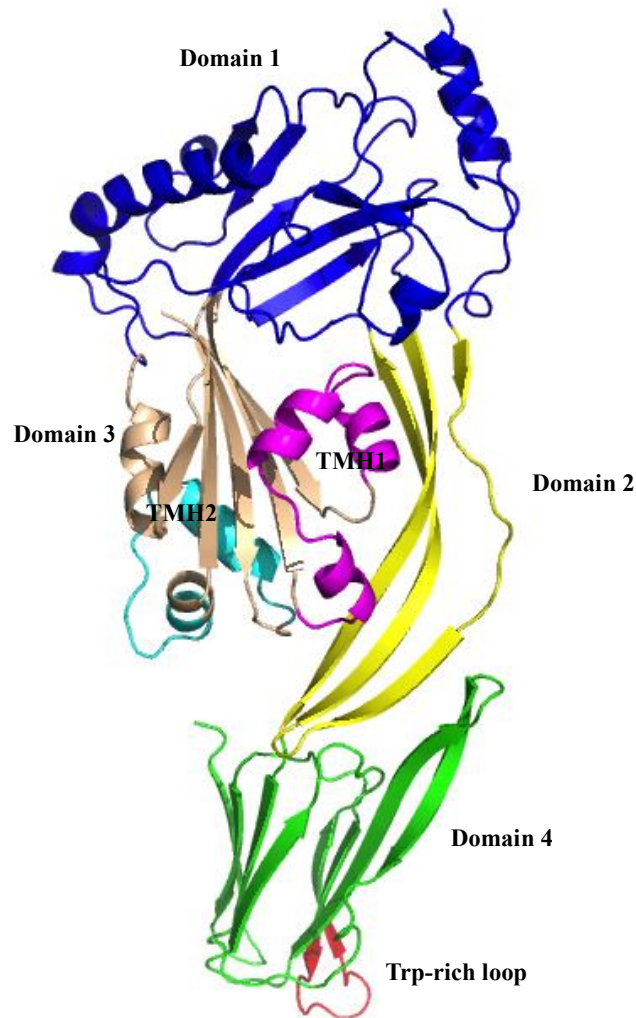


Figure 1-3: Ply crystal structure.

A different colour depicts the four domains, (D1) is blue, (D2) is yellow, (D3) is light brown and (D4) is in green. The Trp-rich loop is coloured in red. Transmembrane hairpins 1, 2 (TMH1 and TMH2) are depicted in purple and cyan respectively.

1.8 Overview mechanism of pore formation

The mechanism of pore formation of the CDCs have been investigated in many studies, via different techniques including, electron microscopy (EM) through negative staining, cryo-EM, atomic force microscopy (AFM), fluorescence imaging, kinetic assays and other biophysical and functional methods (Tveten, 2005, Hotze and Tveten, 2012, Czajkowsky et al., 2004, Lawrence et al., 2015, Palmer et al., 1998, van Pee et al., 2016). Two hypothesis of CDCs pore formation are discussed in the literature. The first based on streptolysin O produced by the *Streptococcus pyogenes*, suggested that monomers oligomerize into arc-shape pores on the cell membrane (Palmer et al., 1998). According

to this study streptolysin O binds and oligomerizes on the membrane surface, and the oligomeric structure is able to insert and open a pore into the lipid bilayer before the ring is completely formed. The second hypothesis, based on work on perfringolysin O suggested that monomers bind to the membrane, oligomerize to form a pre-pore structure, which then inserts into the membrane to form the transmembrane pore (Shepard et al., 2000, Heuck et al., 2003). Figure 1-4 below illustrates the two hypothesis mechanisms of pore formation taken from (Gilbert, 2002). There are two recent contradictory studies about the CDCs assembly on the membrane and pore formation. Leung *et al.* suggested that the assembly of suilysin on the membrane is terminated in the pre-pore state and is not impacted by the pre-pore to pore transition (Leung et al., 2014). However, Gilbert *et al.* suggested that at low toxin concentration the rate of lysis is controlled by the transition of pre-pore to pore to form an incomplete ring. In addition, at high toxin concentration the affinity of the protein for the membrane receptor controlled the rate of lysis (Gilbert and Sonnen, 2016).

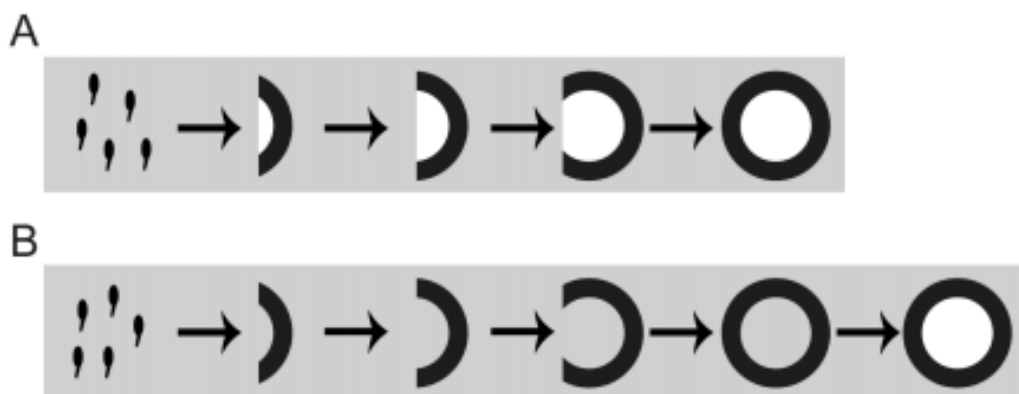


Figure 1-4: Two hypothesis models of pore formation by CDCs.

(A) Shows that the insertion of the toxin followed by oligomerization leading to gradual pore formation. (B) Shows that the toxin monomer binding, oligomerization to form a pre-pore followed by membrane insertion to create the pore.

According to Tweten (Tweten, 2005), during pore formation monomers bind to cholesterol in the membrane via the Trp-rich loop at the base of the D4 (Rossjohn et al., 1998). This orientates the CDCs on the membrane enabling them to diffuse laterally. Secondly, D3 of the toxin rearranges following insertion of the Trp-loop of D4 insertions causing the CDCs monomers to oligomerize to form the pre-pore structure. Thirdly, the N-terminal of the D3 forms the internal part of the transmembrane pore and further

conformational changes occur in D3 in which the two alpha-helical bundles (α HB1 and α HB2) are changed into two extended amphipathic trans membrane beta-hairpins (TMH1, and TMH2), the oligomer is now in the pre-insertion state. Each monomer within the large oligomeric pore complex contributes two TMHs to the formation of the β -barrel pore these TMHs are derived from the two D3 α HBs (Tweten et al., 2015). Finally, the pre-pore vertically collapses and completely inserts into the membrane, and the large beta-barrel-pore is formed which is composed of 35-50 monomers. The resulting pore is approximately 30 nm in size and results in the cell becoming permeable to ions and macromolecules (Sonnen et al., 2014). Oligomer formation was mainly attributed to intermolecular interactions via D1 and D3 (Ramachandran et al., 2002). However, it has been shown that streptolysin, pyolysin and listeriolysin O D4 can oligomerize by themselves on cholesterol crystals (Harris et al., 2011, Weis and Palmer, 2001). A cryo-EM study of Ply confirms that PlyD4 plays a role in oligomer formation through intramolecular and intermolecular interactions of its loops (van Pee et al., 2017). All steps of pore formation in CDCs is shown in (Figure 1-5). A classic study performed by Tilley *et al.* 2005 shows the steps of pore formation by Ply using cryo-EM by taking snapshots of the pore and pre-pore forms of Ply when it interacts with liposomes (Tilley et al., 2005). The crystal structure of Ply supports the theory of the pre-pore complex in which monomers pack side-by-side (Marshall et al., 2015, van Pee et al., 2016).

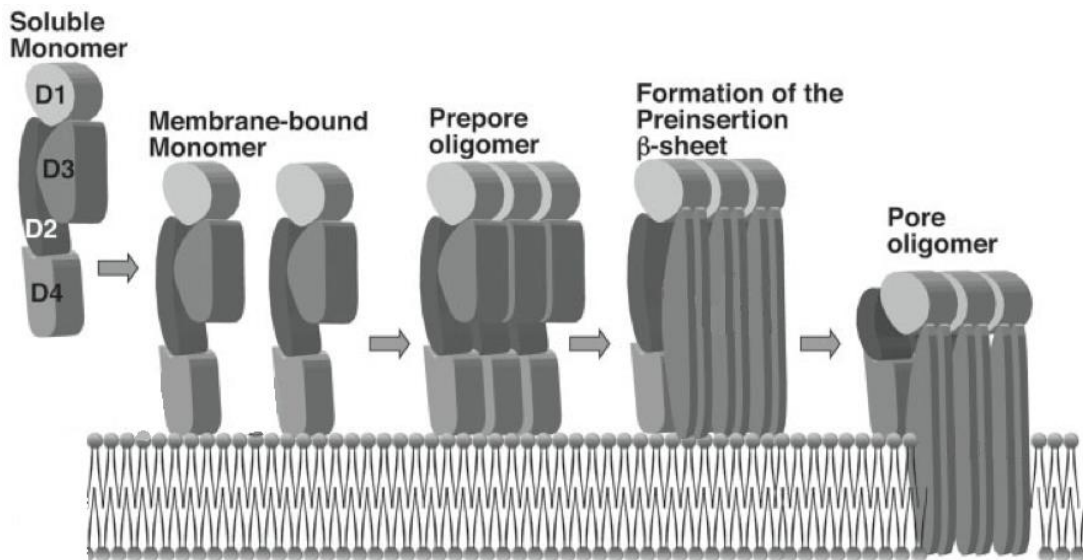


Figure 1-5: Mechanism of pore formation of CDCs family on the lipid bilayer.

As clear from left to right the soluble monomer is anchored to the cholesterol membrane through the Trp-rich loop at the base of D4 which causes a change in D3. The monomers later oligomerized and collapsed downwards through the membrane to form the open pore (Tveten, 2005).

1.9 Role of Ply in pathogenesis

Paton *et al.* demonstrated the key role of Ply towards virulence of the pneumococcus *in vivo* in 1983 (Paton *et al.*, 1983). They showed that mice immunized with a partially inactivated form of Ply, caused moderate protection against a virulent strain of the pneumococcus. In addition, in 1987 the Ply gene was sequenced from a serotype 2 strain of the pneumococcus, D39 (Walker *et al.*, 1987). An isogenic Ply-negative mutant of the pneumococcus was then produced which was called (Ply-N) (Berry *et al.*, 1989). Intranasal challenge of mice with Ply-N showed reduced virulence compare to the wild-type (Berry *et al.*, 1989). Another study confirmed the results from Berry *et al.* 1989, intranasal challenge of mice with Ply-N showed reduced severity of the inflammatory response, a decrease in bacterial growth rate in the lungs and a delayed movement of the bacteria into the blood stream, compared to the wild-type bacteria (Canvin *et al.*, 1995).

Ply has a cytotoxic impact on eukaryotic cells. For example, at sub-cytolytic concentrations, the proinflammatory activity of neutrophils and monocytes is increased as a result of an influx of the extracellular calcium during pore formation (Cockeran *et al.*, 2002). Ply induces an increase in circulating cardiac troponins in the blood stream.

Troponins are indicators of cardiac injury and cause inflammatory cell infiltration into the myocardium (Alhamdi et al., 2015). Moreover, due to activation of proinflammatory immune cells by Ply, reactive oxygen and nitrogen are released and damage host tissues (Cockeran et al., 2001, Houldsworth et al., 1994). Ply is toxic to most eukaryotic cells including epithelial and endothelial cells present in the respiratory tract and brain. Apoptosis of neutrophils, brain cells, macrophages and dendritic cells are induced by pore formation by Ply (Braun et al., 2007, Srivastava et al., 2005, Littmann et al., 2009). The impact of Ply on cells and tissues is well studied but the impact of Ply on the molecular process is less understood. A recent study revealed that Ply is genotoxic, therefore, Ply can damage DNA in the alveolar epithelial cells in the absence of live bacterial cells (Rai et al., 2016).

Ply induces the cytokine production by the white blood cells, which are proteins that regulate the host's immune response to infection (Hirst et al., 2004). Wild-type Ply plays a role in inducing the production of interleukins include IL-1 and IL-18, while these cytokines were not induced by Ply-deficient pneumococcus strains (Shoma et al., 2008). Furthermore, *in vitro* work using human pharyngeal and bronchial epithelial cells showed that Ply encourages the release of pro-inflammatory cytokines IL-6 and 8 (Kung et al., 2014).

Another role of Ply is the activation of the complement system. As a result of complement activation and complement C3 deposition on Ply, activation on the pneumococcus itself is reduced thereby reducing opsonophagocytosis. The mechanism of activation is less well understood. It was reported that Ply activates the CP of the complement system via direct interaction with C1q, due to similarity with C-reactive protein (CRP) (Mitchell et al., 1991). However, another study suggested that C1q does not bind to Ply directly and its binding requires the presence of immunoglobulin. The same study suggested that Ply can also activate the LP via L-ficolin (Ali et al., 2013).

1.10 The mammalian immune system

The immune system is the network of tissues, cells and molecules within an organism that work together to defend the body against diseases mediated by infectious agents including bacteria, viruses, parasites, fungi and other diseases including cancer. It provides protection through innate and adaptive immunity. Innate immunity mediates an initial, immediate and nonspecific immune response against invading microorganisms.

Innate immune components include the phagocyte, complement system, epithelial cells, mucosal membranes and the skin (Mogensen, 2009). Adaptive immunity consists of the specialised lymphocytes and their products involved in the mediation of the antigen-specific immunity. The key cells of adaptive immunity are T and B-lymphocytes (Greter et al., 2012). Adaptive immunity is divided into two branches: cell-mediated immunity, which eliminates intracellular microbes, and is carried out by the T-lymphocytes; and humoral immunity, which protects the body against extracellular microbes by the action of antibodies that are produced by the B-lymphocytes (Jiravanichpaisal et al., 2006). B-cells remain in the bone marrow during maturation, whereas T-cells egress into the thymus.

1.10.1 Complement system

Bordet discovered the complement system in 1896 as a heat-labile component of serum (Jason, 2010). Complement is part of innate and adaptive immunity that provides the first line of defence against invasion by foreign or altered host cells (Ricklin et al., 2010, Kerepesi et al., 2006). The complement system is composed of over 30 soluble plasma proteins and membrane-associated proteins produced mainly by the liver (Kolev et al., 2014). Microorganism can be lysed via assembly of the membrane attack complex (MAC), opsonised by complement proteins or eliminated as a result of immune and inflammatory responses that aid immune cells to fight infection and maintain homeostasis. Three distinct pathways can activate the complement system: the Classical (CP), Lectin (LP), and Alternative (AP) pathways. Each pathway terminates with the MAC (Jason, 2010). Figure 1-6 below illustrates the three complement pathways, all of which generate a C3 convertase that is the central component of the system and cleaves the inactive C3 into C3a, which is an anaphylatoxin, and C3b an opsonin.

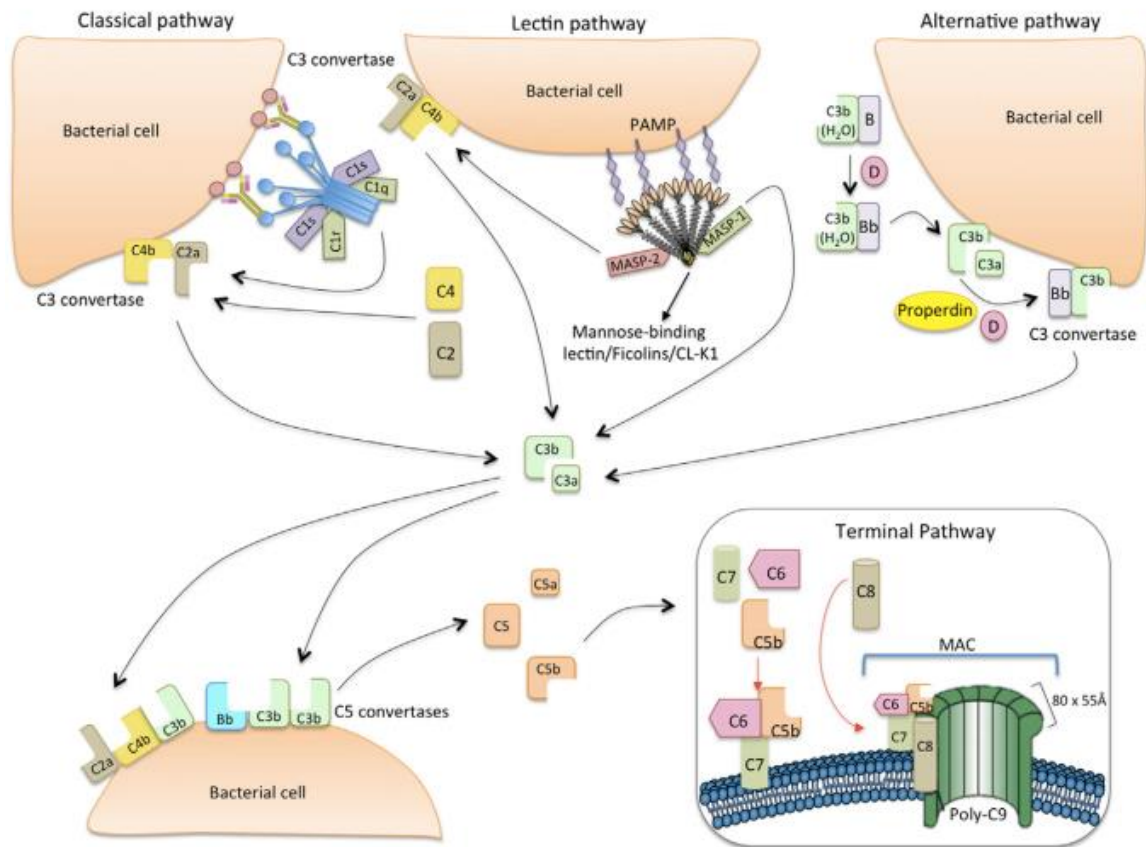


Figure 1-6: Three pathways of the complement system: Classical, Lectin and Alternative pathways (CP, LP and AP).

The CP is activated by C1 consisting of C1q and C1r₂ C1s₂. During activation the recognition molecule C1q binds to IgG and IgM on the surface of pathogens, triggering activation of C1r and C1s. C4 and C4b bound C2 are cleaved by C1s and together form the C3 convertase formation (C4b2a). The LP is activated through the binding of mannose-binding lectin (MBL), serum ficolins, collectin-10 (CL1-10 or CL-L1) and collectin-11 (CL-11 or CL-K1) in complex with MBL-associated serine proteases 1 and 2 (MASP-1 and MASP-2), to acetylated groups and carbohydrates on the surface of pathogens. MASP-2 cleaves C4 and C2 to form the C3 convertase (C4b2a). Spontaneous low-level hydrolysis of C3 in plasma leads to formation of C3b and subsequent activation of the AP. The C3b binds factor B (homologous to C2) to form a C3bB complex. Subsequent cleavage of factor B by factor D forms the alternative pathway C3 convertase (C3bBb). C5 convertases (C3bBbC3b) for the AP and C4bC2aC3b for the CP and LP cleave C5 and initiate the terminal pathway resulting in assembly of the membrane-attack complex (Beltrame et al., 2015).

1.10.1.1 Classical pathway (CP)

The CP is also known as the antigen-antibody dependent pathway because C1q binds to the Fc region of IgG and IgM. However, the CP also activates when the C1q binds to the surface of a wide variety of microbes and apoptotic cells, even in the absence of antibodies (Gaboriaud et al., 2004). C1q is composed of six N-terminal collagen-like arms with C-terminal immunoglobulin-binding globular head domains (Figure 1-7) (Melis et al., 2015). C1q binds to pathogens or altered-self surfaces, and immune molecules and lead to the autocatalysis of associated serine protease C1r followed by cleavage of proenzyme C1s to form activated C1s (Wallis et al., 2010, Forneris et al., 2012). C4 is a substrate of C1s and it is cleaved to generate C4a and C4b, C4a is an anaphylatoxin, whereas, C4b binds covalently to the surface of the pathogens. C2 then binds to the C4b fragment and is cleaved by C1s to form C2a and C2b. C2a binds to C4b to make the C3 convertase complex, C4b2a (Wallis et al., 2010). The C3 convertase cleaves C3 to generate C3b and C3a, the latter is another anaphylatoxin. C3b deposits on the cell surface, where it serves as an opsonin and also forms the C5 convertase, C4b2aC3b. C5 is cleaved by the C5 convertase into C5b and C5a, C5b binds to C6, C7, C8 and multiple copies of C9 to form the MAC (Celik et al., 2001).

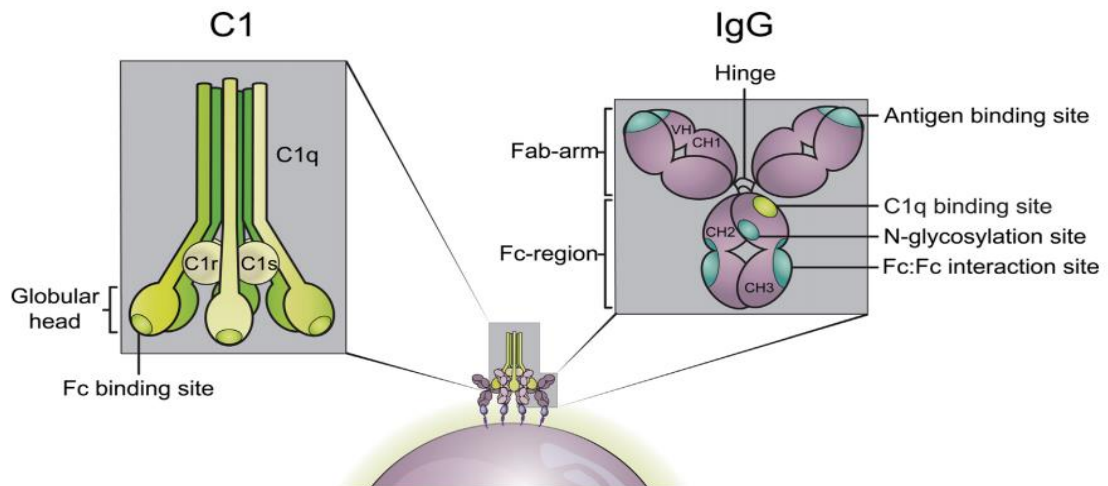


Figure 1-7: Schematic representation of human C1q and human IgG showing how C1q binds to IgG on the pathogen surface.

The highlighted light green region in IgG represents the C1q binding residues D270, K322, P329 and P331 in the CH2 domain of IgG. C1 is composed of the multimeric pattern recognition molecule C1q and a heterotetramer of proteases C1r and C1s. C1q has six globular heads each with an Fc binding region (Melis et al., 2015).

1.10.1.2 Lectin pathway (LP)

Matsushita and Fujita discovered the LP in 1992 (Beltrame et al., 2015). It plays a key role in the innate immune response (Rosbjerg et al., 2014). MBL, CL-L1 and CL-K1, together with H-ficolin, M-ficolin and L-ficolin are the pattern-recognition molecules of the LP (Kjaer et al., 2013, Matsushita et al., 2013). Similar to C1q, the N-terminal region of all LP recognition molecules contains a collagen-like domain, however, the C-terminal recognition domains are different from C1q. Collectins including MBL contain C-type carbohydrate recognition domain (CRD), which recognises patterns of carbohydrates including glucose, mannose, and N-acetyl-glucosamine via Ca^{+2} -dependent interactions (Thielens et al., 2001). Ficolins possess a C-terminal fibrinogen-like domain, which binds to N-acetyl groups, on sugars such as N-acetyl-glucosamine, on the pathogens surface. Ficolins and collectins bind MASPs to activate the LP. During complement activation by the LP, MASP-1 cleaves MASP-2 and MASP-2 subsequently cleaves C4 and C2 (Frederiksen et al., 2005, Krarup et al., 2004). When MBL/MASP-2 or ficolin/MASP-2 complexes bind to the surface of a pathogen, MASP-2 activates through autolysis or via MASP-1 (Heja et al., 2012). The C4 is cleaved by the activated MASP-2 into C4a and C4b and the C4b binds to the pathogen surface. MASP-2 also cleaves C2, and the C2a

fragment binds to C4b producing the C3 convertase (C4bC2a). The cascade continues as previously described for the CP through C5 convertase to the terminal pathway (Heja et al., 2012). Structurally MASPs comprise two N-terminal CUB domains, separated by an EGF-like domain, two CCP modules and a serine protease domain at the C-terminus (Figure 1-8) (Gingras et al., 2011).

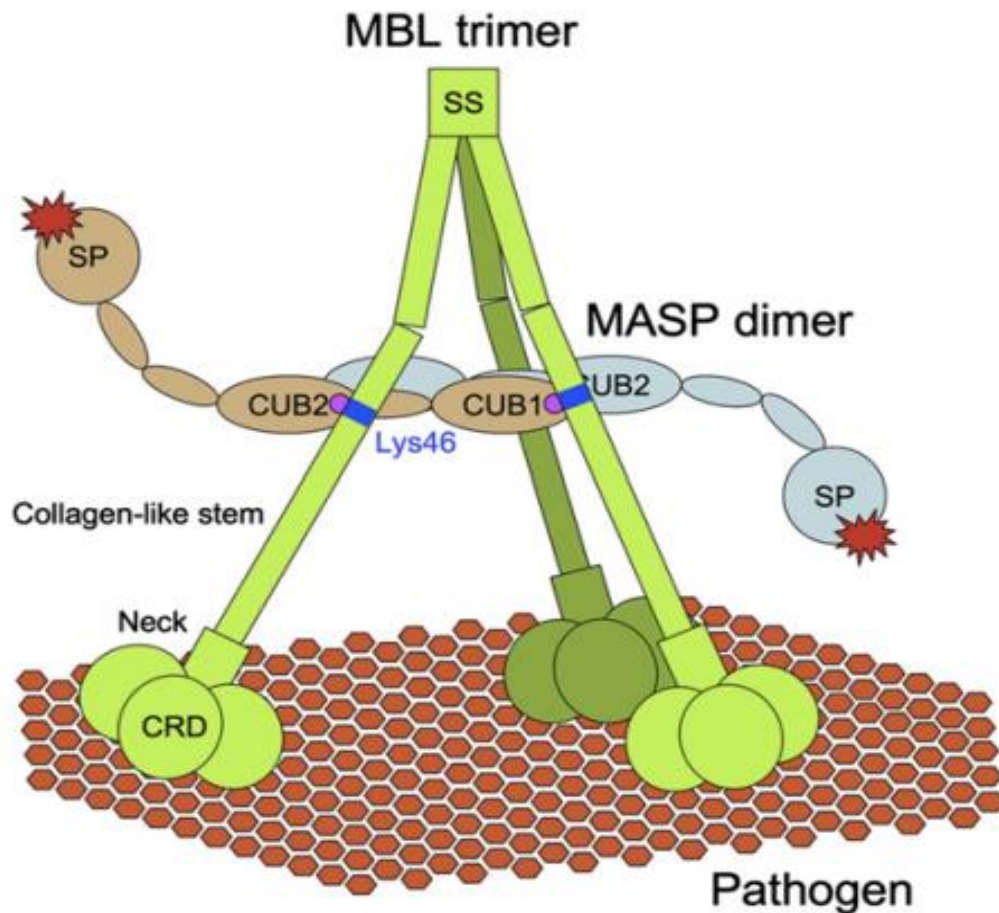


Figure 1-8: Schematic representation of MBL-MASPs binding to a pathogen surface.

MBL is shown associated with the MASPs protease. It is shown in the activated state resulting from pathogen binding. The MASPs needs Ca^{+2} ion to be activated as shown in magenta circles. The carbohydrate recognition domain (CRDs) bind to sugars on the pathogens surface (Hohenester, 2011).

1.10.1.3 Alternative pathway (AP)

In contrast to the CP and the LP, the AP is constitutively active and interacts with cell surfaces without depending on pathogen-recognition molecules (Sahu et al., 1994). AP activation begins in the fluid phase where C3 (H₂O) is formed by hydrolysis of C3. C3 (H₂O) binds to factor B (CFB), which is cleaved, by the factor D (CFD) to form the fluid phase C3 convertase (C3 (H₂O) Bb) (Borza, 2016). This enzyme cuts C3 into C3a and C3b, the later interacts with amine and carbohydrate groups on cell surfaces and engages CFB (Borza, 2016). This complex then binds with another C3b to form the C5 convertase component (Pangburn and Müller-Eberhard, 1986). All these steps are shown in (Figure 1-6).

1.10.1.4 Terminal pathway (TP)

Activation of the TP is induced by the formation of C5 convertase (C4b2aC3b and C3bBbC3b) that cleaves C5 to C5a and C5b. C5b initiates the formation of MAC by binding to C6 and C7 to make the hydrophobic complex C5b67, which inserts into the lipid bilayers. After that C5b67 interacts with C8 and allows binding and polymerisation of C9 to make the MAC pore-forming complex (Figure 1-6). This has a hydrophilic inner surface and an outer hydrophobic surface that allows water and solutes to freely pass across the cell membrane resulting in loss of membrane permeability and eventually lysis of the cells (Lambris et al., 2008).

1.11 Ficolins

Ichijo *et al.* first discovered ficolins as the transforming growth factor β -binding protein from porcine uterus in 1991 (Ichijo et al., 1991). Activation of the LP by ficolins results in cell lysis, opsonisation, phagocytosis, and cytokine production (Endo et al., 2015). Ficolins are structurally similar to Mannose-binding lectin (MBL) and collectins (Zhang and Ali, 2008) but contain fibrinogen-like domains in place of CRDs of collectins (Matsushita and Fujita, 2001). Three different ficolins have been identified in the human plasma: ficolin-1 (FCN-1), ficolin-2 (FCN-2) and ficolin-3 (FCN-3) also known as M-ficolin, L-ficolin and H-ficolin respectively (Bidula et al., 2013). M-ficolin and L-ficolin share 80% sequence identity, whereas H-ficolin has ~50% amino acid identity with both (Kilpatrick and Chalmers, 2012). Only two types of ficolins have been discovered in the mouse and other rodents, ficolin-A (Fcn A) and ficolin-B (Fcn B). These are homologues of L-ficolin and M-ficolin in humans, respectively (Endo et al., 2012). Two ficolins have

also been identified in pigs, called ficolin- α and ficolin- β (Ichijo et al., 1993). Ficolins interact with the MASP-1 and MASP-2 in the presence of Ca^{2+} (Cseh et al., 2002). M-ficolin, L-ficolin and H-ficolin serum concentrations are $\sim 1.4 \mu\text{g/ml}$, $3.4 \mu\text{g/ml}$ and $25 \mu\text{g/ml}$ respectively (Verma et al., 2012).

1.11.1 Human M-ficolin

M-ficolin is also known as FCN-1 or L-ficolin/p35-related protein. This ficolin was identified in 1996 as a by-product during human FCN-2 characterization (Endo et al., 1996, Lu et al., 1996). The M-ficolin gene is *FCN-1*, which is located on chromosome 9 (9q34) (Endo et al., 1996). It is expressed in leukocytes and lung, therefore, has been described as a non-serum ficolin (Liu et al., 2005) but it is not expressed by macrophages or monocytic dendritic cells (Lu et al., 1996, Hashimoto et al., 1999). Human M-ficolin activates the LP through the formation of complexes with MASP-1 and MASP-2 (Liu et al., 2005). It is also found associated with Map-19, which is also known as sMAP. It is formed by alternative splicing of the primary transcript of the MASP-2 gene (Endo et al., 2005). M-ficolin can bind to several carbohydrate ligands on microbes, surface including GlcNAc, N-acetylgalactosamine, and sialyl-N-acetyllactosamine (Liu et al., 2005).

1.11.2 Human H-ficolin

H-ficolin is a serum ficolin discovered in 1978 (Matsushita et al., 2002). Also known as FCN-3, Hakata-antigen or $\beta 2$ -thermolabile macro glycoprotein, it was found in the sera of patients with systemic lupus erythematosus. H-ficolin activates the LP in association with MASP-1, MASP-2, and MASP-3 (Matsushita, 2013). The H-ficolin gene was cloned and characterized in 1998 (Sugimoto et al., 1998). The mRNA of H-ficolin is expressed in liver and lungs (Sugimoto et al., 1998). H-ficolin exists as a mixture of different sizes of oligomers (Yae et al., 1991). Like other ficolins, H-ficolin recognizes the N-acetyl groups and has been shown to bind to *Aerococcus viridians* and *Hafnia alvei* polysaccharide and lipopolysaccharides (Zacho et al., 2012). It has been suggested that IgM interacts with H-ficolin in tumor cell immunosurveillance and this mediates complement activation to defend against tumors (Lei et al., 2015).

1.11.3 Human L-ficolin

Independent studies first described L-ficolin as an elastin-binding protein (EPB-37) and as a corticosteroid-binding protein (hucolin) (Edgar, 1995, Harumiya et al., 1995). Matsushita *et al.* first purified L-ficolin from serum in 1996 (Matsushita et al., 1996). L-

ficolin is also known as ficolin-2, P35, EBP-37 or hucolin. L-ficolin is encoded by the *FCN-2* gene on chromosome 9 (9q34), which contains eight exons and is composed of 314 amino acid residues (Edgar, 1995, Endo et al., 2011, Zhao et al., 2013, Endo et al., 1996, Matsushita et al., 1996). Liver hepatocytes synthesise L-ficolin and it is present in the blood stream at a concentration 1.4 µg/ml (Verma et al., 2012).

The L-ficolin polypeptide has a molecular mass of 35 kDa (Matsushita et al., 1996) and it assembles into tetramers of trimers, with a total of 12-subunits (Hummelshoj et al., 2007). The N-terminal region contains two cysteine residues (Cys7 and Cys27) followed by a collagen-like domain, which is composed of 69 amino acid residues: 15 Gly-X-Y (X and Y representing any amino acid) repeats. The C-terminal fibrinogen-like domain contains 209 amino acids (Hummelshoj et al., 2007).

L-ficolin binds to acetylated compounds, such as GlcNAc, β-1-3-D-glucan and DNA (Kuraya et al., 2005). It also binds to non-saccharide N-acetylated compounds such as, N-acetyl-glycine and N-acetyl-cysteine. Moreover, L-ficolin binds to the lipoteichoic acid cell wall components of Gram-positive bacteria (Lynch et al., 2004). Recent studies reported that L-ficolin binds to the teichoic acid of the *Streptococcus pneumoniae* (Vassal-Stermann et al., 2014). Besides its lectin properties, L-ficolin has been reported to bind to elastin, corticosteroids and DNA (Harumiya et al., 1995, Edgar, 1995). Furthermore, recent studies showed that L-ficolin binds to DNA and heparin via the sulphate and phosphate groups at the S3 ion binding site of the L-ficolin (Laffly et al., 2014).

L-ficolin binds to a variety of bacteria including *Streptococcus pneumoniae* serotype 11F, 11A and 11D (Krarup et al., 2005), *Staphylococcus aureus* serotype 1, 8, 9, 11, and 12 and *Salmonella typhimurium* (Aoyagi et al., 2005). L-ficolin also binds to the unencapsulated pneumococcal strain R6 (Vassal-Stermann et al., 2014) and the encapsulated strain serotype 2 D39 (Ali et al., 2012). In addition, studies have documented that L-ficolin recognises *Mycobacterium tuberculosis* and *Mycobacterium bovis* (Luo et al., 2013). L-ficolin also binds the 1, 3-β-D-glucan structures exist on yeast and fungal cell wall (Ma et al., 2004). A recent study has highlighted the key role of L-ficolin in innate defence against *Aspergillus*, causing opsonophagocytosis by macrophages and neutrophils. It also leads to killing of fungi, by inducing the production of cytokine during infection (Bidula et al., 2015). L-ficolin can also recognise HCV

envelope glycoproteins E1 and E2 to activate complement and mediate cytolytic activity in HCV-infected hepatocytes (Liu et al., 2009).

1.12 Mouse ficolins

Two types of ficolin are produced in mice and other rodents: ficolin-A and ficolin-B.

1.12.1 Ficolin-A

Ficolin-A is highly expressed in the liver and spleen. It is a polypeptide of molecular mass 37 kDa. Like other mammalian ficolins, it binds to acetylated compound such as GlcNAc (Fujimori et al., 1998) and activates complement system via binding to MASP-2. By contrast, mouse ficolin-B does not bind MASPs or activate complement (Endo et al., 2005). As a result of alternative splicing of the ficolin-A gene, two types of ficolin-A exist in the serum called ficolin-A and ficolin-A variant. The latter is composed of a shorter collagen-like domain and has an eight amino acids (Endo et al., 2005). Infection studies, revealed that both ficolins played a crucial role against pneumococcal infection (Endo et al., 2012), with mice deficient in ficolin-A and ficolin-B having reduced survival when infected transnasally with *Streptococcus pneumoniae* D39. Ficolin-A is often referred as the mouse orthologue of human L-ficolin. It binds to GlcNAc, GalNAc and elastin (Fujimori et al., 1998, Giriya et al., 2011). It also binds various microorganisms including Gram-positive and Gram-negative bacteria and fungal cells. Gram-positive bacteria include *Enterococcus faecalis*, *Listeria monocytogenes* and some *Staphylococcus aureus* strains, but not *Streptococcus agalactiae*. Gram-negative targets include *E. coli* and *Pseudomonas aeruginosa* strains, but not *Salmonella* strains. Ficolin-A also binds to clinical isolates of *Aspergillus fumigatus* (Hummelshoj et al., 2012).

1.12.2 Ficolin-B

Ficolin-B was first characterised in 1998. Ficolin-B mRNA is highly expressed in bone marrow and weakly expressed in spleen (Ohashi and Erickson, 1998). It is a homologue of human M-ficolin and like M-ficolin is found within the lysosomes of activated macrophages (Endo et al., 2005, Runza et al., 2006, Endo et al., 2004). Ficolin-B binds to acetylated sugars, including GlcNAc and GalNAc and it binds specifically to sialic acid residues (Endo et al., 2005, Giriya et al., 2011). Mouse ficolin-B cannot associate with MASPs or activate the LP (Endo et al., 2005). However, rat ficolin-B is able to bind to MASP-2 to activate the LP of rat (Giriya et al., 2011). Another study has reported that N-linked glycosylation is required for oligomerization of ficolin-B and its association

with MASPs/sMAP to deposit C4b on immobilized N-acetylglucosamine (Endo et al., 2012).

1.13 Genetics of ficolins

M-ficolin and L-ficolin genes are both located on the chromosome 9q34. M-ficolin is mainly expressed by monocytes and neutrophils, whereas, L-ficolin is expressed by the liver hepatocyte cells and secreted to the blood stream (Teh et al., 2000, Garred et al., 2010). H-ficolin is encoded by the *FCN-3* gene is located on chromosome 1p36.11 and expressed by the liver and lungs (Kilpatrick and Chalmers, 2012, Ruskamp et al., 2009). An overview of the three human ficolins is shown in (Table 1-2). M-ficolin contains 326 amino acid residues whereas; L-ficolin and H-ficolin comprise 313 and 299 amino acids respectively, including the signal peptide (Boldt et al., 2013, Mason and Tarr, 2015).

Table 1-2: A schematic outline of three human ficolins (M-ficolin, L-ficolin and H-ficolin).

Information was taken from the (Mason and Tarr, 2015).

| | FCN-1 | FCN-2 | FCN-3 |
|--------------------------------------|-------------------------|--------------------------|------------------------|
| Proteins name | Ficolin -1 or M ficolin | Ficolin-2 or L-ficolin | Ficolin-3 or H-ficolin |
| Chromosome | 9p34 | 9p34 | 1p36.11 |
| Exon | 9 | 8 | 8 |
| Tissue expression | Monocyte and Neutrophil | Liver | Liver and Lung |
| Serum concentration $\mu\text{g/ml}$ | 1.07 $\mu\text{g/ml}$ | 3.7–5.4 $\mu\text{g/ml}$ | ~26 $\mu\text{g/ml}$ |
| Amino acid residues | 326 | 313 | 299 |

The M- and L-ficolin genes consist of eight exons, whereas H-ficolin comprises nine exons. The signal sequence and the first nine N-terminal residues are encoded by the first exon, the collagen-like domain is encoded by the second and third exon, the fourth exon encodes a short linker and exon five to eight (or nine) encode the fibrinogen-like domain (Kilpatrick and Chalmers, 2012, Mason and Tarr, 2015). Figure 1-9 shows a schematic

representation of the human ficolin genes: *FCN-1*, *FCN-2* and *FCN-3* (Mason and Tarr, 2015).

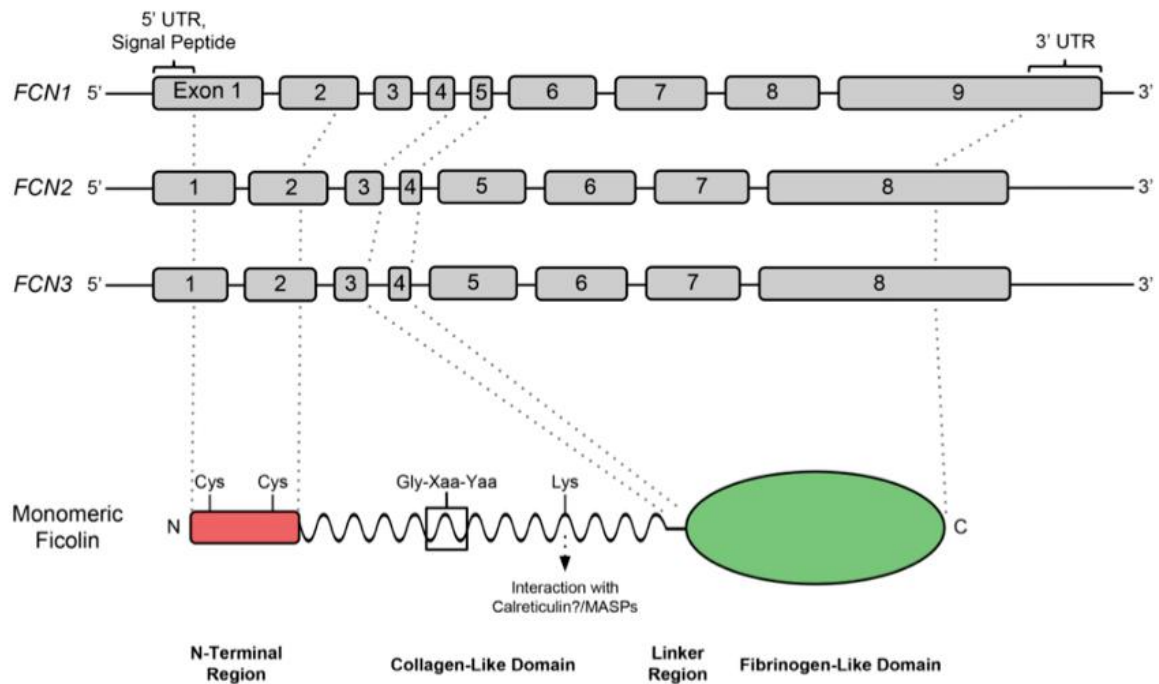


Figure 1-9: Schematic representation of human ficolin genes *FCN-1*, *FCN-2* and *FCN-3*.

The *FCN-2* and *FCN-3* genes composed of eight exons, whereas, *FCN-1* consists of nine exons (Mason and Tarr, 2015). Monomeric ficolin composed of N-terminal cysteine region, collagen like domain, linker region and fibrinogen like domain.

The variants in the promoter region of *FCN* gene leads to polymorphisms in the *FCN* genes that may impact the serum concentrations and/or activity of the encoded ficolins. Three gene polymorphisms at positions -986 A/G, -602 G/A, and -4 A/G in the promoter region of *FCN-2* affect the concentration of L-ficolin in the serum, whereas two polymorphisms at positions 6359C/T and 6424G/T in exon 8 of *FCN-2* gene impacts the GlcNAc binding capacity towards N-acetylglucosamine (Hummelshoj et al., 2005, Cedzynski et al., 2007). Some polymorphisms are associated with disease. For example, *FCN-2* -557 A/G, -64 A/C and +6424 G/T SNPs are associated with the pulmonary tuberculosis (Luz et al., 2013, Xu et al., 2015).

1.13.1 Structure of ficolins

Ficolins are multimeric proteins, consisting of polypeptides of 34-40 kDa. Human L-ficolin is composed of tetramers of a trimeric subunit, with 12-polypeptide chains, each of 35 kDa (Figure 1-10). H-ficolin contains more than 18 polypeptide chains (Yae et al., 1991). Each ficolin polypeptide is composed of a short N-terminal region containing cysteine residues; a central collagen-like domain with Gly-X-Y repeats, a short linker region and a C-terminal fibrinogen-like domain (Figure 1-10 A) (Matsushita et al., 1996, Tanio et al., 2007).

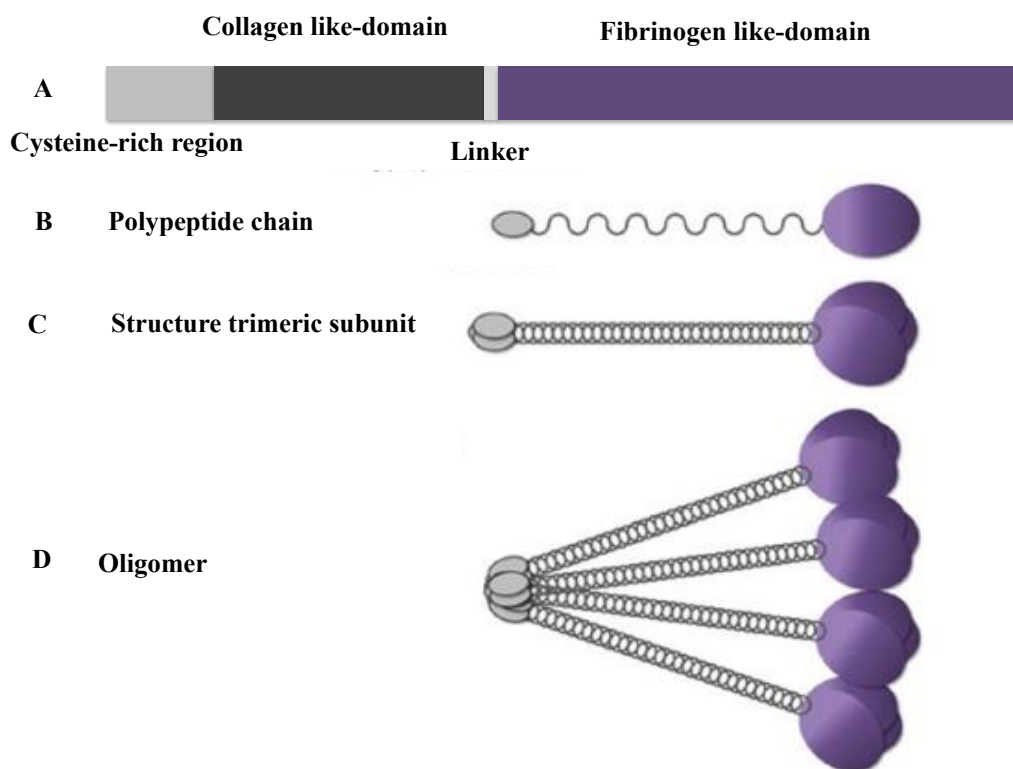


Figure 1-10: Schematic diagram of ficolin structure and domain organisation.

(A) Shows a ficolin monomer, which comprises an N-terminal cysteine region, a collagen-like domain and fibrinogen-like domain. (B) A ficolin polypeptide chain. (C) A ficolin trimeric subunit that contains three fibrinogen-like domains within a C-terminal head. (D) Four trimeric subunits in a tetramer. Disulphide bonds via the N-terminal cysteine-rich domains hold subunits together (Garred et al., 2016).

1.14 Ficolins and disease

High levels of L-ficolin are found in patients with chronic hepatitis C virus (Hu et al., 2013). It has been suggested that L-ficolin neutralises hepatitis C virus by binding to envelope glycoproteins E1 and E2 (Hamed et al., 2014, Zhao et al., 2014). Hoang *et al.*

reported that patients with hepatitis B virus had higher levels of L-ficolin in their serum compared with those with hepatocellular carcinoma (Hoang et al., 2011). Serum L-ficolin levels may be a useful indicator for chronic hepatitis B infection, hepatocellular carcinoma and cirrhosis (Chen et al., 2015). A recent study has suggested that L-ficolin prevents the entry of HIV-1 into cells by binding to the envelope glycoprotein gp120 and serum levels of L-ficolin are higher in HIV patients than the normal population (Luo et al., 2016). It has been documented that both L-ficolin and H-ficolin prevent Influenza A virus infection *in vitro* and *in vivo* by binding to hemagglutinin and neuraminidase (Verma et al., 2012, Pan et al., 2012). M-ficolin has been shown to interact with surface glycoproteins of Zaire Ebola virus (Favier et al., 2016).

Beside the relation between ficolins and viral infections, many studies have shown that neutralisation of ficolins play a key role in parasite diseases. For example, *Trypanosoma cruzi* calreticulin inhibits activation of the CP, as a result of interacting with C1 and the LP by binding to L-ficolin (Valck et al., 2010). In this way *Trypanosoma cruzi* blocks two major arms of the innate immune response (Sosoniuk et al., 2014). Another study has shown that L-ficolin polymorphisms lead to increasing the susceptibility to leishmaniasis (Assaf et al., 2012).

A variety of other studies have highlighted disease associations involving ficolins. For example, it has been reported that L-ficolin serum concentrations are decreased in patients infected with pulmonary *Mycobacterium tuberculosis* (Luo et al., 2013). Deficiency of H-ficolin leads to lack of complement deposition on acetylated structures and is associated with chronic disabling infections and lung damage (Munthe-Fog et al., 2012). H-ficolin concentrations are also decreased in patients with Crohn's disease or ulcerative colitis (Schaffer et al., 2013). M-ficolin concentration in patients with rheumatoid arthritis was 30-fold higher than those with osteoarthritis (Ammitzball et al., 2012).

1.15 Humoral immunity

Antibodies are produced by B-cells and mediate humoral immunity through neutralisation and opsonisation of extracellular pathogens (Kalia et al., 2006). B-cells mature and develop in the bone marrow (Kierney and Dorshkind, 1987, Kurosaka et al., 1999). Antibody production is the only effector function of B-cells and different antibodies are produced according to their specificity towards antigen.

1.15.1 Antibody structure

Immunoglobulins (Ig) are heterodimeric glycoproteins produced by specialized B-lymphocytes known as plasma cells (Schroeder Jr, 2010, Lipman et al., 2005). IgGs are composed of four polypeptide chains with two identical heavy chains (~55 kDa) and two identical light chains (~25 kDa) assembled to form a Y-shaped structure held together by disulfide and non-covalent bonds (Figure 1-11). The resulting molecule is ~150 kDa (Schroeder Jr, 2010, Lipman et al., 2005). In 1890, von Behring and Kitasato reported that diphtheria toxin can neutralize the existence of an agent in the blood followed by known as ‘Antikörper’ or antibodies, it was described as the agent that able to discriminate between two immune substances (Schroeder Jr, 2010). Structurally each antibody heavy chain comprises one N-terminal variable domain (V) which serves as the antigen-binding site and three C-terminal constant domains (C). Each light chain comprises a variable domain and a constant domain. Together the variable domains serve as the antigen-binding sites. Each arm of the antibody is known as Fab fragment, while the central stem is called the Fc portion and it interacts with effector cells and receptors. Each Ig domain consists of approximately 110-130 amino acids, (Schroeder Jr, 2010, Wang et al., 2007).

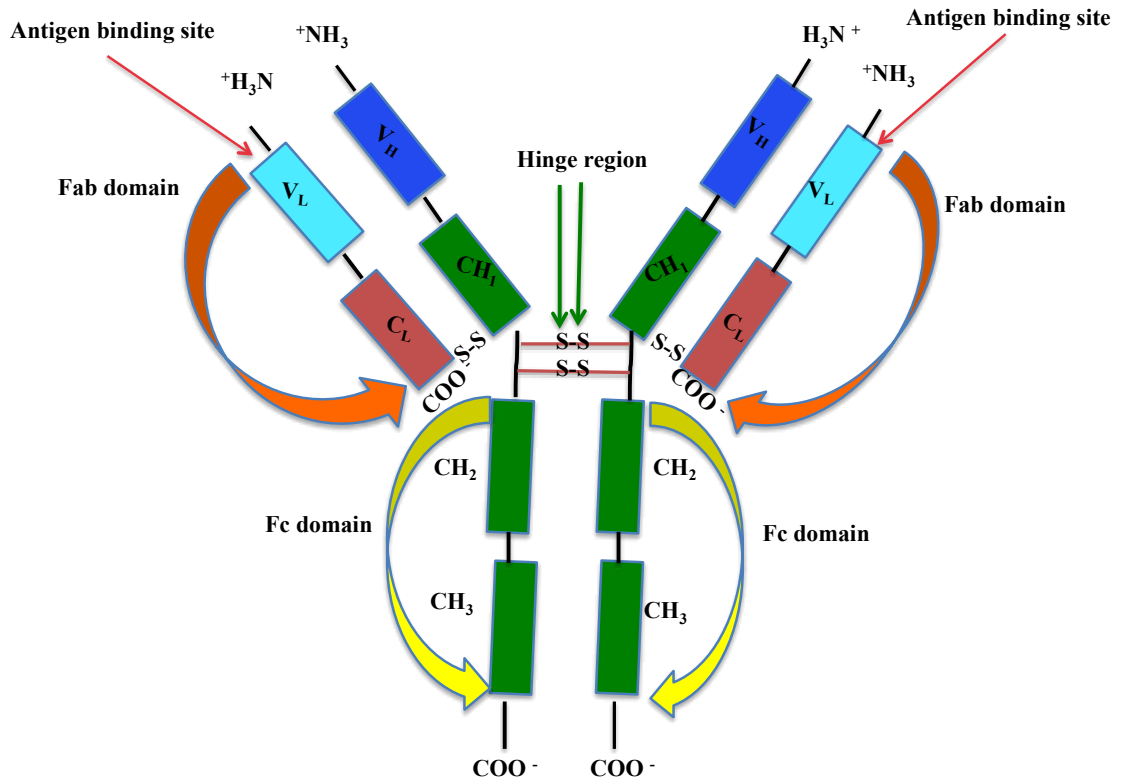


Figure 1-11: Schematic diagram of Ig structure.

The heavy and light chains consist of N-terminal variable (V) domain coloured blue and cyan. The remaining domains form the constant region, with domains coloured as red and green. The hinge region is located between CH₁ and CH₂. Proteolytic enzymes (including IdeS, Papain and Pepsin) are able to split the Ig into Fab domains containing the antigen-binding site and Fc domains that mediate activation of the CP and phagocytosis.

1.15.2 Ig isotypes

There are five Ig or isotypes of Igs: IgG, IgM, IgA, IgD, and IgE. All isotypes are assembled from Ig domains but they differ in the sequences of the constant regions of their heavy chains (Woof and Burton, 2004). Key features of each group are described below. Table 1-3 below shows the general features of each IgG isotype (Vidarsson et al., 2014).

1.15.2.1 Immunoglobulin G (IgG)

IgG is the predominant Ig isotype in human serum (Vidarsson et al., 2014). It comprises 10-20% of the protein in the plasma. IgG a glycoprotein with 82-96% protein and 4-18% carbohydrate. IgG has the longest serum half-life of all isotypes (Schroeder Jr, 2010, Vidarsson et al., 2014). It is classified into four subclasses: IgG1, IgG2, IgG3, and IgG4,

ranked according to their average serum concentration (IgG1> IgG2> IgG3> IgG4) in the blood of normal, healthy individuals (Schroeder Jr, 2010, Liu and May, 2012). IgG isotypes IgG1, IgG2, IgG3, and IgG4 account for approximately 60%, 25%, 10%, and 5% of IgG in blood, respectively (Stoop et al., 1969). An N-linked glycosylation site in all IgG molecules is located in the CH₂ domain at Asn-297. It plays a key role in maintaining the quaternary structure and in the stability of the Fc domain (Mimura et al., 2000, Mimura et al., 2001, Krapp et al., 2003). Some studies have reported differences in the glycosylation pattern of each isotype (Selman and Hansen, 2012, Vestrheim et al., 2014). The number of disulphide bonds differs in each isotype. The disulphide bond in the hinge region of each IgG isotypes is different. In IgG1 and IgG4 is two, IgG2 has four disulphide bonds and IgG3 has eleven disulphide bonds (Liu and May, 2012). The hinge region of each isotype is different with 15, 12, 62 amino acid residues for IgG1, IgG2, IgG4 and IgG3 (Vidarsson et al., 2014). The hinge region determines the stability, flexibility and distances spanned by the two Fabs (Tian et al., 2014).

1.15.2.1.1 IgG1

IgG1 is the predominant IgG subclass and constitutes (10-15 mg/ml) in human serum (Mimura et al., 2000, Mimura et al., 2001). The IgG1 half-life is 3 weeks, whilst, the IgG3 has the shortest half-life of about only 1 week (Dullaers et al., 2012). A deficiency of IgG1 is associated with recurrent infections (Jefferis and Kumararatne, 1990). Serum IgG1 concentrations are increased in Sjogren syndrome, systemic sclerosis, systemic lupus erythematosus and primary biliary cirrhosis diseases (Zhang et al., 2015). IgG1 contains fucosylated N-linked sugar whilst IgG3 showed a non-fucosylated glycoforms. Activation of the complement cascade by IgG1 play a crucial role in protection of the human body against infectious agents (Redpath et al., 1998). It has been reported that the IgG1 and IgG3 are the most efficient IgG isotypes for activating the complement system via the CP by binding to C1q (Bruggemann et al., 1987). Mutations in residues Asp 270, Leu 334, Leu 335 leads to a reduction in complement activation (Michaelsen et al., 2009).

1.15.2.1.2 IgG2

IgG2 accounts for 25% of the total IgG in human blood. It plays a crucial role in protection against *Streptococcus pneumoniae*, *Haemophilus influenzae*, and *Neisseria meningitidis*. IgG2 deficiency may result in the virtual absence of IgG anti-carbohydrate antibodies (Vidarsson et al., 2014). The concentration of IgG2 is decreased in association

with a decreasing levels of IgG4, IgA1 and IgA2 (Latiff and Kerr, 2007). IgG2 can activate the complement system but is considerably less efficient than IgG1 and IgG3 (Burton et al., 1986, Michaelsen et al., 1991).

1.15.2.1.3 IgG3

IgG3 comprises approximately 10% of the total serum IgG. It has a unique elongated hinge region containing ~62 amino acid residues (Stoop et al., 1969, Michaelsen et al., 1977) and is efficient at activating complement. The hinge region is encoded by four exons in IgG3 while only one exon encodes the hinge regions of IgG1, IgG2, and IgG4. IgG3 has a higher molecular weight compared to other subclasses because of its hinge region (Vidarsson et al., 2014). IgG3 is encoded by 13 allotypes, which are the alleles encoding the antibody chain, while IgG1, IgG2, are encoded by 4 allotypes respectively (Lefranc and Lefranc, 2012). IgG3 has a short half-life of ~7 days. This reduction is associated with an arginine at position 435, which is histidine in all other IgG subclasses (Irani et al., 2015). IgG3 deficiency is associated with recurrent respiratory infections including sinusitis (Meyts et al., 2006, Visitsunthorn et al., 2011). The concentration of IgG3 is increased in patients with *Mycobacterium Leprosy* (Hussain et al., 1995).

1.15.2.1.4 IgG4

IgG4 comprises only ~5% of IgG in serum (0.35 to 0.51 mg/ml) (Aalberse et al., 2009, Aalberse and Schuurman, 2002, Aucouturier et al., 1984, Kleger et al., 2015). The hinge region consists of 12 amino acid residues. Unlike all other IgGs, IgG4 can undergo Fab-arm exchange (FAE) in which a bi specific antibody formed (Davies and Sutton, 2015). In this process, the IgG4 heavy chains separate to form half-molecules containing only one heavy and light chain. The half-molecules from separate antibodies associate to produce a bi-specific antibody (Aalberse and Schuurman, 2002). This contributes to the anti-inflammatory properties of IgG4 and limits the ability of IgG4 to form immune complexes and activate complement (Aalberse and Schuurman, 2002). A recent study reported that up to 33% of IgG4 molecules were κ/λ light-chain hybrids (Young et al., 2014). The constant region of IgG4 regions shows 95% amino acid sequence homology to the other IgG subclasses. However, IgG4 binds only weakly to Fc γ receptors, and can not activate complement. IgG4 is associated with autoimmune diseases such as pancreatitis (Kleger et al., 2015). The level of IgG4 is elevated in some cases of infectious bacterial paortitis (Zakir et al., 2015).

Table 1-3: Human IgG isotypes characteristic.

| General property | IgG1 | IgG2 | IgG3 | IgG4 |
|-------------------------------------|------|------|------|------|
| Molecular weight (kDa) | 146 | 146 | 170 | 146 |
| Amino acids in hinge region | 15 | 12 | 62 | 12 |
| Heavy chain disulphide bonds | 2 | 4 | 11 | 2 |
| Serum level g/l | 6.98 | 3.8 | 0.51 | 0.58 |
| Relative abundance % | 60 | 25 | 10 | 5 |
| Half-life weeks | 3 | 3 | 1 | 3 |
| Complement activation (C1q binding) | ++ | + | +++ | - |
| Ab response to proteins | ++ | +/- | ++ | ++ |
| Ab response to polysaccharides | + | +++ | +/- | +/- |
| Ab response to allergens | + | - | - | ++ |

1.15.2.2 Immunoglobulin A (IgA)

IgA is the second most abundant serum antibody after IgG. It is present in plasma at a concentration of ~2 mg/ml, (Roos et al., 2001, Schroeder Jr, 2010). IgA is predominantly secreted and produced by the mucosal surfaces. It is found in secretions such as saliva and breast milk. It protects the body against inhaled and ingested antigens (Leusen, 2015, Carlier et al., 2016). IgA exists as two forms according to location and production. Mucosal secreted IgA (IgA2) is predominantly dimeric while serum IgA (IgA1) is monomeric. Therefore, the function of IgA is likely to be different according to its location. For example, intestinal IgA (a mucosal IgA) is able to neutralize toxins and some pathogens, it also provides a different and spatially diversified population of commensal bacteria (Gutzeit et al., 2014). In addition, the secreted IgA which is present in human colostrum and milk play a key role in both passive and active immune protection of the newborn (Woof and Kerr, 2006). IgA1 has an extra 13 amino acid residues in the hinge region (Carlier et al., 2016, Leusen, 2015, Cerutti and Rescigno, 2008). This elongated hinge prevents recognition by bacterial proteases. IgA2 is more sensitive to these proteolytic enzymes (Schroeder Jr, 2010 Carlier et al., 2016).

1.15.2.3 Immunoglobulin E (IgE)

Ishizaka and Ishizaka identified IgE in 1967 (Poole and Rosenwasser, 2005). IgE is normally present in the plasma at a concentration of less than 1 µg/ml with half-life of about 2 days in serum. It consists of only 0.004% of total Ig in serum (Amarasekera, 2011, Stone et al., 2010, Hamilton, 2010). IgE provides immunity against parasites such as helminths. In addition, it mediates type I hypersensitivity reactions associated with allergic diseases including asthma, allergic rhinitis and atopic dermatitis (Fitzsimmons et al., 2014, Wu and Zarrin, 2014).

1.15.2.4 Immunoglobulin D (IgD)

IgD was discovered in 1965. Serum concentrations of IgD are below IgG, IgA, and IgM but higher than IgE. It represents approximately 0.25% of total Ig in serum (40 µg/ml in adults) and has a short half-life of about 2 days (Vladutiu, 2000, Rogers et al., 2006). IgD is expressed as two forms: membrane IgD (mIgD) and secreted IgD (sIgD), mIgD is co-expressed with IgM in ~90% of mature B-cells (Wu et al., 2016b). In B cells, IgD serves as the B cell receptor and signals the B cells to become activated. Once activated it stimulates the cell to produce antibodies (Ubelhart et al., 2015). The hinge region of IgD is long and susceptible to proteolysis (Gleich et al., 1969, Sire et al., 1982). The serum concentration of sIgD is elevated in some autoimmune diseases including rheumatoid arthritis, systemic lupus erythematosus, Sjogren's disorder and autoimmune thyroiditis (Rostenberg and Penalzoza, 1978, Schmidt and Mueller-Eckhardt, 1973).

1.15.2.5 Immunoglobulin M (IgM)

IgM is considered to be an ancient antibody class, which exists in all vertebrates, except coelacanths, and is important in innate and adaptive immunity in fish (Pleass et al., 2016). Two types of IgM are present in the immune system: membrane-bound receptors on B-cells (mIgM) and secreted IgM (sIgM). The plasma concentration of IgM is 1-2 mg/ml, with a half-life of 5 days. The sIgM molecules are predominantly pentamers and hexamers, while the mIgM is monomeric (Czajkowsky and Shao, 2009, Czajkowsky et al., 2010, Ehrenstein and Notley, 2010). It serves as an opsonin for the clearance of small apoptotic particles, senescent erythrocytes, and even microbes (Racine and Winslow, 2009). IgM activates complement via the CP. It has a 1000-fold greater binding affinity for C1q than IgG (Ehrenstein and Notley, 2010). CP activation on apoptotic cells occurs predominantly via IgM (Zwart et al., 2004). A recent study reported that ethanol-induced

apoptosis in the liver recruits sIgM, facilitating the activation of C1q via the CP (Smathers et al., 2016).

1.16 Biological membrane

Biological membranes are the semi-permeable barrier surrounding all living cells that mediates the exchange of intracellular and extracellular components (Bovigny et al., 2015). They are composed of a bilayer of different phospholipids, proteins and sugars. Lipid molecules can be divided into three main types: phospholipid, glycolipids and sterol (Figure 1-12) (Watson, 2015). Membrane phospholipids are amphiphilic due to the polar head group that has a high affinity for water molecules (hydrophilic) and the non-polar tail group that has a low affinity for water molecules (hydrophobic). The hydrophilic head group is oriented outwards on the outer leaflet and inwards on the inner leaflet of the lipid bilayer, whereas the hydrophobic tails points to the interface between the bilayer leaflets.

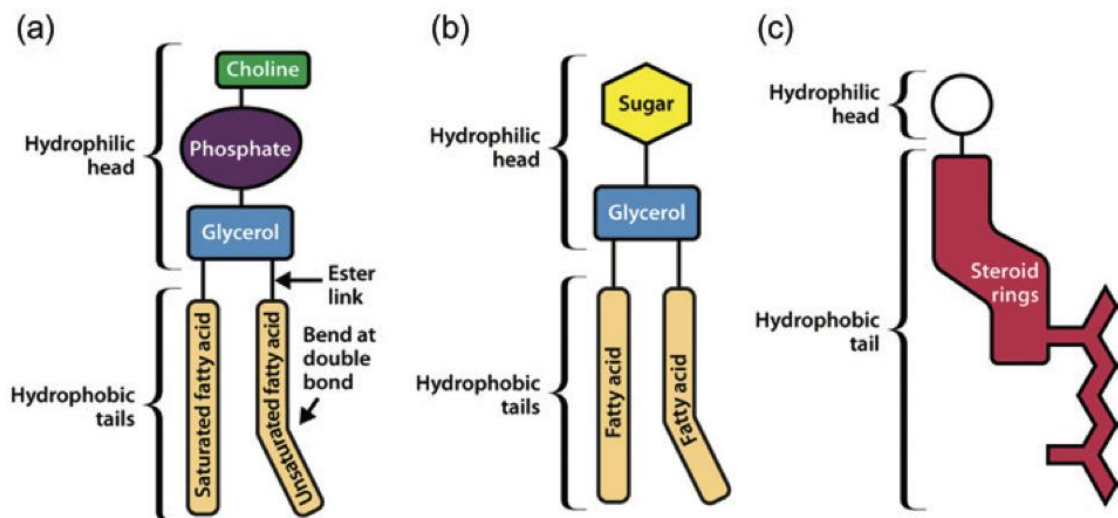


Figure 1-12: Schematic representation of membrane lipid types.

Membrane has three types lipid including a phosphatidylcholine (a), glycolipid (b) and a sterol (c) (Watson, 2015). Phosphatidylcholine composed of hydrophilic head (choline, phosphate and glycerol) and hydrophobic tails which might be saturated or unsaturated. Glycolipid comprises of hydrophilic head (sugar and glycerol) and hydrophobic tails. Steroid as well composed of hydrophilic head and hydrophobic tail.

The fluid-mosaic model is used to describe the properties of biological membranes. The model was proposed in 1972 by Singer and Nicolson based on the thermodynamic principles governing the organization of lipids and proteins in a membrane (Nicolson, 2014). The term, fluid, refers to ability of components to move laterally or diffuse throughout the bilayer. It has been reported that membrane fluidity is regulated by cholesterol (Lombard, 2014). The fluid-mosaic model of biological membranes is illustrated in (Figure 1-13).

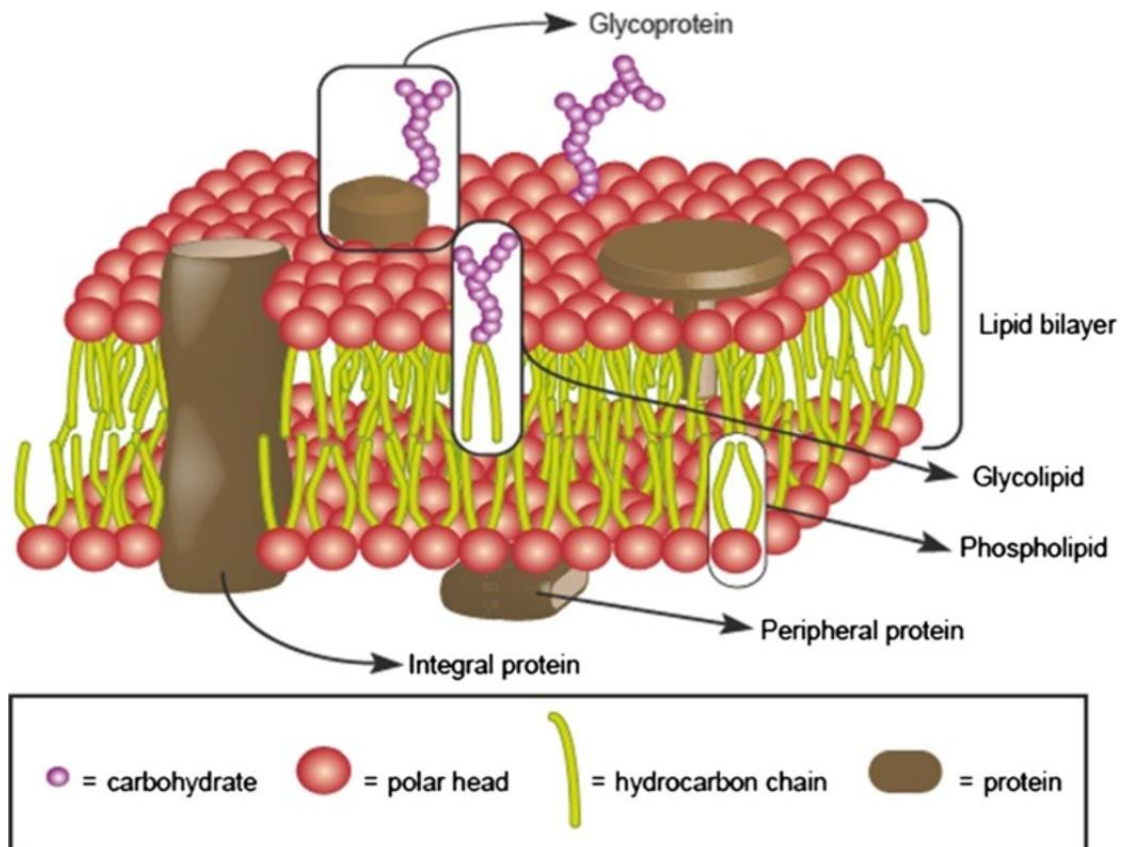


Figure 1-13: Schematic representation of fluid-mosaic model of a biological membrane.

The membrane is composed of the phospholipid bilayers including polar heads and non-polar tails with the glycolipid, glycoprotein, peripheral protein and integral protein (Lombard, 2014).

1.16.1 Structure and biophysical properties of lipid bilayers

1.16.1.1 Lipid molecules

1.16.1.1.1 Phospholipids

Phospholipids comprise the phosphate containing polar head group and fatty acid non-polar tail group. They can be divided into two types of structures: glycerophospholipids and sphingomyelins (SM) (Li et al., 2015). Most of the phospholipids in the eukaryotic cells membrane are the glycerophospholipids which contain a glycerol-2 backbone; this a long acyl chain that typically contains many gauche orientations of the un saturated carbon-carbon bonds leads low density packing (Brown and London, 2000). The backbone is sphingosine in sphingolipids; this contains C16 saturated acyl chain, which can pack tightly together to produce ordered domains in the fluid membrane (referred to as lipid rafts). The presence of sphingolipids in a lipid membrane needs higher temperatures for the main transition compared with membrane comprising pure glycerophospholipids.

1.16.1.1.2 Cholesterol

Cholesterol is an important constituent of animal cell membranes. More than 90% of cellular Chol is incorporated into the membrane. It was discovered in 1815 by the French chemist Michel Eugène Chevreul. Chol is a major determinant of biophysical properties of a membrane because, when incorporated in the membrane, Chol increases mechanical strength, affecting membrane elasticity, it makes the membrane less elastic and hence increases stiffness and the packing density of lipids (Magarkar et al., 2014, Goluszko and Nowicki, 2005). Chol is an amphiphilic molecule with a polar hydroxyl head group that is embedded into the acyl chains of the lipid membrane; it also has a rigid core with four hydrophobic hydrocarbon rings and a flexible acyl tail (Figure 1-14). In addition, Chol plays a key role in lipid metabolism because it is a precursor for some biological compounds such vitamin D, steroid hormones and bile acids. Chol facilitates the proper development and functioning of the nervous system because it is the component of the myelin sheath (Czamara et al., 2015).

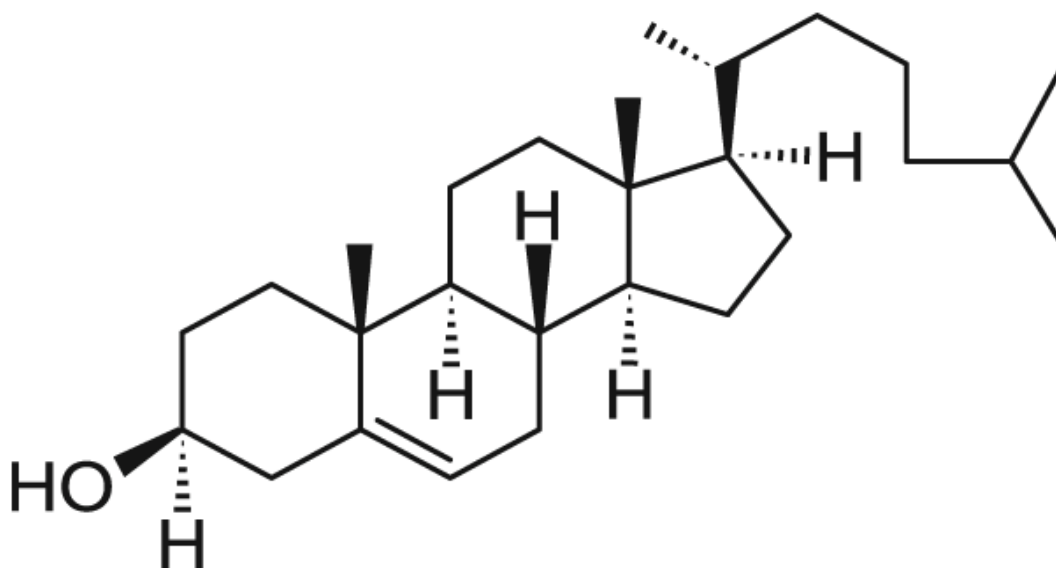


Figure 1-14: Cholesterol chemical structure.

It is composed of weak hydrophilic hydroxyl head, four hydrophobic hydrocarbon rings and flexible acyl tail. Image was taken from Avanti polar lipid website (<https://avantilipids.com/product>).

1.16.1.2 Liposomes as the membrane model

Liposomes are synthetic vesicles with a bilayer structure surrounding an aqueous core. They are useful as a membrane model to study how the shape and morphology of the lipid bilayer is influenced by external factors, including physical, chemical and biological (Kato et al., 2015). They were first characterized in the 1960s by Alec D Bangham at the Babraham Institute, University of Cambridge (Bozzuto and Molinari, 2015). The name, liposome, is derived from the Greek words 'lipos', which means fat, and 'soma', which means body. Phospholipids are the most common component used in the preparation of liposomes, followed by Chol and sphingolipids. Phospholipids have a strong tendency to form membranes because of its amphipathic nature (Bozzuto and Molinari, 2015). Besides the use of liposomes as a model membrane for biophysical and bioanalytical research, they are also used in medicine as a drug carrier (Sercombe et al., 2015). Figure 1-15 shows the structure of a liposome, where a liposomal bilayer provides an interface between the interior content and the surroundings.

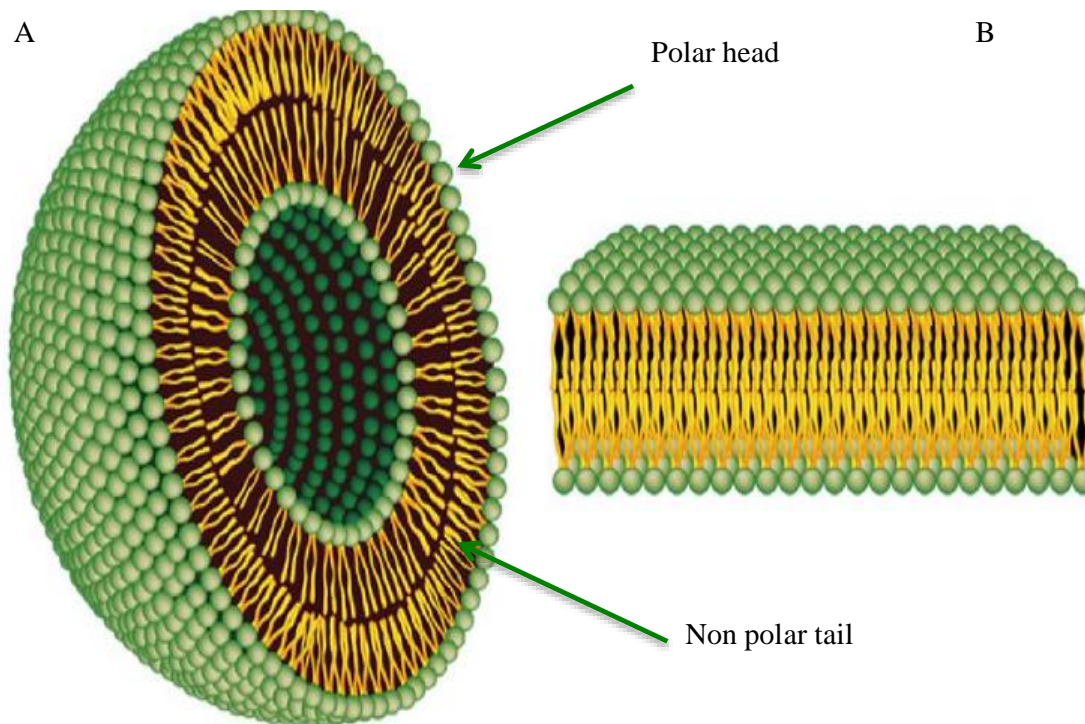


Figure 1-15: Schematic view of a liposome vesicle and a lipid bilayer.

(A) Represents liposome vesicle in which the polar head turns outward whereas, the nonpolar tail turns inward. B, is the lipid bilayer of liposome (Bozzuto and Molinari, 2015).

Liposomes can be classified based on different parameters: firstly, their method of preparation which includes reverse-phase evaporation and extrusion; secondly, their size which encompasses small (<100 nm), intermediate (100 nm to 1 μm) and large (>1 μm) unilamellar vesicles; and, finally, lamellarity which includes unilamellar, multilamellar vesicles. Either unilamellar or multilamellar could be formed depending on the method of formation (Bozzuto and Molinari, 2015). Common phospholipids used in the preparation of liposome is 1,2-dipalmitoyl-sn-glycero-3-phosphocholine (DPPC), 1-palmitoyl-2-oleoyl-sn-glycero-phosphocholine (POPC), 1,2-dioleoyl-sn-glycero-3-phosphocholine (DOPC), and 1,2-dilauroyl-sn-glycero-3-phosphocholine (DLPC) and (Figure 1-16) (Yang et al., 2016). The ratio of phospholipid to Chol that is typically used in the preparation of liposomal bilayers is approximately 1:1 to 2:1 (e.g. 2 parts of lipids and 1 part of cholesterol mole ratio or 1:1 mole ratio (Briuglia et al., 2015).

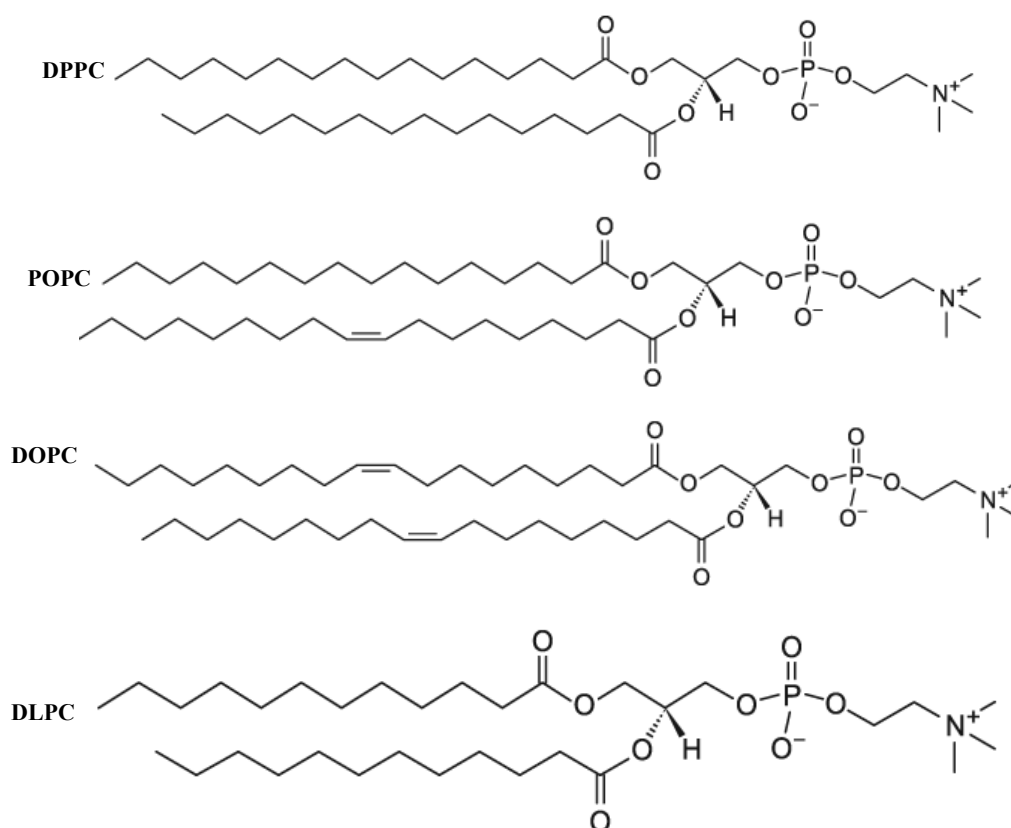


Figure 1-16: Chemical structure of DPPC, POPC, DOPC and DLPC.

All images are taken from Avanti polar lipid website (<https://avantilipids.com>).

1.16.2 Bilayer melting temperatures (T_m)

The T_m of the bilayer or the main transition temperature is defined as the temperature corresponding to the highest specific heat of the lipid bilayer. At this temperature, the physical state of the lipid bilayer is changed from a solid-ordered (gel) phase to a liquid (fluid) phase. When the temperature is below the T_m the membrane state is a gel, whereas, the phase behavior is fluid when the temperature is above the T_m . In the gel phase, lipid molecules are packed in a regular triangular lattice pattern whilst, in the liquid phase the lipid molecules the regular lattice pattern is lost and the lipid molecules are more loosely packed together causing an increase in membrane fluidity and permeability to small molecules (Lewis and McElhaney, 2013). The membrane of most biological cells are in the liquid phase but the gel phase usually exist in the outer leaflet of cells in dry skin tissue (Laggner, 2007). The existence of liquid and gel phases of the membrane is controlled by temperature and the relative amounts of saturated and unsaturated lipids in the bilayer. The change in the membrane from gel to fluid phase is accompanied by an

increase in the hydration state of the lipid head groups (Wolkers et al., 2010). Figure 1-17 shows the membrane phase according to the increasing temperature.

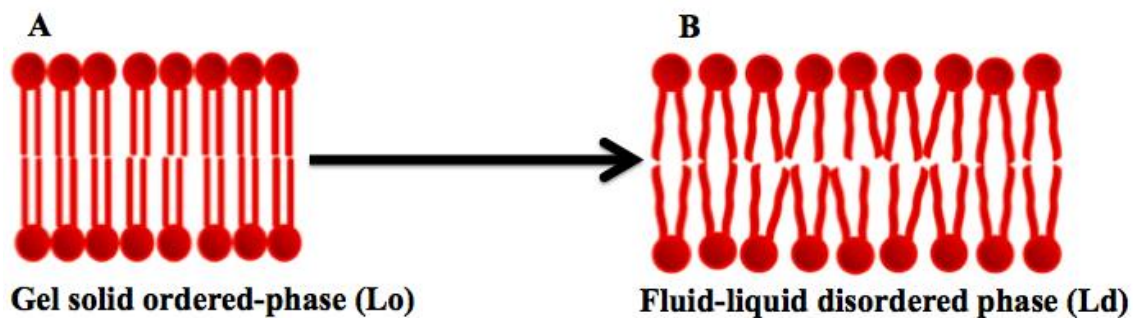


Figure 1-17: Membrane phase transition with increasing temperature.

Increasing of temperature impact the membrane fluidity. (A) The temperature is below the T_m , the lipid molecules are packed tightly. (B) Lipid molecules are likely to melt. Lipids molecule are fully melted and the membrane is changed to the liquid disordered (Ld) or the fluid phase (Zalba and Ten Hagen, 2017).

1.17 Physical states of lipid bilayer

Individual lipid components in synthetic bilayers are classified according to whether they are a high-temperature melting phospholipid or a low-temperature melting phospholipid; where Chol is considered a unique component. At high temperature, the lipids in the bilayer will be mixed uniformly. Chol is important at lower temperature for the coexistence of different phases in separated domains in a binary lipid system. A membrane in the liquid-ordered phase (Lo) is typically enriched in either high- T_m lipids or Chol; the more ordered structure results in a thick membrane. A membrane in the (Ld) is enriched in low- T_m lipids and depleted of Chol; the more disordered structure results in a thin membrane (Veatch and Keller, 2005). The lipids have properties of fast translational diffusion and low acyl chain order in the (Ld) phase and fast translational diffusion but high acyl chain order in the Lo phase. In the solid gel phase (L β), the lipid molecules have slow diffusion and high chain order.

The lipid example DPPC forms stable and well-characterized unilamellar lipid vesicles. The equilibrium phase behavior of unilamellar DPPC bilayers show four distinct phases according to increase temperature such as the crystal (L c), gel (L β), ripple (P β), and fluid or liquid-crystalline (L α) phases (Nagarajan et al., 2012). It has been shown that

the interaction between a saturated lipid and Chol or interaction between mono-unsaturated lipids and Chol results in the presence of Ld and Lo phases of the membrane. The interaction between DPPC and Chol produces a Lo phase, whereas the interaction between POPC and Chol produces Ld phase; and a binary mixture of DPPC and POPC produces a Ld phase (Turkyilmaz et al., 2011). The ternary mixture of DPPC/POPC/Chol has also been examined to show how the interaction between lipid-lipid and Chol-lipid changes the membrane phase from Lo to Ld, and the tighter packing of Chol-lipid combinations to the looser packing of lipid-lipid combinations (Yang et al., 2016).

1.18 General aims of the thesis

This thesis covers three main aims. The first aim was to investigate the interaction between recombinant Ply and the soluble molecules of the immune system that have been identified as potential binding partners, including L-ficolin of the LP and IgGs, which initiate the CP. This work is covered in Chapter 3. The second aim, described in Chapter 4, was to examine the mechanism of pore formation by Ply by characterizing the interaction between Ply monomers during pore assembly. Following on from this work, the third aim covered in Chapter 5 was to observe changes in single cell-sized liposomes by Ply using Raman spectroscopy.

Chapter 2 Production and purification of Ply and Ply domains

2.1 Objectives

In order to study the interactions between Ply and the soluble molecules of the immune system, it was necessary to produce recombinant full-length Ply and Ply fragments comprising PlyD1-3 and PlyD4. The Ply gene was first cloned and sequenced by Walker and colleagues (Walker et al., 1987). In the current study, His₆-tagged full-length Ply and PlyD1-3 were expressed in *Escherichia coli* (*E. coli*) and purified by affinity chromatography on Ni-Sepharose columns followed by gel filtration. PlyD4 was expressed as a maltose-binding protein (MBP) fusion and separated from MBP by cleavage with TEV protease followed by gel filtration.

2.2 Materials and methods

2.2.1 Materials

A plasmid containing the full-length Ply gene in pLEICS-07 (Figure 2-1), a pET-based expression vector, was provided by Dr. Rana Lonnen (Leicester University UK, MSB G43). Promega supplied XL10 and BL21 (DE3) *E. coli* strains competent cells. Platinum Pfx polymerase for (PCR) was from Life Technologies. Protein and DNA markers and amylose-Sepharose affinity resin was supplied by New England Biolabs. Filters (0.2 µm), Ni-affinity resin, Superdex 200 and 75 16/60 columns used for protein purification were purchased from GE healthcare. Qiagen supplied mini and midi prep plasmid extraction kits to purify and extract plasmid DNA. The Quickfold protein refolding kit was from Athena Enzyme Systems. SYBR® Safe DNA gel stain and loading dye were from Invitrogen. Bugbuster protein extraction reagent was from Merck Millipore. Agilent Technologies supplied strata clean resin beads. Isopropyl β-D-1-thiogalactopyranoside (IPTG) and chemicals were purchased from Thermo Fisher Scientific and Sigma. Protease inhibitor tablets were from Roche.

2.2.2 Electrophoresis

PCR products and digested plasmids were separated by electrophoresis on agarose gels (0.5-1.5%) prepared as described in (Sambrook and Russell, 2001). 0.5 µg/ml of SYBR® Safe DNA gel stain was added to the gels before pouring. Gels were run in 1x TBE buffer (45 mM Tris-base, 45 mM boric acid and 1 mM EDTA). DNA samples were diluted 5:1 with 6x loading dye. DNA ladders (100 bp, 1 kb) were used as molecular weight markers.

Gels were run at 80 V and 400 mA for 60 minutes (min), visualised under UV illumination and photographed using UV gel documentation system.

2.2.3 Competent cells and transformation

E. coli XL10 Gold cells were used for plasmid amplification and cloning and *E. coli* BL21 (DE3) were used for protein expression. Competent cells were prepared chemically by the rubidium chloride method described in section 2.2.4. For cloning, 100-1000 ng of ligated recombinant plasmid was used while for normal transformation, supercoiled plasmid (10-50 ng) was used. These were mixed with 100 µl of competent cells, and incubated on ice for 20 min. Cells were heat-shocked at 42°C for 2 min and then put on ice for 2 min. 300 µl of Luria-Bertani (LB) was added to the cells. After 60 min incubation with shaking at 37°C and 220 rpm, the entire content was spread onto LB agar (LBA) containing the appropriate antibiotic e.g. 100 µg/ml ampicillin or 50 µg/ml kanamycin. The plates were incubated at 37°C overnight (Li et al., 2011).

2.2.4 Competent cell preparation by the rubidium chloride method

100 ml LB containing 20 mM MgSO₄ was inoculated with overnight culture and incubated for 2-3 hr in a baffled flask until the OD₆₀₀ reached 0.4-0.6. After that, cells were spun down at 4500 g at 4°C for 5 min. The pellet was resuspended in 40 ml TBF1 buffer (30 mM potassium acetate, 10 mM CaCl₂, 50 mM MnCl₂, 100 mM RbCl containing 15% glycerol at pH 5.8). The suspension was left on ice for 5 min and centrifuged again at 4500 g at 4°C for 5 min. Next, the pellet was resuspended in 4 ml TBF2 buffer (10 mM MOPS or PIPES, 75 mM CaCl₂, 10 mM RbCl, 15% glycerol at pH 6.5) and left on ice for 30 min. Cells were aliquoted into 100 µl fractions and then frozen immediately in liquid nitrogen and stored in -80°C. All buffers were sterilized by filter-sterilize 0.2 µm prior to use (Green and Rogers, 2013).

2.2.5 Sodium dodecyl-polyacrylamide gel electrophoresis (SDS-PAGE)

Proteins were separated by SDS-PAGE using a BioRad mini protein II gel system. In this procedure proteins are unfolded and coated with SDS and separated based on their sizes. The resolving gel was prepared by mixing 375 mM Tris-HCl pH 8.8, 15% v/v acrylamide, 0.1% SDS w/v, 0.1% v/v ammonium persulfate and 0.0004% TEMED. The stacking gel was composed of 125 mM Tris-HCl pH 6.8, 4% v/v acrylamide, 0.1% w/v SDS, 0.002% ammonium persulfate and 0.0004% TEMED. The resolving gel was set under

isopropanol to remove air bubbles until the gel solidified. Then the stacking gel was cast on top and the comb added.

The gel was run in 1x SDS running buffer (25 mM Tris-HCl, 192 mM glycine, 0.1% w/v SDS). Samples were loaded on the gel by mixing 5 μ l of 5x loading buffer (250 mM Tris-HCl pH 6.8, 50% v/v glycerol, 10% w/v SDS, 500 mM DTT, 0.25% w/v bromophenol blue) with 20 μ l of each protein sample. Samples were denatured at 95°C for 5 min before running. Electrophoresis was carried out at room temperature using a constant voltage (200 V) and variable current for approximately 50 min until the dye front reached the end of the gel. Gels were stained with Coomassie blue stain (0.4% w/v in 50% v/v methanol and 10% v/v acetic acid) for 15 min, rinsed with water and destained in (30% v/v methanol containing 7% v/v acetic acid). Gels were scanned with an HP Scanjet G4010.

2.2.6 Expression and purification of full-length Ply

A recombinant pET-based expression plasmid (pLEICS-07), (Figure 2-1) containing the full-length gene was transformed into BL21 (DE3) cells. The encoded protein Ply contains 471 amino acid residues (Figure 2-2). An N-terminal His₆-tagged was added for purification followed by a cleavage site for the Tobacco Etch virus protease (TEV). Cells were grown in (LB) medium with 50 μ g/ml kanamycin to an OD₆₀₀ of 0.5-0.8 at 37°C. Expression was induced with 1mM IPTG, and cells were incubated overnight at 18°C.

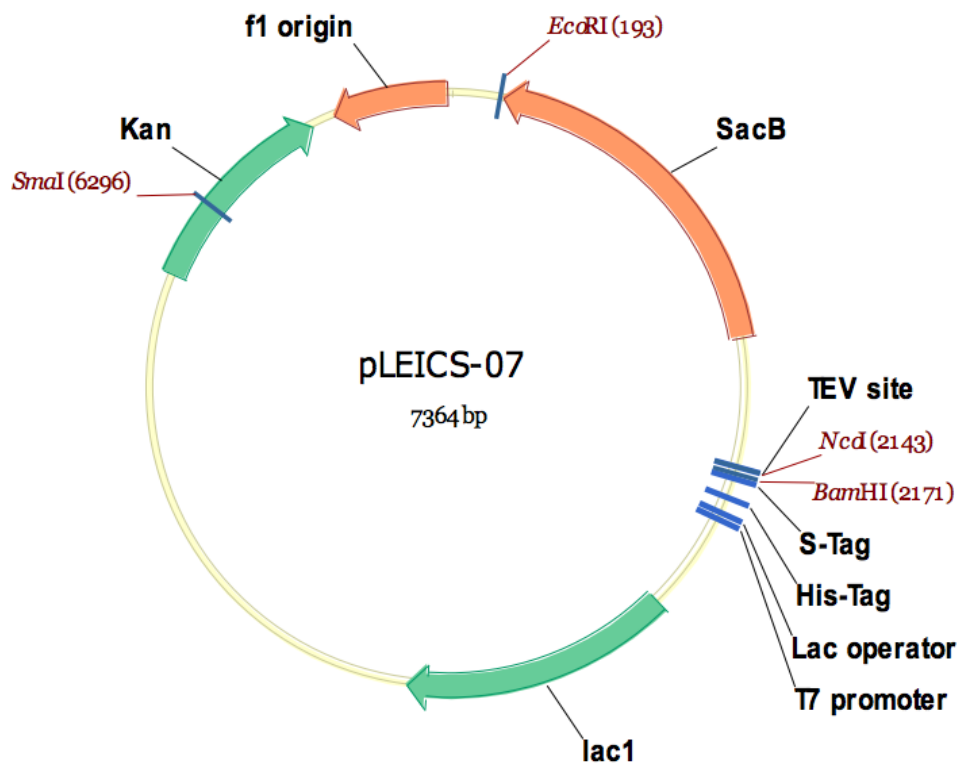


Figure 2-1: Vector map of pLEICS-07.

10 20 30 40 50 60
 MANKAVNDFI LAMNYDKKKL LTHQGESIEN RFIKEGNQLP DEFVVIERKK RSLSTNTSDI
 70 80 90 100 110 120
 SVTATNDSRL YPGALLVVDE TLENNPTLL AVDRAPMTYS IDLPGLASSD SFLQVEDPSN
 130 140 150 160 170 180
 SSVRGAVNDL LAKWHQDYGQ VNNVPARMQY EKITAHSMEQ LKVKFGSDFE KTGNSLDIDF
 190 200 210 220 230 240
 NSVHSGEKQI QIVNFKQIYY TVSVDAVKNP GDVFQDTVTV EDLKQRGISA ERPLVYISSV
 250 260 270 280 290 300
 AYGRQVYLKL ETTSKSDEVE AAFEALIKGV KVAPQTEWKQ ILDNTEVKAV ILGGDPSSGA
 310 320 330 340 350 360
 RVTGKQVDMV EDLIQEGSRF TADHPGLPIS YTTSFLRDNV VATFQNSTDY VETKVTAYRN
 370 380 390 400 410 420
 GDLLLDHSGA YVAQYYITWN ELSYDHQGKE VLTPKAWDRN GQDLTAHFTT SIPLKGNVRN
 430 440 450 460 470
 LSVKIRECTG LAWEWRTVY EKTDLPLVRK RTISIWGTTL YPQVEDKVEN D

Figure 2-2: Ply amino acid residues.

Domains 1, 2, 3, and 4 are coloured blue, green, red and black, respectively.

Cells were harvested by centrifugation at 5000 g for 15 min and resuspended in 40 ml lysis buffer (50 mM Tris-HCl pH 7.5, 150 mM NaCl, 20 mM imidazole, 1% v/v Tween 20 and 1 tablet of protease inhibitor). The mixture was sonicated on ice 5x for 15 sec using the large probe, with a break after each sonication pulse for 45 sec to avoid overheating. The mixture was then centrifuged at 25,000 g for 20 min at 4°C to remove cell debris. Then, the supernatant was loaded onto 1 ml Ni-Sepharose column that was equilibrated with buffer (50 mM Tris-HCl pH 7.5, 150 mM NaCl, 20 mM imidazole). The column was washed thoroughly with the same buffer, and then the Ply eluted with 50 mM Tris-HCl pH 7.5, 150 mM NaCl, 500 mM imidazole. Fractions (0.5 ml) were collected and loaded on 15% w/v SDS-PAGE. Fractions containing Ply were loaded onto a Superdex 200 16/60 gel filtration column, equilibrated with 20 mM Tris-HCl pH 7.5. Fractions (1.5 ml) were collected across the elution peak and Ply was identified by 15% w/v SDS-PAGE. Finally, Ply was concentrated and its concentration was determined by absorbance at 280 nm, using an extinction coefficient (ϵ) of $1.36 \text{ cm}^2\text{mg}^{-1}$ (Morgan et al., 1994). Aliquots were snap frozen in liquid nitrogen and stored at -80°C .

2.2.7 Cloning and amplification of PlyD1-3 by PCR

DNA encoding PlyD1-3 was amplified by PCR from the full-length Ply gene. Primers were designed according to the PROTEX guidelines, which use ligase-independent cloning by recombination (Table 2-1). PCR amplifications were carried out in 50 µl volumes containing 50 ng of DNA template, 0.1 µM forward and reverse primers, 2.5 U of pfx DNA polymerase, 0.1 mM dNTPs, 0.75 mM MgSO₄, and 1x PCR buffer and enhancer. The PCR reaction was performed using an initial denaturation at 94°C for 5 min followed by 32 cycles with denaturation at 94°C for 50 sec, annealing at 61°C for 50 sec, followed by extension at 72°C for 1 min, with a final extension at 72°C for 5 min in a Labnet Multi Gene II thermo cycler. The PCR product was analysed on a 1% w/v agarose gel in TBE buffer. DNA fragments were isolated from the agarose gel and purified using a QIAEX II gel extraction kit. The targeted PCR fragment was cloned into pLEICE-01 vector (Figure 2-3) by PROTEX, which introduces an N-terminal His₆ tag. Sequence verification was carried out by the Protein Nucleic Acid Chemistry Laboratory (PNAACL) at Leicester University using pLEICS-01 sequencing primers.

Table 2-1: Oligonucleotide primers to amplify PlyD1-3.

The start and stop codons are shown in red.

| Primer | Sequence 5'-----3' |
|------------|--|
| FP plyD1-3 | TACTTCCAATCC ATG GCAAATAAAGCAGTAAATGACTTTATA |
| RP plyD1-3 | TATCCACCTTTACTGTC AGT TTCTGTAAGCTGTAACCTTAGTC |

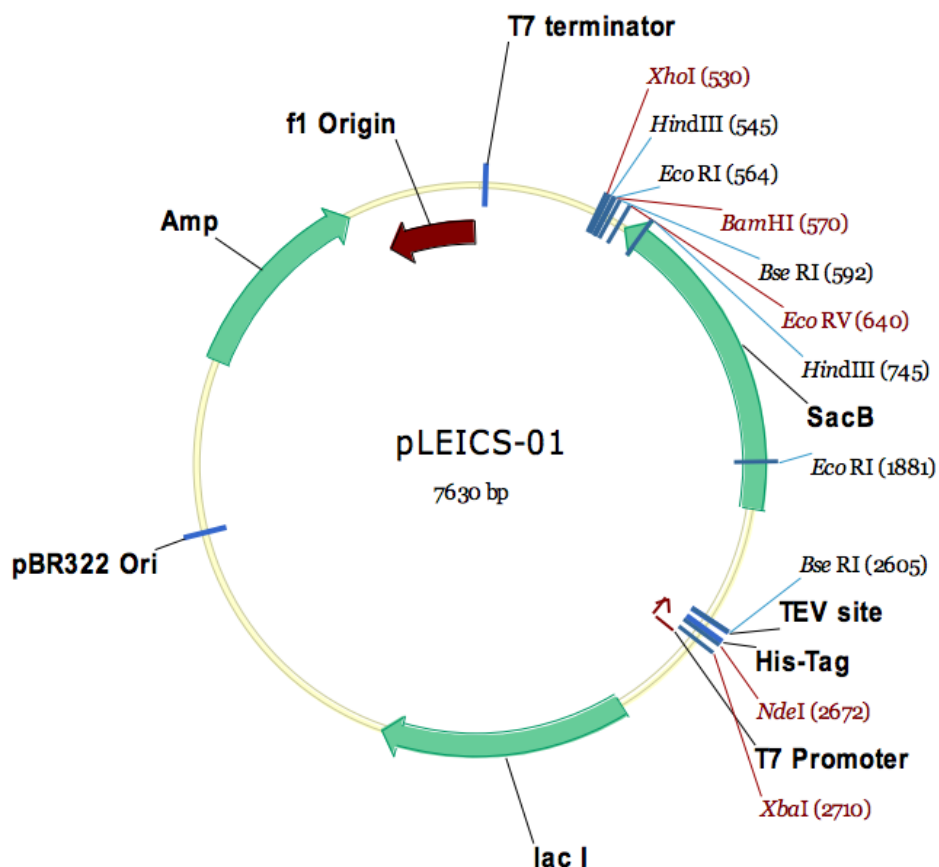


Figure 2-3: Vector map of pLEICS-01.

2.2.8 Small scale expression of PlyD1-3

Briefly, recombinant DNA was transformed into BL21 (DE3) competent cells. 10 ml of LB with 100 mg/ml of ampicillin was inoculated with a single colony of the transformed cells and incubated at 37°C until an OD₆₀₀ of 0.5-0.8 was reached. The culture was induced with IPTG at 1 mM final concentration. After incubation for 3 hr, the cells were centrifuged and washed with PBS. The pellet was resuspended in 100 µl of Bugbuster and incubated at room temperature for 15 min. The sample was then centrifuged and the supernatant collected for analysis. Next, the pellet was mixed with 100 µl PBS. Finally, the supernatant and the pellet samples were analyzed on a 15% w/v SDS-PAGE gel to check for expression and the purity of the protein.

2.2.9 Large scale protein expression

After transformation to BL21 (DE3) cells were grown at 37°C in 500 ml LB media with 100 mg/ml ampicillin. Expression was induced with 1mM IPTG at an OD₆₀₀ of 0.6-0.8 and cells were grown overnight. PlyD1-3 was expressed in inclusion bodies and purified as described below in section 2.2.10.

2.2.10 Inclusion body preparation

Cells were pelleted at 4500 rpm and at 4°C for 20 min. The pellet was washed with 40 ml of PBS. Next the pellet was resuspended in 40 ml lysis buffer (25 mM Tris-HCl pH 8.0, 150 mM NaCl, 0.5 mg/ml lysozyme, 0.5% v/v Triton-X-100 and 1m M EDTA) with 1 protease inhibitor tablet and incubated at room temperature for 30 min with shaking. MgCl₂ (5 mM) and DNase (5 µg/ml) were added to digest the DNA. The suspension was incubated at room temperature with shaking for 15 min and cells were lysed by sonication on ice with the large probe at an amplitude 8 for 10 x 30 sec and with a break of 60 sec. The lysate was centrifuged at 20,000 g at 4°C for 20 min (this speed was used for all subsequent centrifugation steps), then the pellet was washed in 40 ml of 25 mM Tris-HCl pH 8.0 containing 0.5 M NaCl, 1 mM EDTA and 0.5% v/v Triton-X-100 v/v. Additional washes were carried out in 40 ml of 1M urea, containing 0.5 M NaCl, and 1 mg/ml sodium deoxycholate in 25 mM Tris-HCl pH 8.0 and finally 40 ml of 1:10 dilution of Bugbuster protein extraction reagent. Finally, the pellet was mixed with 10 ml 25 mM Tris-HCl pH 8.0 and snap frozen in liquid nitrogen and stored at -80°C (Qoronfleh et al., 2007). After purification samples were checked by SDS-PAGE.

2.2.11 Inclusion body solubilisation

Inclusion bodies were solubilised in 25 mM Tris-HCl pH 8.0 containing 8 M urea and 5 mM DTT. The mixture was incubated at 37°C for 10 min and centrifuged at 14000 rpm for 10 min to remove insoluble cell debris. Finally, the protein concentration of the supernatant was measured at 280 nm with a Nanodrop 1000 Spectrophotometer (Labtech).

2.2.12 Small scale refolding test

The solubilized inclusion bodies were adjusted to a final concentration of 1 mg/ml with 25 mM Tris-HCl pH8, 8 M urea and 5 mM DTT and different refolding conditions were tested using the QuickFold™ Protein Refolding Kit. Solubilized protein (25 µl) was mixed with 475 µl of the 15 different refolding buffers in the screen and incubated

overnight at 4°C. Next each sample was centrifuged at 14000 rpm for 10 min. Soluble protein was checked on a 15% v/v SDS-PAGE gel. Unfolded protein tends to aggregate, so will be removed in the spin step. Samples that gave a clear band on the gel were loaded on to an analytical Superdex 200 10/300 gel filtration column, equilibrated with 20 mM Tris-HCl pH 7.5 and 100 mM NaCl to check for a peak of the expected molecular mass. Fractions were collected across the peaks, concentrated with Strataclean beads and analyzed by 15% w/v SDS-PAGE. Three buffers gave promising refolding results: buffers 2, 4 and 8.

2.2.13 Large scale refolding of PlyD1-3

PlyD1-3 (2 mg/ml) was refolded by drip dilution at 4 °C into buffer 8 (50 mM Tris-HCl pH 8.5, containing 9.5 mM NaCl, 0.4 mM KCl, 2 mM MgCl₂, 2 mM CaCl₂, 0.4 M sucrose, 0.5 Triton X-100, 0.05% polyethylene glycol 3, 550, 1 mM GSH, and 0.1 mM GSSH) to give a final concentration of 0.02 mg/ml. After refolding, the sample was filtered through a 0.22 µm Millipore filter to remove any aggregate and then passed through a 2 ml Ni-Sepharose column, equilibrated with 25 mM Tris-HCl pH 7.4, 150 mM NaCl and 20 mM imidazole using a peristaltic pump. Bound PlyD1-3 was eluted with 500 mM imidazole from the column. Fractions containing protein were collected and the purity was estimated by SDS-PAGE. PlyD1-3 was further purified by gel filtration on Superdex 75 16 / 60 column in 50 mM Tris-HCl pH7.5, 150 mM NaCl. Fractions contain protein were collected across the peak. Typically ~10 mg of pure protein was obtained per litre of culture media.

2.2.14 Cloning, expression and purification of PlyD4

PlyD4 was amplified by PCR as described in section 2.2.7 from the Ply gene using primers described in Table 2-2. The resulting fragment was cloned into pLEICS-10 (Figure 2-4). This vector encodes an N-terminal MBP-tag with a TEV cleavage site that is located between the N-terminus of inserted protein and the tag. After cloning the sequence was confirmed by PNACL.

Table 2-2: Oligonucleotide primer sets for amplify PlyD4.

Start and stop codons are shown in red.

| Primer | Sequence 5'-----3' |
|----------|---|
| FP PlyD4 | 5'GTATTTTCAGGGCGCC ATG CAGAAACGGAGATTACTGCTG3' |
| RP PlyD4 | 5'GACGAGCTCGAATTT AGT CATTCTACCTTATCCTC3' |

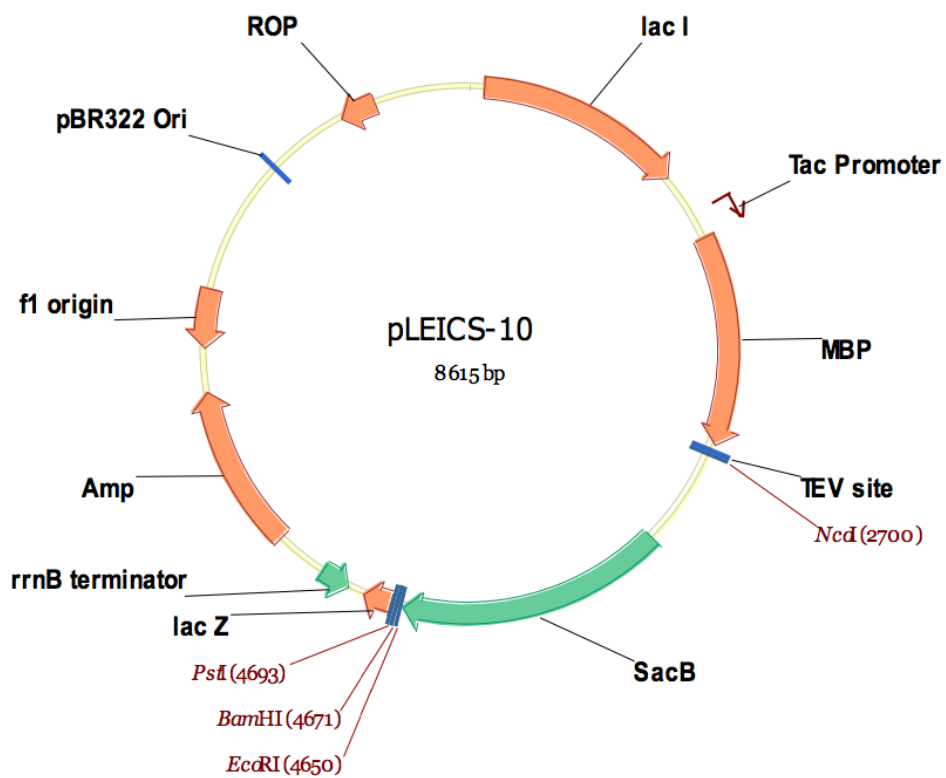


Figure 2-4: Vector map of pLEICS-10.

2.2.15 Expression and purification of PlyD4

The recombinant plasmid was transformed into BL21 (DE3). A small-scale expression was performed by inoculating 10 ml LB media containing 100 µg/ml ampicillin with a single transformed colony and incubated overnight at 37°C. This culture was used to inoculate 500 ml LB containing 100 µg/ml ampicillin and cells were incubated at 37°C in the shaking incubator. At an OD₆₀₀ of 0.5-0.8, expression was induced with 1mM IPTG and the culture was incubated overnight at 30°C. Cells were harvested by centrifugation at 4000 g for 20 min at 4°C. The cell pellet was mixed with 40 ml lysis buffer (50 mM Tris-HCl pH 7.5, 150 mM NaCl and 1% v/v Tween 20) and a protease inhibitor tablet. Sonication was performed 6 x for 15 sec on ice, with 45 sec rest intervals to lysis the cells and the mixture was centrifuged at 20,000g for 20 min at 4°C. The supernatant was passed through a 2 ml amylose-Sepharose column that was equilibrated with 50 mM Tris-HCl pH 7.5, 150 mM NaCl to bind the soluble MBP-tagged PlyD4 fragment. After that the column was washed with 10 ml of 50 mM Tris-HCl pH 7.5, 150 mM NaCl and eluted with 1ml fractions of 50 mM Tris-HCl pH 7.5, 150 mM NaCl and 10 mM maltose. Fractions were collected, analyzed by SDS-PAGE followed by staining with Coomassie blue for 15 min. The fractions contained the fusion protein were pooled and digested with (TEV) protease at 4°C overnight and loaded on a Superdex 75 16/60 gel filtration column that was equilibrated with 50 mM Tris-HCl 7.5, 150 mM NaCl to separate the MBP-tag from the PlyD4. Finally, fractions containing PlyD4 were analysed by SDS-PAGE. Samples were concentrated and snap frozen in liquid nitrogen and stored at -80°C.

2.3 Results

2.3.1 Expression and purification of full-length Ply

The expression plasmid encoding full-length Ply (MSB G43) was transformed into BL21 (DE3) strain and production was induced with IPTG. Ply was initially purified by affinity chromatography on a Ni-Sepharose column, which removes most of the impurities. Fractions containing Ply were analyzed by SDS-PAGE (Figure 2-5).

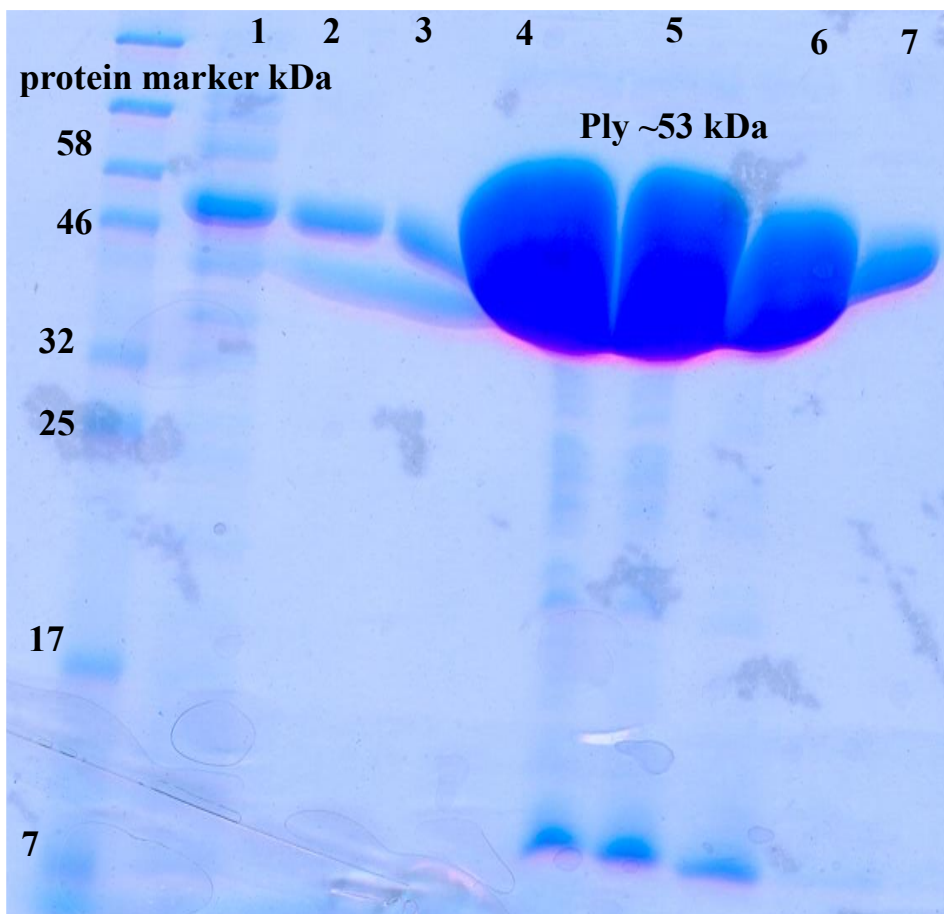


Figure 2-5: SDS-PAGE showing Ply purification by affinity chromatography on Ni-Sephrose column.

Lane 1 is the flow through, lane 2 wash fraction, and lanes 3-7 is the elution fractions of Ply after chromatography. The gel was stained with Coomassie blue. Ply runs at ~53 kDa as expected. The protein bands in lane 4-6 is very thick due to presence of high protein concentration.

The fractions containing Ply were pooled and loaded onto a Superdex 200 16/60 gel filtration column. Ply was eluted as a single peak with a mass of ~50 kDa (Figure 2-6 A) based on the elution of known standards indicating that Ply is monomeric in solution as reported previously (Solovyova et al., 2004, Gilbert et al., 1998, Morgan et al., 1993). Figure 2-6 B shows the SDS-PAGE of Ply after gel filtration. A single protein band was observed with no detectable impurities. The overall yield was typically 20 mg of pure protein per 500 ml of culture.

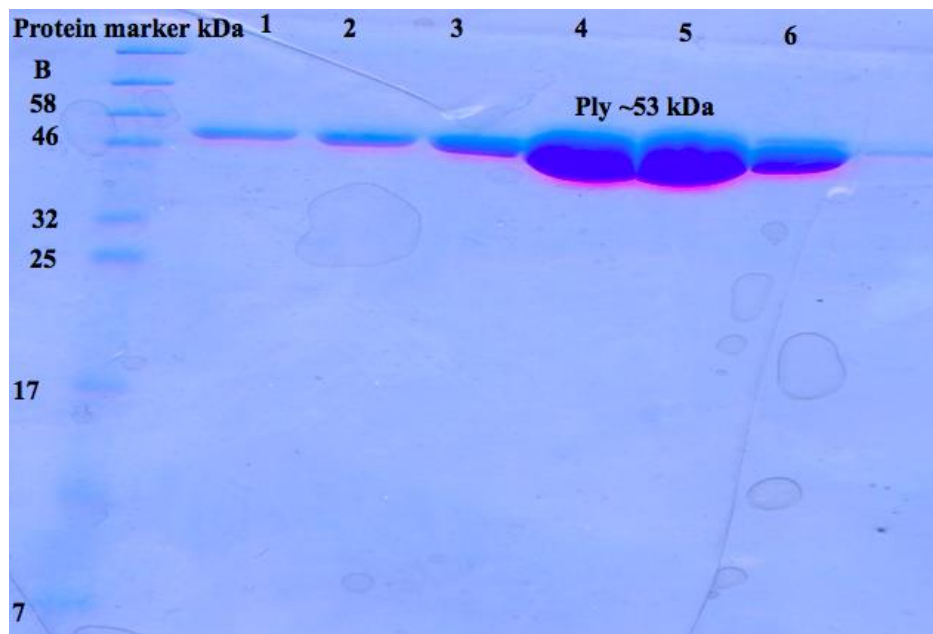
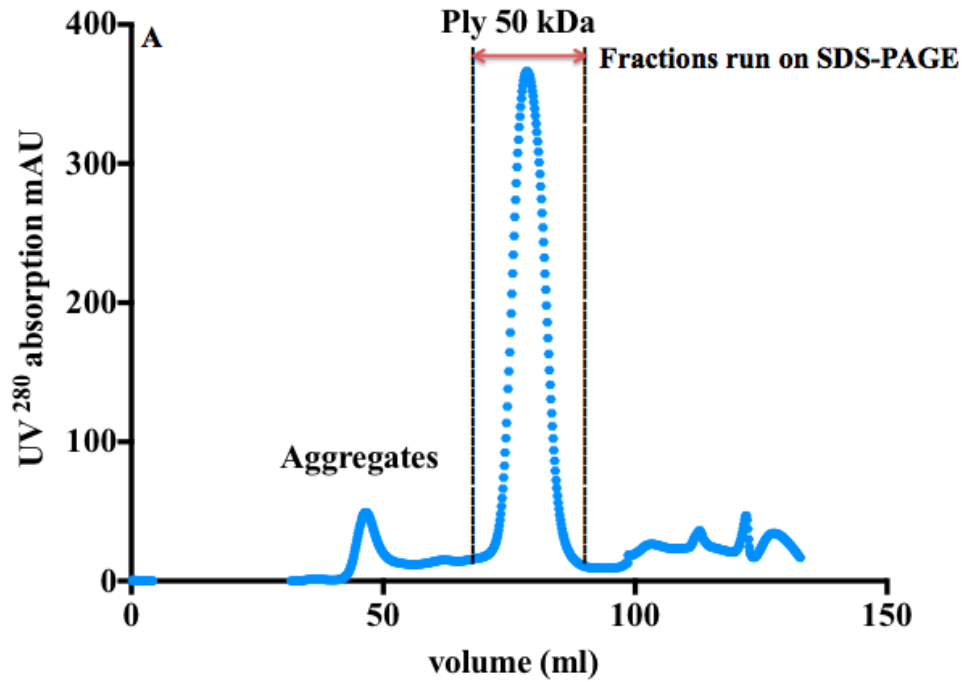


Figure 2-6: Size exclusion chromatography of recombinant full-length Ply on a Superdex 200 16/60 column analysed on a 15% SDS-PAGE gel.

The first peak in A contains aggregates; the main peak is Ply, with an approximate molecular mass of 50 kDa based on the elution position of molecular weight standards. (B) after gel filtration elution fractions were collected from the the main elution peak which labelled in figure A. Lanes 1-6 are fractions collected across the main elution peak which is about 53 kDa. The gel was stained with Coomassie blue.

2.3.2 Cloning, expression and purification of PlyD1-3

PlyD1-3 was produced to help characterize binding between Ply and the IgG isotypes. The gene fragment encoding PlyD1-3 was first amplified from the Ply gene by PCR (Figure 2-7). The mass of the fragment separated on an agarose gel corresponded closely with the expected size of ~1074 bp.

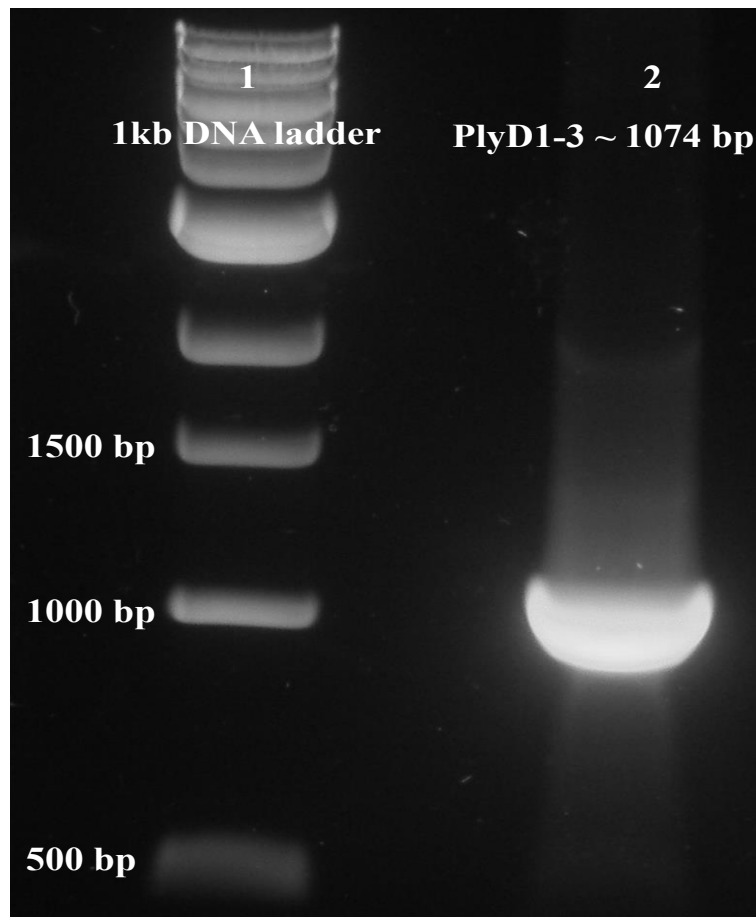


Figure 2-7: Agarose gel showing PCR of PlyD1-3 DNA fragments.

Lane 1 is 1kb DNA ladder lanes 2 is PlyD1-3. The fragment was purified from the gel and cloned into pLEICS-01 expression vector.

The fragment was cloned into pLEICS-01 and sequenced. The resulting expression plasmid was transformed into BL21 (DE3) and test expressions were carried out as described in materials and methods. These preliminary tests showed that PlyD1-3 was expressed in insoluble inclusion bodies (Figure 2-8). These were purified to remove protein, lipid and nucleic acid contaminants and solubilized in 8 M urea. A refolding

screen was then performed to determine the best conditions for refolding, in which PlyD1-3 was diluted into fifteen different buffers as mentioned in materials and methods. Refolding was tested by SDS-PAGE and promising conditions were tested further by gel filtration. Figure 2-9 shows the elution profile of the selected samples from the refolding screens. Although the concentration of protein was very low, peaks of the expected size were observed in three refolding buffers (eluting at ~15 ml from the analytical column).

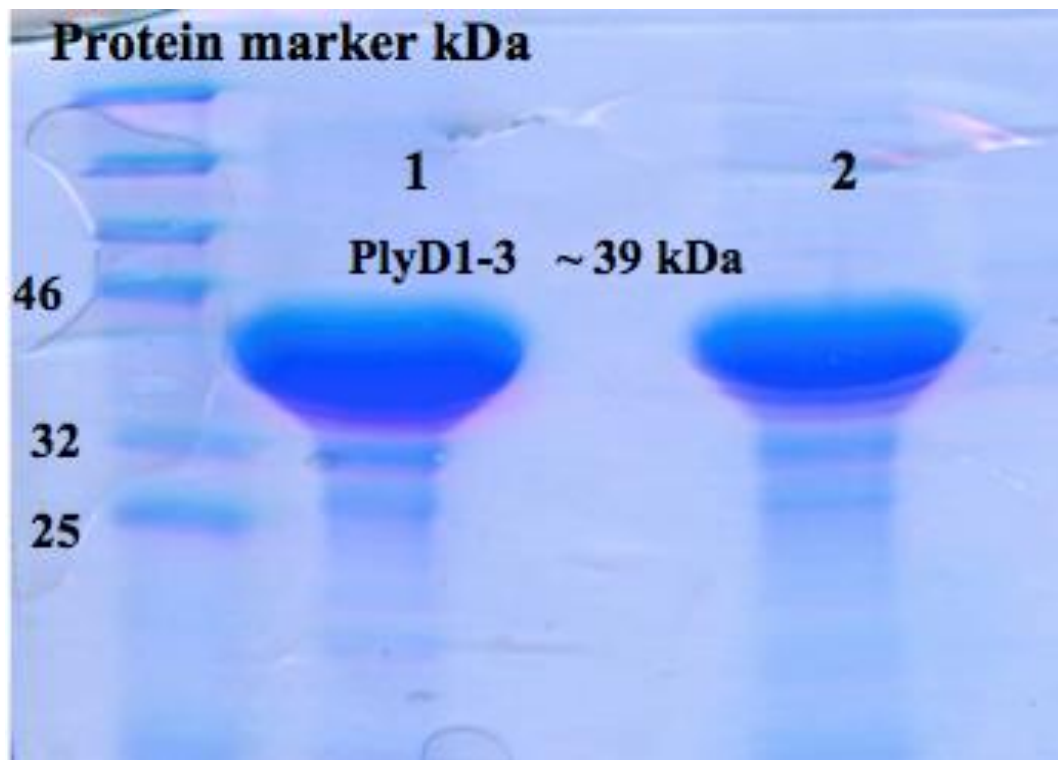
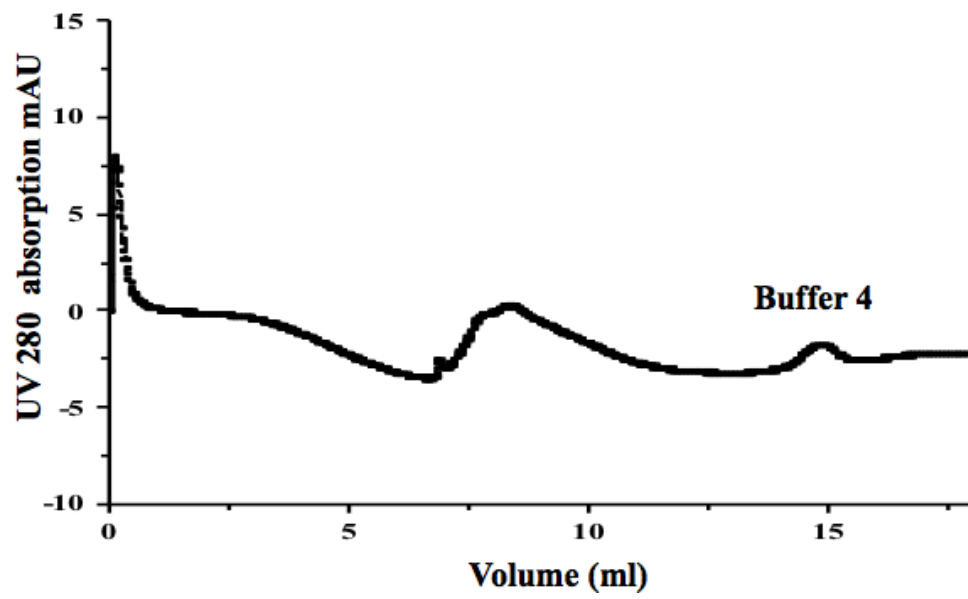
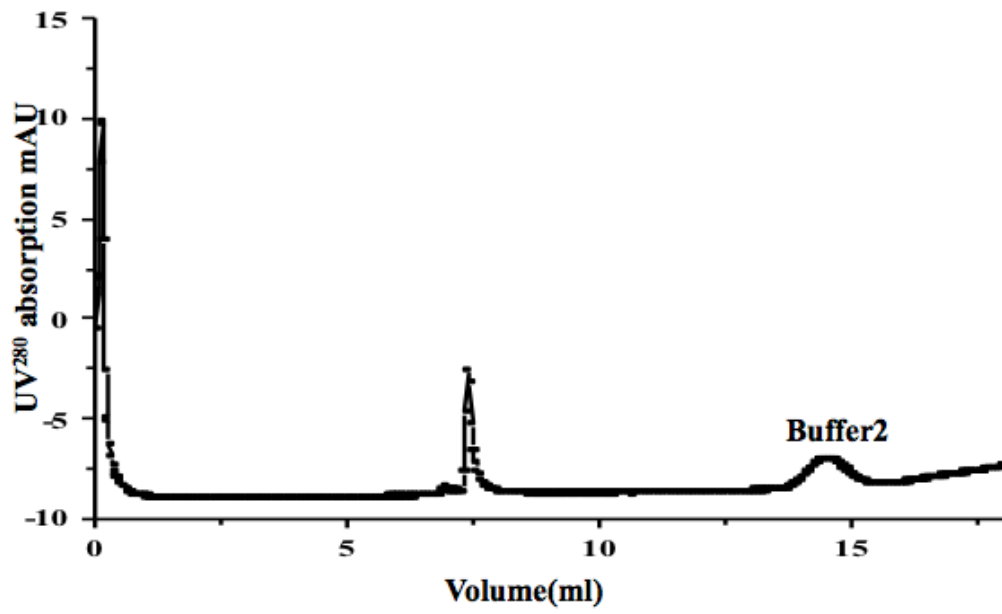


Figure 2-8: 15% SDS-PAGE of small-scale expression of PlyD1-3 in inclusion body.

PlyD1-3 expressed in inclusion body at two different temperatures including 30°C and 37°C. Expressed PlyD1-3 purified and isolated from the *E. coli* cells by Bugbuster. Lane 1 and 2 show purified PlyD1-3 at 30°C and 37°C subsequently.



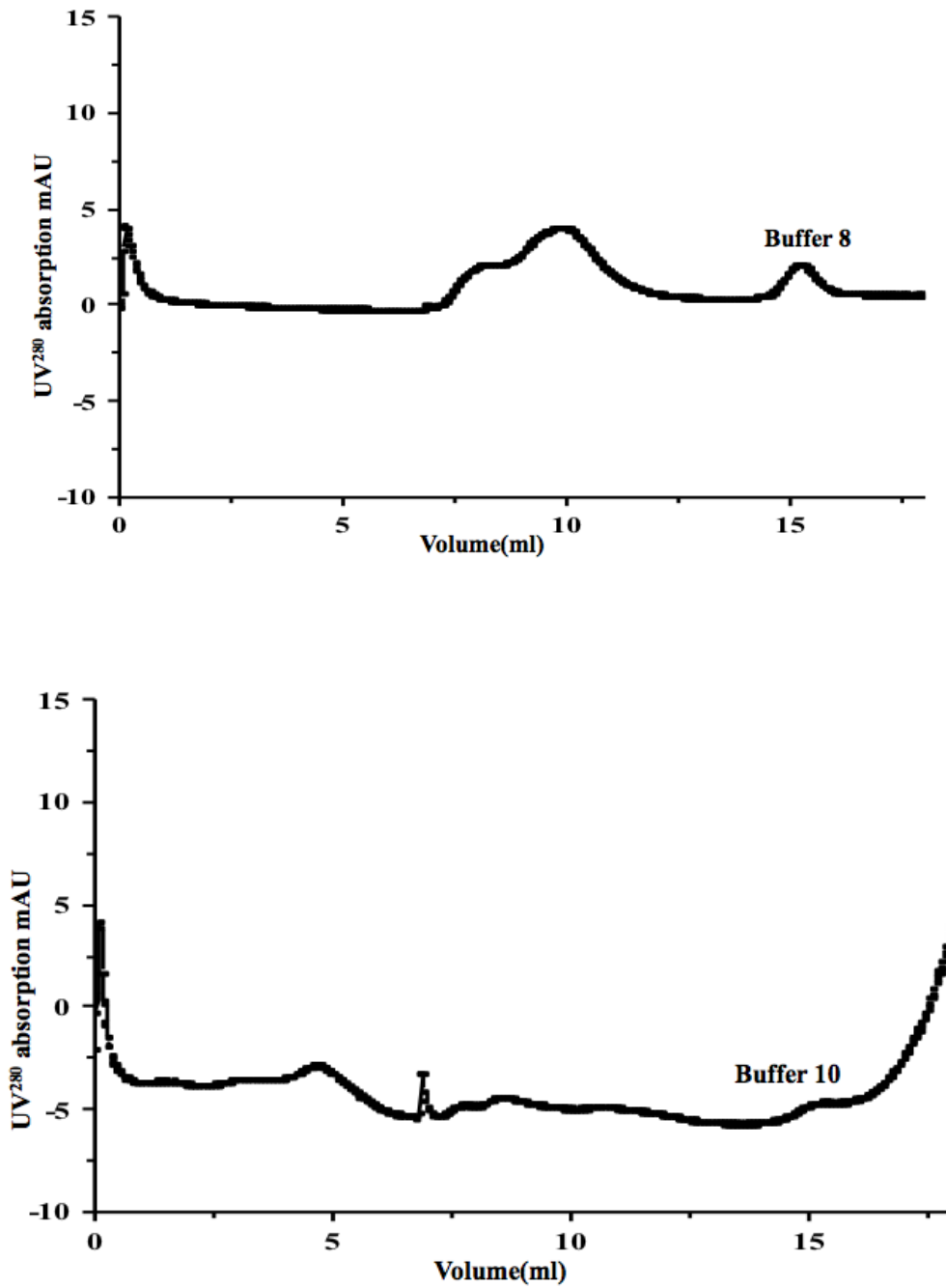


Figure 2-9: Elution profile of the purified PlyD1-3 on Superdex 200 10/300 after refolding screens.

PlyD1-3 refolded in four different buffer samples include 2, 4, 8 and 10 according to the QuickFold™ Protein Refolding Kit. Refolded samples subjected to gel filtration on a Superdex 200 10/300. Small peaks at ~15 ml correspond to PlyD1-3.

After gel filtration on Superdex 200 10/300, each refolded samples were concentrated with Strataclean beads and analysed by SDS-PAGE under reducing conditions (Figure 2-10). PlyD1-3 was refolded successfully in three refolding screen conditions: buffers 2, 4 and 8. This means any of these can be used to refold PlyD1-3.

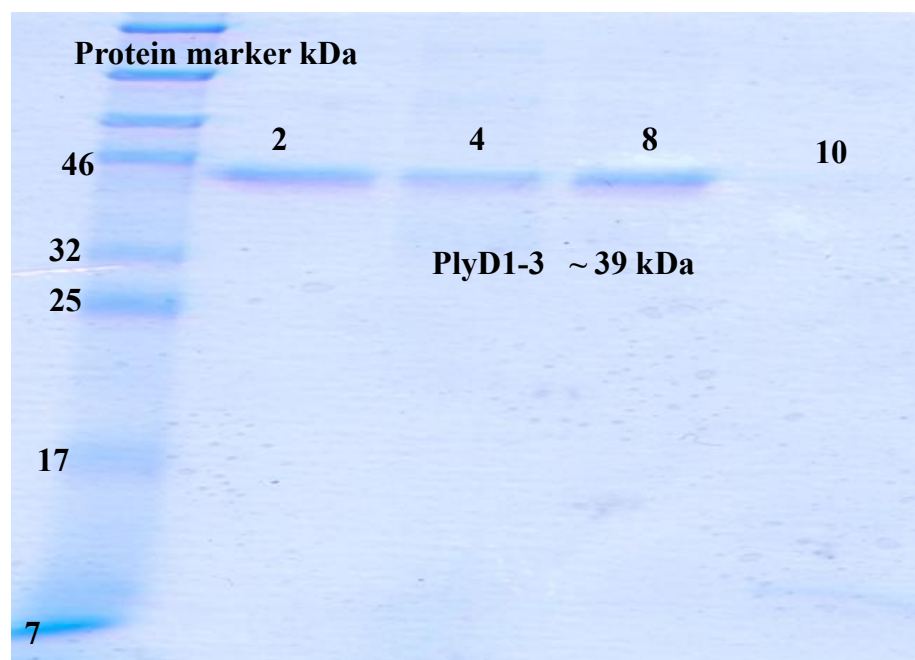


Figure 2-10: Purified refolded recombinant PlyD1-3 after analytical size exclusion chromatography assessed by SDS-PAGE.

After gel filtration samples were concentrated with Strataclean beads. Concentrated samples were resuspended in 5x loading dye and incubated 5 min at 95°C before loading onto the gel. Protein marker was loaded on the left side of the gel and the number of the right side corresponds to the number of the refolding buffer.

For large-scale purification, solubilized inclusion bodies were refolded by drip dilution into buffer 8 (50 mM Tris-HCl pH 8.5, containing 9.5 mM NaCl, 0.4 mM KCl, 2 mM MgCl₂, 2 mM CaCl₂, 0.4 M sucrose, 0.5 Triton X-100, 0.05% polyethylene glycol 3,550, 1 mM GSH, and 0.1 mM GSSH). PlyD1-3 contains 359 amino acid residues (Figure 2-2) and was expressed with an N-terminal His₆ tag, enabling purification by Ni-affinity chromatography (Figure 2-11 A). The sample was eluted from the Ni-Sepharose column with imidazole and further purified by gel filtration on a Superdex 75 16/60 column to remove minor impurities. It eluted as a large peak with a smaller shoulder as labeled with the red circle (Figure 2-11 B). No differences was detected by SDS-PAGE (Figure 2-12) suggesting that the shoulder may represent a dimer. When fractions corresponding to the

main peak or the shoulder were reapplied to the gel filtration column, protein eluted as a single peak at the same position as the main peak, consistent with dimerization at high protein concentrations. Given that full-length Ply is a monomer, removal of domain 4 probably exposes a hydrophobic surface that facilitates self-association. The purity of the protein was checked on 15% SDS-PAGE (Figure 2-12). The expected size of PlyD1-3 is ~39 kDa. Yields of PlyD1-3 were typically 10 mg per litre of culture.

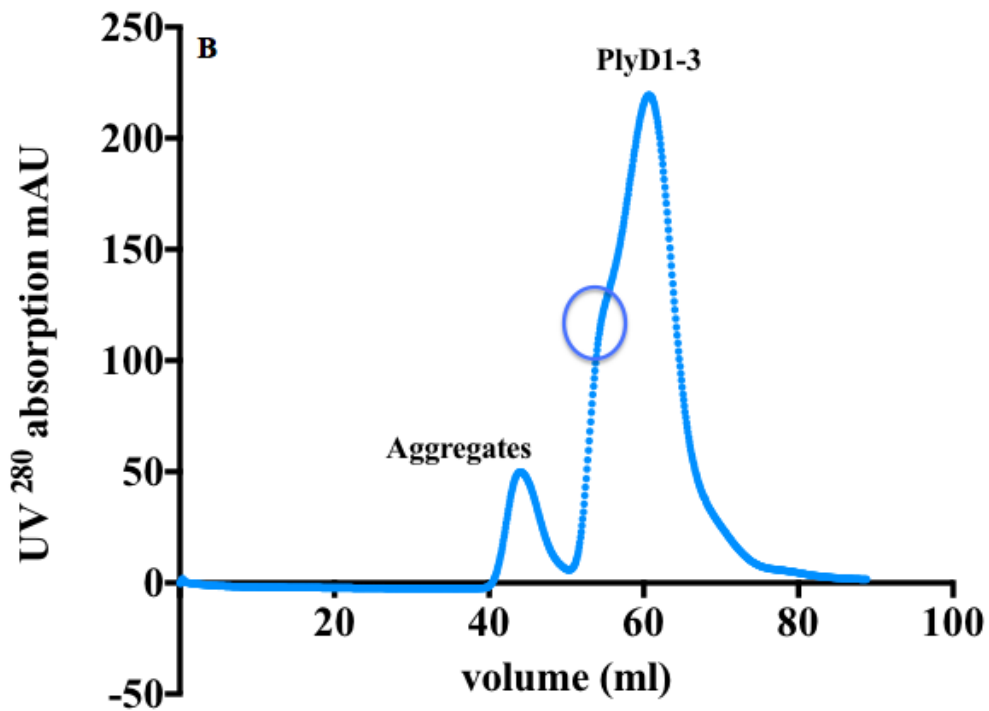
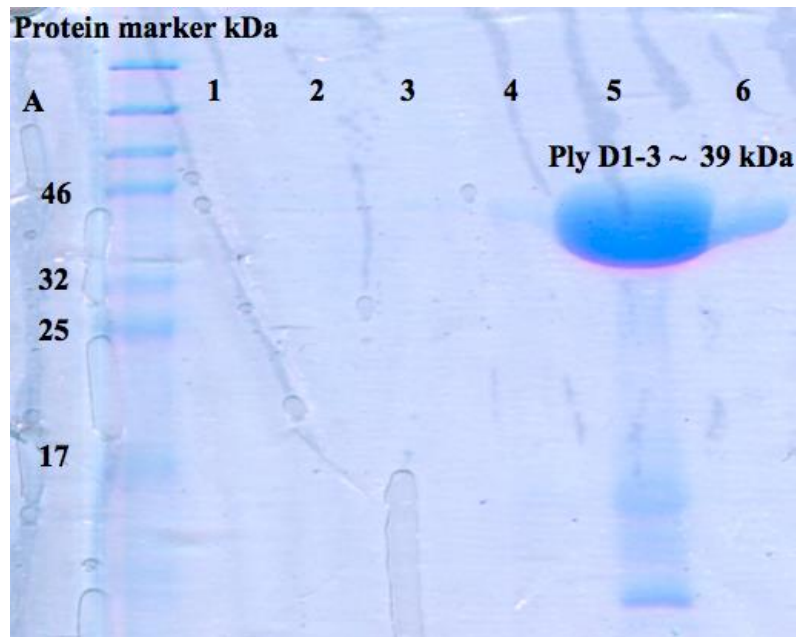


Figure 2-11: 15% SDS-PAGE of PlyD1-3 after purification on Ni-Sepharose column and size exclusion chromatography profile of PlyD1-3 on Superdex 75 16/60 column.

(A) Lane 1 and 2 is the flow through and wash respectively, lane 3-6 is 1ml elution fractions. The expected size of PlyD1-3 is ~39 kDa. (B) Gel filtration profile of the plyD1-3 on a Superdex 75 16/60 column. Peak fractions were collected and analysed by SDS-PAGE. The shoulder on the PlyD1-3 peak is labelled in blue circle.

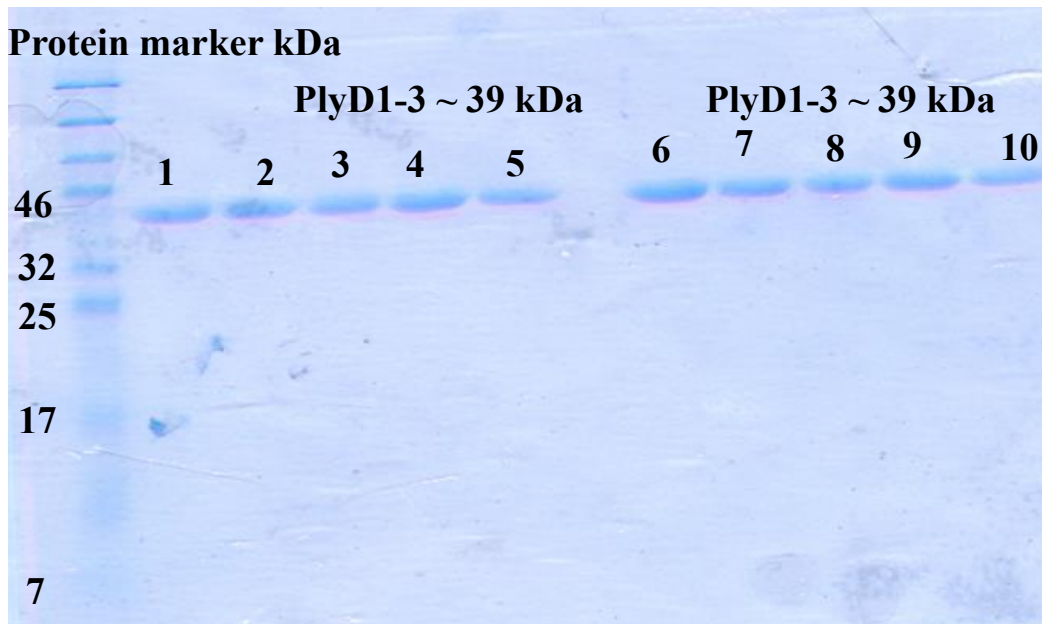


Figure 2-12: SDS-PAGE of purified PlyD1-3 after gel filtration on Superdex 75 16/60.

After gel filtration the elution fractions across the PlyD1-3 peak were collected and run on SDS-PAGE. Lane 1-5 shows the protein without DTT (unreduced), and lane 6-10 shows the protein with DTT (reduced). The expected size of PlyD1-3 is ~39 kDa. The gel was stained with Coomassie blue.

2.3.3 Cloning, expression and purification of PlyD4

PlyD4 is the membrane-binding domain of Ply and comprises residues 360-471 of the full-length protein (Figure 2-2). A gene fragment encoding the domain was amplified, and inserted into pLEICS-10 vector (Figure 2-4). After transformation, colonies only grew on LB agar plates in the presence of 2% of glucose, which reduces the background expression of recombinant proteins from pET-based vectors, suggesting that PlyD4 may be toxic to the BL21 (DE3) cells. Attempts to produce a His-tagged form of PlyD4 were unsuccessful with no soluble protein produced. However, PlyD4 was expressed as a

soluble fusion with an N-terminal MBP tag, which enhances the solubility of the expressed proteins (Nallamsetty et al., 2005). The fusion protein was purified by affinity chromatography on an amylose-Sepharose column (Costa et al., 2014, Fox and Waugh, 2003) and was eluted from the column with 10 mM maltose. The resulting protein was ~53 kDa, with MBP ~42 kDa and PlyD4 ~13 kDa (Figure 2-13). The tag was removed from PlyD4 by overnight digestion with TEV protease and the proteins were separated by gel filtration chromatography on a Superdex 75 16/60 column. PlyD4 eluted from the column as a single peak after 140 ml, much later than expected for its size, probably as a result of weak interaction with the column (Figure 2-14). PlyD4 migrated with a molecular weight of ~13 kDa on SDS-PAGE gels as expected (Figure 2-15).

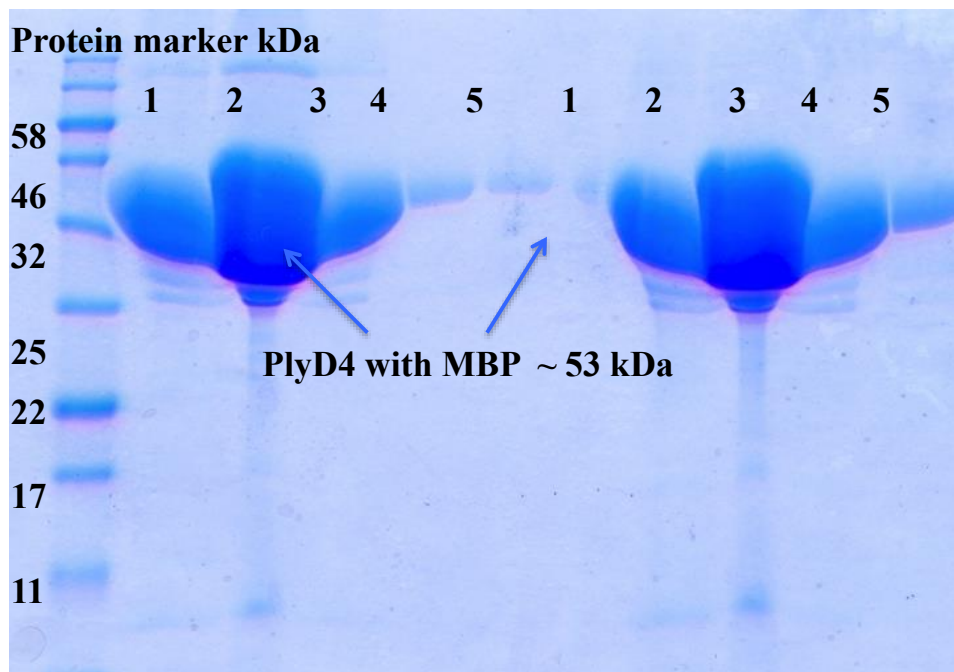


Figure 2-13: 15% SDS-PAGE of purified PlyD4 tagged with MBP after affinity chromatography on amylose resin column.

After chromatography elution fractions were run on the SDS-PAGE. Lane 1-5 of the left side shows elution fraction of the protein that was run under non-reducing condition (without DTT). Lane 1-5 of right side shows same elution fractions of the protein but run under reducing conditions (with DTT). The expected size of PlyD4 with MBP tag is ~53 kDa. The gel was stained with Coomassie blue.

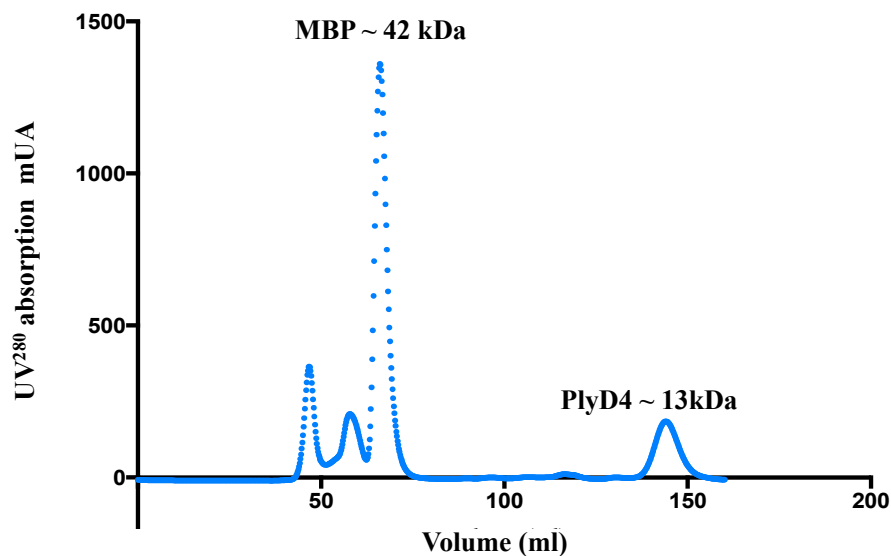


Figure 2-14: Elution profile of PlyD4 after digestion with TEV protease on a Superdex 75 16/60 gel filtration column.

MBP tagged PlyD4 after chromatography digested with TEV protease and run on the gelfiltration column. After digestion the MBP peak is shown high absorbance because it was expressed more than the PlyD4. PlyD4 eluted after 140 ml from the gel-filtration column.

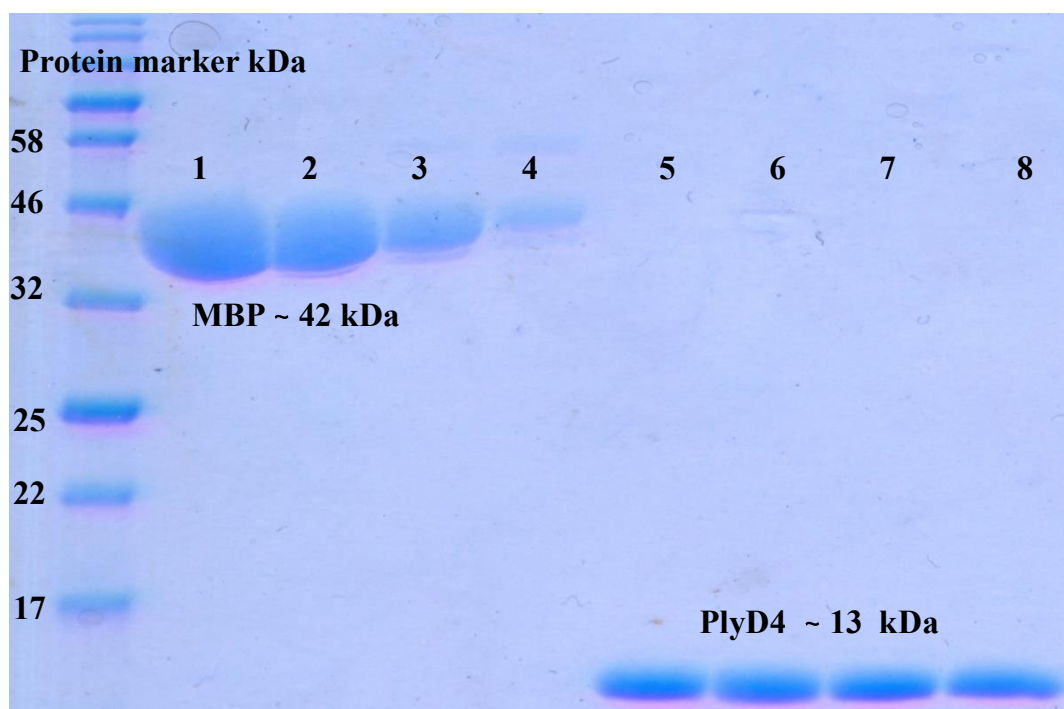


Figure 2-15: 15% SDS-PAGE of purified PlyD4 after digestion with TEV protease on Superdex 75 16/60 gel filtration.

After gel filtration eluted protein across the MBP and PlyD4 peaks were collected and run on the 15% SDS-PAGE. After digestion with TEV the protein split into MBP and PlyD4. Lanes 1-4 is MBP (~ 42 kDa), and lanes 5, 6, 7 and 8 correspond to PlyD4 (~13 kDa).

2.4 Discussion

In the work described in this chapter full-length Ply and Ply fragments comprising domains 1-3 (PlyD1-3) and domain 4 (PlyD4) were cloned, expressed and purified. Previous studies have shown that an N-terminal His₆-tagged protein does not compromise the haemolytic activity of Ply (Wu et al., 2012). Ply migrated with the expected molecular mass on gel filtration indicating that it is monomeric. Based on SDS-PAGE, the purity was >99%, with yields of 20 mg. Unlike the full-length protein, PlyD1-3 was insoluble when expressed in *E. coli* at 37°C. Nevertheless, it was refolded successfully by drop dilution. PlyD1-3 dimerized at high concentrations, probably through the interactions between the exposed interfaces exposed by removal of D4. PlyD4 only expressed well with an N-terminal MBP-tag, which is known to increase the solubility of expressed proteins (Nallamsetty et al., 2005). It eluted from the gel filtration column much later than expected, indicating that it binds to the column matrix. Superdex is made from dextran

covalently attached to highly cross-linked agarose. It has been suggested that D4 may function as a lectin by binding to sLeX (Shewell et al., 2014) and this could explain why it is retained on the column. However, full-length Ply elutes at the expected position on the same column, so the interaction between D4 and Superdex is probably non-specific.

Chapter 3 Interaction of Ply with human L-ficolin and IgG isotypes

3.1 Introduction

Many studies have reported that the CP and the AP of the complement play a crucial role against pneumococcal infections (Hazlewood et al., 1992, Homann et al., 1997, Janoff and Rubins, 1997). The antigenic structure of the pneumococcus activates the CP and the AP of the complement pathways (Paton et al., 1984). For example, the AP is activated by teichoic acid whereas the CP is activated by capsular polysaccharide and Ply (Paton et al., 1984). Brown *et al.* reported that the CP of the complement is the key pathway against the pneumococcus infection in mice (Brown et al., 2002b). Another study has confirmed that the CP is vital for complement-mediated phagocytosis of the pneumococcus. In this work, C2 deficiency increases susceptibility to the pneumococcus (Yuste et al., 2008). CP and AP play a critical role in host defense against the pneumococcus during the early stage of OM (Li et al., 2012). C1q interacts with pneumococcal surface-exposed proteins directly, even in the absence of specific antibodies and mediates binding to host cells (Agarwal et al., 2013). A recent study reported that mouse strain deficient in MASP-2 was highly susceptible to pneumococcal infection and it was not able to opsonize pneumococcus. However, that mouse strain was able to activate both CP and AP of the complement. This suggests that the LP is also important against pneumococcus infection as well as the CP and the AP (Ali et al., 2012).

Studies have reported that Ply activates complement directly. By directing complement activation away from the bacterium itself, this activity may reduce deposition of C3b on its surface (Yuste et al., 2005, Paton et al., 1984). It has been suggested that complement activation on Ply occurs via the CP and the LP. A direct interaction between C1q and Ply has been proposed due to similarity between PlyD4 and C-reactive protein (CRP), which itself activates the CP (Mitchell et al., 1991). However, Ali *et al* (2013) reported that complement activation depends on the presence of the IgG, suggesting that C1q may not bind to Ply directly. The most recent data suggested that Ply activates the CP via IgG3 and IgM (Ali et al., 2013). L-ficolin was also identified as binding to Ply (Ali et al., 2013). Furthermore, in C1q-deficient human serum Ply activated complement via the LP suggesting that L-ficolin is likely to be the recognition molecule responsible for

activation. No activation was detected in C1q-deficient mouse serum and ficolin-A did not bind to Ply (Ali et al., 2013). The pneumococcus evades complement via several different mechanisms. For example, the pneumococcus prevents binding of C4b and Factor H to its surface, thus reducing the function of both classical and alternative pathways (Li et al., 2012). The capsular polysaccharide prevents binding of IgG and CRP, thereby reducing CP activity, and reducing the AP activity through decreasing the degradation of C3b (Hyams et al., 2010). In addition, direct binding of C1q with pneumococcal endopeptidase O attenuates the CP to facilitate pneumococcal escape (Agarwal et al., 2014). Ply itself can activate the CP (Paton et al., 1984). This activation may prevent host defense against the pneumococcus by depleting components from serum (Boulnois et al., 1991).

3.2 Objectives

Ali *et al* (2013) reported that Ply interacts with the human L-ficolin in the serum. This chapter will focus on the interaction between Ply and L-ficolin. Recombinant proteins (Ply and L-ficolin) were used to measure the interaction between them. Because Ply has been implicated in binding to IgG to initiate the activation of CP, this chapter also focuses on determining the molecular interaction between Ply and IgG isotypes.

3.3 Materials and methods

3.3.1 Materials

DNA restriction enzymes and T4 DNA ligase were obtained from New England Biolabs. Promega supplied pGEM-T easy cloning vectors and acetylated BSA. DXB11 CHO cells line, pED4, and pET28a, were kindly provided by Prof. Russell Wallis (Lab 218 MSB Leicester University). Tissue culture media including Minimal Essential Media α with and without nucleosides (MEM α^+ , MEM α^-), CHO-S-SFMII and phosphate buffered saline (PBS) were purchased from Life Technologies. Bovine serum albumin (BSA), carbonate/bicarbonate buffer, anti-human IgG conjugated with alkaline phosphatase, anti-human L-ficolin and p-nitrophenyl phosphate disodium salt (pNnp), dialyzed heat fetal bovine serum (DHFBS), methotrexate (MTX), Penicillin/Streptomycin (P/S), Trypsin EDTA (10X TE), N-acetyl glucoseamine (GlcNAc), calf-thymus DNA, dimethyl sulfoxide (DMSO), and 5-bromo-4-chloro-3-indolyl- β -D-galactoside (X-Gal) were purchased from Sigma. Tissue culture flasks were purchased from Thermo Fisher Scientific and Nunc. Oligonucleotide primers were from Eurofins Genomics. IgG

isotypes were supplied by Athens Research & Technology. Qiagen supplied DNeasy blood and tissue kits.

3.3.2 PCR amplification of the L- ficolin cDNA

DNA was extracted from DXB11 cells previously transfected with L-ficolin cDNA provided by Prof. Wilhelm Schwaeble at Leicester University using the DNeasy blood and tissue kit. Full-length L-ficolin was amplified and assembled using different sets of primers (Table 3-1).

Table 3-1: Sequence of oligonucleotides using in the cloning of the human L-ficolin.

Restriction sites (*PstI* and *EcoRI*) are underlined, start and stop codon are in bold and an optimised Kozak sequence, to facilitate better levels of gene expression, was put before the start codon and is highlighted in red. F represents forward and R is reverse.

| Primer | Sequence 5'-----3' |
|--------------------------|---|
| L-ficolin <i>pstI</i> F | GACATC <u>CTGCAG</u> GCCACC ATG gagctggacagagct |
| L-ficolin <i>EcoRI</i> R | GTCATC <u>GAATTC</u> CTAG gcaggctgcacctt |
| L-fic mat F | ctccaggcggcagacacctgtccagaggtga |
| L-fic colfib F | aacggagcacctggggagccccagccg |
| L-fic colfib R | cggctggggctccccaggtgctccgtt |
| L-fic Sig F1 | tgggcgtgccaccctgctgctctcttcttctggcatggcctgggctctccaggcggcagaca cct |
| L-fic Sig F2 | <u>CTGCAG</u> GCCACC ATG gagctggacagagctgtgggggtcctg ggcgtgccaccct |

3.3.3 Cloning of full-length L-ficolin into pGEM-T easy vector

The amplified L-ficolin cDNA was initially cloned into pGEM-T easy cloning vector. An A-tail was added to the blunt-ended PCR product by incubating 10 µl of the PCR product with 5U Taq DNA polymerase, 0.1 mM dNTP and 2 µl 10 x Taq polymerase buffer and 1 µl of MgCl₂ (0.75 mM) at 70°C for 30 min. 3 µl of the mixture was then added to 1 µl

of pGEM-T easy vector (0.05 µg), 5 µl 2 x rapid ligation buffer, and 1 µl T4 DNA ligase (3 Weiss units) and incubated at 4°C overnight. The ligated product was introduced into competent XL10 cells by transformation, as described in section 2.2.3. Cells were plated onto LB agar (LBA) plates containing 100 mM IPTG, 50 mg/ml X-Gal plates and 100µg/ml ampicillin. White colonies, containing the inserts were used to inoculate 1.5 ml of LB broth containing 100 µg/ml ampicillin and incubated overnight at 37°C. Plasmids were isolated using Qiagen plasmid mini kit. Constructs containing the insert were sequenced by the PNAACL facility at Leicester University.

3.3.4 Cloning of full-length L-ficolin into pED4

The mammalian expression vector pED4 (10 µg) was digested by mixing 44 µl of pED4 with 4 µl *EcoRI* and 4 µl *PstI*, 3 µl BSA, 30 µl NEB buffer 3 and 215 µl H₂O and incubating for 3 hr at 37°C. The product was separated on a 1% w/v agarose gel in TBE buffer and extracted and purified from the gel using a Qiaex II gel extraction kit. A fragment encompassing the entire L-ficolin cDNA was digested with the same enzymes. For ligation, 0.5 µg of digested pED4 was mixed with the cDNA at different molar ratios together with 1 µl of 10 x ligase buffer, 1 µl of T4 DNA ligase and water in a 10 µl reaction and incubated at 4°C overnight. Each ligation reaction was transformed into XL10 cells and plated onto LBA containing 100µg/ml ampicillin. Individual colonies were grown up in 1.5 ml LB broth containing 100 µg/ml ampicillin, plasmid DNA was extracted and the presence of the insert was confirmed by restriction digestion with enzymes *EcoRI/PstI* followed by DNA sequencing performed by PNAACL.

3.3.5 Expression vector pED4

The mammalian expression vector pED4 (Figure 3-1) expresses the gene of interest as a dicistronic mRNA along with the dihydrofolate reductase (*DHFR*) gene. *DHFR* is required for the synthesis of purines, thymidine, and certain amino acids and is used as a selectable marker in the *DHFR*-deficient CHO cell line, DXB11. Following transfection into DXB11 cells, only those cells containing the pED4 vector are able to grow in the absence of external nucleotides. Expression of the gene of interest can be further increased by selection of transfected cells in increasing concentrations of MTX, an inhibitor of dihydrofolate reductase, up to 0.5 µM (Kaufman et al., 1991).

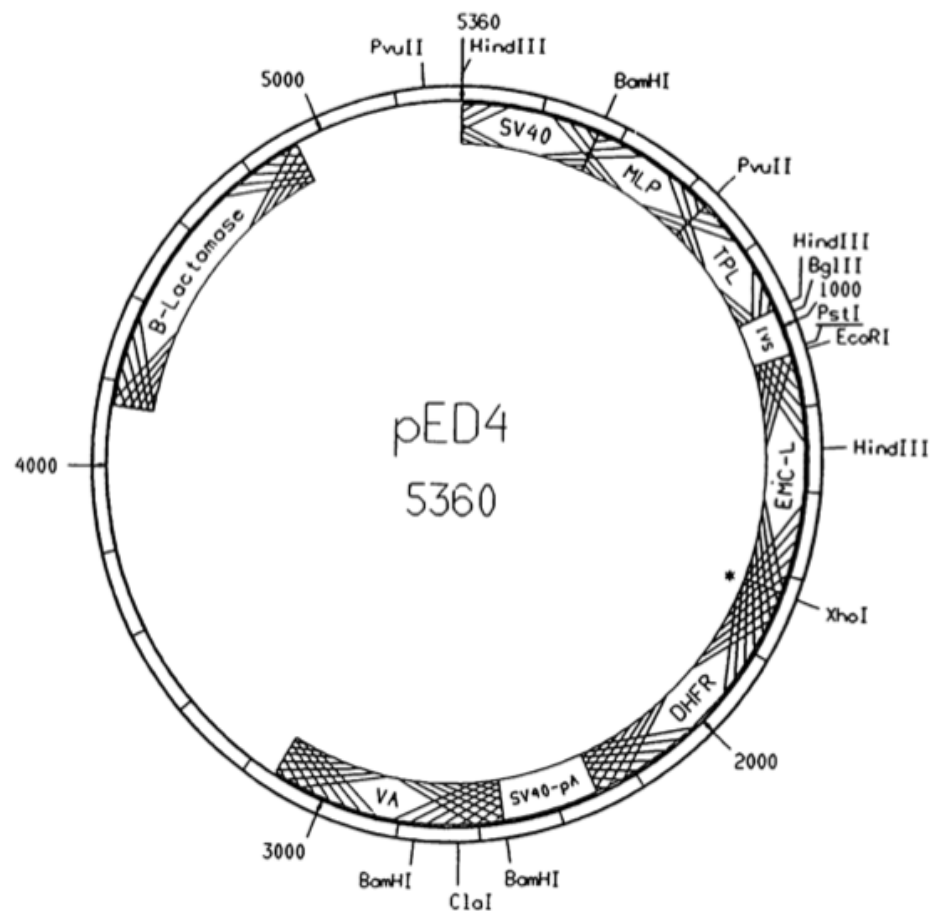


Figure 3-1: Map of a pED4 expression vector.

This vector is a discistronic mRNA expression vector of 5360 bp, containing the *DHFR* gene as a selectable marker and the B-lactamase gene conferring ampicillin resistance for selection in bacteria. The L-ficolin gene was cloned into the *PstI/EcoRI* sites within the polylinker region (Kaufman et al., 1991).

3.3.6 Cell culture

DXB11 cells, which are deficient in the *DHFR* gene, were used to express L-ficolin (Urlaub and Chasin, 1980). Two days before the transfection the DXB11 cell line was grown in minimal essential medium containing nucleosides (MEM α +) with 10% v/v DHFBS and P/S at final concentrations of 500 units/ml and 500 μ g/ml respectively. Cells were grown in Nunc tissue culture flasks (25 cm²) at 37°C with 5% CO₂.

3.3.7 DNA precipitation

DNA was precipitated by adding 1/10 volume of 3 M sodium acetate pH 5.2 and two volumes of 100% cold ethanol. The mixture was incubated on dry ice for 15 min and the DNA pelleted by centrifugation for 15 min at 13000 rpm in a microcentrifuge. The pellet was washed in 1 ml of 70% cold ethanol and dried in the tissue culture laminar flow cabinet for 15-30 min under sterile conditions.

3.3.8 Transfection of mammalian cells by the calcium phosphate method

The recombinant plasmid was introduced into DXB11 CHO cells by transfection using the calcium phosphate method (Graham and van der Eb, 1973). In this method the DNA binds to the calcium phosphate and can enter to the eukaryotic cells by endocytosis. Briefly, the DNA together with 100 μ l of 10 mg/ml calf thymus DNA was diluted in 1 ml of sterile ddH₂O containing 120 μ l of 2 M CaCl₂ in a 15 ml falcon tube. This was mixed with 1 ml of 2 x HEPES buffered saline pH 7.1 (HBS; 0.5g HEPES, 0.8 g NaCl/50 ml) and 40 μ l 100 x phosphate buffer (70 mM Na₂HPO₄ and 70 mM NaH₂PO₄). The mixture was left for 30 min at room temperature to allow a precipitate to form. 1 ml was added to 50% confluent DXB11 cells in MEM α + medium containing 10% v/v DHFBS and P/S in a (25 cm²) flask, and incubated overnight. The next day, cells were washed with PBS at pH 7.2 and the MEM α + medium was replaced. Cells were incubated overnight until they reached confluence. The cells were trypsinized and resuspended in MEM α - containing 10% v/v DHFBS, with P/S. Media (200 μ l) was added to each well of a 96 well tissue culture plate and incubated for 2 weeks at 37°C with 5% CO₂. When the clones had reached confluence, they were transferred to 24 well plates (Nunc). Cells were passaged into MEM α - containing 10% v/v DHFBS, with P/S and increasing concentrations of MTX up to 0.5 μ M.

3.3.9 Expression and purification of full-length L-ficolin

L-ficolin was purified from the cell line as described previously for MBL (Wallis and Drickamer, 1999). The cells were grown in 3 layered tissue culture flasks in MEM α - containing 0.5 μ M MTX, 10% v/v DHFBS with P/S. Once the cells were fully confluent, the media was replaced with CHO-S-SFM II without nucleosides containing 50 mM HEPES, pH 7.55 as an additional buffer during the cell growth, 0.5 μ M MTX and P/S. Media was harvested every other day, spun at 1500 rpm for 2 min to remove any cell debris and stored at -20°C. L-ficolin was purified by affinity chromatography on a

GlcNac-Sepharose column. Culture media (500 ml) was diluted with an equal volume of high salt loading buffer (25 mM Tris-HCl pH 7.5, 1 M NaCl and 10 mM CaCl₂). This was loaded onto a 2 ml GlcNac-Sepharose column that was equilibrated with the same buffer. The column was then washed with high and low-salt loading buffer (25 mM Tris-HCl pH 7.5, 150 mM NaCl and 5 mM CaCl₂). Protein was eluted with 25 mM Tris-HCl pH 7.5, 150 mM NaCl containing 300 mM GlcNac. Purified protein was dialyzed to remove GlcNac in 20 mM Tris-HCl pH 7.5 and 150 mM NaCl. Yields were ~0.35 mg from 1 liter of culture medium. The amino acids sequence of L-ficolin is shown in (Figure 3-2).

```

      10      20      30      40      50      60
MELDRAVGVL GAATLLLSFL GMAWALQAAD TCPEVKMVGL EGSDKLTILR GCPGLPGAPG

      70      80      90      100     110     120
PKGEAGTNGK RGERGPPGPP GKAGPPGPNG APGEPQPCLT GPRTCKDLLD RGHFLSGWHT

     130     140     150     160     170     180
IYLPDCRPLT VLCMDTDGG GWTVFQRRVD GSVDFYRDWA TYKQGFGRSL GEFWLGNDNI

     190     200     210     220     230     240
HALTAQGTSE LRVDLVDFED NYQFAKYRSF KVADEAEKYN LVLGAFVEGS AGDSLTFHNN

     250     260     270     280     290     300
QSFSTKDQDN DLNTGNCAVM FQGAWWYKNC HVSNLNGRYL RGTHGSFANG INWKSQKGYN

     310
YSYKVSEMKV RPA

```

Figure 3-2: Amino acids sequence of human L-ficolin.

The signal sequence is shown in blue, the N-terminal domain in black, the collagen-like domain in green and the fibrinogen-like domain in red.

3.3.10 Cell storage

Transfected cells were stored by mixing 1ml of trypsinized cells from a 25 cm² flask with 2 ml DHFBS containing 10% v/v DMSO. The cells were split into two 1ml cryovials and frozen in dry ice. Cells were stored at -196°C.

3.3.11 Cloning, expression and purification of the fibrinogen-like domain of L-ficolin

3.3.11.1 Amplification of the cDNA encoding the fibrinogen-like domain of L-ficolin

The cDNA encoding the fibrinogen-like domain of L-ficolin was amplified using primers shown in (Table 3-2). The DNA was separated on a 1% agarose gel and the DNA fragment excised and purified. The PCR product was cloned into the pGEM-T easy vector as described in section 3.3.3 and the sequence was verified by PNACL. The cDNA fragment was then digested with *Nco1/EcoR1* and cloned into the polylinker region of the expression vector pET28a (Figure 3-3) and digested with the same restriction enzymes. The resulting plasmid was sequenced by PNACL.

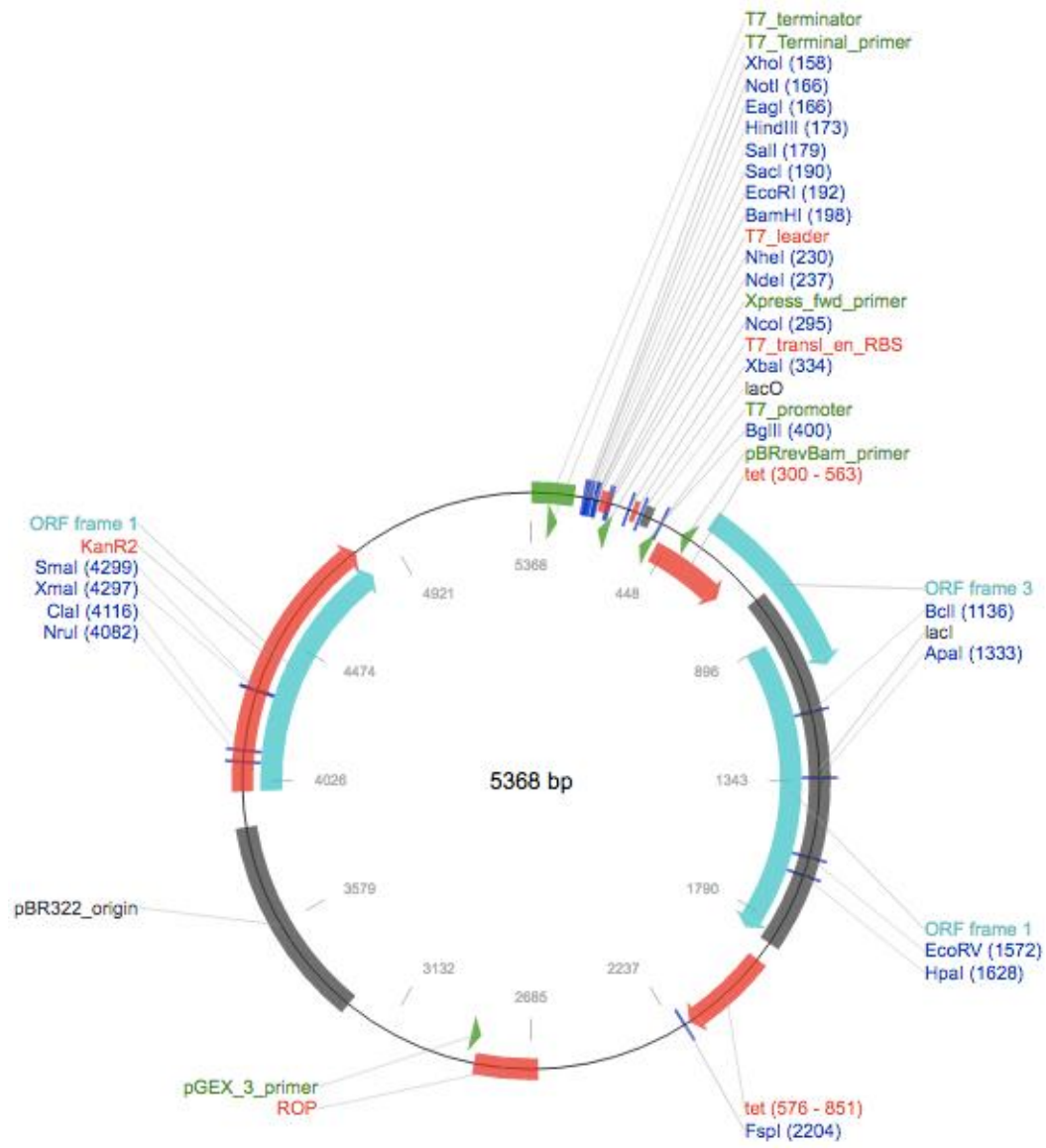


Figure 3-3: Map of the bacterial expression vector pET28 a.

This vector is 5368 bp and contains the kanamycin antibiotic resistance gene as a selectable marker. The cDNA encoding the fibrinogen-like domain was cloned into *NcoI/EcoRI* restriction sites.

Table 3-2: Oligonucleotide sequences used to amplify the cDNA encoding the fibrinogen-like domain of L-ficolin.

The restriction sites are underlined, start and stop codon are highlighted in red. The sequence encoding the His-tag on the forward primer is in bold. F and R represent forward and reverse respectively.

| Primer | Sequence 5'-----3' |
|--------------------------|--|
| L-ficolin N His fib F | agctag <u>CCATGGCT</u> catcatcaccatcaccac cccagcccgctgacctgac |
| L-ficolin <i>EcoRI</i> R | cgatca <u>GAATTCCTAG</u> gcaggctgcacctt |

3.3.11.2 Expression and purification of the fibrinogen-like domain of L-ficolin

The protein was expressed as inclusion bodies and refolded by drip dilution as described in section 2.2.13. Refolded protein was purified by affinity chromatography on a 2 ml Ni-Sepharose column pre-equilibrated with 25 mM Tris-HCl pH 7.4, 150 mM NaCl and 20 mM imidazole. After loading, the column was washed with 25 mM Tris-HCl pH 7.4, 150 mM NaCl and 20 mM imidazole. Protein was eluted from the column with the same buffer containing 500 mM imidazole. Protein was further purified by gel filtration on a Superdex 75 16/60 column, equilibrated with the 50 mM Tris-HCl pH 7.4, 150 mM NaCl, 50 mM GlcNAc and 2 mM EDTA.

3.3.12 ELISA binding between Ply and L-ficolin

Flat-bottomed Nunc Maxisorp plates (Nunc) were coated with 5 µg/ml (100 µl) of Ply in coating buffer (0.3 M NaHCO₃, 0.2 M Na₂CO₃ at pH 9.6) and left at 4°C overnight. Acetylated BSA and BSA were used as positive and negative controls respectively. Wells were blocked with 1% w/v BSA in Tris-buffer saline (TBS; 10 mM Tris-HCl pH 7.4, 140 mM NaCl) and left at room temperature for 1 hr. Then 100 µl of 2-fold serially diluted serum was added in BBS buffer (4 mM barbital, 145 mM NaCl, 2 mM CaCl₂, and 1 mM MgCl₂ pH 7.4). Separate experiments were carried out using purified L-ficolin as the soluble ligand. The plates were allowed to stand at room temperature for 1 hr. Binding was detected using (1/2000) rabbit polyclonal or monoclonal anti L-ficolin antibodies. After 1hr at room temperature the secondary antibody conjugated to alkaline phosphatase was added (1/5000 either anti-rabbit or anti-mouse IgG) and incubated at room temperature for 1hr. The substrate pNnp (100 µl; 1 mg/ml) was added to each well and incubated for 15 min at room temperature. Absorbance was measured at 405 nm. Wash

steps were carried out three times using 200 μ l of wash buffer (10 mM Tris-HCl pH 7.4, 140 mM NaCl, 5 mM CaCl₂, 0.05% v/v Tween 20) and plates were dried upside down on paper towels.

3.3.13 ELISA binding between Ply and IgG isotypes

Nunc Maxisorp microtiter plates were coated with 100 μ l ligand at 5 μ g/ml (either Ply, PlyD1-3, PlyD4 or BSA) in coating buffer (0.3 M NaHCO₃, 0.2 M Na₂CO₃ at pH 9.6) and incubated at 4°C overnight. The plate was blocked with 200 μ l/well of 1% w/v BSA in PBS and allowed to stand at room temperature for 1 hr. Next, two-fold serial dilutions of the IgG isotypes, the Fab or Fc fragments were added in PBS. Plates were allowed to stand at room temperature for 1hr. Binding was detected with anti-human IgG conjugated with alkaline phosphatase and incubated for 1hr at room temperature. Finally, (100 μ l; 1mg/ml) substrate pNNp was added and the absorbance was read at 405 nm. The plate was washed three times with washing buffer after each binding step as described above.

3.3.14 Inhibition assay

Plates were coated with Ply and blocked with 1% BSA as described above. Serial dilutions of Ply (starting at 1mg/ml; 50 μ l) were mixed with IgG Fab and Fc (50 μ l; 200 μ g) and incubated for 10 min before transfer to the coated wells. The resulting samples were incubated at room temperature for 1hr. After washing, wells were incubated with anti-human IgG followed by substrate pNNp. Absorbance was read at 405 nm. Graph pad prism 7 programme was used to make the figures. The data was analyzed in prism programme by choosing Nonlinear regression, Dose response curves - Inhibition and then the equation [Inhibitor] vs. response -- Variable slope]. To find the IC₅₀ of inhibition. The equation is $Y = \text{Bottom} + (\text{Top} - \text{Bottom}) / (1 + ((X^{\text{HillSlope}}) / (\text{IC}_{50}^{\text{HillSlope}})))$.

3.3.15 IgG4 digestion with IdeS enzyme

IgG4 (4 mg Human Myeloma Plasma, Kappa) was prepared in 20 mM phosphate buffer pH 7.4, 150 mM NaCl and 0.05% sodium azide. For each 1 mg of IgG4, 1000 units of IdeS (IgG-degrading enzyme from *Streptococcus pyogenes*) was added and the mixture was incubated for 5 hr at 37°C and overnight at 4°C. IdeS was prepared in ddH₂O according to GENOVIS instruction (A0-FRI-050) at 67 units/ μ l. After digestion, the Fab and Fc regions were separated by gel filtration on a Superdex 200 16/60 column. Fractions were analyzed by SDS-PAGE. Fab and Fc fragments were concentrated to 3 mg/ml and 1.8 mg/ml stored at -80°C.

3.4 Results

A previous study has reported that Ply binds to L-ficolin to activate the LP pathway of complement (Ali et al., 2013). To characterize this process in more detail, I produced recombinant full-length L-ficolin and smaller fragment encompassing the fibrinogen-like domain. The advantage of using recombinant proteins rather than purifying the ficolin from serum is that preparations are free from contamination by serum components including complement components.

3.5 Cloning, expression and purification of L-ficolin

3.5.1 PCR amplification of full-length L-ficolin

PCR was used to amplify the cDNA encoding the full-length L-ficolin. Initial attempts to clone the full-length cDNA were unsuccessful because the template lacked a functional signal peptide. PCR1 was carried out with (L-ficolin *pst1* F and L-fic colfib R) primers to check the presence of signal peptide in the cDNA, no band appeared (Table 3-1 and Figure 3-4). PCR2 (~249 bp) was carried out to check the existence of mature sequence in the cDNA with (L-fic mat F and L-fic colfib R) (Table 3-1 and Figure 3-4). In order to generate the full-length cDNA, multiple steps were used. PCR3 was performed to amplify the DNA encoding the N-terminal, collagen and fibrinogen-like domains of L-ficolin; the product was approximately 1kb as expected (Figure 3-4). This was then used as a template for adding the signal peptide (incorporated within the primer Lfic Sig F1) in PCR4. The product was used as a template to generate PCR5 (~1 kb), which encodes the full-length L-ficolin with signal peptide (Figure 3-4).

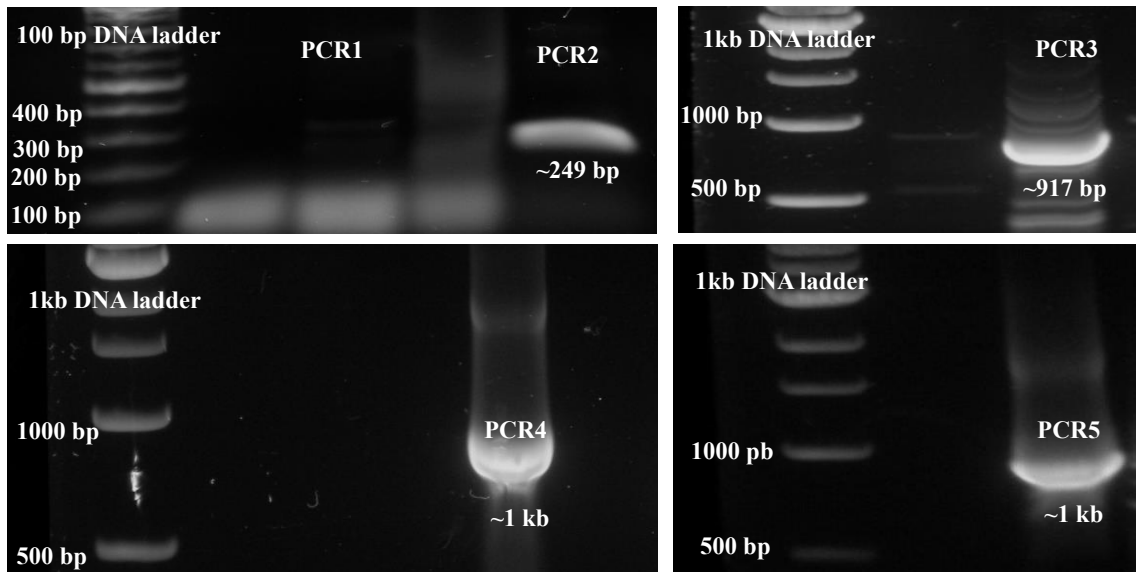


Figure 3-4: 1% w/v agarose gel electrophoresis showing PCR steps to amplify cDNA of the L-ficolin.

PCR1 and 2 were used to analyse the L-ficolin cDNA in the template cell line with (L-ficolin *pst1* F and L-fic colfib R) primers. No product was detected in PCR1 indicating that the ficolin lacked a signal sequence. PCR2 (~249 bp) was carried out with (L-fic mat F and L-fic colfib R) confirmed that the L-ficolin cDNA was present in the cell line. In PCR3 the N-terminal, collagen and fibrinogen-like domains were amplified but minus the signal peptide. In PCR 4 and 5 a functional signal sequence was added and the full length L-ficolin cDNA was amplified with both Lfic Sig F1 and Lfic SigF2.

The final L-ficolin PCR product was A-tailed and cloned into the cloning vector pGEM-T easy vector (Figure 3-5 A). A *PstI/EcoRI* fragment encompassing the entire gene was then inserted into pED4. Clones were confirmed by restriction digestion (Figure 3-5 B) and sequenced to ensure that no mutations were introduced by the PCR.

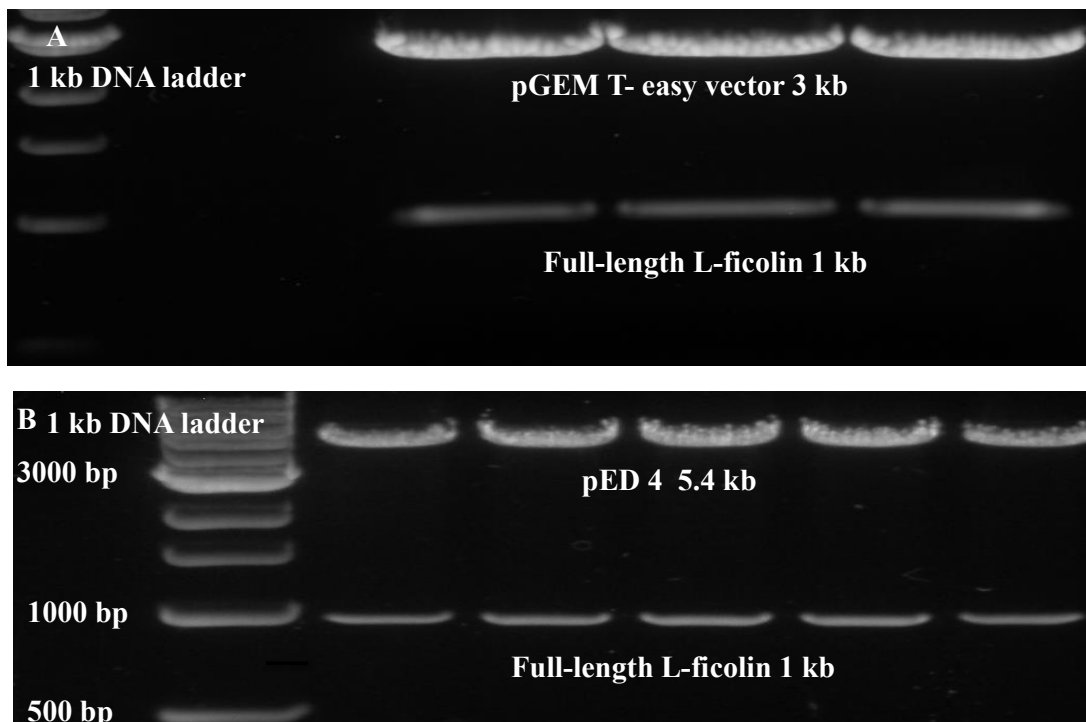


Figure 3-5: A restriction digestion of L-ficolin cDNA in pGEM-T easy (A) and pED4 (B) with *PstI/EcoRI* enzymes.

The plasmids pGEM T-easy and pED4 in A, and B figures were digested with *PstI/EcoRI* at 37°C for 3 hr. After digestion of recombinant pGEM T-easy the right size bands of L-ficolin was cut from the gel and purified. Then the purified product cloned into pED4. This also digested with the *PstI/EcoRI* enzymes to check the existence of the L-ficolin. In each case the upper bands correspond to the pGEM-Teasy and pED4 vectors (3 and 5.4) kb in size respectively. The lower bands represent the L-ficolin cDNA and the expected size is 1kb.

3.5.2 Production and purification of full-length L-ficolin

Full-length L-ficolin was produced by expression in CHO DBX11 cells. This cell line carries out the post-translation modifications that are essential for function, including hydroxylation of proline residues and hydroxylation and glycosylation of Lys residue in the collagen-like domain, together with disulphide bond formation, (Wallis and Drickamer, 1999). L-ficolin was harvested in serum-free medium and was purified by affinity chromatography on a GlcNac-Sepharose column. About 0.35 mg of purified recombinant L-ficolin was obtained per liter of culture media. The ficolin migrated as a single band of ~35 kDa under reducing condition (Figure 3-6) as expected from the amino acid sequence (Matsushita, 2010, Endo et al., 2011).

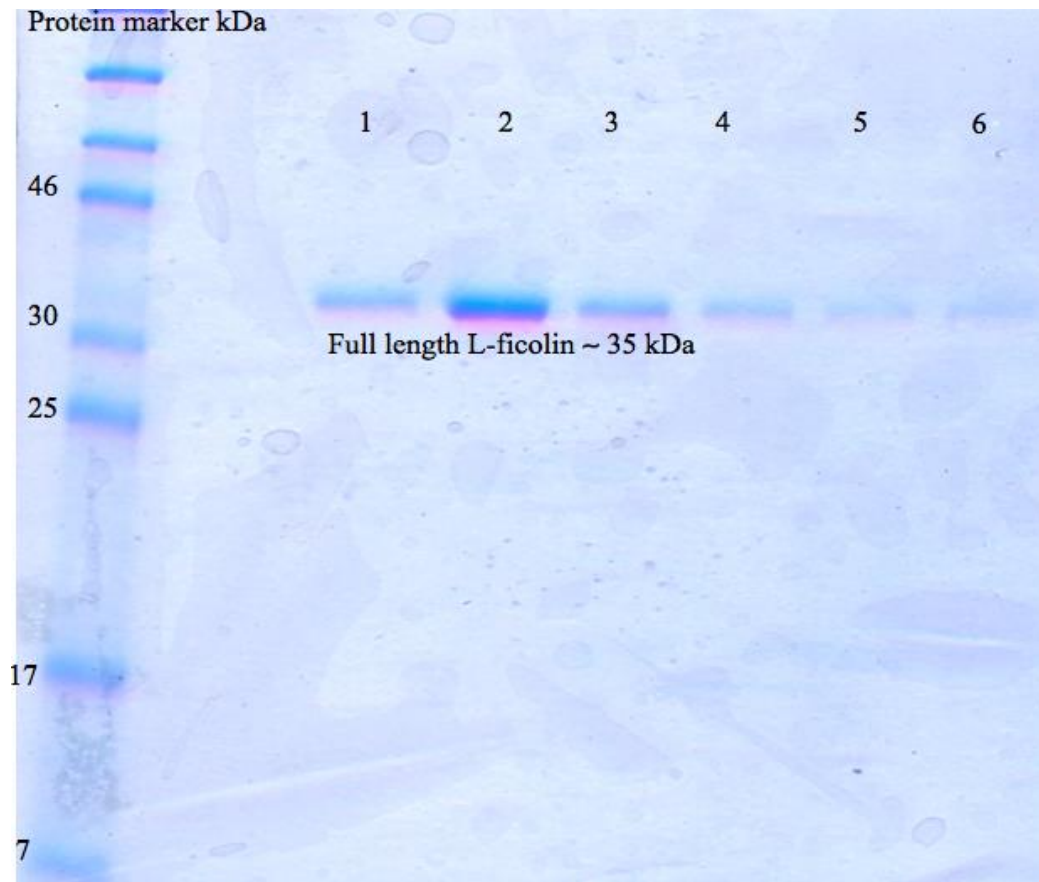


Figure 3-6: 15% SDS-PAGE gel analysis of recombinant L-ficolin after chromatography on a GlcNac-Sepharose column.

L-ficolin was expressed in CHO DBX11 cells line and purified by affinity chromatography on a GlcNac-Sepharose column. Lane 1-6 show the L-ficolin elution fractions after chromatography. A 15% gel was run under reducing condition (with DTT) and stained with Coomassie blue.

3.6 Cloning expression and purification of fibrinogen-like domain of L-ficolin

3.6.1 PCR amplification and cloning of fibrinogen-like domain of L-ficolin

To localise the interaction between Ply and L-ficolin an additional fragment was made encompassing the fibrinogen-like domain of L-ficolin. This was amplified by PCR as described in the methods section, separated on a 1% agarose gel (~660 bp), purified and cloned into pGEM-T easy vector (Figure 3-7 A and B). The fragment was then excised by restriction digestion with *NcoI* and *EcoRI* and cloned into pET28a digested with the same enzymes (Figure 3-8). Initial attempts to express the protein in *E. coli* resulted in

poor yields, so the fragment was re-cloned with the addition of an N-terminal His-tag, which improved expression levels. We have found that adding an N-terminal tag often helps to improving the yields of mammalian proteins in *E. coli*.

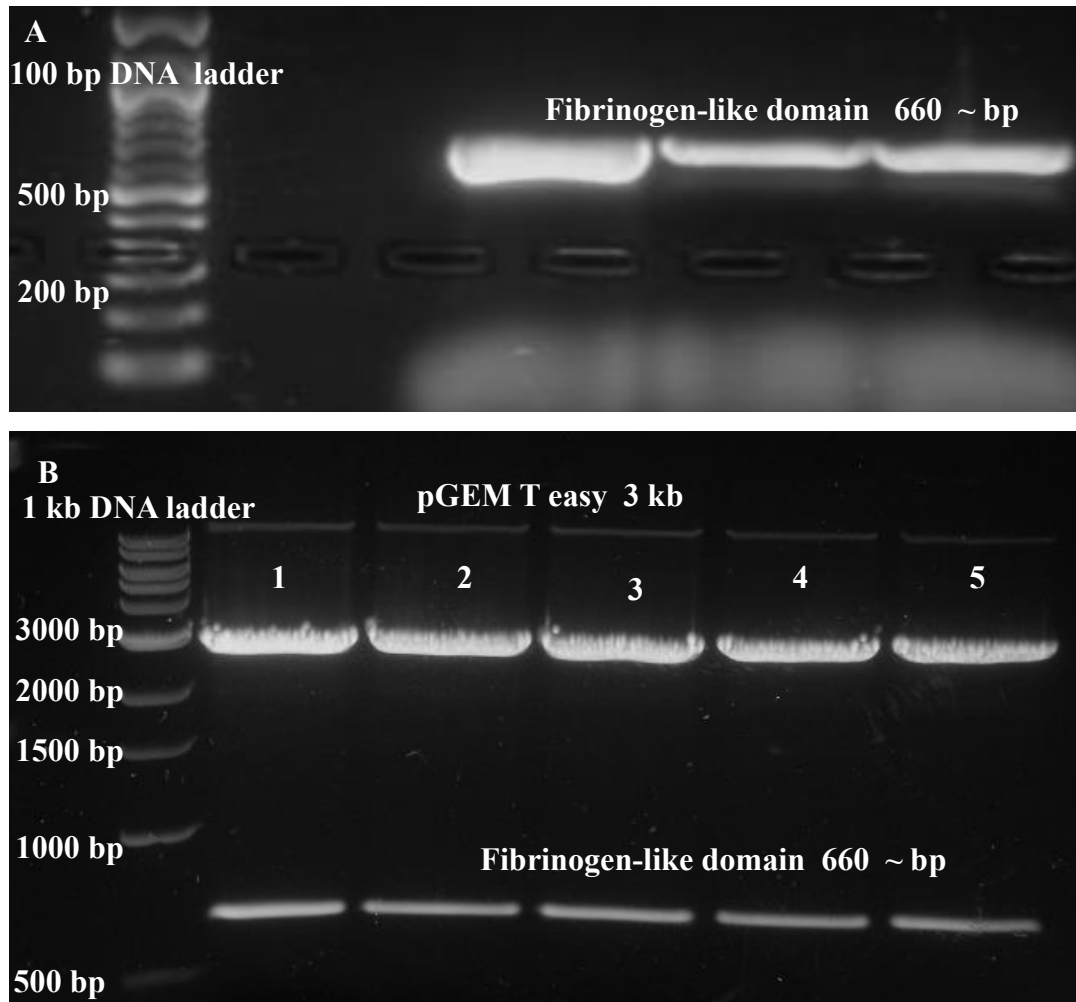


Figure 3-7: A 1% agarose gel showing PCR amplification of the cDNA encoding fibrinogen-like domain of L-ficolin and restriction digestion of the resulting clones in pGEM-T easy vector.

(A) Amplified fibrinogen-like domain of ~ 660 bp. The first lane is 100 bp DNA ladder and other lane is the amplified product. (B) *NcoI/EcoRI* restriction digestion of recombinant pGEM-T easy vector containing the 660 bp insert, five different clones are shown.

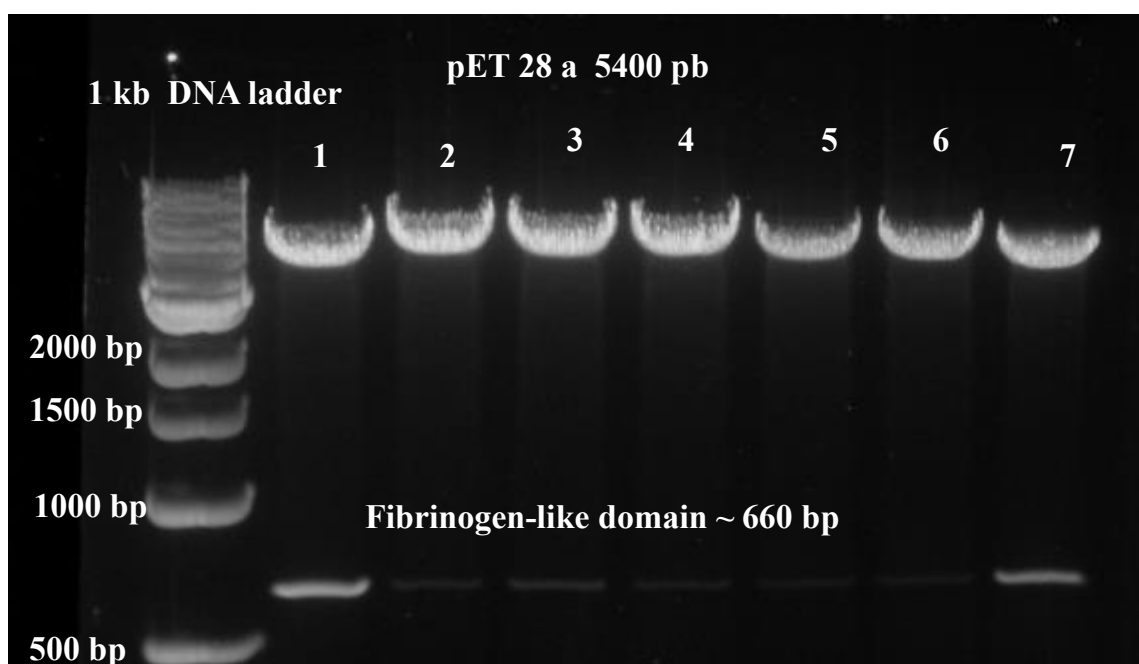


Figure 3-8: A 1% agarose gel of *NcoI/EcoRI* restriction digestion of seven different fibrinogen-like domain clones in pET28a.

All seven clones contained the insert giving two fragments on digestion: the vector (5.4 kb) and the smaller insert (~660 bp). The difference in the intensity of the smaller product in lane 2-6 is probably due to incomplete digestion.

3.6.2 Expression and purification of fibrinogen-like domain of L-ficolin

The fibrinogen-like domain was expressed in *E. coli* BL21 (DE3) and purified from inclusion bodies (Figure 3-9 A) by drop dilution as described in the section 2.2.13. It was purified by affinity chromatography on a Ni-Sepharose column (Figure 3-9 B). The fibrinogen-like domain migrated at the expected size of ~27 kDa by SDS-PAGE.

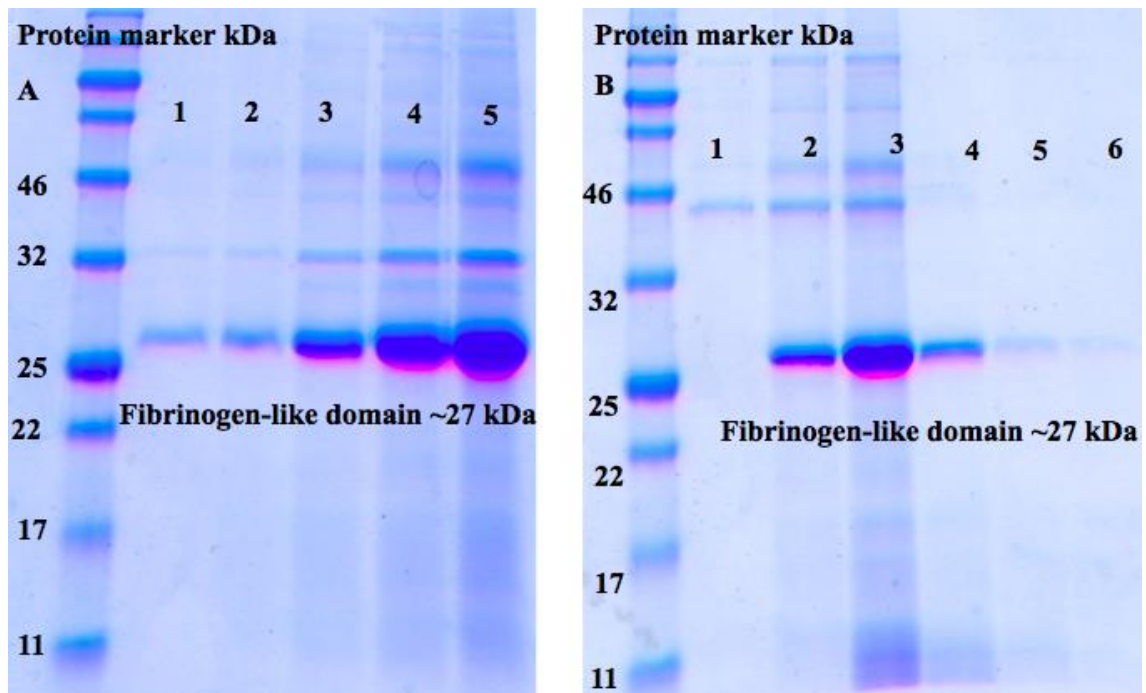


Figure 3-9: SDS-PAGE of the fibrinogen-like domain of L-ficolin.

(A) Purified inclusion bodies (increasing amounts loaded from left to right). The fibrinogen-like domain migrates at the expected molecular mass of ~27 kDa. (B) Purification of the fibrinogen-like domain on a Ni-Sepharose column. Protein was eluted in 6 fractions using 500 mM imidazole. Proteins were separated on 15% gels and stained with Coomassie blue.

Further purification was carried out by gel filtration on a Superdex 75 16/60 column (Figure 3-10 A). Protein eluted with an apparent molecular mass of ~80 kDa consistent with trimerization of the fibrinogen-like domain as described previously (Tanio et al., 2007). Proteins migrated at ~27 kDa by SDS-PAGE indicating that trimerisation is mediated by non-covalent interactions (Figure 3-10 B). Yields were relatively low (0.25 mg from 500 ml of culture).

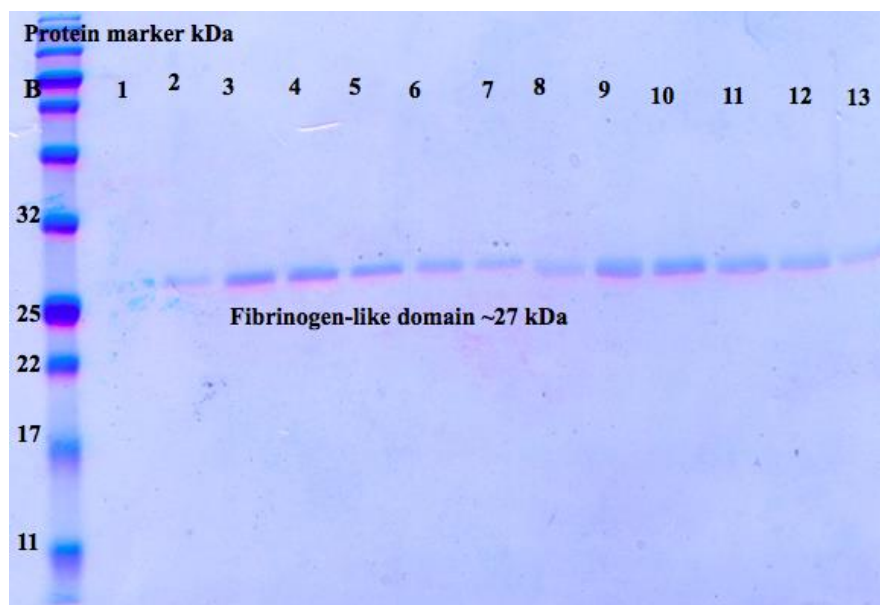
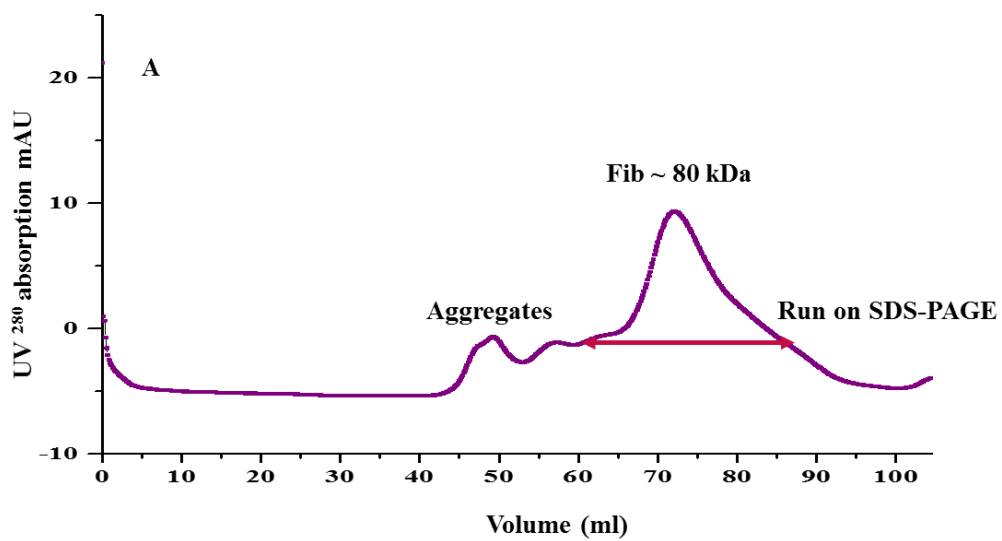
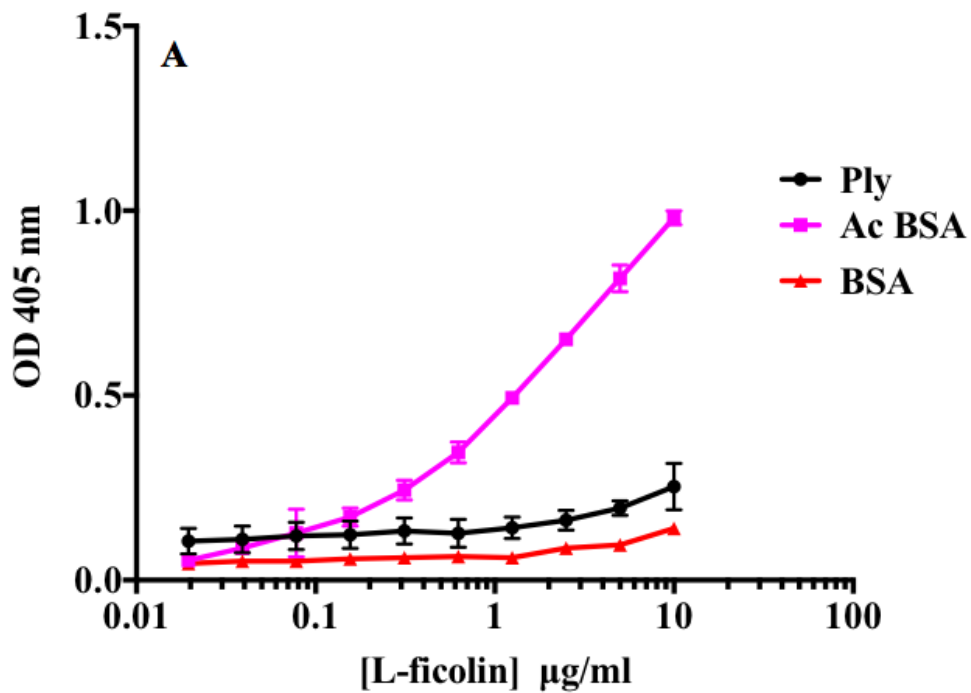


Figure 3-10: Size exclusion chromatography of recombinant fibrinogen-like domain on a Superdex 75 16/60 column analysed on a 15% SDS-PAGE gel.

(A) The elution profile of the fibrinogen-like domain on a Superdex 75 16/60 gel filtration column. The main peak labelled by red arrow is fibrinogen like domain is about ~ 80 kDa. The first peak is aggregate. (B) Fractions were collected across the main peak of fibrinogen-like domain and run on the SDS-PAGE under reducing with DTT (lanes 1-6) and non-reducing without DTT (lanes 7-12) conditions.

3.6.3 Analysis binding between recombinant Ply and L-ficolin

Binding of purified Ply to recombinant human purified L-ficolin was investigated using a solid-phase binding assay in which Ply was immobilized in the wells of an ELISA plate and incubated with increasing concentrations of recombinant L-ficolin. Bound ficolin was detected using a polyclonal anti-L-ficolin antibody (Figure 3-11 A and 3-11 B). Surprisingly, no binding was detected between recombinant Ply and recombinant L-ficolin. Two recombinant ply preps were used as labbled Ply and Ply1 in (Figure 3-11) to confirm the result. L-ficolin did bind to acetylated BSA, a known ligand, indicating that L-ficolin was functional. To exclude the unlikely possibility that bound L-ficolin was not recognized by the antibody, the experiment was repeated using the same monoclonal anti L-ficolin antibody used in the original published study (Figure 3-12). Again no binding was detected. These studies suggest that the conclusions of the original study were incorrect, possibly due to contamination of Ply preparations by an L-ficolin ligand.



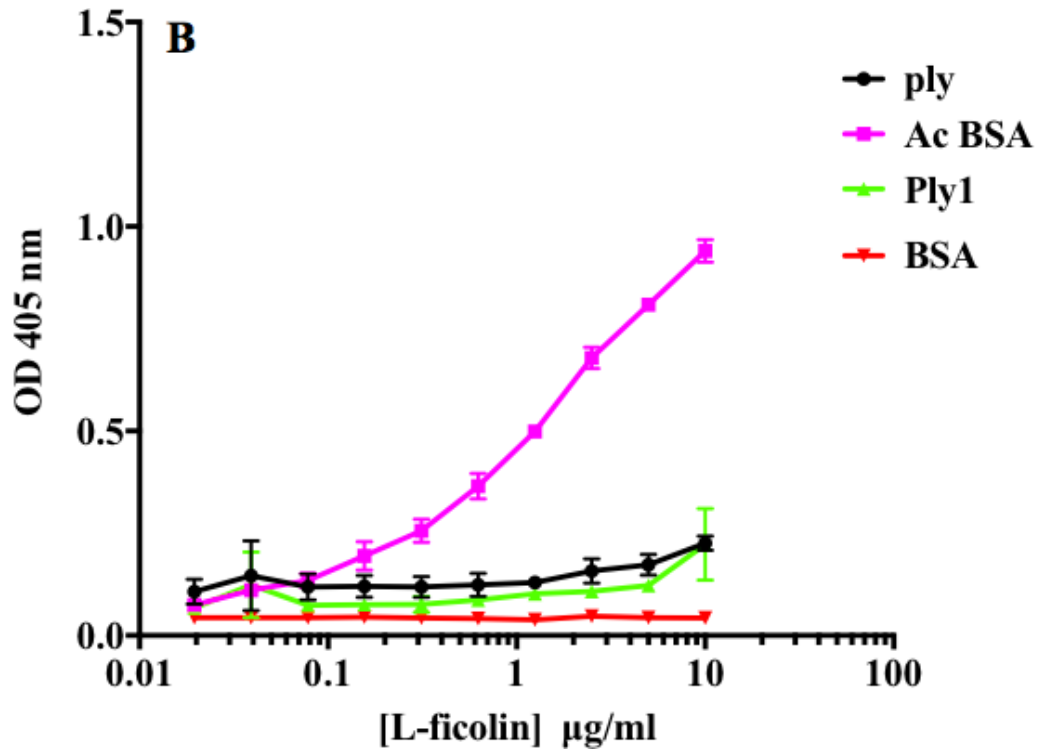


Figure 3-11: No binding between recombinant Ply and purified recombinant L-ficolin by ELISA.

Nunc Maxisorp plate wells were coated with Ply and Ply1, acetylated BSA (Ac BSA) or BSA and blocked with 1% w/v BSA. Purified recombinant L-ficolin was incubated with the coated wells at room temperature and binding was detected using a rabbit polyclonal anti L-ficolin antibody. The primary antibody was detected with an anti-rabbit IgG antibody conjugated with alkaline phosphatase and the colour changed to yellow. Absorbance was determined at 405 nm. The data was recorded in triplicate and the error is the SEM. Graph pad Prism 7 programme was used to make the figures.

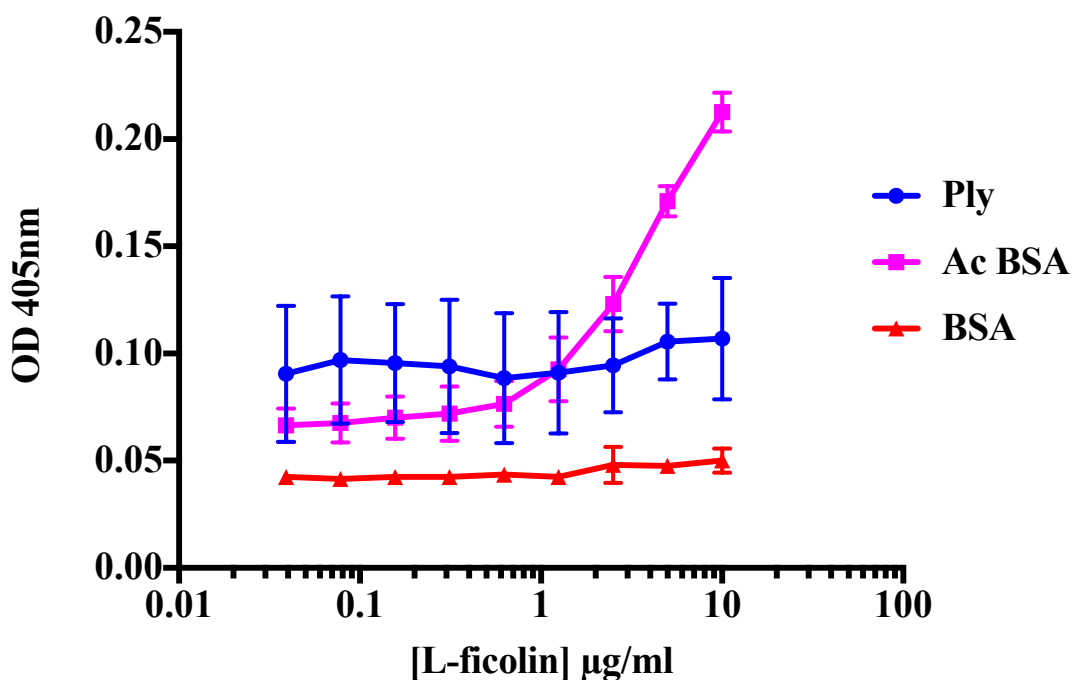
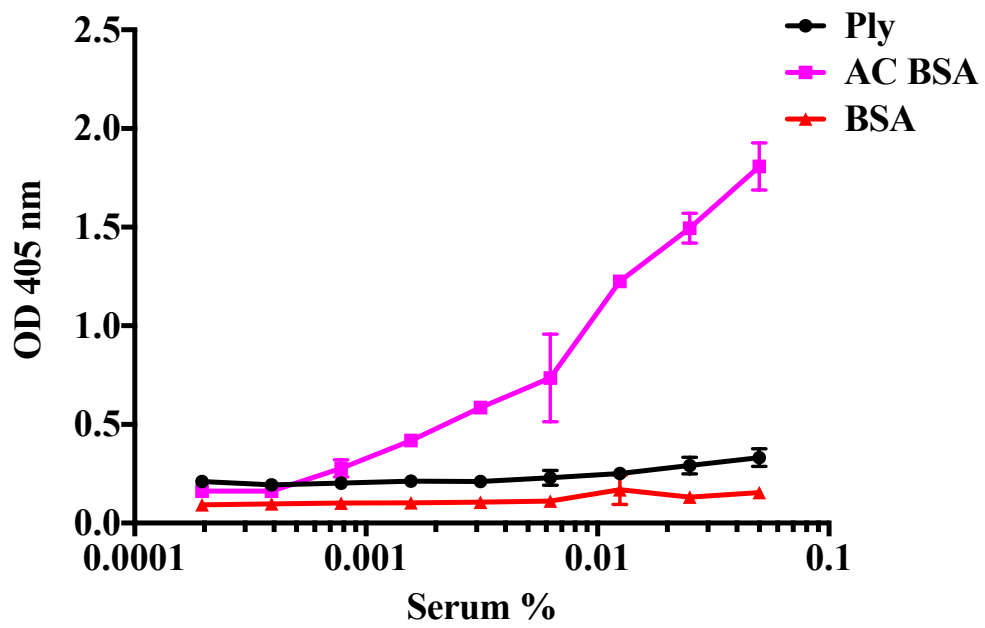
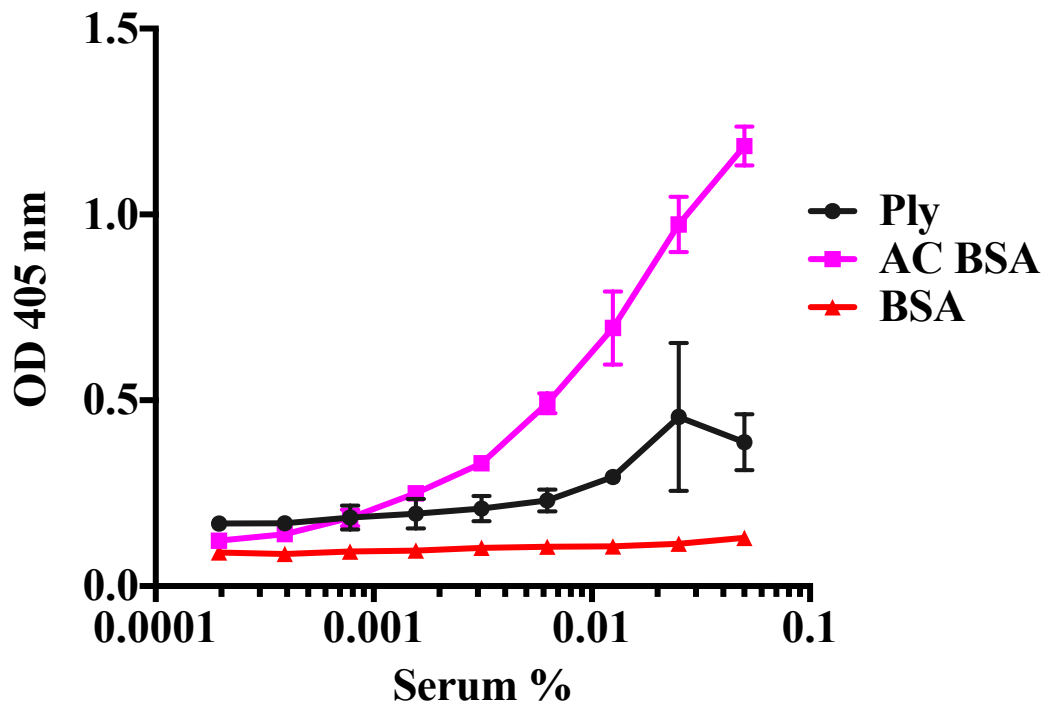
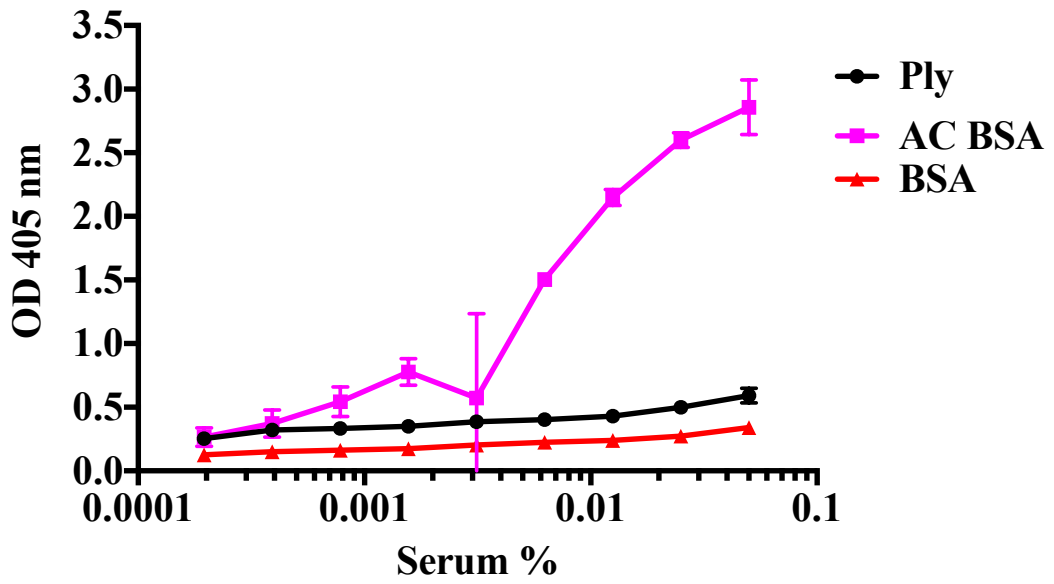
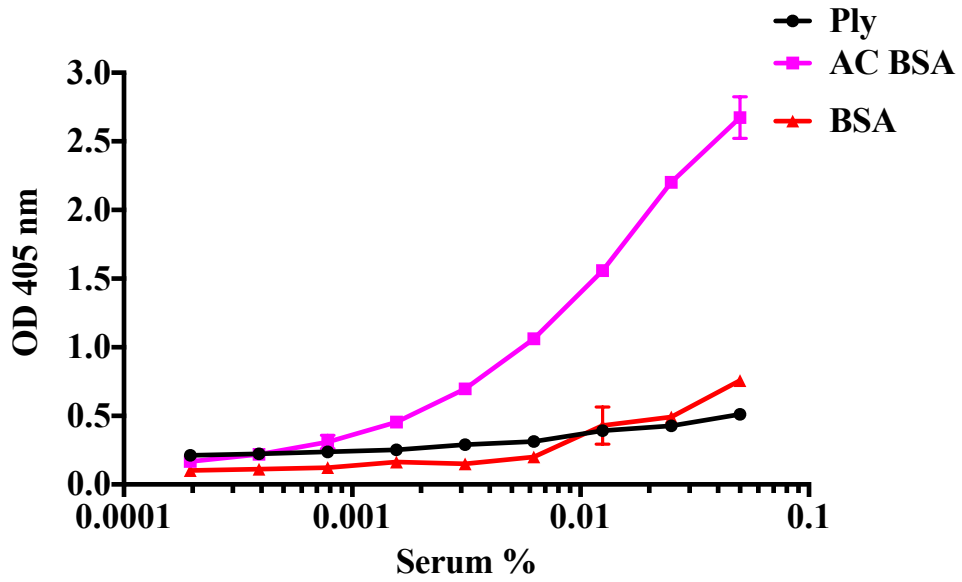


Figure 3-12: L-ficolin binding to recombinant Ply using monoclonal anti L-ficolin antibody by ELISA.

The experiment was carried out in the same way as in (Figure 3.17) above except that binding was detected using a monoclonal anti L-ficolin antibody as the primary antibody, and an anti-mouse IgG antibody conjugated with alkaline phosphatase for pNPNP substrate. The data was recorded in triplicate and the error is the SEM.

Given the unexpected findings described above, it was important to investigate what might have gone wrong in the initial study. One possibility is that antibody might have reacted against a contaminant in whole serum rather than L-ficolin. I therefore reproduced the binding experiments described in the previous report using L-ficolin from human serum. Binding was investigated using the same assay except that serial dilutions of serum were used instead of purified L-ficolin. Binding was detected using the polyclonal anti-L-ficolin antibody. As can be seen in (Figure 3-13) no binding was detected between Ply and serum L-ficolin. As before L-ficolin bound to acetylated BSA but not the BSA control. Experiments were repeated using different Ply preparations and using serum from different donors. Thus L-ficolin does not bind to Ply. Moreover the previous erroneous conclusion cannot be explained by the detection method. The most likely explanation is that preparations of Ply were contaminated by the L-ficolin ligand.





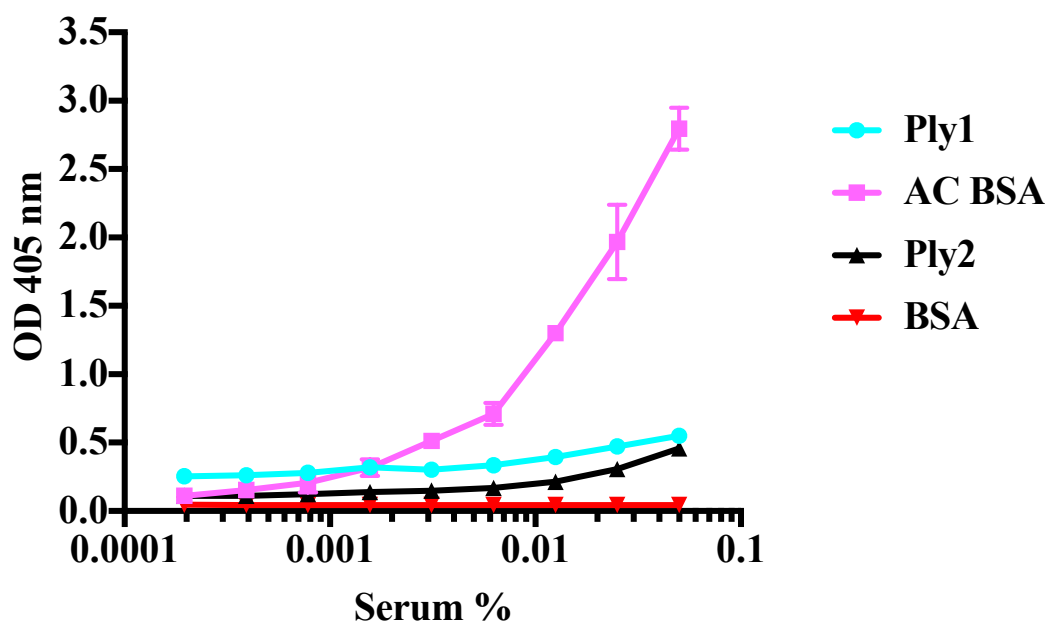
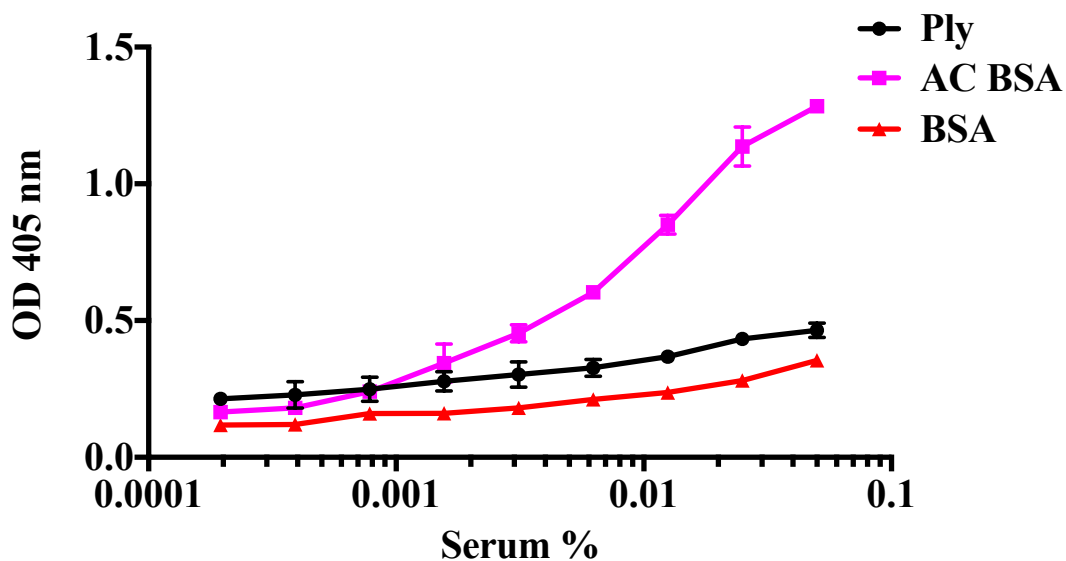


Figure 3-13: ELISA binding of Ply with serum L-ficolin.

Nunc Maxisorp plate wells were coated with two Ply prep as designate as Ply, Ply1, acetylated BSA (AC BSA) or BSA. 1% BSA was used for blocking the plate after that the plate was incubated with serial dilutions of different serum from different donars. After washing the binding was detected using a rabbit polyclonal anti L-ficolin antibody as the primary antibody, and anti-rabbit IgG conjugated with alkaline phosphatase. After incubation with pNPN substrate, absorbance was measured at 405 nm. The data was recorded in triplicate and the error is the SEM. Graph pad Prism 7 programme was used to make the figures.

3.7 ELISA binding between Ply and IgG isotypes

An ELISA was performed to test binding between Ply and different IgG isotypes. Following previous studies that described CP was activated on Ply pre-incubated with polyclonal non-immune serum IgG preparations. I aimed to show which IgG isotypes mediate this binding with Ply with using monoclonal IgG from human myeloma plasma (Mitchell et al., 1991). Immobilized Ply was incubated with the serial dilutions of human IgG isotypes including monoclonal IgG1, IgG2, IgG3 and IgG4. Monoclonal preparations were obtained from the serum of myeloma patients, where one isotype of IgG is overproduced. Unlike whole IgG, these IgGs are clonal so any binding is unlikely to be caused by "classical" antibody-antigen interactions via the variable regions of the antibody. Ply bound to the whole IgG, IgG2, IgG3 and IgG4 but not to IgG1 (Figure 3-14 A and B).

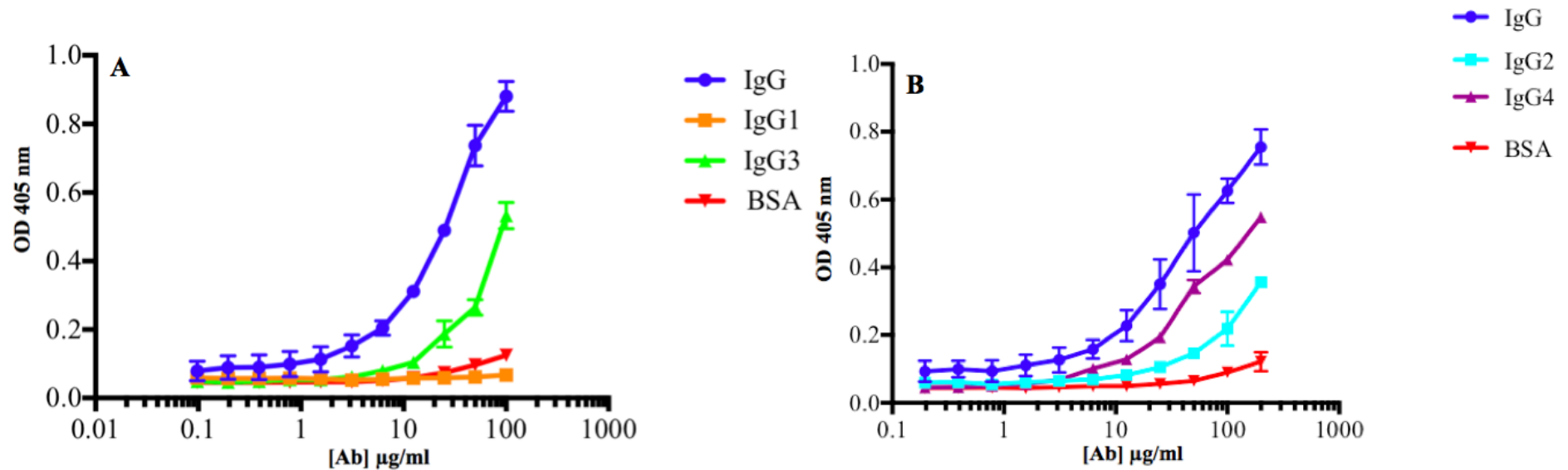


Figure 3-14: ELISA binding assay between Ply and IgG isotypes.

Nunc Maxisorp plate wells were coated with Ply and BSA. After coating plate was blocked with 1% BSA. After blocking plate was incubated with serial dilutions of IgG isotypes. Binding was detected using anti-human IgG antibody, conjugated with alkaline phosphatase. After incubation with pNPP substrate, absorbance was measured at 405 nm. The data was recorded in triplicate and the error is the SEM. Graph pad Prism 7 programme was used to make the figures.

3.8 ELISA binding between PlyD1-3 and PlyD4 with IgG isotypes

To localise the binding between Ply and IgG, binding was tested towards Ply fragments: PlyD1-3 and PlyD4, produced as described in Chapter 2. As before, binding was investigated by immobilizing the Ply fragments and adding each IgG isotype in turn. Detection was using an anti-human IgG antibody. As shown in Figure 3-15 A, no binding was detected between PlyD4 and IgG2, IgG3, IgG4 or IgG1. However, PlyD1-3 bound to all IgG isotypes except IgG1 (Figure 3-15 B). Thus a similar binding pattern was observed as with full-length Ply suggesting that Ply interacts through domains 1-3.

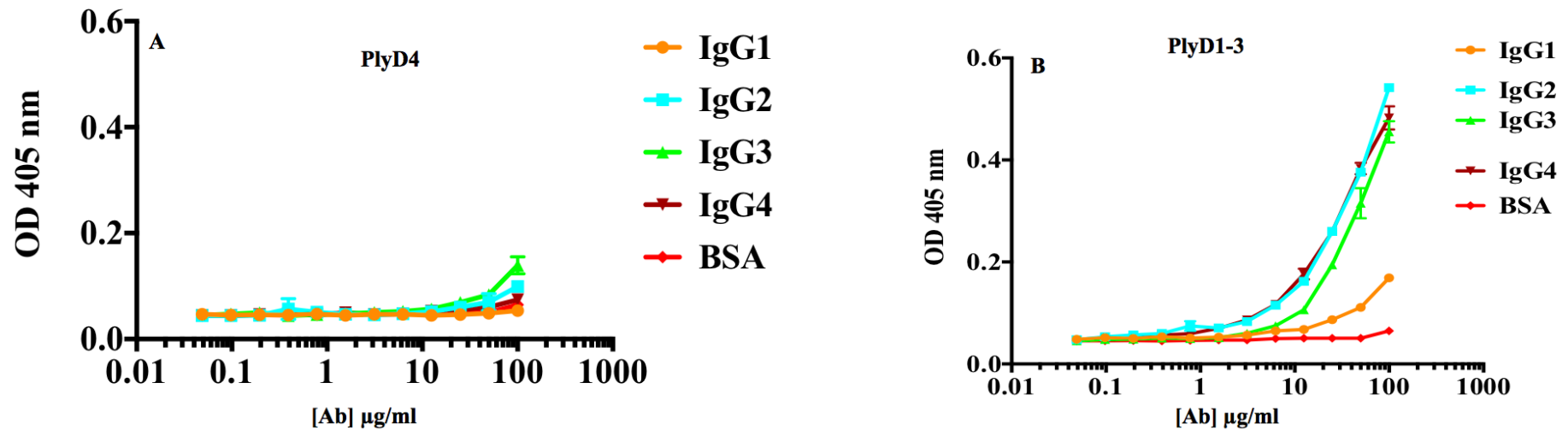


Figure 3-15: ELISA binding of Ply domains with IgG isotypes.

Nunc Maxisorp plate wells were coated with Ply domains (PlyD4 and PlyD1-3) or BSA. Plate was blocked with 1% BSA. Then it was incubated with serial dilutions of IgG isotypes. Binding was detected using anti-human IgG antibody, conjugated with alkaline phosphatase. After incubation with pNPN substrate, absorbance was measured at 405 nm. The data was recorded in triplicate and the error is the SEM. Graph pad Prism 7 programme was used to make the figures.

3.9 ELISA binding between Ply and Ply domains with IgG fragments

In order to localise the binding site on IgG, Ply was immobilized and incubated with the serial dilutions of Fc and Fab. These fragments were generated by digestion of whole antibodies (supplied by Athens Research), so comprise mixtures of IgG isotypes. Binding was detected using the anti-human IgG antibody. It was found that, Ply bound to the Fab fragment of IgG not to the Fc fragment (Figure 3-16 A). Similarly, PlyD1-3 also bound to the Fab fragment, not to Fc (Figure 3-16 B). As expected, PlyD4 did not bind to the Fab and Fc fragments (Figure 3-16 C). In summary, Ply binds to IgG3, 2 and 4 via the Fab fragment of the antibody and D1-3 of Ply. These findings contradict previous work that suggested Ply binds to the Fc portion of IgG (Mitchell et al., 1991).

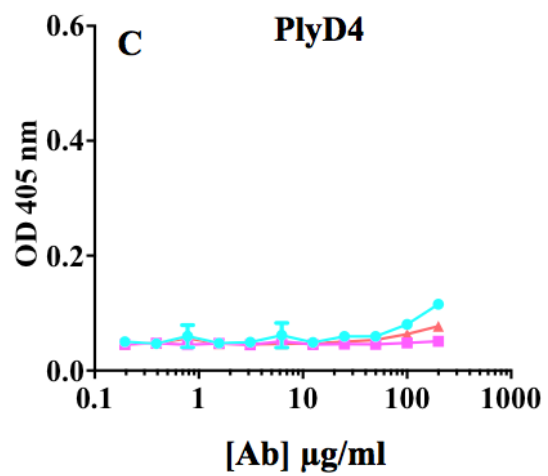
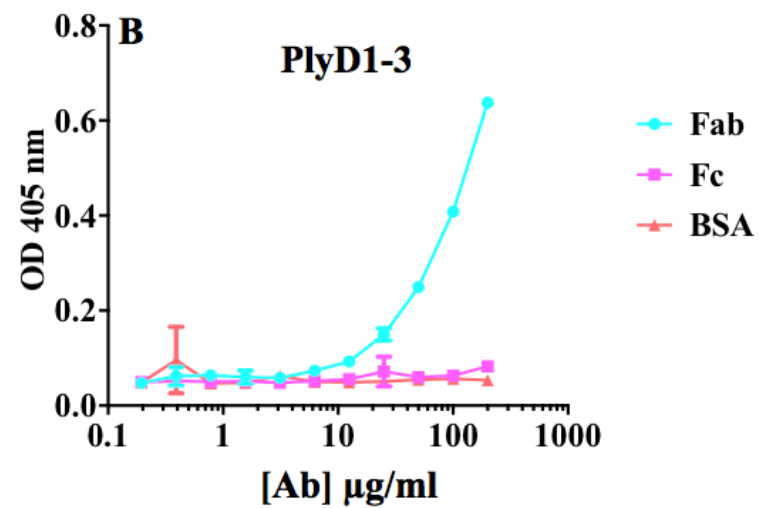
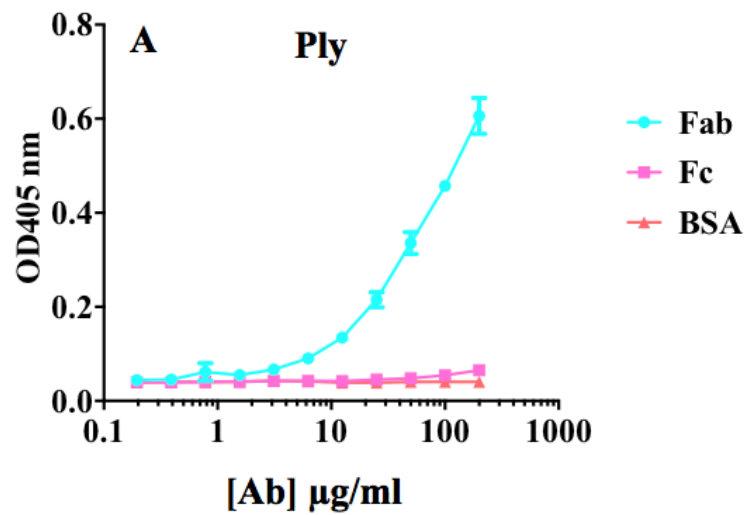


Figure 3-16: ELISA binding of Ply and Ply domains with IgG fragments.

Nunc Maxisorp plate wells were coated with Ply and Ply domains and BSA. Plate was blocked with 1% of BSA. After that it was incubated with serial dilutions of Fab and Fc fragments. Binding was detected using anti-human IgG antibody, conjugated with alkaline phosphatase. After incubation with pNPN substrate absorbance was measured at 405nm. The data was recorded in triplicate and the error is the SEM. Graph pad Prism 7 programme was used to make the figures.

3.10 Digestion of IgG4 with IdeS enzyme

To generate monoclonal Fc and Fab fragments, IgG4 was digested using IdeS enzyme, which cleaves the IgG below the hinge region and produces two fragments: Fab₂ and Fc (An et al., 2014). IgG4 was chosen because it bound strongly to Ply in our assays. Because cleavage is below the hinge the Fab fragment generated is a dimer (~100 kDa) linked by disulphide bonds. Fragments were separated by gel filtration (Figure 3-17). Two peaks were observed, a larger peak corresponding to the Fab₂ fragment (~100 kDa) and a smaller peak corresponding to Fc (~50 kDa). Fractions were collected across the Fab and Fc peaks and analyzed by SDS-PAGE under reducing and non-reducing condition (Figure 3-18 A and B) respectively. Under non-reducing condition the Fab and Fc region migrated at ~100 kDa and ~ 24 kDa respectively. Under reducing condition the Fab was separated into two fragments of ~31 kDa and ~24 kDa corresponding to the heavy and light chains respectively (Figure 3-18 B).

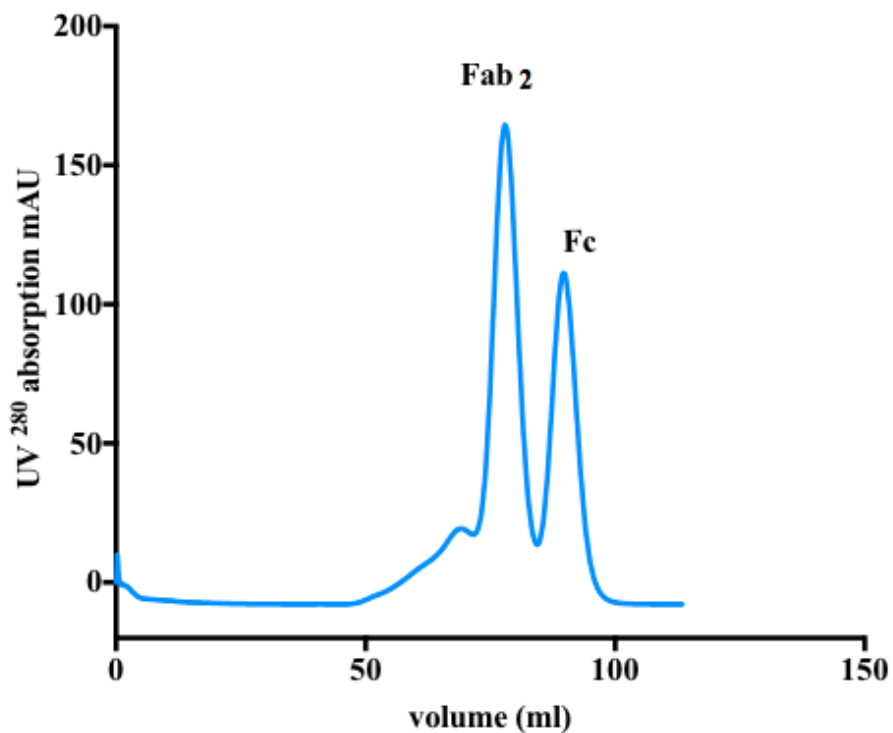


Figure 3-17: Elution profile of an IgG4 digestion with IdeS enzyme on Superdex 200 16/60.

4 mg of IgG4 digested with IdeS enzyme 67 Unit/ μ l and incubated 5hr at 37°C and left at 4°C overnight and subjected to gel filtration column. After digestion the IgG4 splitted into two parts include Fab2 and Fc fragment as labled in the figure. The small peak before the Fab2 peak is the aggregates. Fab2 and Fc peaks were run on the SDS-PAGE.

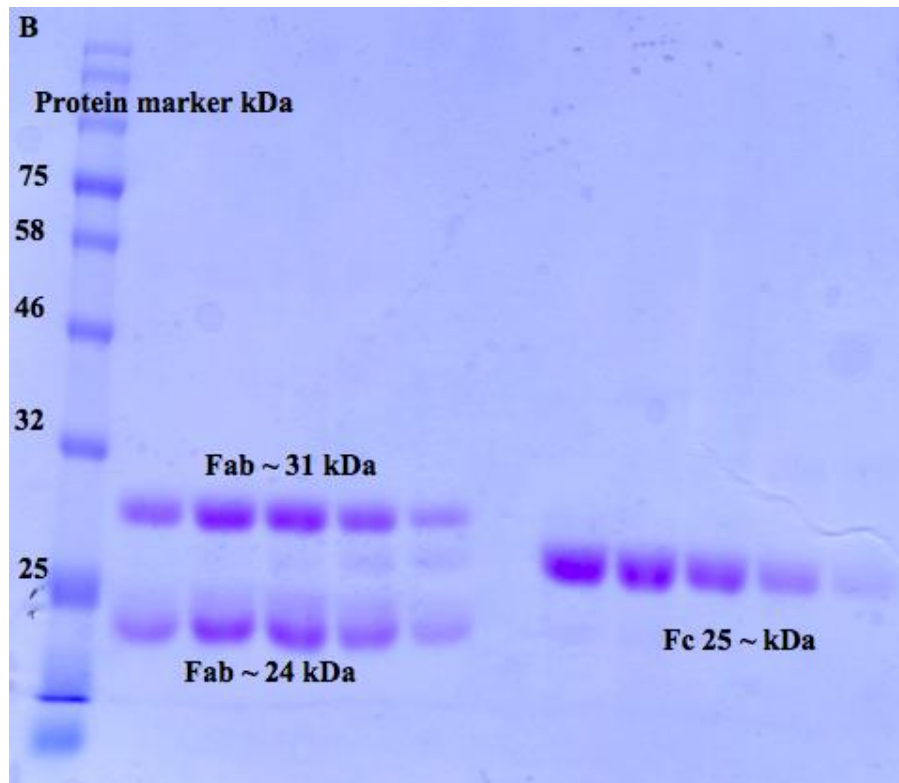
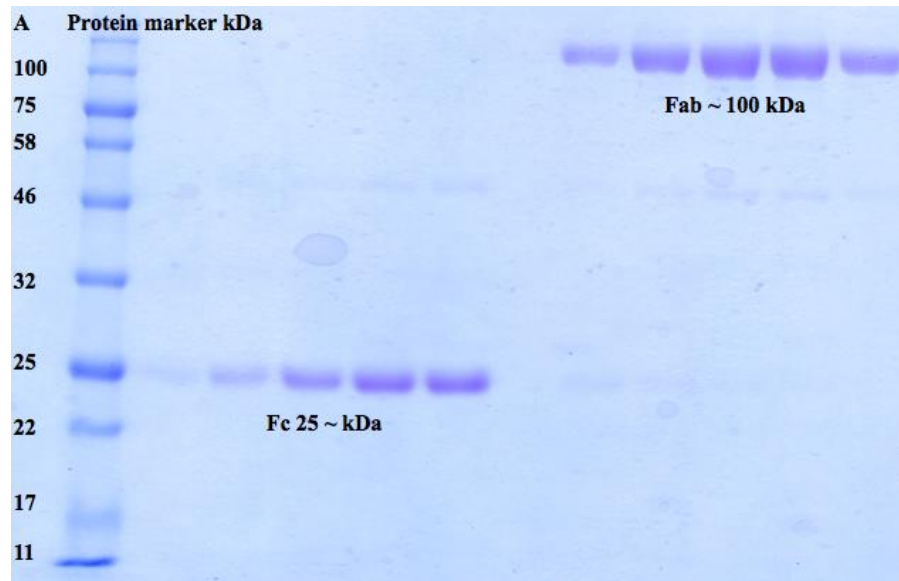


Figure 3-18: Analysis of digested IgG4 on SDS-PAGE.

(A) Under non-reducing condition. The Fab and Fc fragments migrate at the expected molecular masses of $\sim >100$ kDa and ~ 25 kDa respectively. (B) Digested IgG4 under reducing condition the Fab₂ is separated into two bands ~ 24 kDa and ~ 31 kDa, the light and heavy chains.

3.11 ELISA binding between monoclonal Fab and Fc with the Ply, PlyD1-3 and PlyD4

In the previous experiment, Fc and Fab fragments were isolated from whole IgG, so contain mixtures of the four IgG isotypes. Moreover, Fab fragments will be polyclonal. Thus it is possible that binding of Ply to Fab could occur via antibody-antigen interaction. The experiment was therefore repeated using monoclonal Fab₂ and Fc fragments. The result of this experiment was similar to the previous finding. Figure 3-19 A shows that Ply and PlyD1-3 bound to the monoclonal Fab₂. No binding was observed between Fc and Ply, PlyD1-3 or to PlyD4 (Figure 3-19 B). Thus, this experiment confirms our previous finding that the interaction between Ply and IgG was occurs via PlyD1-3 and the Fab of IgG.

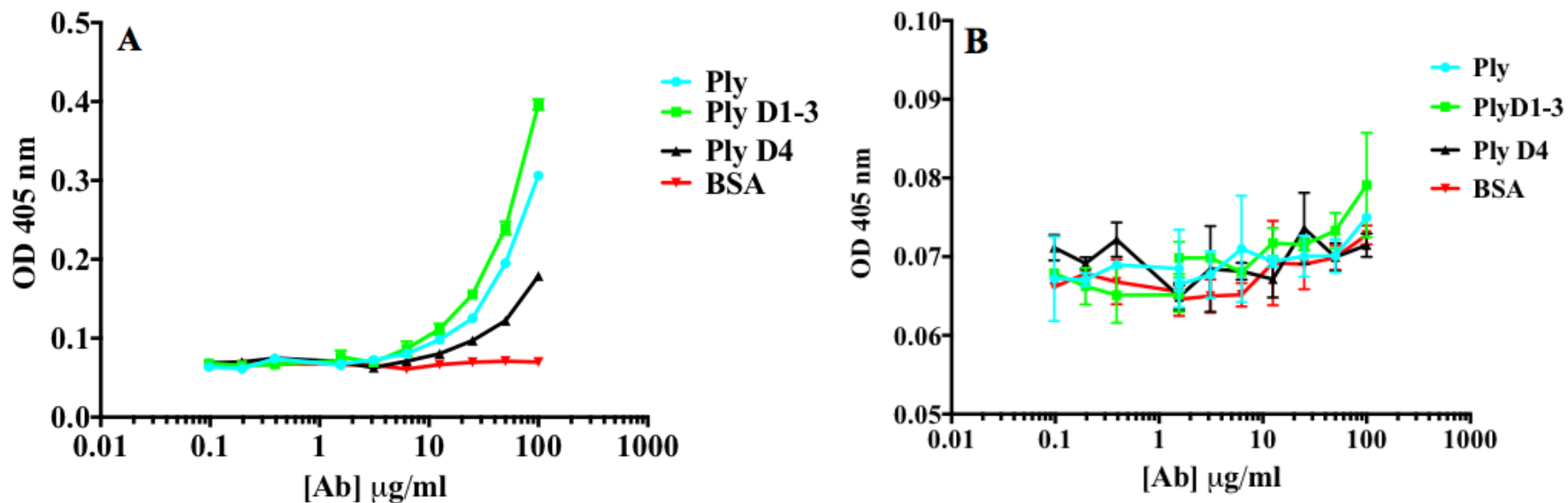


Figure 3-19: ELISA binding of Ply and Ply domains with the monoclonal Fab and Fc of digested IgG4.

(A) represents the binding between Fab with the Ply, PlyD1-3, PlyD4 and BSA. (B) represents the binding between Fc with the Ply, PlyD1-3, PlyD4 and BSA. Nunc Maxisorp plate wells were coated with Ply and Ply domains and BSA and incubated with serial dilutions of monoclonal Fab and Fc fragments. Binding was detected using anti-human IgG antibody, conjugated with alkaline phosphatase. After incubation with pNPNP substrate, absorbance was measured at 405 nm. The data was recorded in triplicate and the error is the SEM. Graph pad prism 7 programme was used to make the figures.

3.12 ELISA binding between Ply D385N and IgG isotypes

Previous studies have suggested that the mutation D385N knocks out complement activation (Mitchel and Andrew, 1997). Therefore, PlyD385N (produced in Lab 218) was tested using the ELISA binding assay to see if loss of complement activity is caused by loss of binding to IgG. As shown in (Figure 3-20) the point mutation D385N still bound to IgG. Wild-type Ply and mutant D385N Ply showed similar binding to IgG2, IgG3 and IgG4. No binding was detected with the IgG1. This suggests that failure to activate complement by PlyD385N is not caused by loss of binding to IgG.

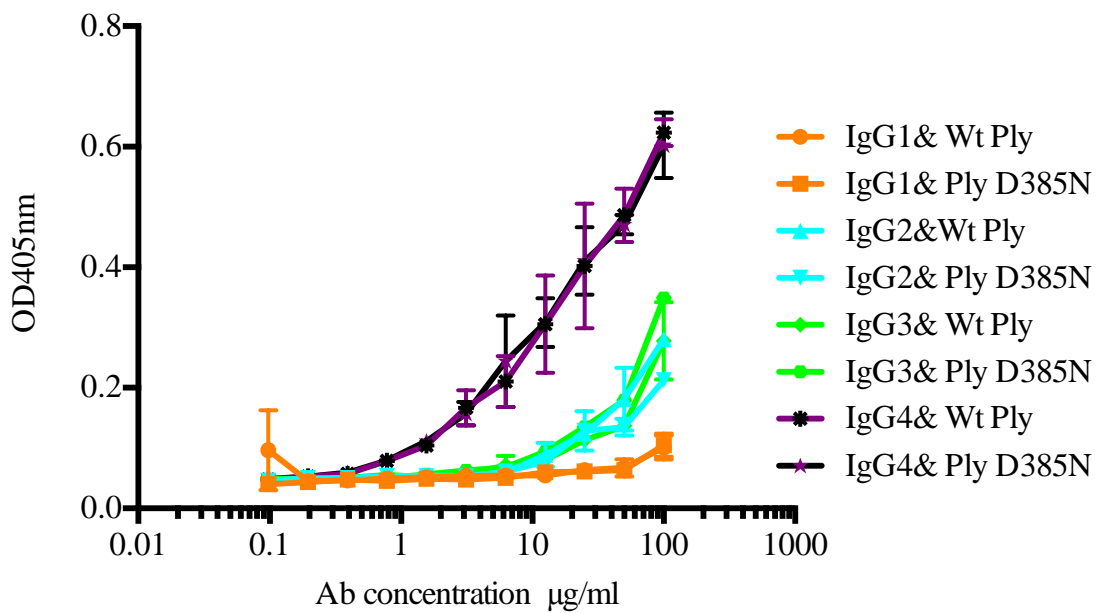


Figure 3-20: ELISA binding comparison of wild-type Ply and mutant PlyD385N with IgG isotypes.

Nunc Maxisorp plate wells were coated with Ply, Ply D385N or BSA and incubated with serial dilutions of IgG isotypes. Binding was detected using anti-human IgG antibody, conjugated with alkaline phosphatase. After incubation with pNPN substrate, absorbance measured at 405 nm. The data was recorded in triplicate and the error is the SEM. Graph pad prism 7 programme was used to make the figures.

3.13 Inhibition assay

Inhibition assays were used to measure binding between components in solution. Plates were immobilized with Ply and serial dilutions of Ply were incubated with a fixed amount of IgG, Fab or Fc. The amount of IgG bound to the plate was detected using anti-human IgG antibody. Figure 3-21 A shows that the whole IgG binds to Ply in solution leading to a concentration dependent decrease in the amount of IgG binding to the plate. The IC₅₀ (the concentration of an inhibitor where the response (or binding) is reduced by half) for Ply with IgG was (3.8 mg/ml), figure B, shows that Fab fragment also binds to Ply in solution. The IC₅₀ was (4.5 mg/ml) after analyzing the data in Prism program, whereas Fc fragment does not bind. The detecting antibody (anti-human IgG) recognizes both Fc and Fab fragments. Thus, IgG binds tightly to Ply via the Fab fragment.

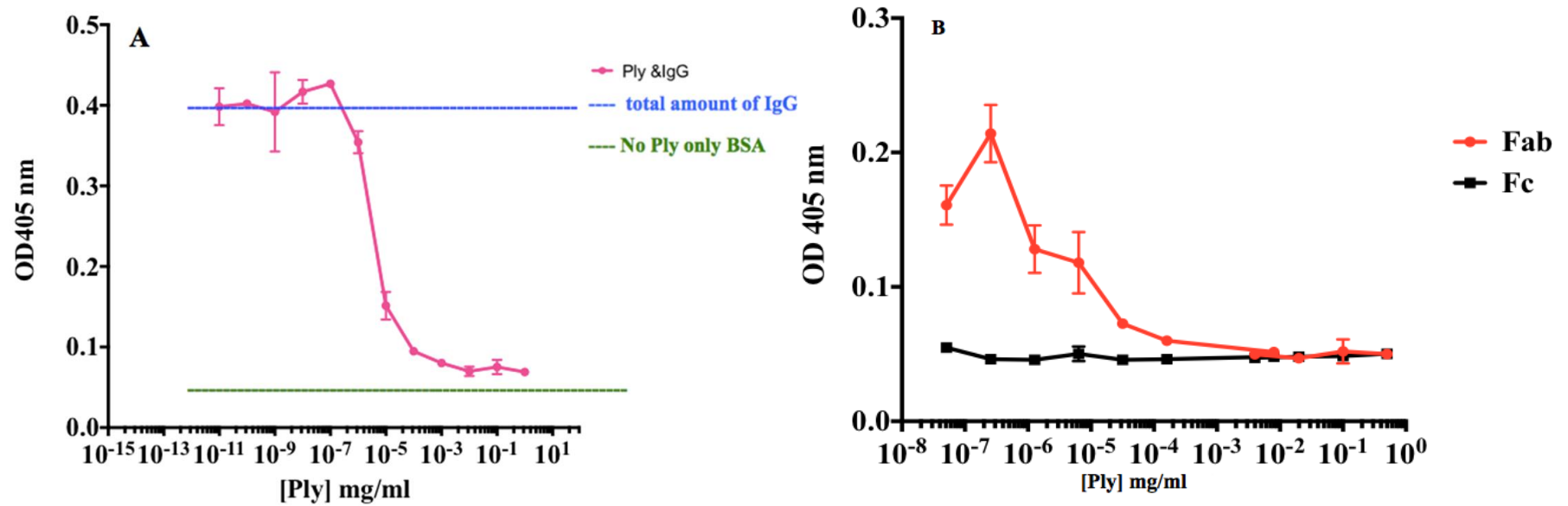


Figure 3-21: Inhibition of binding of IgG, Fab and Fc to Ply.

In figure A , B 10 x serial dilution of Ply was incubated with IgG and IgG fragments (Fab or Fc) at concentration of 100 $\mu\text{g/ml}$. 100 μl from the pre-incubated mixture was transferred to the Ply immobilized plate and absorbance measured at 405 nm. The data was recorded in triplicate and the error is the SEM. Graph pad prism 7 programme was used to make the figures.

3.14 Discussion

3.14.1 Binding between Ply and L-ficolin

Human L-ficolin is a soluble protein of the innate immune system that recognizes pathogens through its fibrinogen-like domains and activates the LP through MASPs (Vassal-Stermann et al, 2014). Previous published work (Ali et al., 2013) suggested that L-ficolin also binds Ply. In this chapter, the interaction between Ply and human L-ficolin was reassessed to characterize the interaction in more detail. Surprisingly, no binding between Ply and L-ficolin was detected using native serum L-ficolin as well as recombinant protein. Ply lysed RBCs (Chapter 4) and L-ficolin bound to acetylated BSA (a known ligand) confirming that both components were functional. The most likely explanation for the erroneous conclusions of the previous study was that the preparations of Ply were contaminated by L-ficolin ligand. This finding highlights the importance of using pure proteins in binding analysis, particularly in this case where a pathogen-recognition receptor (L-ficolin) is used because even minor contamination from e.g. a bacterial cell wall component can lead to false positives.

3.14.2 Binding between Ply and IgG isotypes

Ply activates the complement system through the CP by binding to IgG (Yuste et al., 2005, Paton et al., 1984, Mitchell et al., 1991). The likely function of this interaction is to deplete the host of complement components and diverting the immune response away from the bacteria. This study was undertaken to better understand how Ply interacts with IgG and identify which IgG isotypes interact with Ply. My results showed that Ply bound to IgG4, IgG3 and IgG2 but not IgG1 (Figure 3-14). The four IgG isotypes share greater than 90% sequence identity, and the variation is mostly found in the hinge region and the constant domain CH2 within the Fc fragment, which can be excluded (Vidarsson et al., 2014). In this study all monoclonal IgGs had kappa light chains, so differences in binding between IgG1 and IgGs 2, 3 and 4 must be due to differences in the heavy chain within the Fab region. The sequence alignment of the CH1 region of each IgG isotype reveals that three amino acids (CSR) are conserved in IgG2, IgG3 and IgG4. While they are (SSK) in the IgG1 (Figure 3-22).

```

IgG1    ASTKGPSVFPLAPSSKSTSGGTAALGCLVKDYFPEPVTVSWNSGALTSGVHTFPAVLQSS
IgG3    ASTKGPSVFPLAPCSRSTSGGTAALGCLVKDYFPEPVTVSWNSGALTSGVHTFPAVLQSS
IgG2    ASTKGPSVFPLAPCSRSTSESTAALGCLVKDYFPEPVTVSWNSGALTSGVHTFPAVLQSS
IgG4    ASTKGPSVFPLAPCSRSTSESTAALGCLVKDYFPEPVTVSWNSGALTSGVHTFPAVLQSS
*****. * : * * * . *****

IgG1    GLYSLSSVVTVPSSSLGTQTYICNVNHKPSNTKVDKRV
IgG3    GLYSLSSVVTVPSSSLGTQTYTCNVNHKPSNTKVDKRV
IgG2    GLYSLSSVVTVPSSNFGTQTYTCNVDHKPSNTKVDKTV
IgG4    GLYSLSSVVTVPSSSLGTQTYTCNVDHKPSNTKVDKRV
*****. * : * * * * * : * * * * * : * * * * * * *

```

Figure 3-22: Alignment of the IgG CH1 amino acid sequences.

The amino acid sequences are highly conserved in all IgG isotypes, but three amino acids are conserved in IgG2, IgG3, and IgG4 (CSR) under line in black. In IgG1 is (SSK) under line in red.

Ply bound to IgG4 but it is worth noting that the IgG4 does not activate complement. Activation of CP complement pathway is initiated by human IgG subclasses in the rank order IgG3 > IgG1 > IgG2 while IgG4 shows no significant activation (Burton and Woof, 1992, Isenman et al., 1975, Tao et al., 1993). The findings presented in this chapter revealed that, the IgG Fab fragment bound to the PlyD1-3 of Ply, which is in contrast to the previous study published in 1991 by Mitchell *et al*, where the Fc fragment was identified. Binding to Fab would leave the Fc fragment free to interact with C1q. Furthermore, this study showed that IgG2, IgG3 and IgG4 all bound to Ply D385N, which was previously described as a mutant form of the toxin that was deficient in complement activation (Mitchell and Andrew, 1997). Thus it can be concluded that failure to activate complement by PlyD385N is not caused by a failure to bind to IgG as previously reported. It was suggested that the residue Asp 385 of Ply is provided in antibody binding via Fc region. This binding cause activate of the CP.

Chapter 4 Inhibition of Ply by disruption of intermolecular packing

4.1 Objectives

Ply monomers pack side-by-side in crystals like the molecular packing of molecules in the pre-pore complex (Marshall et al., 2015). The concave face of one monomer packs against the convex face of its neighbour (Figure 4-1). There is some charge complementarity between the convex (negatively charged) and concave faces (positive charged). The concave interface comprises 44 binding residues whereas convex face has 41. The major contribution towards oligomerization on the membrane surface is likely to be surface complementarity between the concave and convex interfaces, as there are relatively few hydrogen bonds.

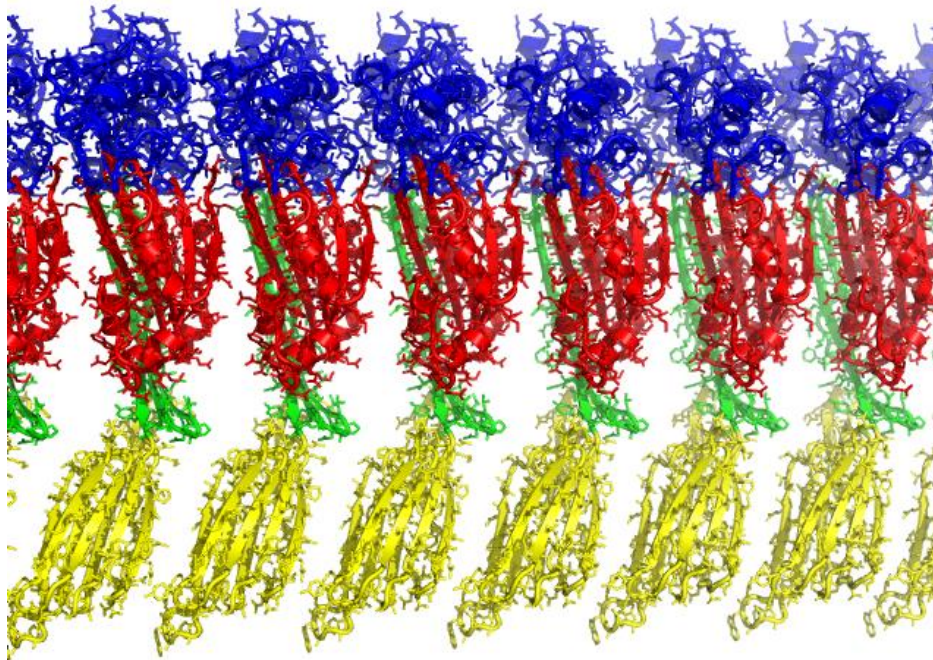


Figure 4-1: Packing of monomers in the Ply crystal reveals the packing of the pre-pore complex.

Each molecule of Ply molecule packs against each other in both concave and convex face. Such that the large concave side interacts with its partner's convex side.

To test whether the interactions observed in the crystal structure are important for pore formation (Figure 4-2), residues at the interface were mutated and the cytolytic activities of the resulting mutants were tested. Selected mutants include D205R, N339R and T304R were also analysed by EM and calcein leakage from liposomes. As well as single mutants, two disulphide-locked forms of Ply were created. Mutations were introduced into residues in TMH1 and TMH2 with the aim of generating a locked form of Ply that can still bind to membranes but cannot undergo the conformational changes to form pores. Locked mutant contained pairs of Cys residues at specific sites in Ply. This was done in order to lock different parts of the Ply molecule with the intention of preventing them moving apart during pore formation. The amino acids that were replaced by Cys in Ply were Thr 55, Val 163, Ala 262 and Trp 278. In this case Ply carries two mutations and they created by SOE-PCR. The mutants included; Thr55Cys + Val163Cys (intended to lock D2 to TMH1 of D 3 of Ply and A262 + W278C (intended to lock TMH2). The lock mutants were designed by Adnan Muhammad at Leicester University. These mutants can not form pores so they can be activated if DTT added to reduce the disulphide bond.

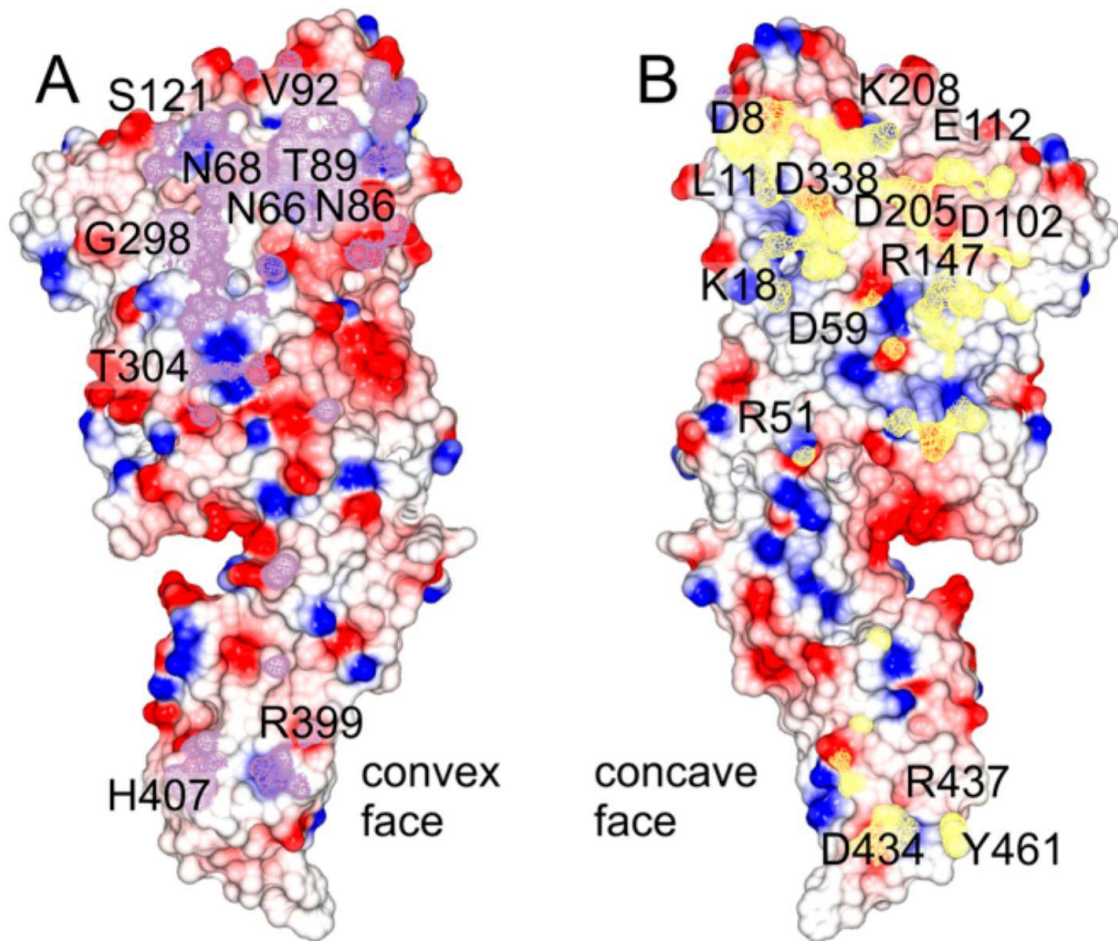


Figure 4-2: Ply residues contribute in the intermolecular interaction.

(A) The convex and (B) concave interacting surfaces showing the electrostatic potential. Regions buried by the interaction are shaded in yellow and purple and the key residues are labelled.

To further study the mechanism of pore formation by Ply, individual fragments (PlyD1-3 and plyD4) were crystallized. Although, PlyD1-3 crystals did not diffract, two separate structures of PlyD4 were determined. The structures suggest that changes in the conformation of the Trp rich-loop at the base of Ply upon membrane binding are likely to facilitate the interaction between Ply monomers, by creating new interactions, thus promoting oligomerization on the cell surface.

4.2 Materials and methods

4.2.1 Materials

All PCR components that were used to make the single and double mutants are described in section 2.2.1. The vector pLEICS-93 was provided by PROTEX at Leicester University, PBS was purchased from Life Technologies. Guanidine-HCl (Gdn-HCl), L- α -phosphatidylcholine, cholesterol, dihexadecyl phosphate, glycerol and calcein were supplied by Sigma. Sheep red blood cells (RBCs) were provided by Thermo Scientific. Nunc supplied the round and flat bottom 96 well plates. Crystallization screens: Morpheus, PACT, JCSG, and Proplex were purchased from Molecular Dimensions. sLeX was supplied by Calbiochem. Hidex sense plate reader, 96 well black plates was from Perkin Elmer. MRC Maxi 48 well crystallization plates were purchased from the Hampton Research, and TTP Labtech provided triple sitting drop 96 well plate.

4.2.2 Construction of Ply mutants by SOE-PCR

Point mutations were introduced into Ply by SOE-PCR (Hussain and Chong, 2016) using a two-step procedure. Mutations were introduced by producing two half fragments, which then combined to generate the full-length Ply gene sequence with the mutants by two rounds of PCR. In the first round PCR the 5' fragments of all mutants were generated using 10 pmol of forward wild-type Ply pLEICS-93 primer with mutant reverse primers as illustrates in (Table 4-1) (Thr88Glu, Arg226Ala, Thr304Arg, Leu11Arg, Asp205Arg, Lys268Ala, Asn339Arg and Val341Arg). Similarly, by first round, PCR the 3' fragments were generated with 10 pmol reverse wild type Ply pLEICS-93 with forward mutant primers (Thr88Glu, Arg226Ala, Thr304Arg, Leu11Arg, Asp205Arg, Lys268Ala, Asn339Arg and Val341Arg). The PCR reaction was explained in section 2.2.7 with the following settings: 5 min at 94°C, 50 sec at 94°C, 50 sec at 62°C, and 1 min at 72°C) for 32 cycles with a final cycle of 5 min at 72°C. Subsequently, the amplified PCR products were run on 1% agarose gel in TBE buffer followed by purification from the gel with Qiagen purification kit. Next, the second round PCR were performed to make the full length Ply. Equal amount of both halves fragments of DNA (20 ng), was used to obtain the full length Ply gene. In each case 2 μ l of short fragment was mixed with the 4 μ l of long fragment with both external forward wt Ply and reverse wt Ply pLEICS-93 (Table 4-1) and the PCR was performed as normally done. PCR was carried out as described previously using a denaturation step of 5 min at 94°C followed by 32 cycles of: 50 sec at 94°C, 50 sec at 62°C, and 1 min at 72°C. PCR products were run on 1% agarose gel and

purified from the gel using a Qiagen purification kit. The resulting mutant Ply genes were introduced into pLEICS-93 (Figure 4-3) by recombination. All clones were sequenced by PNACL. Recombinant plasmids were transformed into *E. coli* BL21 (DE3) and proteins were expressed and purified by Ni-Sepharose affinity chromatography and gel filtration as described for wild-type Ply in section 2.2.6.

Table 4-1: Mutagenic Primer sequences to make the single point mutants.

Mutant amino acid nucleotides are shown in red, start and stop codons are shown in green and aqua respectively. Wild-type is abbreviated to wt.

| First round PCR | Sequence 5'-----3' |
|---------------------------|--|
| Forward wt Ply pLEICS-93 | GTATTTTCAGGGCGCCATGGCAAATAAAGCAGTAAATGACTT |
| Reverse Thr88Glu primer | ATCGACCGCAAGAAGTTCGGGATTATTCTCTAA |
| Reverse Arg226Ala primer | CTCTGCAGAAATTCAGCCTGTTTTAAATCCTC |
| Reverse Thr304Arg primer | CATATCCACCTTGCCACGTACAACCTCGGGCACC |
| Reverse Leu11Arg primer | ATCGTAATTCATAGCGGTATAAAGTCATTAC |
| Reverse Asp205Arg primer | TGGATTTTTAACAGCACGTACGCTGACTGTATA |
| Reverse Lys268Ala primer | AGCTACCTTGACTCCGGCTATCAAAGCTTCAAA |
| Reverse Asn339 Arg primer | AAAGGTCGCAACTACGGGTACACGTAAAAAAGA |
| Reverse Val341Arg primer | ATTTTGAAAGGTGCGCACGTACATTGTCACGTAA |
| Reverse wt Ply pLEICS-93 | GACGGAGCTCGAATTCACATAGTCATTTTCTACCTTATCTTCTA |
| Forward Thr88Glu primer | TTAGAGAATAATCCCGAATTCTTTCGGGTCGAT |
| Forward Arg226Ala primer | GAGGATTTAAAACAGGCTTGAATTCTGCAGAG |
| Forward Thr304Arg primer | GGTGCCCGAGTTGTACGTGGCAAGGTGGATATG |
| Forward Leu11Arg primer | GTAAATGACTTTTATACGGCTATGAATTACGAT |
| Forward Asp205Arg primer | TATACAGTCAGCGTACGTGCTGTAAAAATCCA3 |
| Forward Lys268Ala primer | TTGAAGCTTTGATAGCCGGAGTCAAGGTAGCT |
| Forward Asn339 Arg primer | TCTTTTTTACGTGACCGCTAGTTGCGACCTTT |
| Forward Val341Arg primer | TTACGTGACAATGTACGTGCGACCTTTCAAAT3 |
| Second round PCR | Sequence 5'-----3' |
| Forward wt Ply pLEICS-93 | GTATTTTCAGGGCGCCATGGCAAATAAAGCAGTAAATGACTT |
| Reverse wt Ply pLEICS-93 | GACGGAGCTCGAATTCACATAGTCATTTTCTACCTTATCTTCTA |

PCR was carried out as described previously using a denaturation step of 5 min at 94°C followed by 32 cycles of: 50 sec at 94°C, 50 sec at 62°C, and 1 min at 72°C. PCR products were run on 1% agarose gel and purified from the gel using a Qiagen purification kit. The resulting mutant Ply genes were introduced into pLEICS-93 (Figure 4-3) by recombination. All clones were sequenced by PNACL. Recombinant plasmids were transformed into *E. coli* BL21 (DE3) and proteins were expressed and purified by Ni-

Sepharose affinity chromatography and gel filtration as described for wild-type Ply in section 2.2.6.

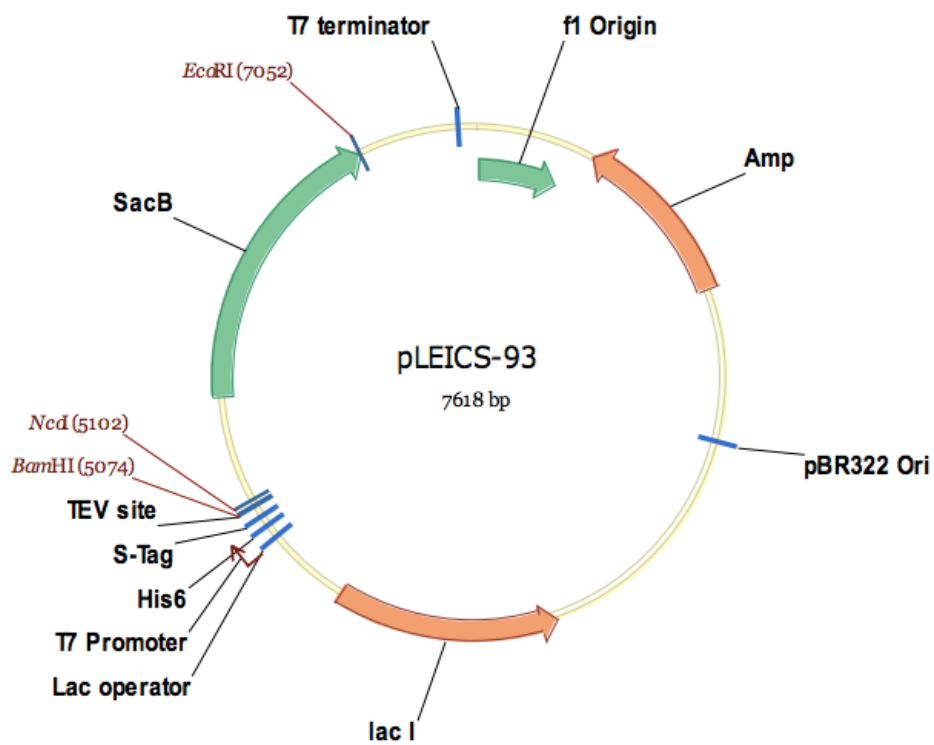


Figure 4-3: Vector map of pLEICS-9.

4.2.3 Mutations in the TMH1 and TMH2 region of Ply

Mutations were also introduced into the TMH1 and TMH2 regions of Ply and two disulphide-locked mutants were created. Oligonucleotide primers are shown in (Tables 4-1 and 4-2).

Table 4-2: Primer sequences of the TMH1 and TMH2 mutants.

The cysteine codons in all primers are shown in a bold red.

| Primers TMH1 | Sequence 5'-----3' |
|-------------------|---|
| Tyr55Cys forward | AAGCGGAGCTTGTCG TGT AATACAAGTGATATT |
| Tyr55Cys reverse | AATATCACTTGTATT ACA CGACAAGCTCCGCTT5 |
| Val163Cys forward | ATGGAACAACCTCAAG TGT AAGTTTGGTTCTGAC |
| Val163Cys reverse | GTCAGAACCAAACTT ACA CTTGAGTTGTTCCAT |
| Primer TMH2 | Sequence 5'-----3' |
| Ala262Cys forward | GATGAAGTAGAGGCT TGT TTTGAATCTTTGATA |
| Ala262Cys reverse | TATCAAAGATTCAAAA ACA AGCCTCTACTTCATC |
| Trp278Cys forward | GCTCCTCAGACAGAG TGT AAGCAGATTTTGACA |
| Ala278Cys reverse | TGTCAAAATCTGCTT ACA CTCTGTCTGAGGAGC |

4.2.4 Fluorescence spectroscopy

Fluorescence spectroscopy has long been used to study protein folding and dynamics. The protein conformation changes are mostly dependent on the tryptophan (Trp) and tyrosine (Tyr) residues because these are the natural fluorophores in proteins (Munishkina and Fink, 2007, Zhang et al., 2013). The dominant source of the intrinsic protein fluorescence is Trp, because it has the highest quantum yield. The Trp emission maximum $\lambda_{em, max}$ is sensitive to the polarity of its environment. The $\lambda_{em, max}$ of buried of Trp is around 335 nm, whereas for fully solvent accessible Trp this value increases to 355 nm (Ghisaidoobe and Chung, 2014, Munishkina and Fink, 2007). The intrinsic fluorescence of Phe in proteins is usually relatively unimportant (in proteins containing Tyr and Trp) due to that phe has low absorptivity and quantum yield. The quantum yield of Tyr is similar to Trp, but the Trp indole group is considered as the dominant source of UV

absorbance at ~280 nm and emission at ~350 nm in proteins (Ghisaidoobe and Chung, 2014).

In this study, fluorescence spectroscopy was performed to investigate stabilities of all mutants. Ply has 41 aromatic residues including 19 Tyr, 8 Trp and 14 Phe residues. Gdn-HCl was used as the protein denaturant (Rashid et al., 2005).

4.2.5 Stability of mutants

Fluorescence spectra were taken for all mutants using a linear titration of Gdn-HCl over the concentration range of 0.55-2.0 M. The protein concentration of all mutants was 1 μ M in 20 mM Tris-HCl pH 7.5 in a total volume of 300 μ l in the low volume quartz fluorescence cuvette (Sigma). Fluorescence measurements were performed using a Fluoromax-4 (Horiba Jobin Yvon). Proteins were excited at 280 nm with a 2.5 nm slit width and fluorescence was detected between 300 and 400 nm at 1 nm intervals with a 2.5 nm slit width. All spectra were collected at 20 °C. The cuvette was placed in the heat block inside the fluorimeter for 150 sec to allow equilibration before collecting spectra.

4.2.6 Preparation of liposomes

Liposomes were prepared according to (Nollmann et al., 2004) by mixing Chol/ α -phosphatidylcholine/dihexadecyl phosphate at a molar ratio of 130:130:13 μ moles (50, 100, and 7.1 mg) respectively. This mixture was dissolved in 5ml 1:1 (v/v) methanol/chloroform in a volumetric flask and solubilized by shaking. Then it was dried under a dry stream of nitrogen on ice. After all the liquid had evaporated, the translucent lipid film was rehydrated in 5 ml PBS and dissolved by vortexing and sonicating at room temperature for 90 sec and stored at 4°C for one week.

4.2.7 Fluorescence data collection with liposomes

Fluorescence spectra were collected with liposome for wild-type Ply and all mutants (Thr88Glu, Arg226Ala, Thr304Arg, Leu11Arg, Asp205Arg, Lys268Ala, Asn339Arg and Val341Arg, Thr55Cys+V163Cys and A262Cys+Trp278Cys) against fixed concentration of liposome. The final concentration of each mutant and cholesterol were adjusted at 1 μ M, and 10 μ M in PBS respectively. First 270 μ l of PBS mixed with 30 μ l of proteins and the spectra were collected. Then 270 μ l of liposome mixed with 30 μ l of proteins and spectra were collected again in a total volume of 300 μ l in the low volume

quartz fluorescence cuvette (Sigma). Fluorescence measurements were performed using a Fluoromax-4 (Horbia Jobin Yvon). Proteins were excited at 280 nm with a 2.5 nm slit width and fluorescence was detected between 300 and 400 nm at 1 nm intervals with a 2.5 nm slit width. All spectra were collected at 20 °C. The cuvette was placed in the heat block inside the fluorimeter for 150 sec to allow equilibration before collecting spectra.

4.2.8 Haemolytic assay

To prepare 1% v/v of sheep red blood cells (RBCs), cells were washed 3 times in chilled PBS. Cells were pelleted by centrifugation at 1734 g, at 4°C for 15 min. Two-fold serial dilutions of Ply were aliquoted into round-bottomed 96-well microtitre plates with a final volume of 50 µl. These dilutions were mixed with an equal volume of 1% v/v sheep RBCs. Plates were incubated at room temperature for 30 min, and then centrifuged at 1734 g, at 4°C to remove unlysed RBCs and cellular debris. Then 80 µl of the supernatant was transferred into flat-bottomed 96-well microtiter plate, and the absorbance was measured at 410 nm to measure haemoglobin.

4.2.9 Transmission electron microscopy (TEM)

Electron microscopy was used to check oligomerization of Ply on unilamellar liposome vesicles. Each mutant (1µM) was mixed with a 1/50 dilution of liposomes in PBS and left at room temperature for 10 min. Then 5 µl of each sample was applied to a freshly glow-discharged 400 mesh carbon-coated grid (Agar Scientific Ltd). Grids were discharged for 60 sec in a Q150T ES machine. The excess sample was removed by touching a piece of filter paper to the side of the grid. Grids were negatively stained with 5 µl of 1% (w/v) uranyl acetate for 5 sec and immediately blotted dry. Then a further 5 µl of stain was added to the grid and left for 10 sec and blotted dry. Negatively stained specimens were viewed on a JEOL 1400 TEM with an accelerating voltage of 100 kV. The digital images were collected with a Megaview III digital camera with iTEM software at Leicester University.

4.2.10 Preparation of liposomes with calcein

Unilamellar liposomes were prepared as described in section 5.4 and rehydrated in 1ml of 70 mM calcein, it was dissolved in 1M KOH until dissolution occurred then the pH was brought back to 7.4 by adding 2M HCl (Chongsiriwatana and Barron, 2010). Unilamellar liposome vesicles were extruded 20 times through 1 µm polycarbonate

membrane to entrap the calcein. The mixture was centrifuged at 500 rpm for 20 min and the liposome pellet was washed in 1ml PBS four times to eliminate free calcein. The liposome pellet was resuspended in 1ml PBS and stored at 4°C for one week.

4.2.11 Calcein-leakage assay

Leakage of the self-quenching calcein from liposomes upon exposure to Ply was measured in a spectrofluorometer (HIDEX Sense) using Optiplate-96 F black bottom (Perkin Elmer) at an λ_{ex} of 485 nm and λ_{em} of 560 nm at 37°C. Complete release of calcein was obtained by exposing liposomes to Triton X-100 at a final concentration of 0.25 mM. Self-quenching calcein from the liposome vesicles were measured for the wild-type Ply, mutant Asp205Arg, Asn339Arg, Ply D1-3 and PlyD4. In this experiment 2.5 μl of liposomes with calcein was added to each well with a final volume of 100 μl with different concentration of each protein (20 mM, 10 mM, 8 mM, 6 mM, 4 mM, 2 mM and 0 mM). The kinetics mode of the spectrophotometer was measured every minute for about 30 min at 37°C.

4.2.12 PlyD1-3 crystallization and optimization

Sitting drop were set up with commercial crystallization screens: Morpheus, PACT, JCSGs, and Proplex by mixing 0.1 μl reservoir buffer with 0.1 μl of purified PlyD1-3 (10 mg/ml) on MRC crystallization plates using a Mosquito NanoDrop crystallisation robot. Screens were tested at room temperature and at 4°C. After one-week crystals were observed in most screens. The best quality crystals were observed in the Proplex screen: 0.2 M sodium acetate, 0.1 M sodium citrate pH 5.5 and 5% PEG 4000 at 4°C. Variants of this condition were set up manually to try to improve the quality of the crystals by changing the precipitant concentration. Table 4-3 shows the optimization buffers. For larger drops, 1.5 μl of PlyD1-3 (10 mg/ml) was mixed with 1.2 μl reservoir buffer.

4.2.13 PlyD4 crystallization with sLeX

PlyD4 (5 mg/ml) crystallization trials were set up with sLeX trisaccharide (20 mM) using JCSG and PACT screens as described in section 4.2.12. Plates were kept at room temperature and checked daily. Promising crystals were observed in JCSG screen: 0.1 M potassium thiocyanate, and 30% PEG MME 2000. Based on the initial screen, larger drops were set up changing the concentration of the PEG precipitant to 15, 20, 25, 30, 35, 40%. 1.5 μl of protein with sLeX was mixed with 1.2 μl of the reservoir solution and

incubated at room temperature. After one-month small crystals grew in 0.1 M potassium thiocyanate, and 35% PEG MME 2000.

Table 4-3: Optimisation crystallisation condition for PlyD1-3.

| | |
|----|---|
| 1 | 100 mM HEPES pH 7.5, 8% ethylene glycol EG and 20%, 18%, 16%, 14%, 12%, 10% PEG 8000 |
| 2 | 200 mM Potassium thiocyanate, 100mM BTP pH8.5 and 20%, 18%, 16%, 14%, 12%, 10% PEG 8000 |
| 3 | 100 mM HEPES pH 7.5, 12% PEG 8000 and 14%, 12%, 10%, 8%, 4%, 2% EG |
| 4 | 100 mM Trizma-Ac pH 8, 200mM potassium thiocyanate and 20%, 18%, 16%, 14%, 12%, 10% PEG 8000 |
| 5 | 100 mM Trizma -Ac pH 8.5, 200mM potassium thiocyanate and 20%, 18%, 16%, 14%, 12%, 10% PEG 8000 |
| 6 | 100 mM HEPES pH 7.5, 12% PEG 8000, 10% EG and different volume drops of the protein and the buffers |
| 7 | 100 mM HEPES pH 7, 10% EG and 20%, 18%, 16%, 14%, 12%, 10% PEG 8000 |
| 8 | 100 mM Trizma -Ac pH 8, 10% EG and 20%, 18%, 16%, 14%, 12%, 10% PEG 8000 |
| 9 | 100 mM Trizma -Ac pH 8.5, 10% EG and 20%, 18%, 16%, 14%, 12%, 10% PEG 8000 |
| 10 | 0.1 M Sodium acetate pH4.5 and 1.8, 1.6, 1.4, 1.2 1 and 0.8M ammonium phosphate dibasic |
| 11 | 0.2 M Sodium acetate, 0.1M sodium citrate pH 5.5 and 7% PEG4000 incubated at 4°C |
| 12 | 0.1 M MgCl ₂ 0.1 M HEPES pH 7.5, 10% PEG 4000 at room temperature |
| 13 | 0.2 M Sodium acetate, 0.1 M sodium citrate pH5.5 10% PEG4000 at room temperature |

4.2.14 X-ray diffraction of PlyD1-3 and PlyD4 crystals

PlyD1-3 crystals were picked with litho loops in buffer containing 30% v/v glycerol as a cryoprotectant. Crystals were frozen in a stream of nitrogen gas. Prof. Russell Wallis carried out this work. Diffraction data were collected at 100K at beam line Diamond LS and were analysed using CCP4 by Prof. Russell Wallis. Phases for the D4 structures were determined using D4 of the Ply structure as a search model. Manual refinement in Coot was used to optimize the models (Emsley and Cowtan, 2004) in combination with refinement in Refmac5, part of the CCP4 software suite (Krissinel, 2015) and in Phenix

(Adams et al., 2010).

4.2.15 Crystallization theory

150 years ago protein crystallization was discovered by chance and in the late 19th century it was developed as a powerful purification tool and as a demonstration of chemical purity (McPherson and Gavira, 2014). Two steps are generally used to obtain crystals. The first is the identification of crystallization conditions, which depends on the chemical, biochemical and physical conditions. Then, the crystal conditions are optimized by changing the initial conditions by incremental amounts to obtain the better quality crystal for diffraction analysis (McPherson and Gavira, 2014). Crystallization proceeds in two inseparable steps: nucleation and growth. To obtain crystals, the protein is brought to supersaturation. This is a non-equilibrium condition in which the concentration of the macromolecule is increased above the solubility limit (McPherson and Gavira, 2014). Weak protein-protein interactions that may be specific or nonspecific lead to crystal formation, leading to nucleation, which is the critical step in the crystallization. Nucleation is followed by crystal growth (McPherson and Gavira, 2014, Durbin and Feher, 1996). The crystallization process encompasses four zones: undersaturation, nucleation, metastable and precipitation zones (Figure 4-4) (Chayen, 2004). In the precipitation zone, the protein concentration reaches a high supersaturation, so precipitates. At lower concentrations the system moves to the nucleation zone where nucleation can occur. Crystal growth occurs in the metastable zone. As the crystal grows so the solubility of protein decreases. Eventually, crystal growth stops in the undersaturation zone.

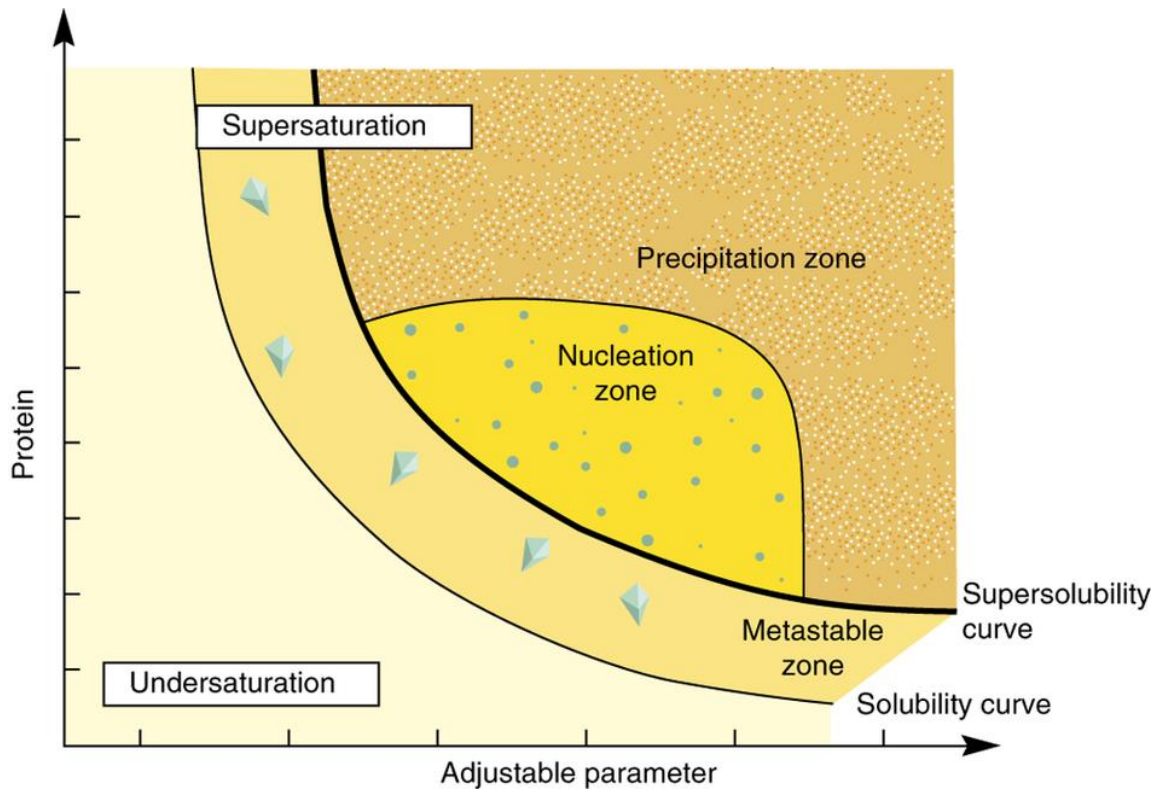


Figure 4-4: Schematic diagram of protein crystallization phase.

The changeable factor can be additive concentration or precipitant, pH, temperature. The solubility curve is defined as the concentration of protein in the solute that is in equilibrium with crystals. Whereas, the supersolubility curve is defined as the line that splits conditions where spontaneous nucleation or precipitation occurs from conditions where the crystallization solution remains clear if it is left undisturbed. Four zones including precipitation, nucleation metastable and undersaturation condition these zones are produced as a result of the different degree of supersaturating conditions (Chayen, 2004).

4.2.16 X-ray diffraction

X-rays are specifically a powerful approach to achieving insight into the inner structure of material because the wavelength of X-rays corresponds to the interatomic distances in macromolecules. For this reason, constructive and destructive interference occurs between X-rays that are scattered from atoms and the scattered waves are said to diffract (Pouget et al., 1975). In 1912 Max von Laue and Co discovered that crystalline substances act as three-dimensional diffraction gratings for X-ray wavelengths identical to the spacing of planes in a crystal lattice (Bunaciu et al., 2015). X-ray diffraction is the most contributive experimental method in structural biology.

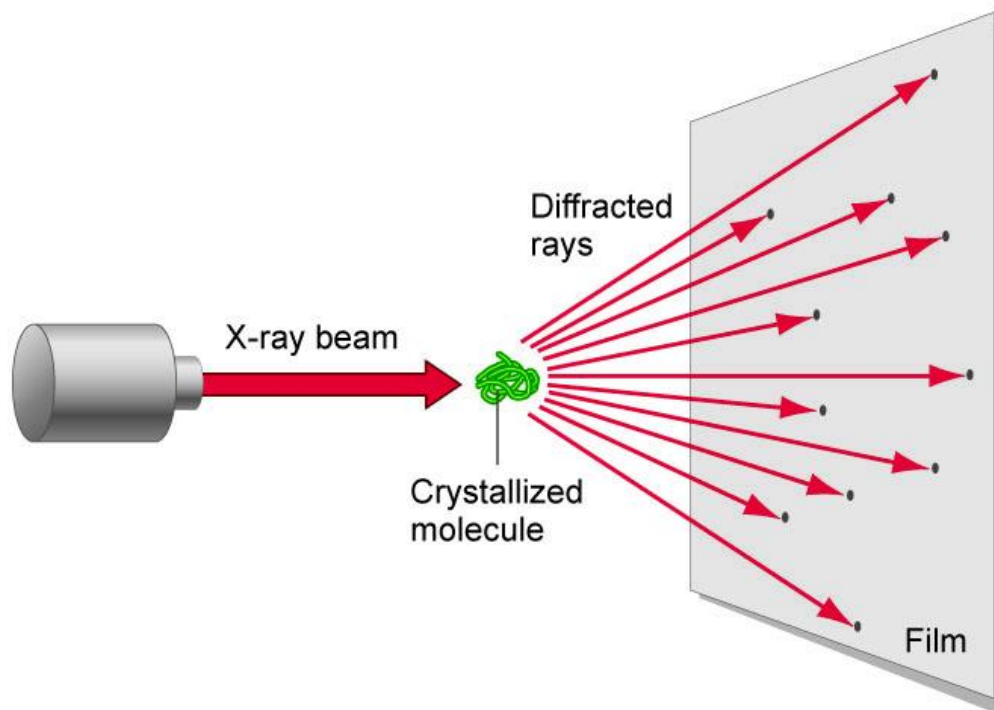


Figure 4-5: X-ray diffraction.

When X-ray beams hit the crystal, the beam is diffracted, depending on the arrangement of atoms within the structure. At specific angles, constructive interference produces spots on the film or detector.

Scattering can be detected when a large number of the molecules are arranged in a well-defined configuration in the crystal. Typical X-ray wavelengths are about 0.1-100 Å, which is on the order of the atomic spacing in a solid (Scheck, 2013). The diffraction of the X-ray can be calculated by Bragg's law: $n\lambda = d\sin\theta$ (n is an integer, the wavelength of the X-rays is λ , the spacing between the planes in the atomic lattice is d , the angle between the incident ray and the scattering planes as θ (Jenkins, 2000).

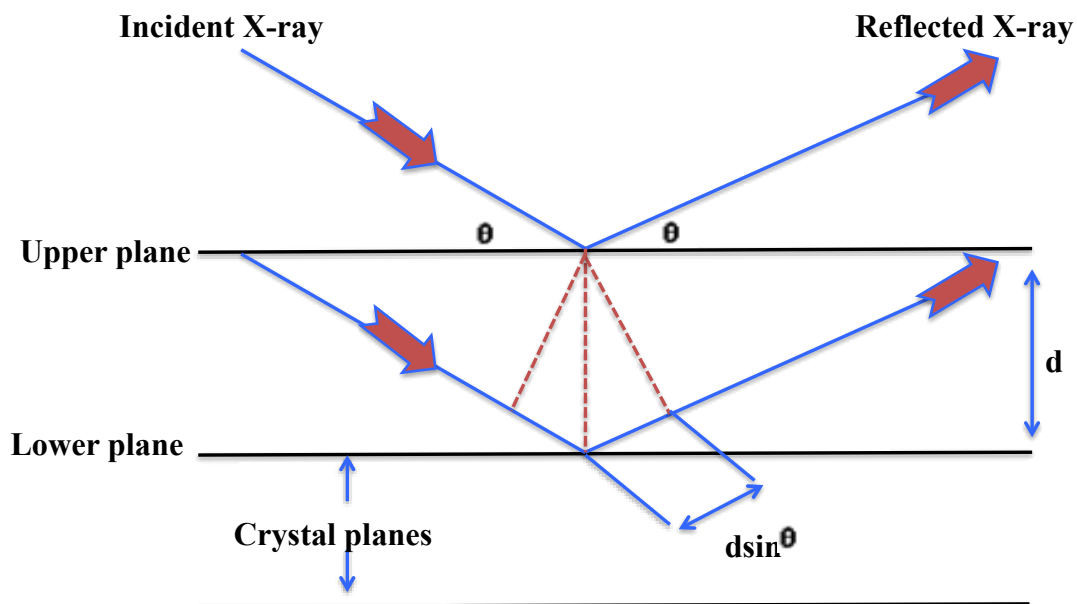


Figure 4-6: The two-dimensional representation of the reflected X-ray from two crystal planes.

Suppose that the X-ray beam is incident at the angle θ in one of the crystal plane then the beam is reflected from an atom of both planes (upper and lower planes). The reflected beam from the lower surface travels further from the upper surface reflected beam by a distance of $2d \sin \theta$. The reflected beam from both planes is combined to make the constructive interface when this path difference is equal to some integral multiple of the wavelength λ .

4.3 Results

4.3.1 SOE-PCR construction of single mutant Ply

In the crystal structure of Ply, individual Ply monomers are packed side-by-side, which resembles the molecular packing of the pre-pore complex. To test whether the intermolecular interactions observed in the crystal are also essential for the cytolytic activity of the toxin, mutations were introduced into those residues at the interface. In total eight point mutations were introduced. These mutations were designed to change surface exposed residues and thereby to disrupt the intermolecular packing. Most residues were changed to large charged groups (Glu or Arg) because these are likely to be most disrupting of the surface complementarity: Leu11Arg, Thr88Glu, Asp205Arg, Val341Arg, Thr304Arg and Asn339Arg (L11R, T88E, D205R, V341R, T304R and N399R). Other mutations Lys268Ala, Arg226Ala (K268A and R226A) were made to

disrupt polar intermolecular interactions.

SOE-PCR was used to generate all mutants of Ply using two rounds of PCR. In the first round, the mutation was introduced into the Ply gene to create two overlapping fragments. In the second round the fragments were amplified to generate the full-length mutant gene. First round and second round PCR is shown for two of the mutants including Asp205Arg (fragments of 615bp and 804bp) and Lys268Ala (fragments of 615bp and 804bp) both mutants are designated as D205R and K268A in (Figure 4-7). A similar strategy was used to create all mutants. Once the full-length mutant clones were produced, they were cloned into pLEICS-93 by PROTEX. DNA sequencing by PNACL was used to verify the mutations and to confirm that no additional changes were introduced by the PCR. Proteins were expressed in BL21 (DE3) and purified by Ni-chromatography followed by size exclusion chromatography on a Superdex 200 16/60 as described for the wild-type protein. Yields of all proteins were high with ~35 mg of protein from 1L of culture.

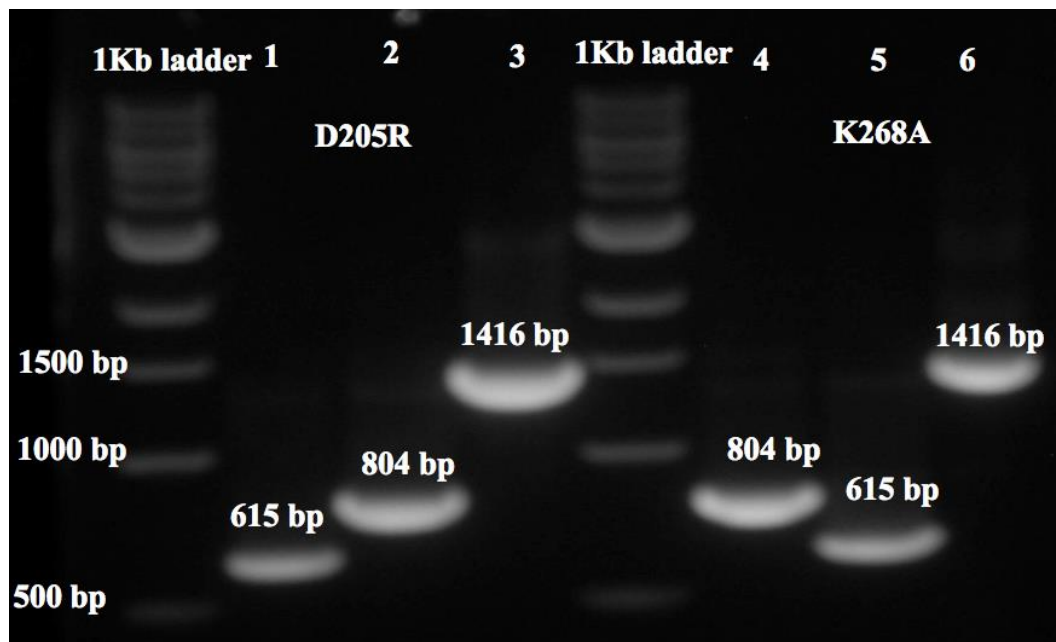


Figure 4-7: SOE-PCR to introduce the mutations D205R and K268A into Ply.

In the first round, PCR products of 615 bp and 804 bp (D205R) and 804 bp and 615 bp (K268A) were produced which matched the expected size of the fragments. These products were combined to generate the 1416 bp gene of full length Ply.

4.3.2 Mutations in TMH1 and TMH2 region of Ply

Two double mutants were introduced into Ply gene to create disulphide-locked mutants: Thr55Cys+Val163Cys and Ala262Cys+Trp278Cys. These mutations were introduced into the regions of Ply that form the transmembrane structures of the pore. D3 of Ply consists of a 5-stranded antiparallel β -sheet that is surrounded by the two α -helical bundles that become (TMH1 and TMH2) (Shepard et al., 1998, Shatursky et al., 1999, Lawrence et al., 2015). When Ply binds to the membrane, TMH1 and TMH2 unfurl to make two β -hairpins, which insert into the membrane. TMH1 was initially identified in PFO as residues S190-N217 (Shepard et al., 1998) and TMH2 as K288-D311 (Shatursky et al., 1999). Residues M158-E187 (TMH1) and D257-Q280 (TMH2) represent the corresponding stretches in Ply (Figure 4-8).

```
10      20      30      40      50      60
MANKAVNDFI LAMNYDKKKL LTHQGESIEN RFIKEGNQLP DEFVVIERKK RSLSTNTSDI

      70      80      90      100     110     120
SVTATNDSRL YPGALLVVD E TLLENNPTLL AVDRAPMTYS IDLPGLASSD SFLQVEDPSN

      130     140     150     160     170     180
SSVRGAVNDL LAKWHQDYGQ VNNVPARMOY EKITAHSMEQ LKVKFGSDFE KTGNSLDIDF

      190     200     210     220     230     240
NSVHSGEKQI QIVNFKQIYY TVSVDAVKNP GDFVQDTVTV EDLKQRGISA ERPLVYISSV

      250     260     270     280     290     300
AYGRQVYLKL ETTSKSDEVE AAFEALIKGV KVAPQTEWKQ ILDNTEVKAV ILGGDPSSGA

      310     320     330     340     350     360
RVVTGKVDMV EDLIQEGSRF TADHPGLPIS YTTSFLRDNV VATFQNSTDY VETKVTAYRN

      370     380     390     400     410     420
GDLLLDHSGA YVAQYYITWN ELSYDHQGKE VLTPKAWDRN GQDLTAHFTT SIPLKGNVRN

      430     440     450     460     470
LSVKIRECTG LAWEWWRVTV EKTDLPLVRK RTISIWGTTL YPQVEDKVEN D
```

Figure 4-8: Ply amino acid residues forming TMH1 and TMH2.

Residues M158-E187 and D257-Q280 highlighted as black and navy blue bold respectively form the TMH1 and TMH2 regions of Ply. Blue, green, red and black residues indicate domains 1, 2, 3 and 4, respectively.

Figure 4-9 summarizes the construction of the double mutants (Thr55Cys+Val163Cys and Ala262Cys+ Trp278Cys Ply genes encoding the locked mutants. Single mutations were introduced first and these were used as templates to generate the final double mutant. Mutant Plys gene were introduced into pLEICS-93 vector by recombination and were produced in BL21 (DE3) as described for the single mutants.

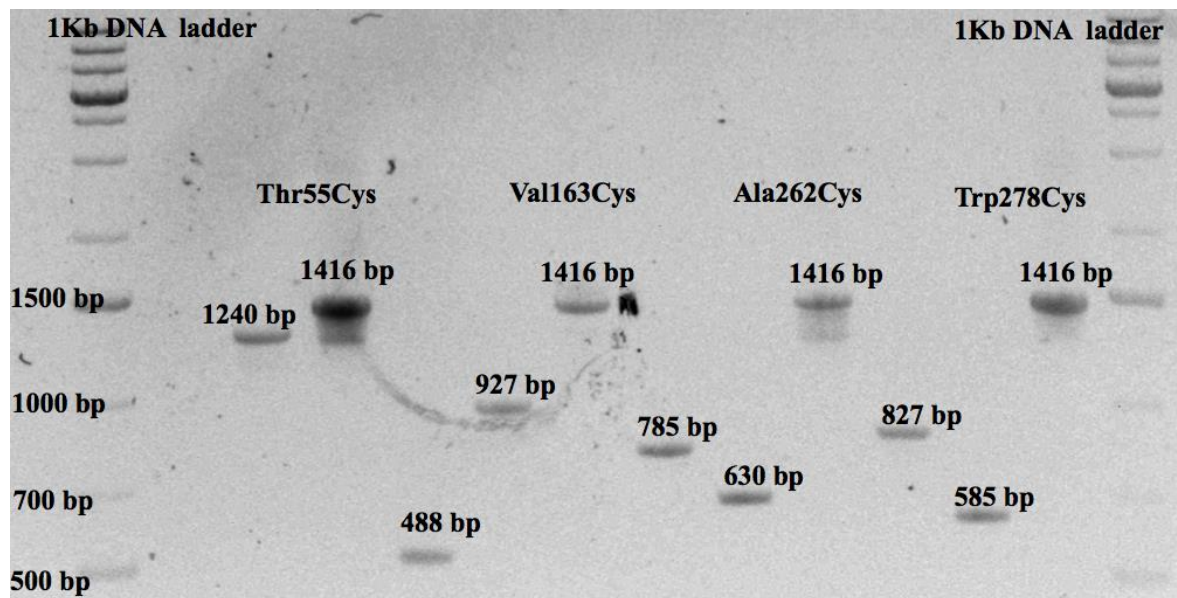


Figure 4-9: Result of SOE-PCR showing the construction of the Ply Thr55Cys+Val163Cys (TMH1) and Ala262Cys+Trp278Cys (TMH2) mutants.

PCR was used to produce the full-length double mutants Ply in a multi-step process. Products from the initial reactions, after producing two half fragments were combined and used as a template to generate the full-length single mutants Thr55Cys. This was used as template to make Val163Cys and finally Thr55Cys+Val 163Cys was produced. Ala262Cys was created and used as template to make Trp278Cys and finally Ala262Cys+Trp278Cys was produced.

4.3.3 Cytolytic activities of Ply mutants

The haemolytic activities of mutant Plys was compared with wild-type protein using sheep RBCs. Haemolysis was measured by absorbance at 410 nm to detect the released haemoglobin following lysis. The ability of Ply to lyse sheep RBCs was reduced in all mutations, but by different degrees, as shown in (Figure 4-10 A and Table 4-4). The greatest effects were observed for Asn339Arg and Asp205Arg, which failed to lyse sheep RBCs at the highest concentrations tested (10 μ M) reflecting >3000-fold decreases in haemolytic activity. Both mutations are located towards in the middle of the binding

interface within D1. Other mutations including Thr88Glu and Arg226Ala in D1 also caused substantial decreases of about 25.6 and 15.6 folds in their haemolytic activity respectively. The mutation Thr304Arg within D3 resulted in a 300-fold decrease in the hemolytic activity. The Thr side chain forms part of a β strand, which packs against the hydrocarbon portion of side chain of Lys268. The activities of Leu11Arg and V341Arg were also lower but only by ≤ 2 -fold. Interestingly, these residues are situated in the posterior region of D1 that forms the outer part of the pre-pore ring. Residues in this region of the toxin may be less important for oligomerization, perhaps reflect some flexibility when monomers assemble. In summary, disruption of the surface complementarity and polar intermolecular interactions of Ply in the crystal structure also reduce the ability of the toxin to produce pores. These findings support our hypothesis that the packing observed in the crystal lattice mimics the packing of Ply during pore formation.

Analysis of the two disulphide locked mutants showed that both had reduced haemolytic (5%, 1.5% of Ala262Cys+Trp278Cys and Tys55Cys+Val163Cys of wild type Ply) (Figure 4-10 B) activities, as expected, but neither completely abolished haemolysis. The simplest explanation for the residual activity is that a small proportion of each mutant contained reduced cysteine residues so could still form pores. As expected, neither D4 nor D1-3 had haemolytic activity (Figure 4-10 B), indicating that the full-length Ply is required for pore formation. The hemolytic activity test of locked mutants were carried out separately and highlighted as grey in (table 4.4).

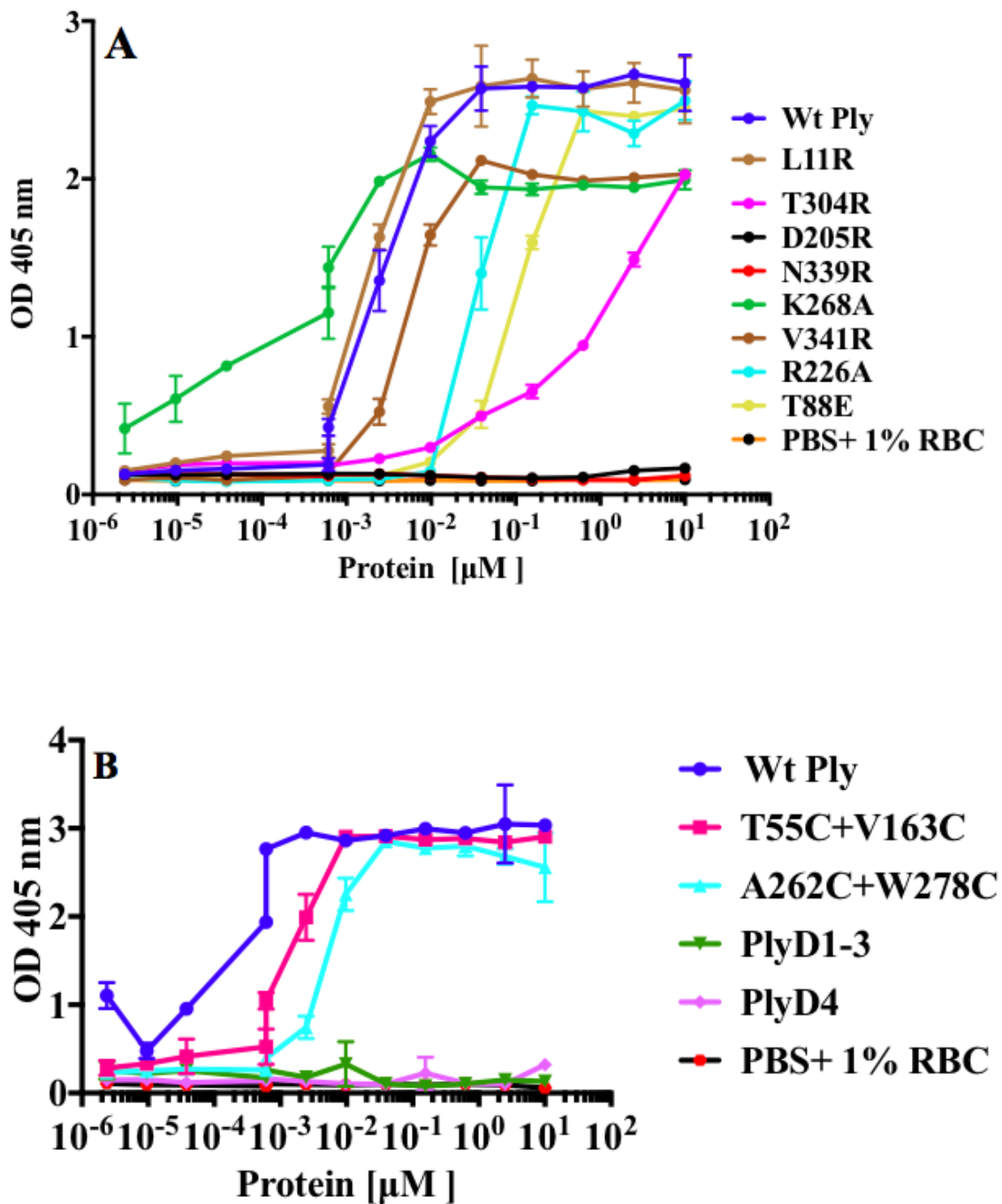


Figure 4-10: Haemolytic activities of wild-type Ply, mutants Ply and ply truncated fragments.

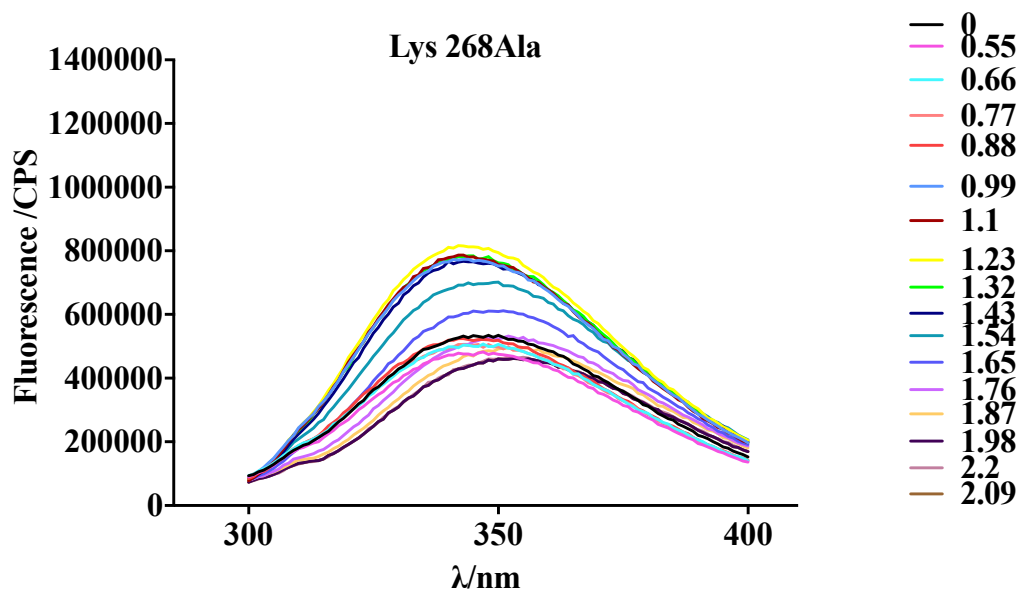
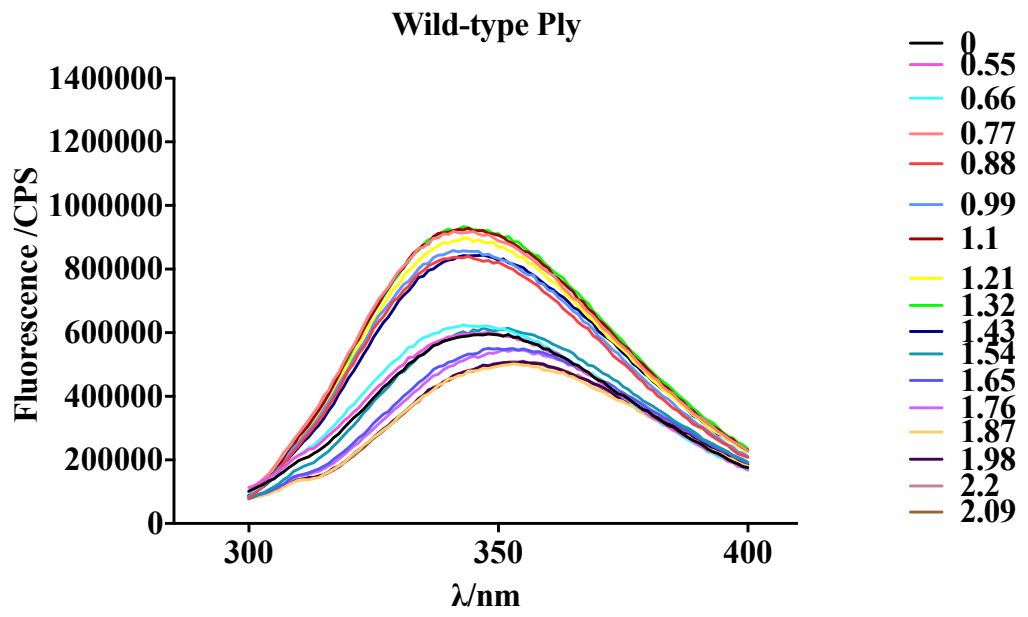
Figure A, and B is shown the haemolytic activity of single mutants, double mutants and Ply fragments. The absorbance of haemoglobin was measured at 410nm absorbance after 30 min incubation at room temperature PBS was used as a negative control. The data was recorded in triplicate and the error is the SEM. Graph pad prism 7 programme was used to make the figures.

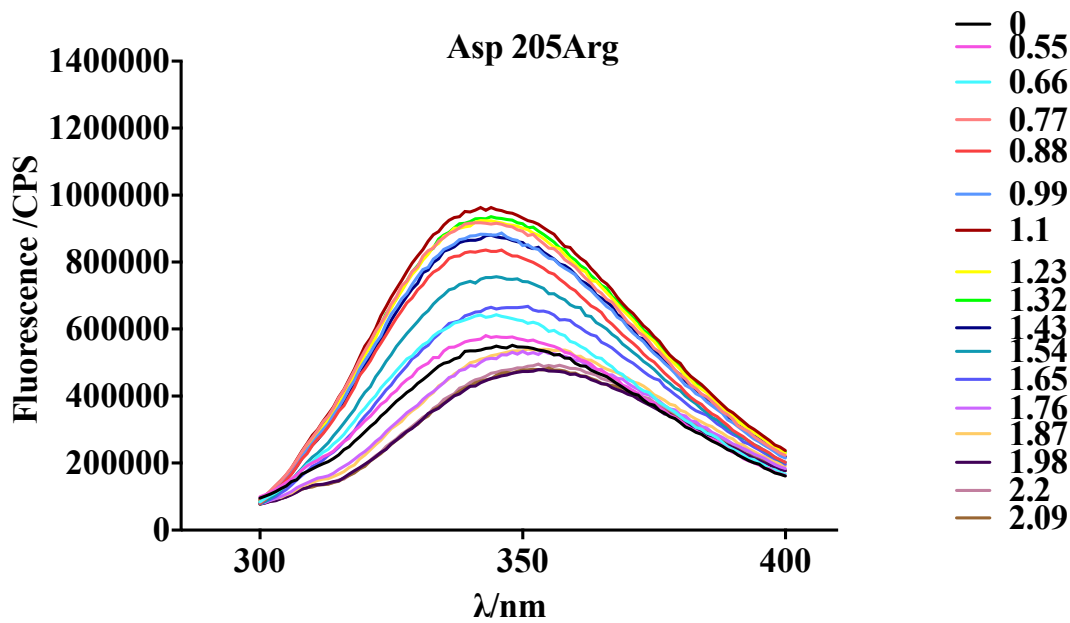
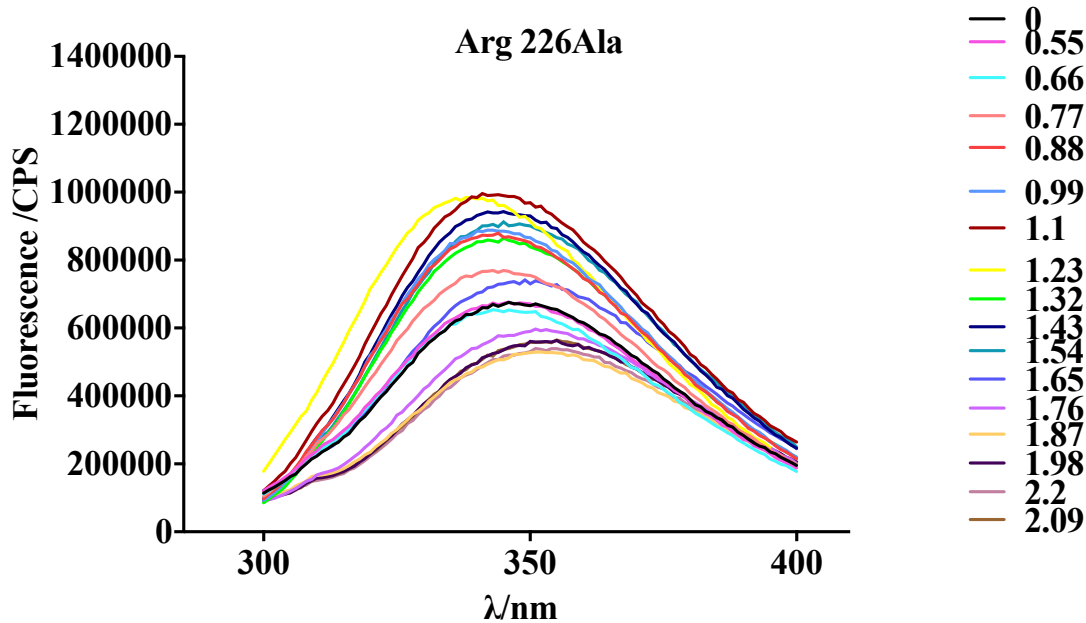
Table 4-4: Cytolytic activity of wild-type Ply and Ply mutants. The haemolytic activity of single mutants and double mutants were carried out at different time. Therefore, the relative activity of wild-type Ply is different.

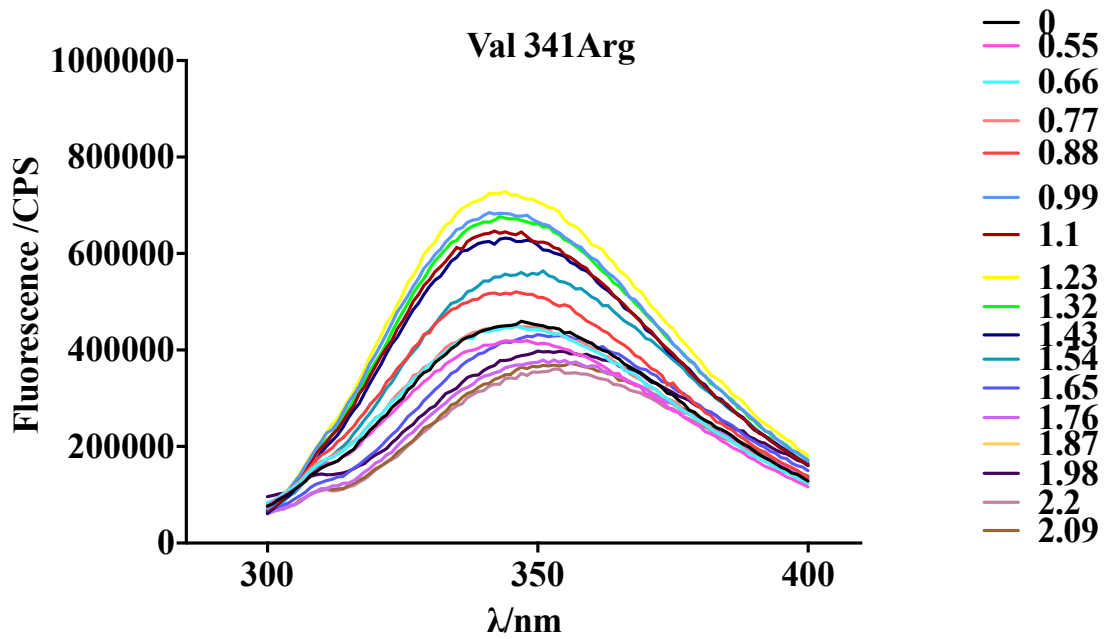
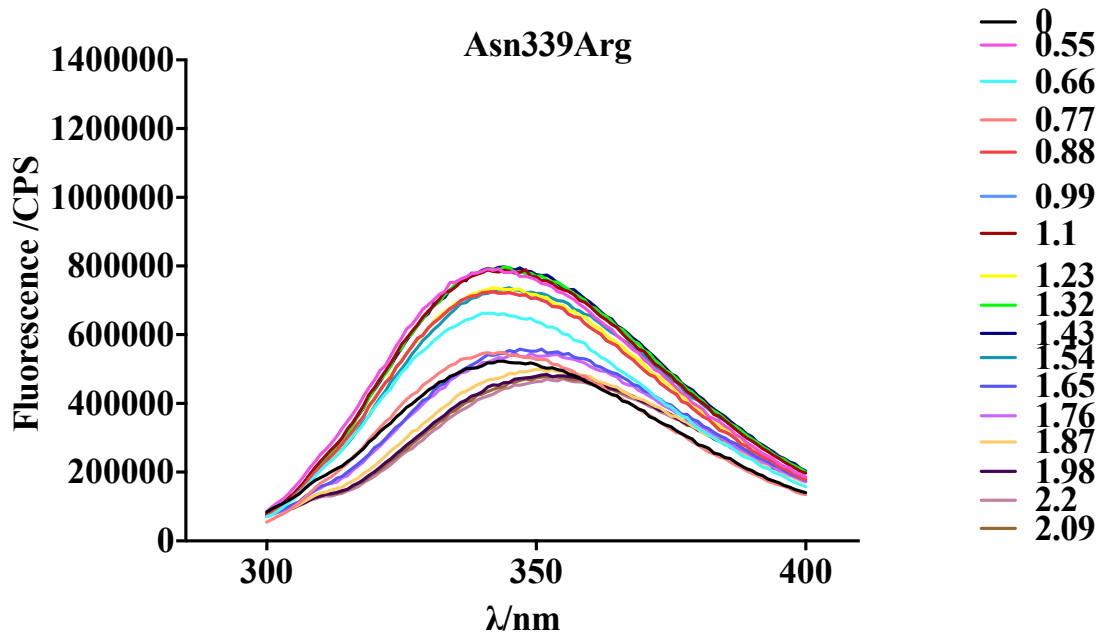
| Protein | EC50 (nM) | Relative haemolytic activity |
|---------------|-----------|------------------------------|
| Wild-type Ply | 2.6 | 1.0 |
| L11R | 4.6 | 0.565 |
| T88E | 76 | 0.034 |
| D205R | >10000 | <0.0003 |
| N339R | >10000 | <0.0003 |
| R226A | 48 | 0.054 |
| T304R | 900 | 0.0031 |
| K268A | 6.3 | 0.412 |
| V341R | 2.5 | 1.04 |
| Wild-type | 6.4 | 1 |
| T55C+V163C | 4.07 | 1.5 |
| A262C+W278C | 1.8 | 3.5 |

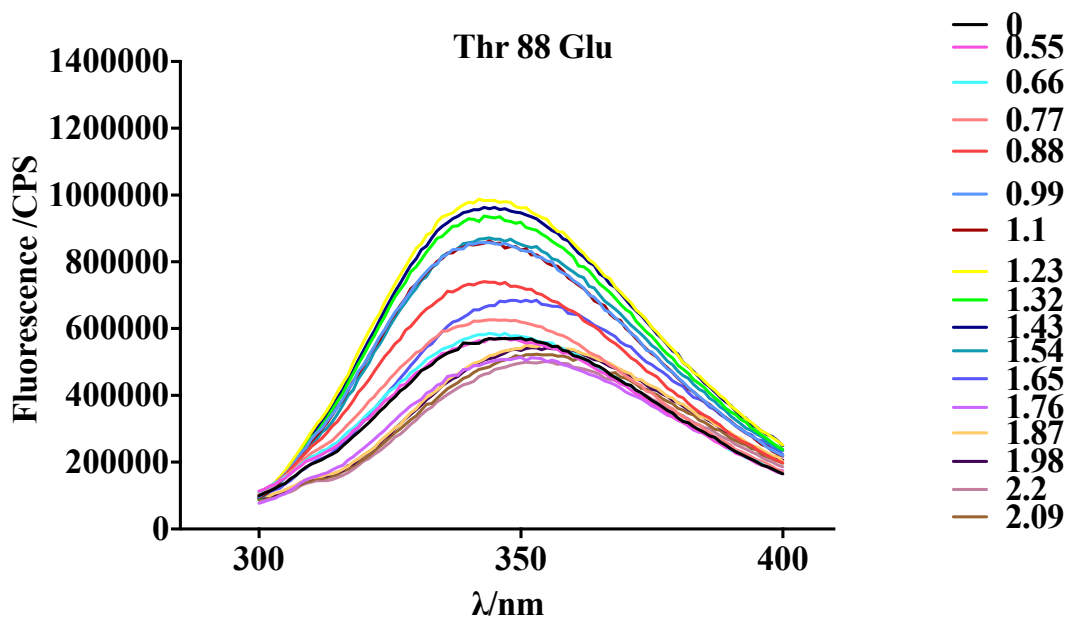
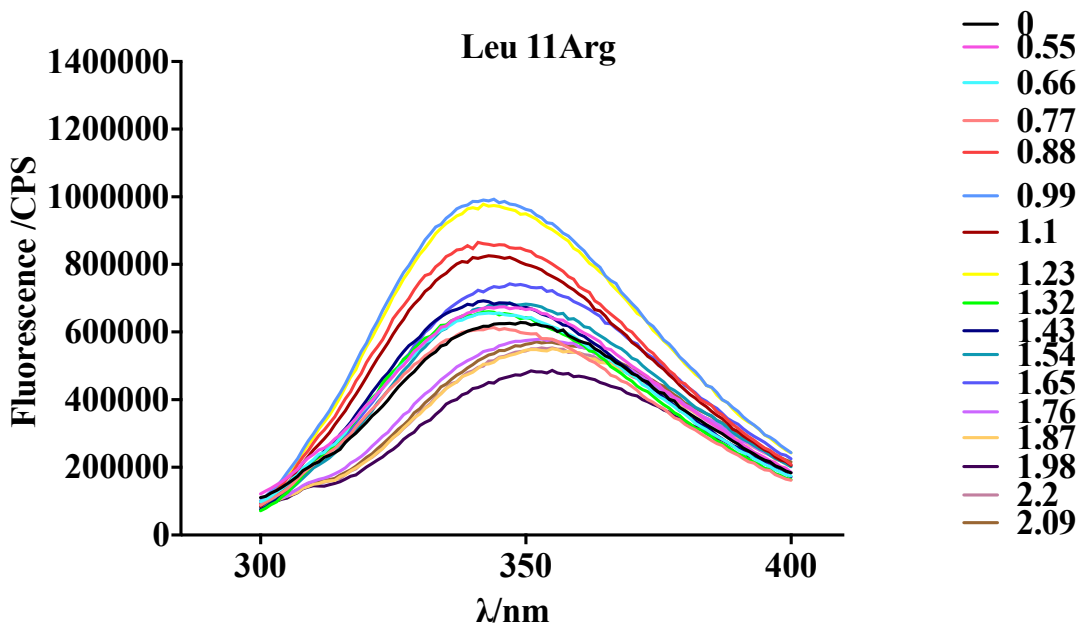
4.3.4 Stability measurement of mutants by Gdn-HCl denaturation

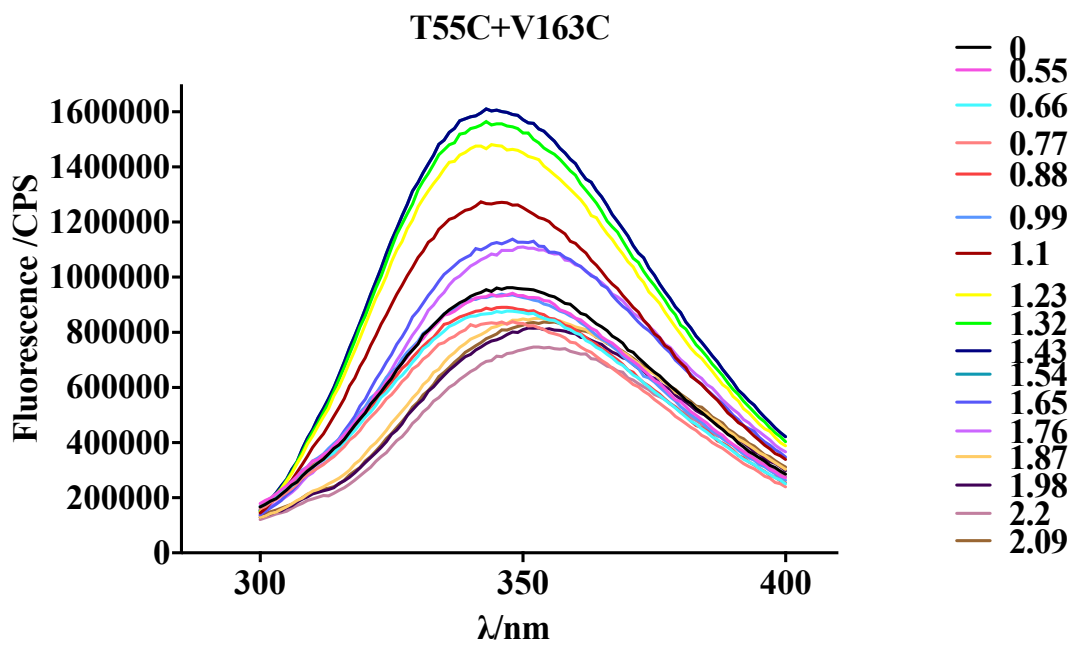
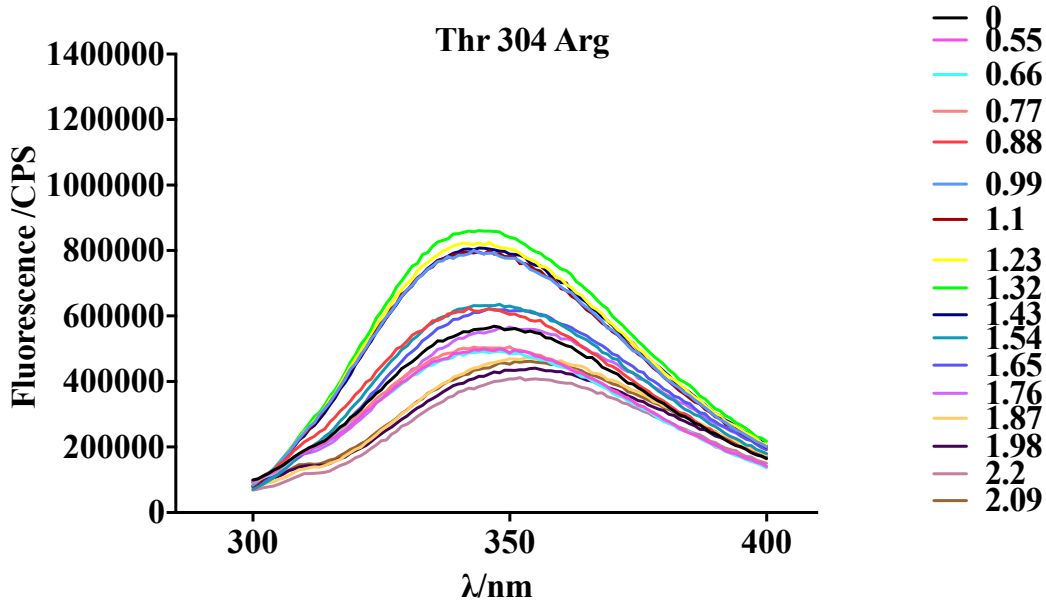
To check that change in haemolytic activities was not caused by destabilisation of the mutants, proteins were denatured with Gdn-HCl and unfolding was measured by fluorescence. Figure 4-11 shows the emission spectra of all mutants in increasing concentrations of Gdn-HCl.











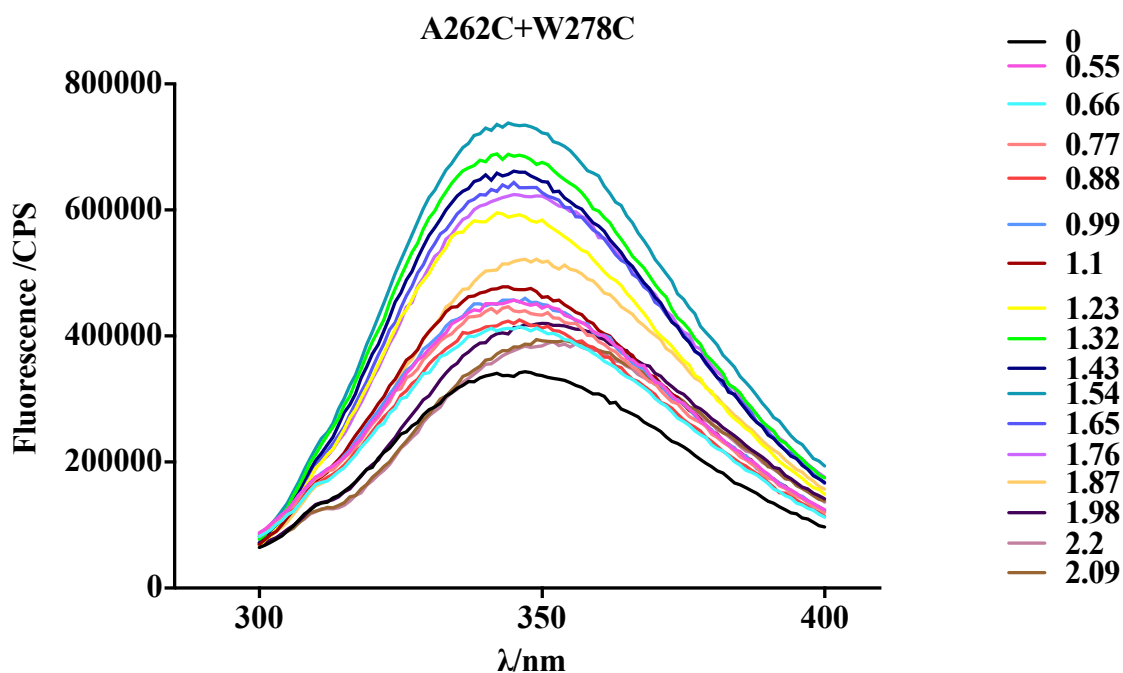
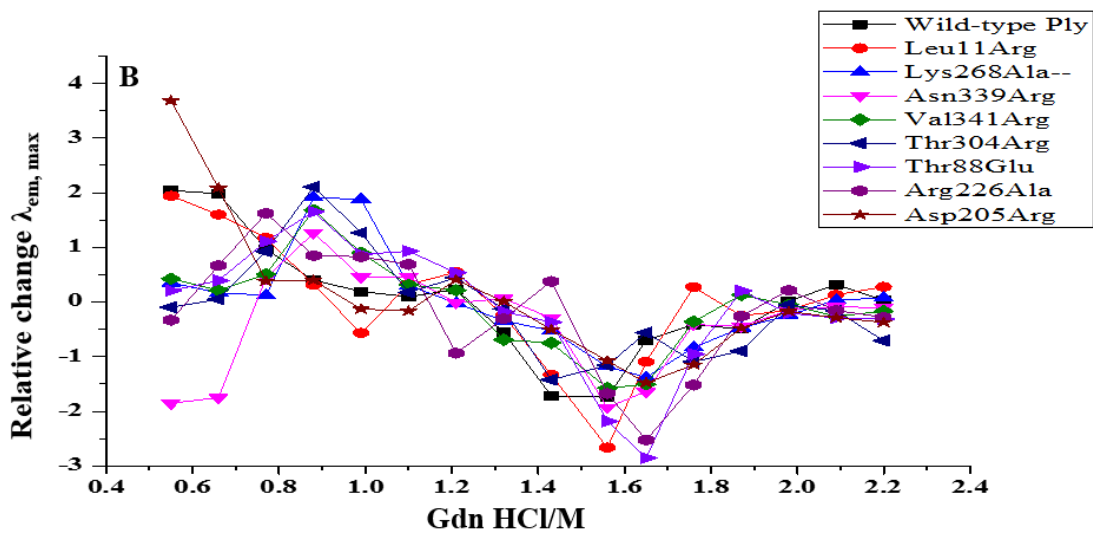
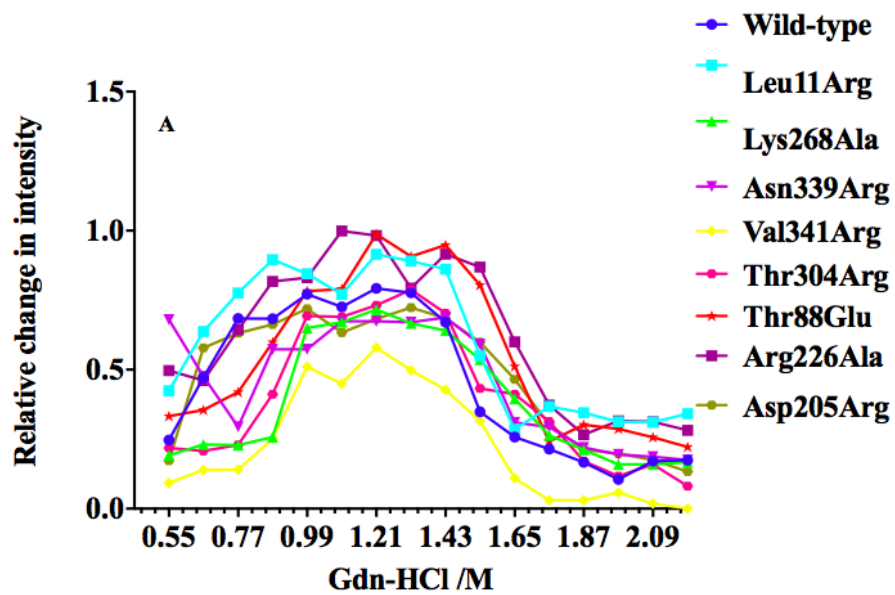


Figure 4-11: Fluorescence emission spectra of wild-type Ply and mutants in Gdn-HCl.

All mutant Proteins were excited at 280 nm with different concentration of Gdn-HCl from (0.5-2.2) M with a 2.5 nm slit width and fluorescence was detected between 300-400 nm at 1nm intervals with 2.5 slit width. All spectra were collected at 20°C. Each graph represents the denaturation profile of each Ply toxin, where the protein was exposed to 0.55 M to 2.2 M Gdn-HCl M.

The fluorescence of the wild-type and all mutants were measured in increasing concentrations of Gdn-HCl. In every case, the fluorescence intensity increased over the range of 0.99-1.54 M of Gdn-HCl and then decreased from 1.54-2.2M of Gdn-HCl (Figure 4-12 A). The changes probably reflect unfolding of the different Ply domains (e.g. D4 and D1-3). Above 2.2 M Gdn-HCl, the fluorescence intensity did not change suggesting that all toxins were fully unfolded. All mutants had the same denaturation profile as the wild-type Ply, indicating that they are not destabilised appreciably by the mutations. The shift in the fluorescence maximum is shown in (Figure 4-12 B). For each protein the $\lambda_{em, max}$ was between 347-349 nm at 1.65 M Gdn-HCl and increased to 352-354 nm with increasing concentrations of Gdn-HCl. The graph represent tha data after calculation of 1st derivative IN Origin programe. This is consistent with the buried Trp residues becoming exposed to the polar solvent as the protein unfolds.



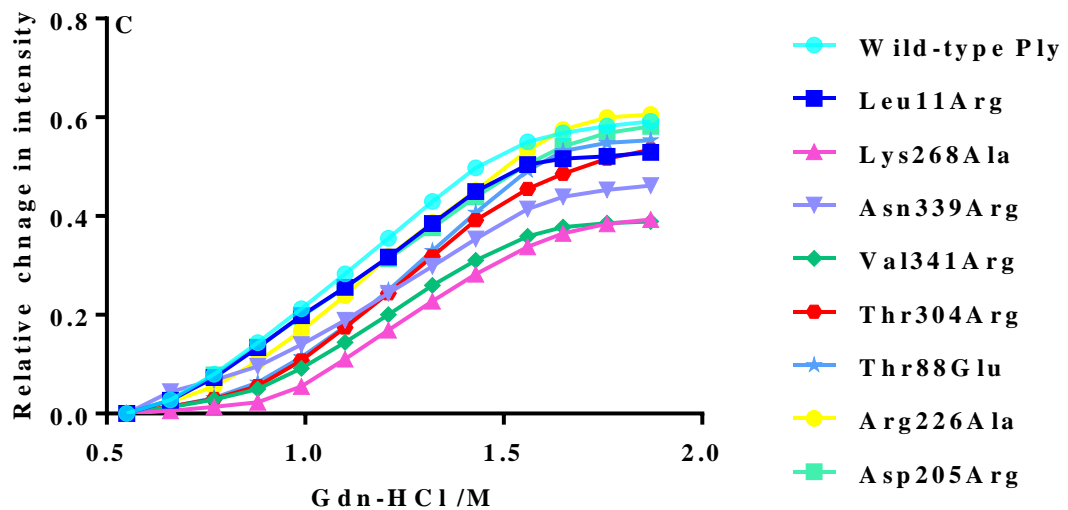
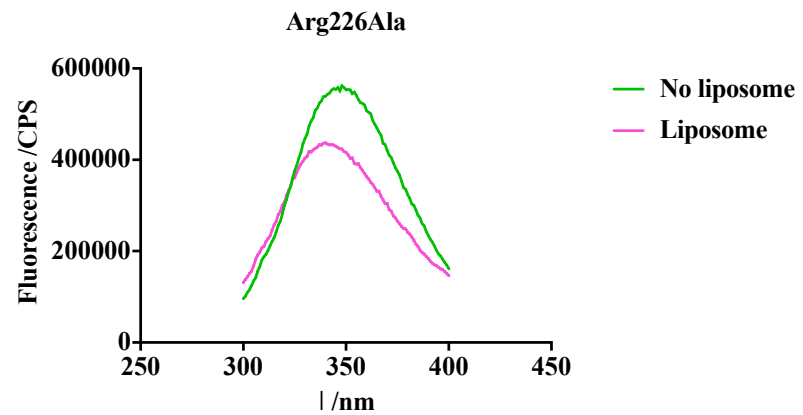
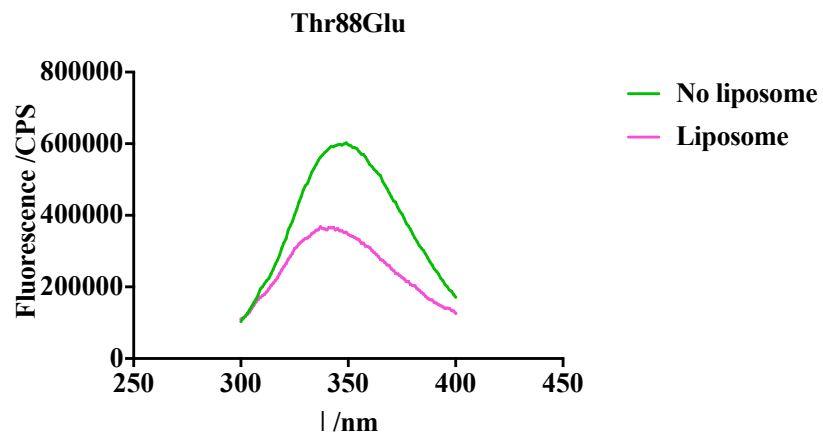
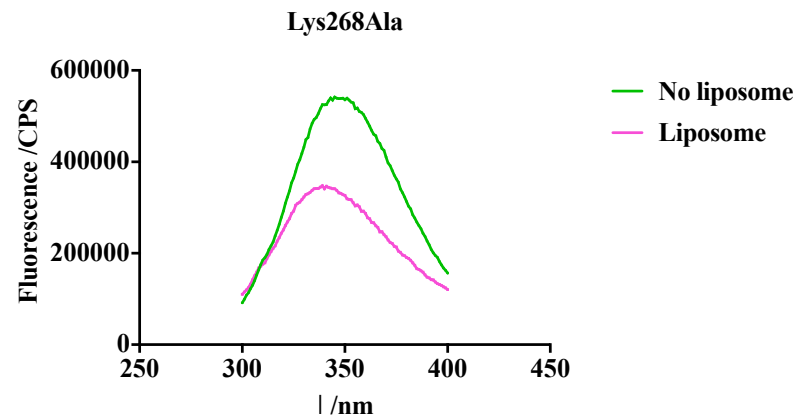
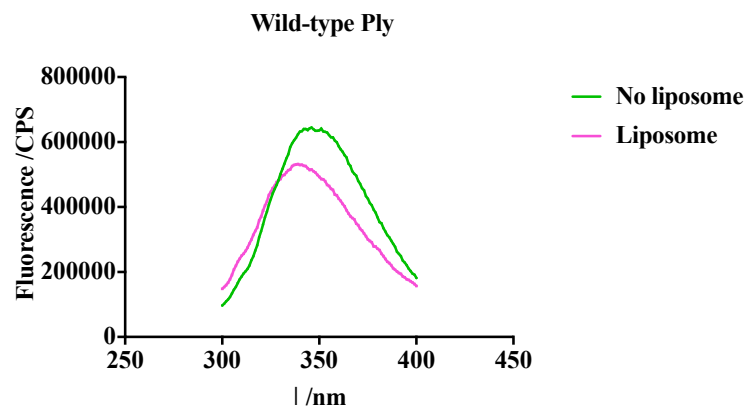


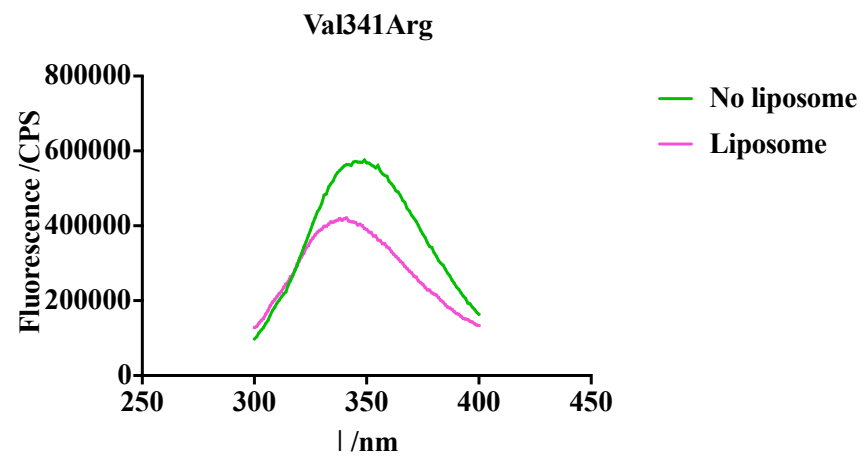
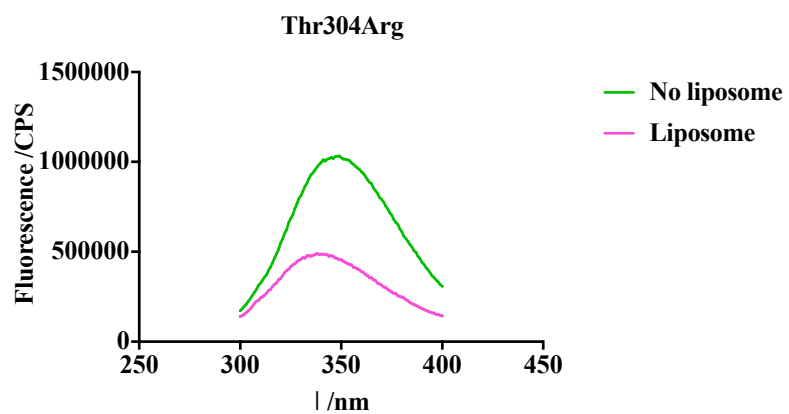
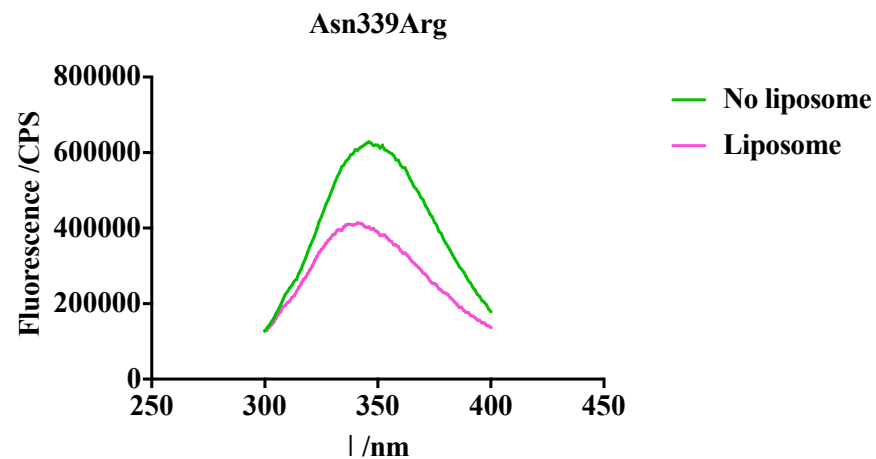
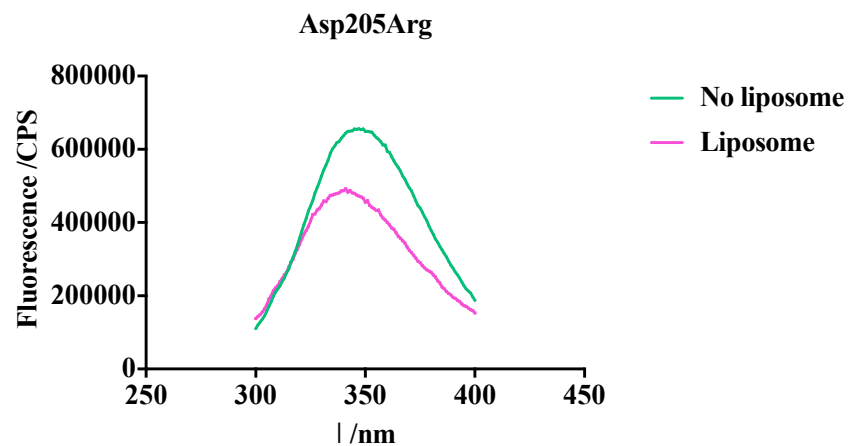
Figure 4-12: Unfolding of wild-type and mutant Plys in Gdn-HCl.

(A) Shows the relative change in fluorescence intensity and B, change in, $\lambda_{em, max}$ after calculation of 1st derivative. It was calculated in origin programe (analyze, Mathatics and then differentiate). (C) change in the relative intensity after finding of the area under curve in Origin programe (analyze, Mathatics and then integrate). The experiment was carried out using $1\mu\text{M}$ of the protein and $\lambda_{ex} = 280\text{ nm}$.

4.3.5 Liposome binding

The Gdn-HCl denaturation measurements confirmed that the mutations did not compromise protein stability. To investigate membrane binding, Ply was added to cholesterol-containing liposomes, and fluorescence was used to detect any changes in the environment of the Trp residues. Data are shown in (Figure 4-13).





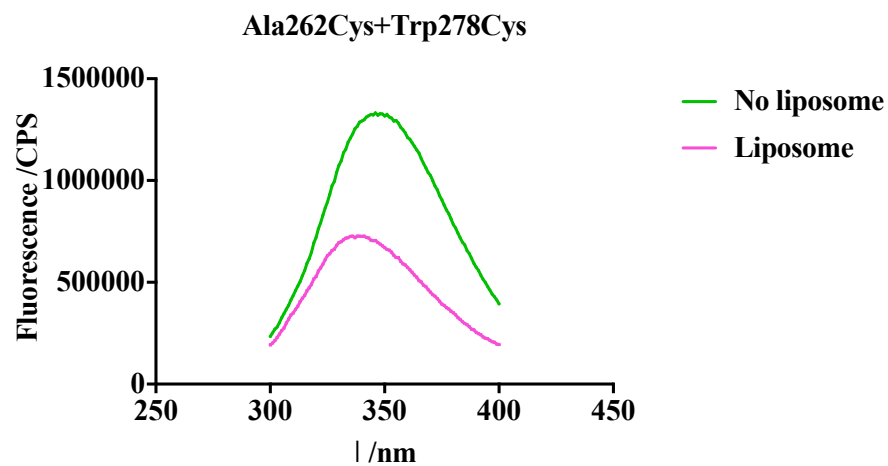
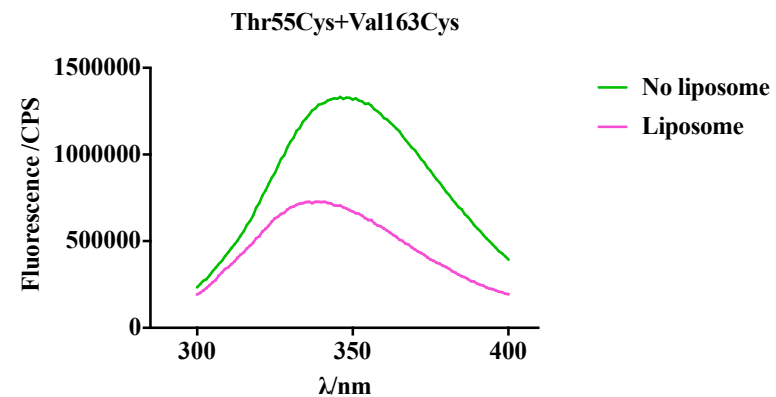
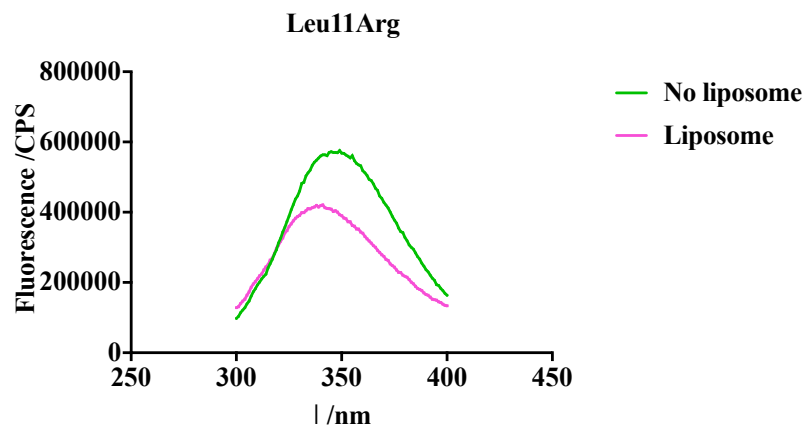


Figure 4-13: Fluorescence emission spectra of wild-type Ply and mutants in the presence and absence of cholesterol containing liposomes.

Final protein concentration and liposome were 1 μ m, 10 μ m respectively. Proteins were excited at 280 nm with a 2.5 nm slit width and fluorescence was detected between 300 and 400 nm at 1 nm intervals with a 2.5 nm slit width. All spectra were collected at 20°C. Pink and green lines show the fluorescence spectra of protein with and without liposome respectively.

There are eight Trp residues in Ply with six in D4 and three of in the Trp-rich loop. Incubating the toxins with liposomes, lead to a reduction in the $\lambda_{em\ max}$ indicating a change to a more hydrophobic environment. This probably reflects Trp residues in the binding loop becoming buried in the hydrophobic membrane. This is in agreement with a previous study by (Ohno-Iwashita et al., 1988) on PFO toxin. Importantly, all the mutants behaved similarly to the wild-type toxin indicating that the mutations do not prevent lipid binding.

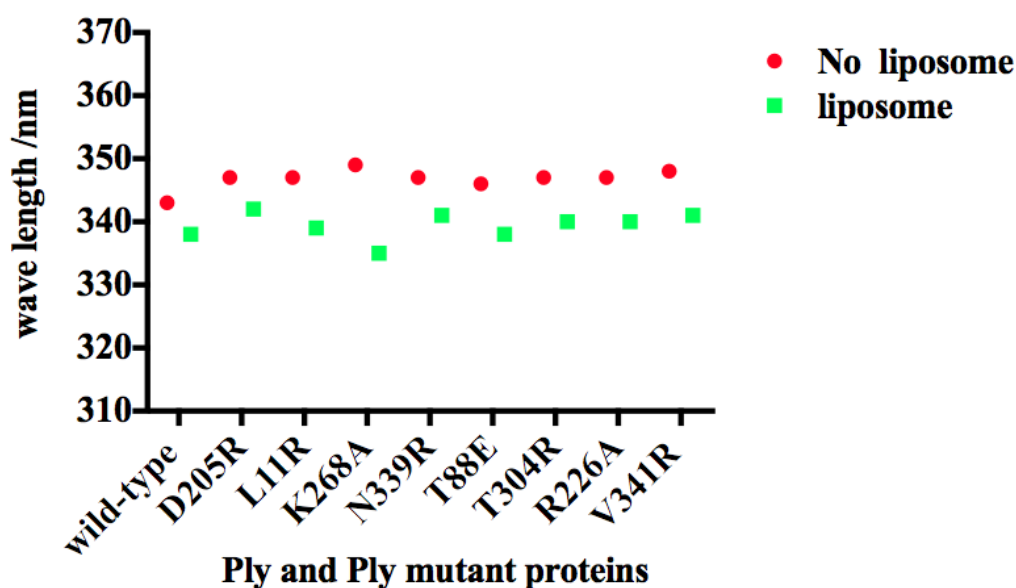
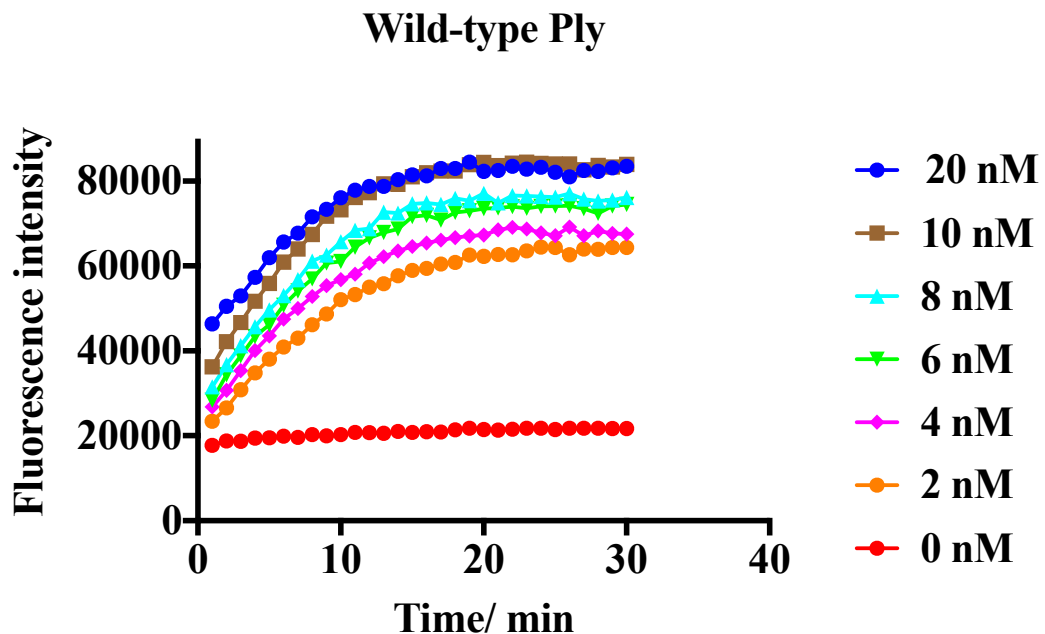


Figure 4-14: Change in the $\lambda_{em\ max}$ of wild-type Ply and mutants in the presence and absence of liposomes.

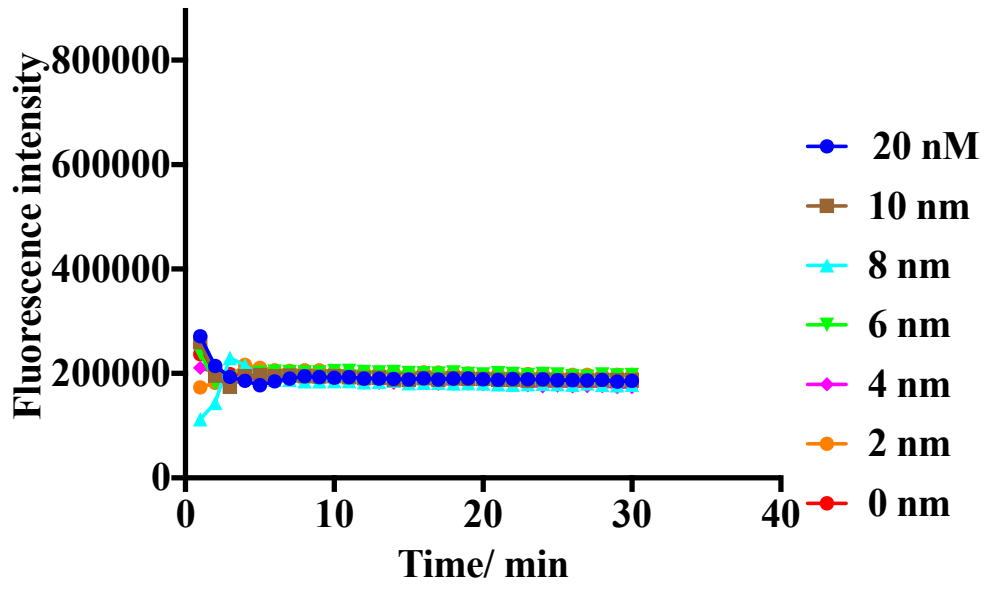
The green dots represent the $\lambda_{em\ max}$ of Ply in solution with liposomes, the red dots show that same without liposomes. Ply has an initial fluorescence maxima wavelength Between 343 and 347 nm that, on average, decreases by 5 nm with the addition of liposomes. The $\lambda_{em\ max}$ of all mutants decreases in the presence of liposomes, reflecting a change in the location of one or more Trp residues into a more hydrophobic environment. The $\lambda_{em\ max}$ of each mutant is taken from the data and plotted against the mutant's name.

4.3.6 Calcein leakage from liposomes in the presence of Ply

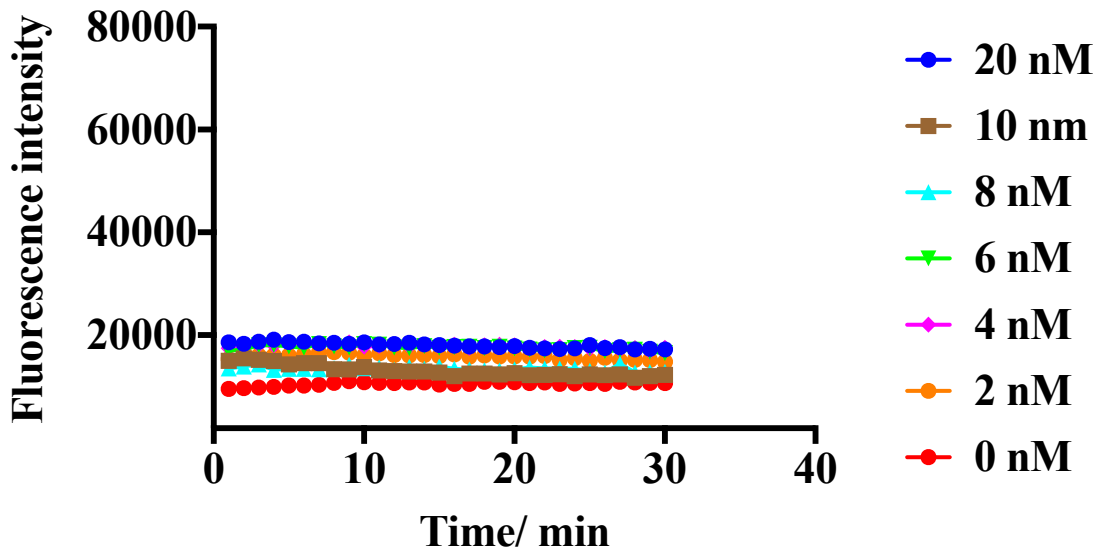
Ply point mutations Asp205Arg, and Asn339Arg completely abolished lysis of sheep RBCs. To test the effect of the mutants on membrane integrity, calcein leakage from liposomes was quantified by steady-state fluorescence spectroscopy. Calcein is a fluorescent molecule that is self-quenching on membranes. Dissociation from the membrane leads to an increase in the fluorescence (Menestrina, 1988) enabling the time course of pore formation to be measured. Figure 4-15 shows the calcein fluorescence changes from liposomes with wild-type Ply, Asp205Arg, Asn339Arg PlyD4 and PlyD1-3. Leakage appears as an increase in the fluorescence, which reaches a steady state. To calibrate the system, complete release of calcein was obtained by exposing liposomes to Triton X-100, which dissolves liposomes by destabilizing their membranes (Lin and Thomas, 2003). Wild-type Ply showed increasing calcein release over time. More release was observed with increasing concentrations of Ply. By contrast no release was observed with PlyD4 and PlyD1-3. No change of fluorescence was seen for either Asn339Arg or Asp205Arg, confirming that neither mutant forms pores in synthetic liposomes.



plyD1-3



PlyD4



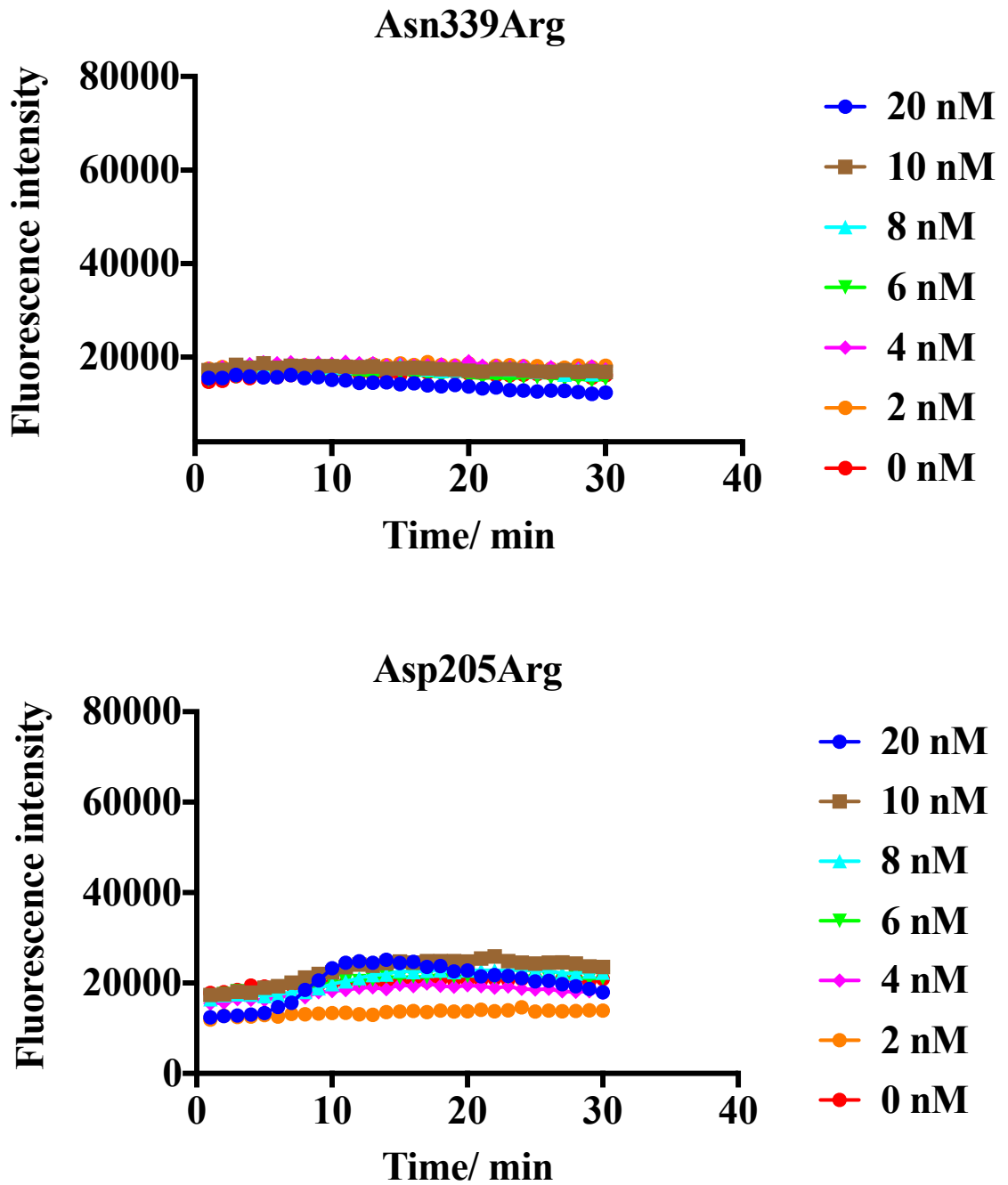


Figure 4-15: Calcein release from liposomes by Ply. Calcein leakage was measured as a function of time.

Protein concentration was $1\mu\text{m}$ and no release was detected for PlyD4, and plyD1-3 or for the point mutants Asp205Arg or Asn339Arg, indicating that they do not form pores in liposomes, unlike wild-type Ply.

4.3.7 Pore formation of Ply on Chol-containing liposomes by EM

Wild-type Ply, and selected mutants were incubated with Chol-containing unilamellar liposomes to visualize their oligomeric structures by negative-stain electron microscopy. Mixtures were stained with 1% uranyl acetate on a copper grid, and oligomers were visualized by transmission EM. As shown in (Figure 4-16) wild-type Ply formed complete rings that covered most of the liposomes indicated in the figure by cyan arrows (Koster et al., 2014, Sonnen et al., 2014). The interior of lysed liposomes stained more darkly indicating that transmembrane pores were formed and the lipid was removed (Dang et al., 2005). In contrast, the non haemolytic mutant Asp205Arg bound to and oligomerized on unilamellar liposomes mainly in the form of long chains (Figure 4-17 orange arrow). The Ply monomers still self-associated, but these structures did not form pores. Ply Asp339Arg, which is also non haemolytic, did not form pores or arcs. Instead the mutant appeared to completely cover the liposomes which remained undamaged (with no darker internal staining) (Figure 4-18, blue arrow). PlyD4 also bound the membrane to form arrays (Figure 4-16 by the green arrow). The mutant Thr304Arg reduced the haemolytic activity of Ply by ~300-fold. It is located in the domain 3. Addition of Arg prevent the threonine side chain forms part of a β strand that packs against the hydrocarbon portion of the side chain of Lys268. This strand may displaced upon oligomerisation on the membrane to allow the monomers to pack together to form the ring. To visualize the oligomeric structures of T304R negative-stain electron microscopy was performed. The mutant was incubated with unilamellar liposome membrane and after that checked by the transmission EM. As shown in (Figure 4-16) mutant Thr304Arg can form complete ring and incomplete ring on the liposome membrane.

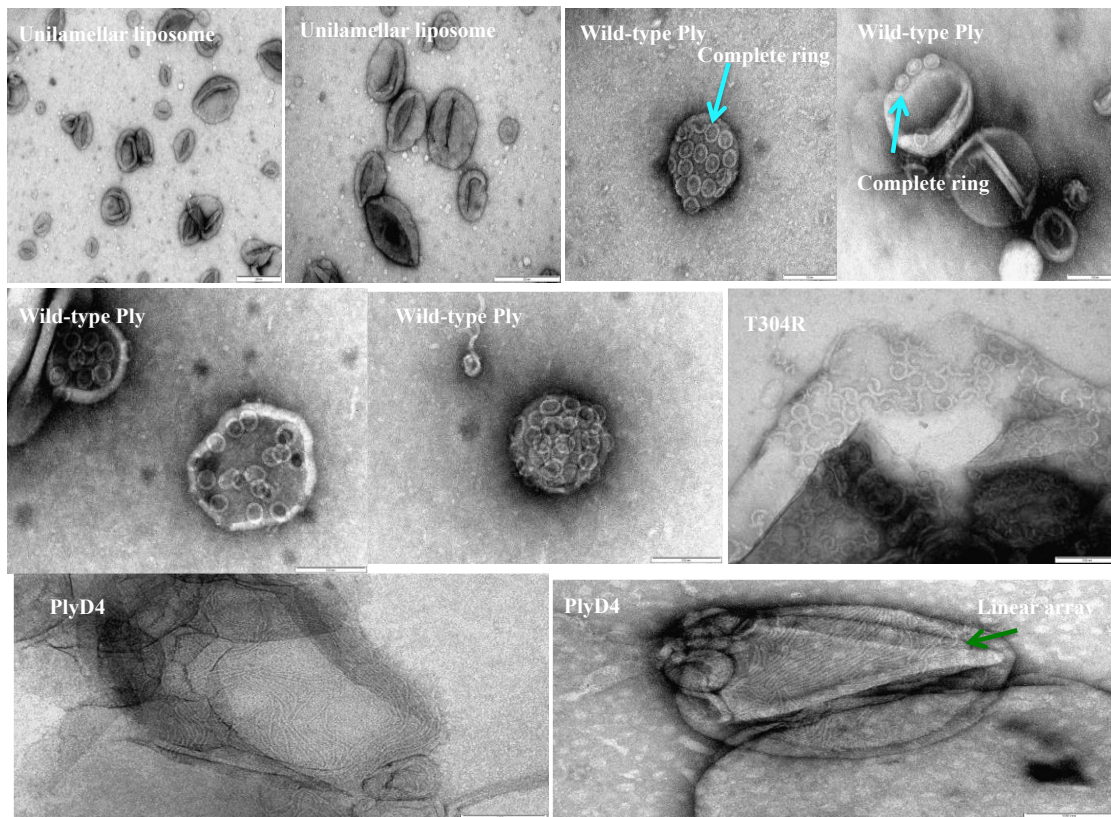


Figure 4-16: Negative-stain EM of wild-type Ply, mutants Ply Thr304Arg, and PlyD4 with unilamellar liposome containing-Chol.

Liposomes were incubated with wild-type Ply, mutant Ply and PlyD4 for 10 min at room temperature and imaged by EM. The complete ring is produced by the wild-type Ply; In the case of PlyD4, it is also oligomerized on the membrane as an array.

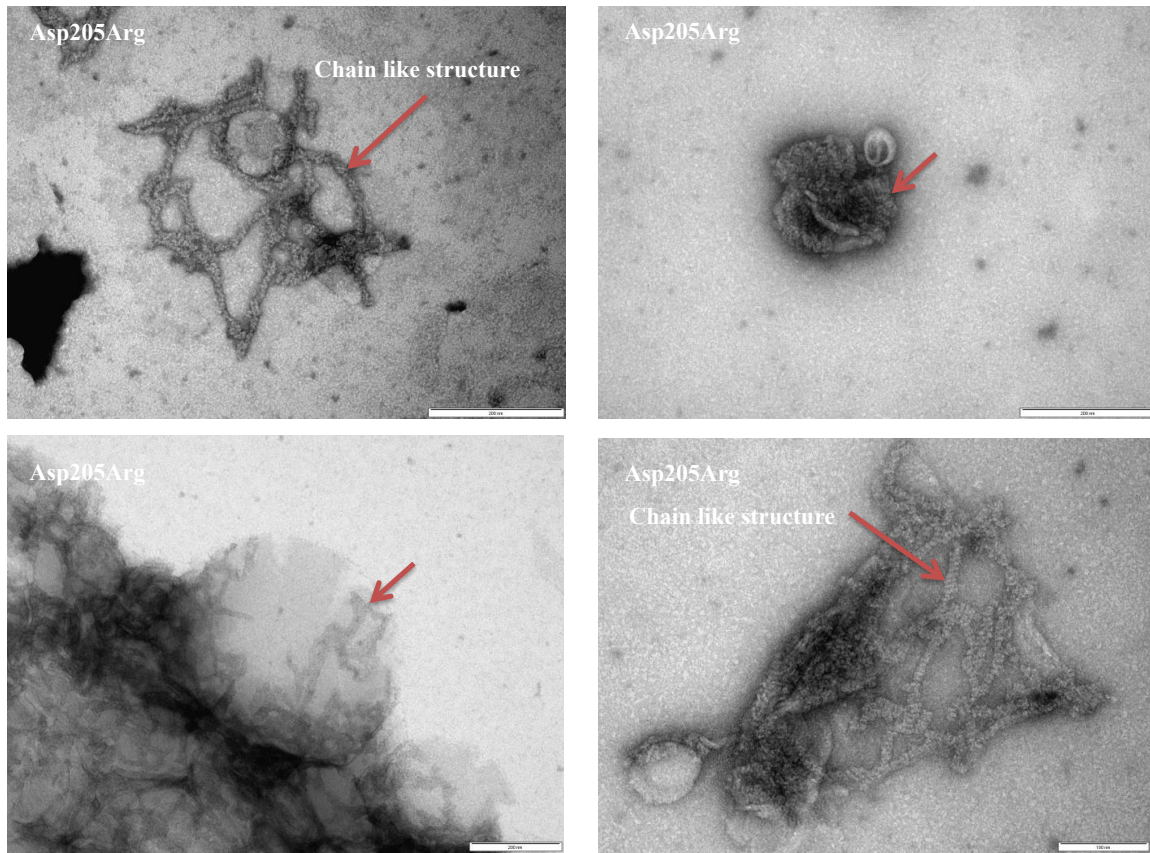


Figure 4-17: Negative-stain EM of Ply Asp205Arg, with the unilamellar liposome containing-Chol.

Liposomes were incubated with Asp205Arg mutant for 10 min at room temperature and imaged by EM. This mutant makes chain like structures. The scale bar is written in the bottom right of each image, which is 100 nm.

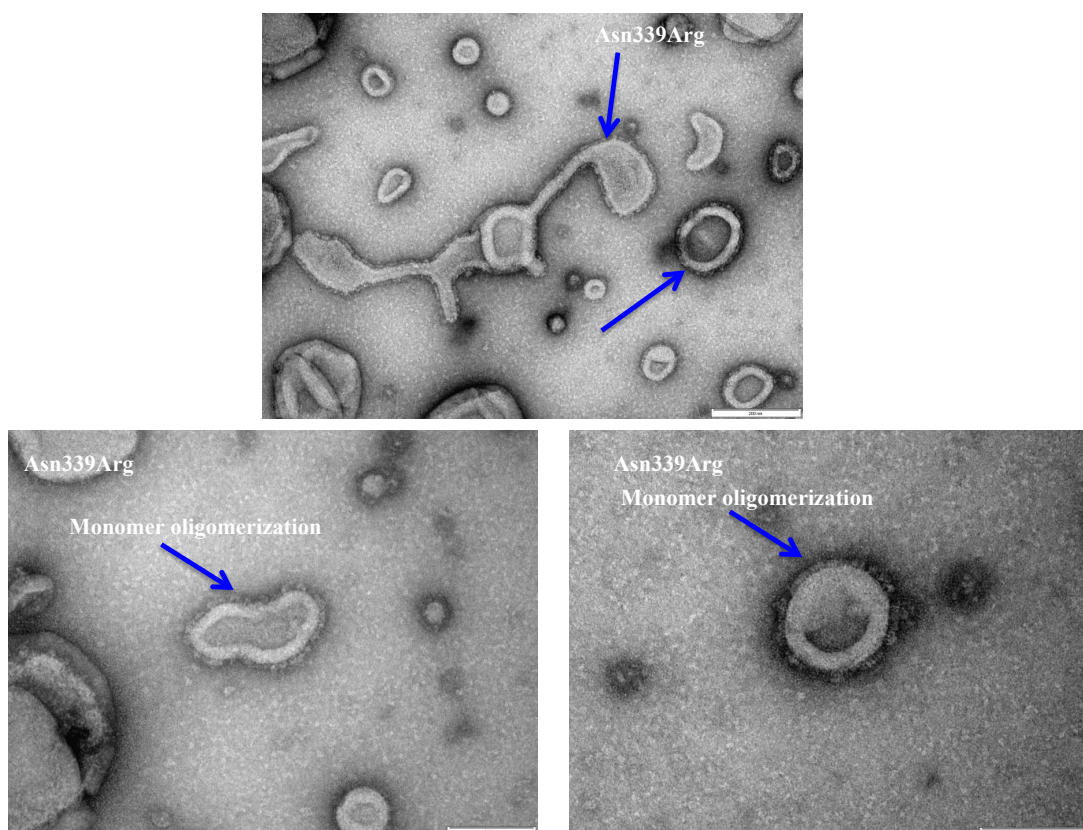


Figure 4-18: Negative-stain EM of Ply Asn339Arg, with the unilamellar liposome containing Chol.

Liposomes were incubated with Asp339Arg mutant for 10 min at room temperature and imaged by EM. This mutant only coats the liposomes. The scale bar is written in the bottom right of each image, which is 100 nm.

4.3.8 Crystallization of PlyD1-3 and D4

Crystals of PlyD1-3 were grown in 0.1M sodium citrate pH 5.5, containing 0.2M sodium acetate and 7% PEG 4000 at 4°C by the sitting drop method. Cryoprotected crystals were picked, and tested for diffraction at 100K; but unfortunately no crystals diffracted. Crystals of PlyD4 were grown in 0.1M potassium thiocyanate containing 35% PEG MME 2000 at room temperature. Crystal took ~4 weeks to grown and diffracted to 2.1Å resolution at Diamond Light Source. Two different structures were determined only one structure is shown in (Figure 4-19). Refined models had good stereochemistry (Table 4-7). Although crystals were grown in the presence of sialyl Lewis-X (which is proposed to serve as a co-receptor on host cells (Shewell et al., 2014), no sugar was detected in the

density map (Figure 4-19). Structures were solved by molecular replacement using the structure of the full-length Ply as a search model.

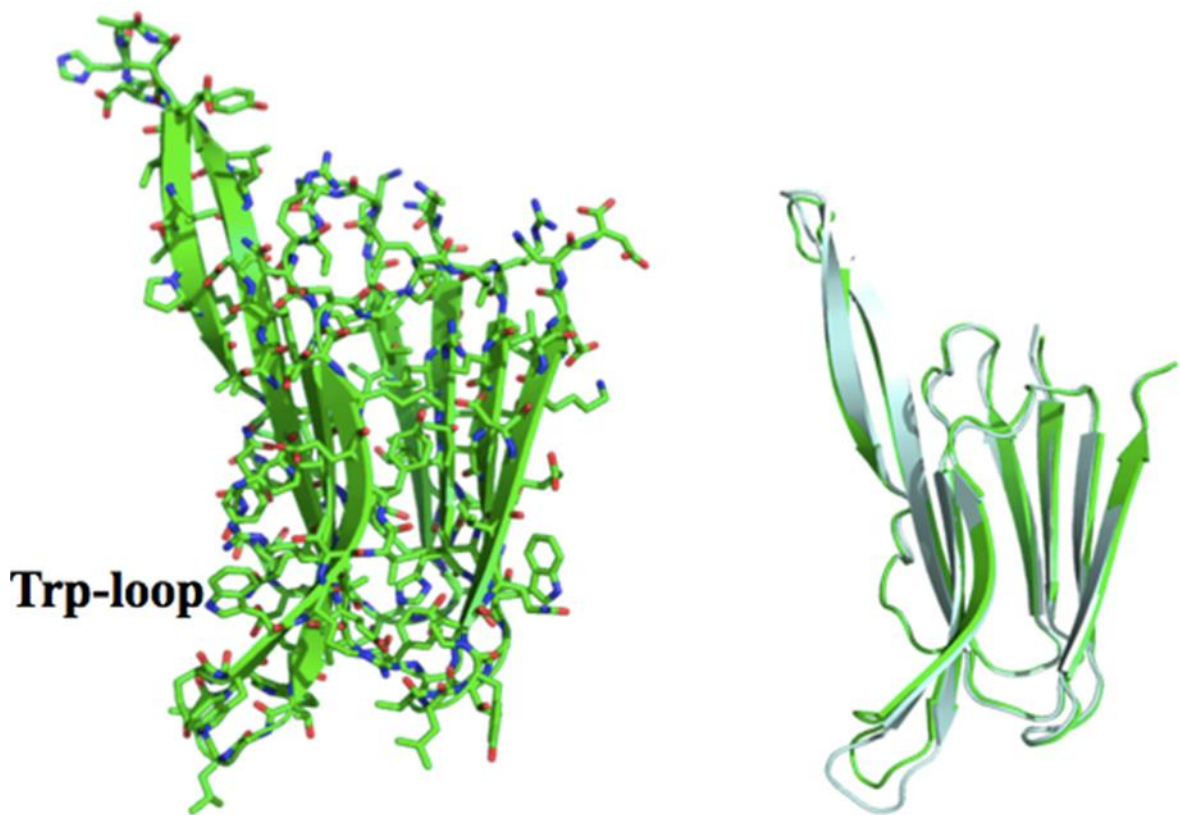


Figure 4-19: PlyD4 crystal structure the Trp loop in the green structure is flip down.

PlyD4 is the binding domain of Ply. This domain was crystalized after one-month and small crystals grew in 0.1 M potassium thiocyanate, and 35% PEG MME 2000. The Trp loop is responsible for binding to cholesterol, its receptor in the membrane. The protein data bank ID of PlyD4 is 5CR8.

In the structure of full-length Ply, the Trp-rich loop is extended as would be expected when bound to a membrane. In the structures of PlyD4 alone, the loop is partially folded back (Figure 4-20). In the PFO structure the loop is fully bent back against the body of D4 (Rossjohn et al., 1997). Taken together the structures are consistent with the previous suggestion that when the toxin binds to the membrane of mammalian cells the loop springs outwards and downwards to project into the membrane (Rossjohn et al., 1997).

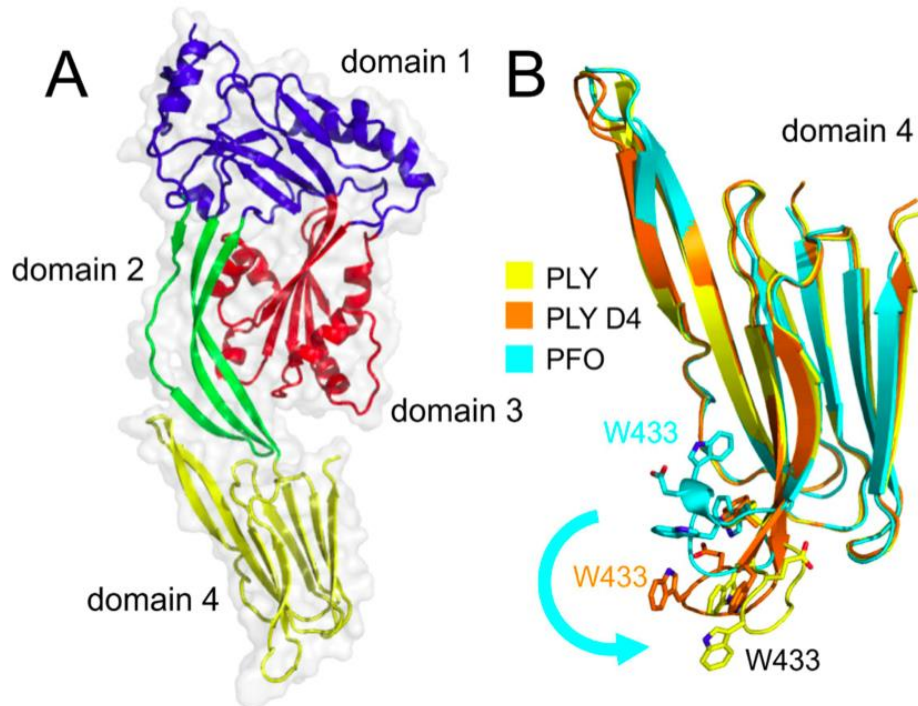


Figure 4-20: Ply domain structure and the likely changes upon membrane binding.

(A) Domains 1, 2 and 3 are contiguous and connected to the C-terminal membrane-binding domain (D4) via D2. The protein data bank ID of Ply is 5CR6. (B) Overlay of D4 of full-length Ply, PlyD4 and perfringolysin O (PFO; PDB: 1PFO) structures. The structures show the likely changes that occur upon membrane binding. Remarkably, the Trp-rich loop flips outwards and downwards (cyan arrow) showing Trp433, to enable binding to the membrane (Marshall et al., 2015). The protein data bank ID of PlyD4 is 5CR8.

Table 4-5: Data collection and refinement statistics (Marshall et al., 2015).

| | |
|--------------------------------------|----------------------------|
| Data collection | PlyD4 |
| PDB ID | 5CR8 |
| Beam Line | Diamond I03 |
| Space group | I121 |
| a,b,c, Å | 48.7, 47.7, 97.5 |
| $\alpha, \beta, \gamma, ^\circ$ | 90, 101.4, 90 |
| Resolution, Å | 46.53 – 2.05 (2.12 – 2.05) |
| R _{sym} | 0.091 (0.451) |
| I/ σ (I) | 6.8 (2.0) |
| Completeness | 99.4 (97.8) |
| Redundancy | 2.9 (2.4) |
| Refinement | |
| Resolution | 46.53 – 2.05 (2.12 – 2.05) |
| No. reflections | 40468 (2447) |
| R _{work} /R _{free} | 0.218/0.271 |
| No of atoms | 2021 |
| Protein | 1870 |
| water | 151 |
| B-factors, Å ² | 35.0 |
| Protein | 35.1 |
| water | 33.6 |
| Rms deviations | |
| Bond lengths, Å | 0.004 |
| Bond angles, ° | 0.83 |

4.3.9 Discussion

Pore formation by Ply kills host cells and plays a major role in the damage caused during pneumococcal infections. In this chapter, mutations were introduced into Ply with the aim of disrupting packing between adjacent molecules during pre-pore and pore-formation. Residues were selected based on the recent crystal structure of Ply in which monomers pack side-by-side in linear arrays. Eight mutations were made: Leu11Arg, Asn339Arg, Asp205Arg, Thr88Glu, Arg226Ala, and Val341Arg in D1, Lys268Ala and Thr304Arg in D3. When tested all 8 mutations reduced the ability of Ply to lyse RBCs, confirming that these residues are important and supporting the hypothesis that the packing of molecules in the crystals mimics the interactions that occur during pore formation. Several other CDCs have been crystallized. Although most pack differently, two recent structures of intermediolysin and listeriolysin O, show similar side-by-side packing to Ply (Johnson et al., 2013). Interesting contacts in the three structures involve equivalent regions of the CDC polypeptides, and many of the interacting residues are conserved, suggesting that CDCs pack together in the same way during pore formation (Marshall et al., 2015). In line with our findings Lawrence *et al.* and Van *et al.* also showed that the mutations in Ply interface residues significantly influence the Ply pore formation activity (Lawrence et al., 2015, van Pee et al., 2016). This confirms the idea that the monomer-monomer interactions observed in the structure are necessary for pore-formation by the CDCs (Hotze et al., 2012).

Mutations in this study were mostly located in PlyD1 and PlyD3, because these regions form the majority of the interface between monomers. During pore formation, PlyD4 anchors Ply to the membrane. PlyD1 participates in oligomerization and acts as a bridge between D2 and D3. PlyD3 undergoes a large conformational change in which the helical regions form β -hairpins that penetrate into the membrane (Tween et al 2005, Tilley et al., 2005). PlyD2 is relatively mobile and collapsed down and rotates as the pre-pore is converted to the functional pore.

As indicated above, all mutants reduced the haemolytic activity of Ply but to different degrees. Remarkably, two mutants Asp205Arg and Asn339Arg completely lost their haemolytic activities. Stability and membrane binding tests showed that the loss of haemolytic activity was not caused by destabilization of Ply or a failure to bind to cholesterol-containing membranes. Interestingly, EM indicated that loss of activity was

caused by distinct changes in the Asp205Arg and Asn339Arg mutants (Figure 4-17 and 4-18). Ply Asp205Arg monomers oligomerized on the membrane to form linear chains, but these structures were not curved and failed to make pores in the membrane. Alternatively, mutant Asn339Arg was still able to bind to the membrane, but monomers could not oligomerize. Overall both residues are important for oligomerization and assembly of functional pores. This interesting finding provides further understanding of Ply oligomerization on the cell surface and could facilitate the production of inhibitors for Ply toxin.

Finally, PlyD4 was successfully crystallized to give two new structures. The Trp-loop is partially folded back against the body of Ply. In solution it is likely that the Trp loop is fully bent back as seen in the structure of PFO structure (Rossjohn et al., 1997). Upon membrane binding the loop moves away and swings outward and downwards enabling interaction with the cell membrane. This conformation change at the base of the toxin promotes monomer-monomer interactions upon membrane by binding the loop that springs outwards and downwards, allowing additional contacts between D4 of adjacent monomers.

Chapter 5 The conversion of monomers of Ply to pre-pore complexes promotes microdomain formation in lipid bilayers

5.1 Raman spectroscopic analysis of lipid bilayers

5.1.1 Raman spectroscopy

Raman spectroscopy is the optical analysis technique discovered by Professor Sir Chandrasekhara Venkata in 1928. He was awarded a Nobel Prize in 1930 for his work on this phenomenon (Lawton et al., 2014). Raman spectroscopy is the useful technique to determine the chemical composition and molecular structures in cells and tissues. It is defined as a vibrational spectroscopy technique, which occurs as a result of interaction of light with molecules leading to inelastic scattering. The shift in the wavelength gives information about the frequencies of vibrational modes of molecules present in the sample (De Luca et al., 2015). This technique is mostly used in biology, analytical chemistry, and medicine specifically to identify molecular fingerprints of disease and evaluation of living cells and tissues (Redding et al., 2015). When the light is passed through the transparent substance, it can be elastically scattered by the molecules with the same frequency. This is known as Rayleigh scattering (Lambert et al., 2006). In the Raman effect the incoming wavelength is different from the scattered wavelength i.e. this is an inelastic light scattering process (Lambert et al., 2006). Raman scattering is classified into two different kinds: Stokes and anti-Stokes scattering. In Stokes scattering, the photons have lost energy to the molecules, whereas, in anti-Stokes scattering, the photons have gained energy from the molecule (Richard, 2001). Both scattering include the Raman scattering types and the Rayleigh scattering (Figure 5-1).

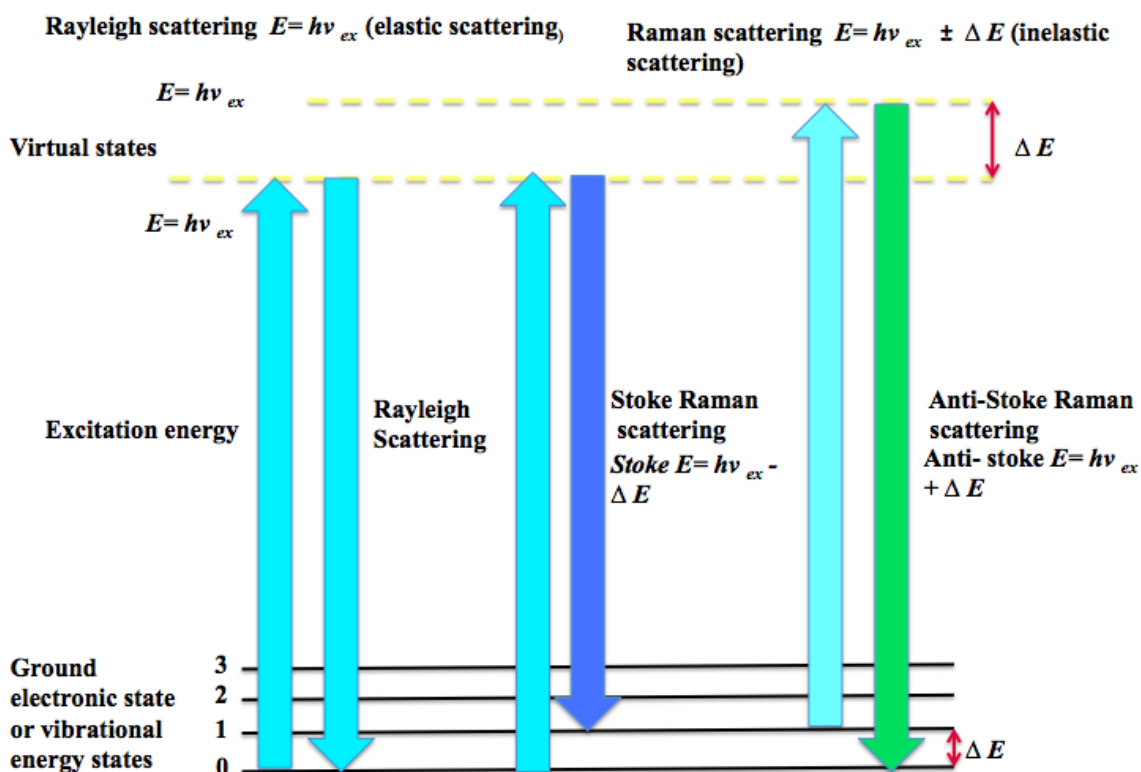


Figure 5-1: Rayleigh and Raman scattering.

The molecule is excited light from its ground state to the virtual state. Left: Rayleigh scattering. Middle: Stokes Raman scattering. Right: anti-Stokes Raman scattering. Inelastic scattering therefore; their previous and the electronic ground state are different.

5.1.2 Lipid Raman spectra

Lipids are an important class of biomolecules; particularly they are important in cellular signaling, energy storage and component of the cells membrane. Raman spectroscopy can be used to deduce the lipid composition and structure (Kochan et al., 2013). Biological membranes contain phospholipids with different chemical structures and degree of saturation, such as the phosphatidylcholine and phosphatidylethanolamine are saturated and unsaturated lipid respectively. However, they have similar properties because both are composed of two fatty acid chains with identical glycerol-based backbones and their acyl chains are approximately equal in length (Czamara et al., 2015). Raman spectroscopy in combination with optical tweezing was used to study the structure of the LUVs lipid

bilayer. The hydrophobic lipid tail groups at 1050-1150 cm^{-1} and 2800-3200 cm^{-1} respectively represent the Raman spectra of the skeletal C-C and C-H stretching mode of the lipid bilayer. This was the first example of the Raman spectrum recorded from the individual vesicles (Cherney and Harris, 2010). In addition, Raman spectroscopy in combination with optical tweezers was also used to analyse the composition of the liposome membrane by Sanderson and Ward (Sanderson and Ward, 2004). The Raman assignment peaks of some lipids are well established. For example, 2851 and 2882 cm^{-1} represent the symmetric (d^+) and antisymmetric (d^-) methylene stretching vibrations of DMPC respectively (Lhert et al., 2002, Snyder et al., 1982). However, in the bilayer of POPC, the methylene stretching is at 2855 cm^{-1} and 2893 cm^{-1} ; the latter value is shifted to higher frequency because the lipid chains are more fluid (Snyder et al., 1982, Aslanian et al., 1986). The shoulder at 2928 cm^{-1} and the peak around 2972 cm^{-1} is assigned to a Fermi resonance of the symmetric methyl stretch (rFR^+) and antisymmetric methyl stretch (r^-) respectively of the fatty acid chains (Lhert et al., 2002). The lipid Raman spectrum is characterized by the presence of the hydrocarbon chain, which is observed in three regions for all lipids including 1500-1400, 1300-1250 and 1200-1050 cm^{-1} in the fingerprint. The bands in the 1500-1400 cm^{-1} range is the CH_2 assignment fingerprint and $\sim 1300 \text{ cm}^{-1}$ is assigned to the CH_3 vibrations groups in the lipids. Bands in the 1200-1050 cm^{-1} regions are attributed to the C-C stretching vibrations, which represent the skeletal modes. It needs to be taken account that the Raman spectra of individual lipids are considerably different according to their saturation, phase, geometrical isomerism and polymorphic/polytypic and presence of a hydrophilic group (Czamara et al., 2015).

It is very well understood that the transition temperature are different for different lipid molecules such as POPC, DPPC, DOPC, DLPC and PC24. They are different in their temperature of the gel phase to the fluid phase (Dmitriev and Surovtsev, 2015). The disordering process in the lipid bilayer from gel to fluid is determined by different structural and spectroscopic techniques including infrared absorption, electronic spin resonance, NMR and Raman (Binder et al., 1998, Naumann et al., 1992, Heimbürg et al., 1992, Sassi et al., 2015). It has been reported that the frequency of the CH_2 peak positions increase with the increasing of the temperature; for example they are increased by about 2 cm^{-1} at 50 K and 263 K, larger increase of temperature is caused transition from gel-fluid phase (between 263 K and 275 K) (Surovtsev and Dzuba, 2014, Kodati et al., 1994, Casal and Mantsch, 1984). The conversion from gel to liquid-crystalline phases is

accompanied by an increase in the symmetric CH₂ stretching band in both FTIR and Raman spectra; the wavenumber shifts from 2851-2853 cm⁻¹ in the FTIR spectra of hydrated lipids; similarly in Raman spectra, the wavenumber is shifted from 2851.5-2853.5 cm⁻¹ (Sassi et al., 2015). In addition, when cholesterol is added to DPPC and POPC lipids near the gel-fluid phase transition, the Raman frequencies for both CH₂ and C-C stretching are altered (Surovtsev and Dzuba, 2014). Raman spectroscopy can be combined with optical tweezing (known as Raman tweezing) to enable a confocal spectroscopic measurement on cell-sized structures. This was used first time in 1986 and has recently been extended to trap and record the Raman spectra from particles in microfluidic flow channels (Redding et al., 2015). Raman Tweezers are typically composed of two lasers: one for trapping a cell-sized particle and another for Raman excitation. The lasers can be configured on a microscope apparatus (Ajito and Torimitsu, 2002).

5.1.3 Optical tweezers (OT)

Different types of synthetic bilayers can be studied. Two common variants are solid-supported planar lipid bilayers and unilamellar lipid vesicles. The former is unsatisfactory for the study of transmembrane protein complexes because the solid support would interfere with penetration of the protein in the lipid bilayer. Thus, we have utilised unilamellar lipid vesicles in this research. There is a very useful approach that can be used in experiments employing unilamellar lipid vesicles in which a single vesicle is suspended at a fixed point in a liquid sample by OT. Physical changes to the single vesicle can then be monitored by optical microscopy or microspectroscopy. Arthur Ashkin discovered the physical principles of optical tweezing (OT) in 1970 (Heller et al., 2014). He showed that the radiation pressure from the laser beam causes the acceleration of microparticle (Ashkin, 1970), and two counter propagating beams could create an optical trap for the particle by the radiation pressure. Later, he showed that a single laser beam could lead to levitation of the microparticle by the balance of the radiation pressure and the gravitational force on the particle (Ashkin and Dziedzic, 1971). OT is attractive because of its capability as a non-contact and non-invasion method that can be widely used in different applications in physics, biology, chemistry, medical science and nanoscience (Guo and Li, 2013). Another configuration of OT uses a highly focused laser beam to trap particles. The laser beam is focused by a high-quality microscope objective

to a diffraction-limited spot in the specimen plane, which makes an optical trap to hold a small particle at the beam waist (Guo and Li, 2013). OT is a useful tool for the trapping and manipulation of biological cells, and has been utilised in different areas in biomedical research, such as fertilization, cell-cell interaction, cell adhesion, embryology, microbiology... etc (Zhang and Liu, 2008).

The mechanism of trapping by a highly focussed laser beam relies on two kinds of forces namely scattering force which tends to push the particle along an axis parallel to the direction of light propagation and the gradient force which tends to pull the particle towards the high intensity region. The gradient force is produced by the field gradient density (Figure 5-2) (Zhang and Liu, 2008, Basu et al., 2010, Redding et al., 2015). Both forces exerted on the particle depend on the particle size (r) and the wavelength of the laser beam (λ) (Zhang and Liu, 2008). Optical trapping is usually performed with deep red and near-infrared lasers. The short wavelengths of the laser minimise photon damage to the trapped particle (Celliers and Conia, 2000). A particle trapping by the OT is classified into three different regimes including Mie regime ($r \gg \lambda$); Rayleigh regime ($r \ll \lambda$); and regime in between them ($r \sim \lambda$). If a particle is within the Mie scattering region, which is when the particle is of the identical scale as the incident light. The optical force can be divided into two components. The first component is the pressure force resulting from the back scattering of incident photons from the laser; this force acts along the direction of the propagating laser beam. The second, and more important form of energy transfer occurs through the refraction of photons through the particle (Ashkin, 1992).

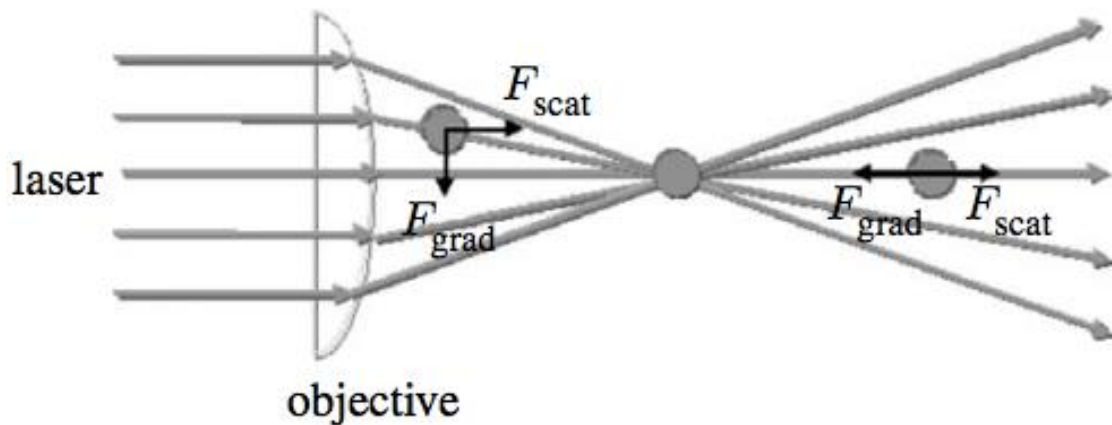


Figure 5-2: The gradient force mechanism in OT.

The objective lens of the microscope focuses the light to a diffraction-limited beam waist, to create a three-dimensional light gradient.

5.1.4 Microfluidic device

This device makes it possible to deliver unilamellar vesicles into an optical tweezer, and then after a single vesicle is held by the tweezers, the surrounding fluid can be exchanged. How this is done is explained in the next section. Microfluidic devices enable small liquid volumes of liquids to be controlled precisely (Tehranirokh et al., 2013). According to the microfluidic technology liquid flow can be manipulated in channels with dimensions of (10-100) micrometers (Yu et al., 2009). The microfluidic system allows two various solutions to flow without mixing in a channel. The micro channels lead to interesting flow characteristics that are integral to the function of microfluidic devices (Eriksson et al., 2007).

The fluid flow in the microfluidic device is controlled by the Reynolds number which is defined as the ratio of momentum forces to viscous forces (Squires and Quake, 2005). The Reynolds number equation is shown as $Re = \rho \times v \times d / \mu$, (d represents the pipe diameter, v is the average velocity, and ρ is the fluid density and μ is the dynamic viscosity (Saint-Michel et al., 2014). Three types of fluid flow in the channel pipe have been described: turbulent, laminar and transient. For instance, if the Re value is lower than 2300, the flow is laminar and the two fluids will flow in parallel streams to each other without mixing; whereas, if $Re > 4000$, the flow is turbulent and both fluids are mixed

completely. In addition, if $Re\ 2300 < Re < 4000$, the flow is transient and the fluids will be partially mixed (Squires and Quake, 2005). Microfluidic devices are produced by Soft-lithography with an elastomer rubber, polydimethylsiloxane (PDMS) (Velve-Casquillas et al., 2010).

5.2 Objectives

In this chapter, the structural changes of the lipid bilayer in a liposome is described once exposed to Ply and a number of Ply mutants. Using a combination of OT, microfluidic device and Raman spectroscopy. A microfluidic device was created to allow manipulation of the liposome into a solution of Ply using OT. It is consisting of laser beam tightly focused through an objective lens, which is used to isolate single particles in suspension. A change in the structure of the lipid membrane in a liposome ($\sim 1\ \mu\text{m}$ in diameter unilamellar vesicles) was detected by measuring inelastic back-scattered light via Raman spectroscopy.

5.3 Materials and methods

5.3.1 Materials

Chol, POPC, Micro-Extruder and polycarbonate membrane were supplied by Avanti polar lipid. Boron-doped silicon (100) wafer purchased from (MicroChemical GmbH), negative photoresist (SU-8-2002) supplied by (MicroChem Crop). The base hardener silicon adhesive with Trimethylisocyanate and 85% oil immersion were purchased from the Sigma 1.0 mm biopsy puncher was purchased from World Precision Instruments.

5.4 Preparation of lipid vesicles (Liposomes)

Different batches of liposomes were prepared: pure POPC, binary mixtures of POPC/Chol (1:1, 1:2 and 4:1 mole ratio) and a ternary mixture of POPC/Chol/SM (1:1:1). Liposomes were prepared according to the Avanti Polar Lipids protocol 10 mg POPC was mixed with 5 mg Chol (for a 1:1 mole ratio) they were dissolved in 1ml chloroform this was dried under a gentle stream of N_2 at room temperature to evaporate the solvent completely. After that the white film rehydrated in 1 ml PBS. Then it was extruded 20 times through the $1\ \mu\text{m}$ pore size polycarbonate membrane at 50°C in order to control the phase transition temperature. In addition, to produce LUVs that are homogeneous with

the respect of size but might be different in the composition. Liposomes were stored at 4°C and used within a week.

5.5 Microfluidic laminar flow cell

A microfluidic device was prepared to enable controlled mixing of a single liposome in PBS with a solution-containing Ply that is flowing in parallel by laminar flow. Microfluidic devices were made by soft lithography. A photomask containing negative images of the pattern of microfluidic channels was reproduced and printed by (JD Photo-Tools, Oldham, Lancashire) made from Boron-doped silicon with a diameter of 50 mm and a thickness of 280 μm . A single copy of the pattern is composed of two inlets and one out let (Figure 5-3 A). The perimeter of the inlet for the protein solution is bordered by two rows of isosceles trapezia (Figure 5-3 B) these are separated by 8 μm in the inner circle, and 5 μm in the outer circle. Two rows of isosceles trapezia provide removing of any particles present in the protein solution, which would be drained into the focus of the optical-tweezing laser. The width of the fluidic channels into which the liposome dispersion and the protein solution are injected is 100 μm , and these converge at a Y-shaped junction into a fluidic channel of 200 μm -width.

The master template of the device was produced by dispensing approximately 1 ml of a permanent negative photoresist (SU-8-2002) onto the wafer and distributed on the wafer surface on the chuck of the spin. Then, it was spun onto the wafer at 500 rpm for 30 sec followed by 1500 rpm for 30 sec to create a uniform 100 μm . Next the wafer was baked on a hot plate at 95°C for 45 min. An in-house vacuum chuck photography apparatus was used to clamp the coated silicon wafer and then a predesigned mask was placed on the wafer, which was exposure to UV radiation at 365 nm to the wafer with the 15% power at the illumination of 550-650 mJ cm^{-2} using a LED curing lamp (DELOLUX80/365, Delo industrial adhesive). The UV initiates cross-linking of the epoxy resin; the parts of the resin not exposed to UV are removed following developing. After UV exposure the wafer was put on the hot plate to bake at 95°C for 10 min, and rinsed in Microposit EC solvent developer for 2 min and then cleaned with isopropyl alcohol and dried.

Replicas of the pattern shown in (Figure 5-4 A) were produced by PDMS. PDMS consists of two components, the base and hardener silicon adhesive; they were mixed in a ratio 10:1 and cast over the pattern with ~5 mm thickness (Figure 5-4 B). Then the cast was

placed into the vacuum desiccator to remove air bubbles, before casting the wafer was salinized in 85% Trimethylisocyanate in a vacuum left overnight to reduce the sticking of PDMS on the wafer and to prolong the lifetime of the wafer. The wafer was then incubated in an oven at 65°C for 2 hr to harden the PDMS. Then the PDMS slab was carefully excised from the wafer with a sharp scalpel. The template was then reused to make another microfluidic device.

The 1 mm-internal diameter biopsy puncher was used to punch holes to create the outlet and inlet in the fluidic patterns transferred onto the PDMS. The PDMS blocks were cleaned with adhesive tape to remove debris from both sides and they were taped to eliminate any dust from collecting. Glasses cover slip cleaned it in 14 ml of the 95% H₂SO₄ and 6 ml of 30% H₂O₂ at room temperature for 15 min then it washed in 40 ml (18.2 MU, Milli-Q, Millipore) for 5 min finally they put into the methanol for a few sec and dried in oven at 60°C for 10 min. Next the PDMS was sealed with a glass cover slip. Next the PDMS and the glass cover slip for PDMS sealing were treated with oxygen plasma to activate the PDMS and the cover glass (Menzel-Glaser, 24 mm by 50 mm) for 1min at 0.1 mbar and 28 W (ManiFesto-PC-MFC, Gala Instrument GmbH) (Friend and Yeo, 2010). Then the PDMS was bonded to the cover glasses; a weight was placed on top of the PDMS to secure to the glass surface and the device was placed in the oven at 80°C overnight. This procedure promotes complete bonding and allows the cover glasses to bind to the PDMS and seal the flow channels of microfluidic device. Figure 5-3 C shows the Y-shape device with two inlets and outlet and the laminar co-flowing streams of two fluids: pure water and a solution containing a blue dye

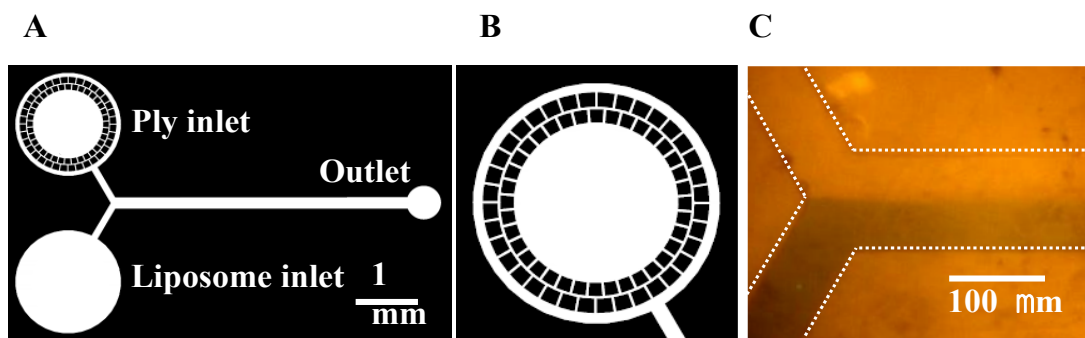


Figure 5-3: Microfluidic device pattern.

(A) Display microfluidic pattern replica. (B) Shows the inlet of the microfluidic device, which was used to inject Ply. (C) illustrates the laminar flow of co-flowing streams of pure water and a dye solution in the microfluidic device at 10 nl/min.

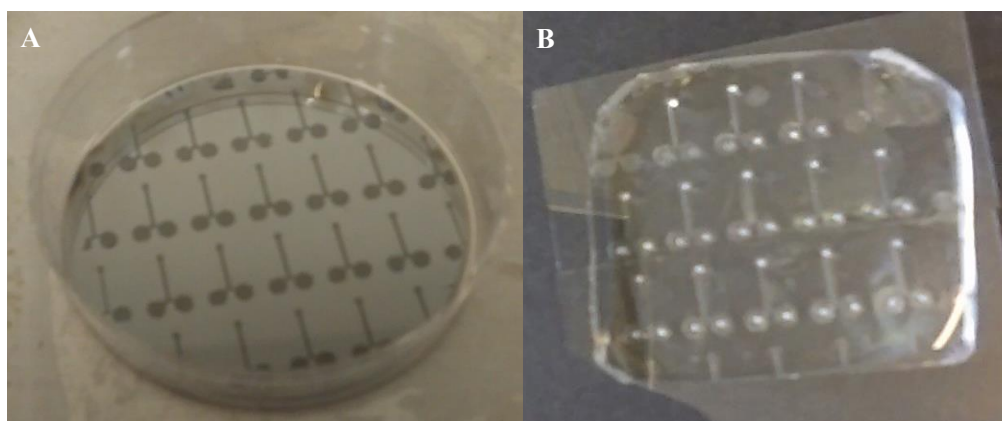


Figure 5-4: Microfluidic device preparation.

(A) Represent the silicon wafer with printed Y-shaped patterns. (B) is the sealed microfluidic component; inlets were made with a 1 mm biopsy punch after casting.

5.6 Raman tweezers of a single liposome with the wild-type Ply and Ply mutants

For the flow cell experiment 9.5 nM (0.5 $\mu\text{g/ml}$) of Ply and a 1:100 dilution of liposome were prepared separately in PBS. Delivery of the two fluids was done using a dual syringe pump (Harvard Scientific). Both were delivered to the separate inlets of the microfluidic component using PTFE tubing. The flow rate was set initially at 100 nl/min, and then after the microfluidic channels were fully filled the flow rate was lowered to 5 nl/min to enable the optical trapping of the liposomes. OT of a single liposome was carried with a 1070 nm IR laser at a power of 10 mW that was controlled by the LabView software (National Instruments). First the liposome was trapped in the original solution PBS and

its Raman spectra was collected at 37°C. Then the liposome was transferred into the Ply solution site in the microfluidic device (Figure 5-5) again the Raman spectra were recorded with 100 Raman spectra recorded over 30 sec using WinSpec3 software.

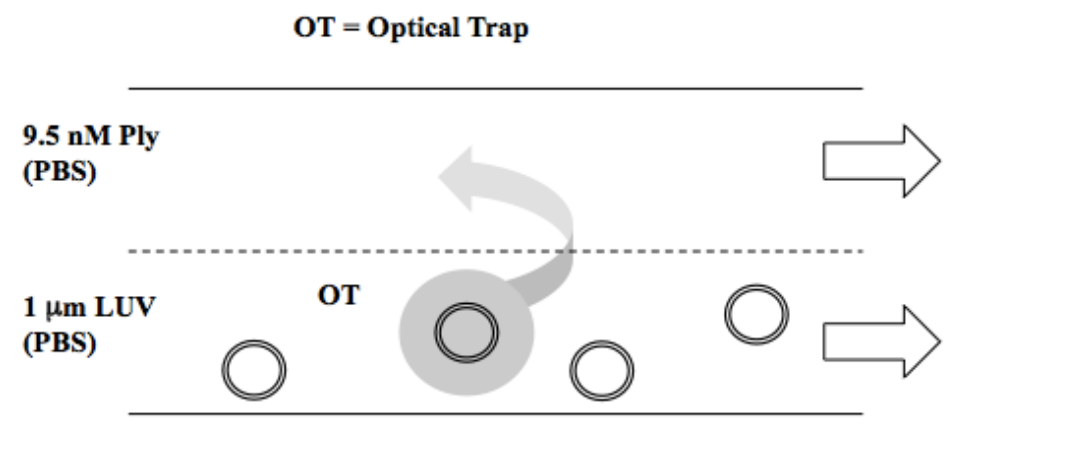


Figure 5-5: Liposome manipulation between two different solutions including PBS and Ply by OT.

Two solutions comprising liposomes (LUVs) in PBS and Ply flow together but do not mix because of a laminar boundary inside the microfluidic device.

5.7 Raman measurement and data collection

The combination of dichroic mirrors, DM1 and DM2 (z700dcxr; Chroma) (Figure 5-6) allowed the Raman-scattered light, from the 488 nm laser, to be collected by the objective lens. The signals were gathered from the samples utilizing at 13.5 mW for all Raman experiments depicted in this work. Focusing of the 160 mm achromatic lens system (Comar), onto a 150 μm pinhole (Comar) in the confocal image plane allows spatial filtering of the Raman wavelength. The second achromatic lens 160 mm was used to recollimate the spatial filtered light. Then the 50 mm achromatic lens was focused onto the 100 μm -width entrance slits of a spectrograph with a 0.500 m imaging triple grating monochromator (Acton Research Potbelly, Spectra Pro 2500i; 1800 seam /mm grating; 500 nanometre blaze wavelength). The detector was a -80 °C cooled, back-illuminated, charge-coupled device (Princeton Instruments, Pixis I 00B). Increments of 0.018 nanometer (~ 0.5 centimetre⁻¹) was used to measure the spectral data points.

The optical resolution of the spectrograph was 2cm^{-1} , and the precision of the wavenumber was 0.5 cm^{-1} . Acquisition time for an individual spectrum was 30 sec and was controlled by the WinSpec3 software. The background signal of the lipid-Raman spectrum (which includes the stretching set of water molecules) was subtracted using Excel, and all Raman spectra were normalized in order to have the same integrated intensity for the overlapping C-H stretching bands (between 2800 and 3040 cm^{-1}), which is the region of interest of the lipid. Figure 5-6 represents the schematic diagram of the OT and measuring the inelastic scattering of light.

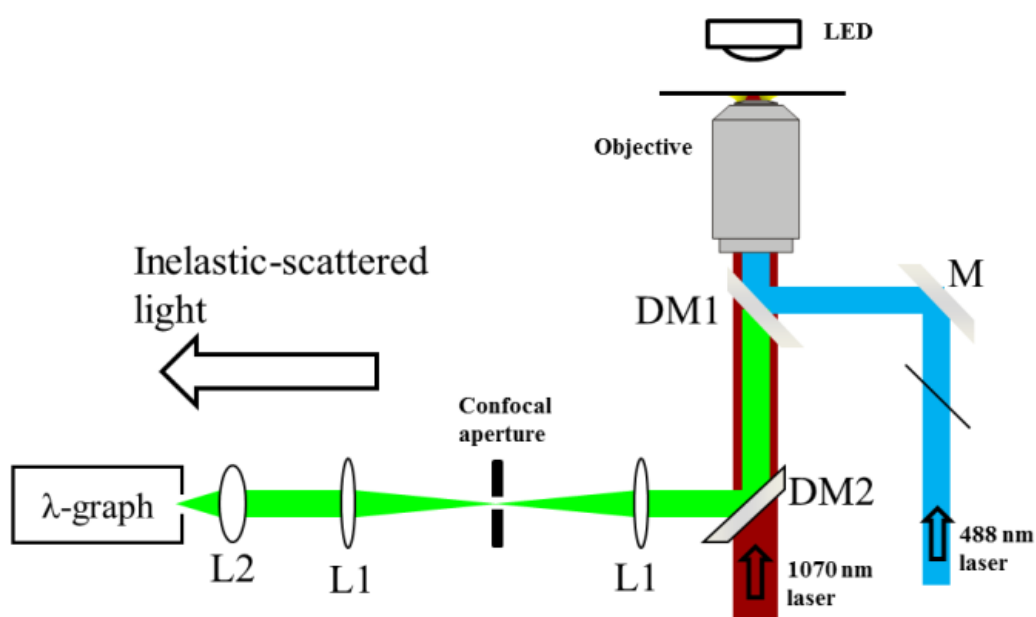


Figure 5-6: Schematic of Optical tweezers.

The blue path is the Raman excitation laser at 488 nm lasers. The mirror DM1 reflects the beam onto the objective. The inelastic back-scattered light of the Raman is collected back through the objective by the short wave pass dichroic mirror DM2. The DM1, DM2 are the dichroic mirrors, with the long-wave pass. L1-achromatic lens, L2-achromatic lens, are included 160 mm, 50 mm respectively. M is the silver mirror and λ -graph is a Raman spectrometer.

5.8 The OT setup

The experiments were performed using a custom built inverted microscope. The sample stage was composed of the aluminum plate and the insulated flexible heater ring shape. A K-type thermocouple was used to monitor the temperature of the aluminum plate. A 1cm

delrin plate was used to isolate the sample stage from the microscope body. The aluminum plate and delrin plate have a circular opening matched to the inner diameter of the heating element. The oil-immersion infinity corrected, objective lens (Nikon Inc., 1.25 NA, 100×) make contact between the microscope and the lower surface of the 1.5 cover glass through the circular opening. The white light LED 400-800 nm and the condenser illuminated the sample. The trapping laser at 1070 nm had a 7 mm diameter beam. This was expanded to 21 mm by two achromatic lenses (L1 and L2). In order to create an optical trap in the sample plane, the back aperture of the objective lens was over filled by a continuous-wave infra-red (IR) laser (1070 nm-wavelength). The liquid-crystal-on-silicon and the spatial light modulator controlled the focal point of the optical trap in the lateral and axial position, which is located near the IR source beam. This instrument capability enables a trapped particle is correctly positioned at the focal point of a second laser beam of 488 nm wavelength which is combined with the IR laser by the DM1 dichroic mirror. More than 95% of the 488 nm was reflected by the DM1 dichroic mirror with the transmission of IR 1070 nm and approximately 50% of the laser 488 nm was used to measure the light scattering because it is not sufficient to trap the particle. The Notch filter was placed in front of the CCD for both laser sources. The advantage of using two different laser sources for the optical trapping and the Raman excitation is that the trapped particle can be manipulated freely with sensitivity and the set up allows alignment of the particle into the focal spot of the excitation laser to optimize the Raman intensity. Another advantage of using two lasers with the different wavelengths is minimising damage of the sampl by selecting a suitable wavelength for the optical trapping laser.

5.9 Raman data normalization

Raman data was normalized using a multistep process. Firstly, the cosmic background anomalies of all Raman data were removed by estimating the values that would have been recorded without interference and replacing them with the average of the two neighboring data. After this correction any changes in the data can be identified. Secondly, the base line was adjusted to zero to normalize the intensity of the Raman data because in the raw data the Raman spectra lies on a slope due to overlapping signals in the Raman. This was solved by taking three sections using a linear equation due to the change in gradient in stages. For example, the data was separated into three sections including 1st section

between 562.200-564.989 nm, the 2nd section between 565.001-572.989 nm and the 3rd section lies between 573.006-574.200 nm. The large broad signal of PBS was excluded because lipid intest peaks are contained in those three sections. The equation to normalize the intensity of each section was performed by Dr. Andrew Hudson in the Chemistry department at Leicester University. All equations are displayed in the appendix. The final step was the calculation of the Raman shift, in which the wavelength of the region of interest was converted into wavenumbers of the Raman shift.

5.10 Results

5.10.1 Lipid vibrational spectroscopy

LUVs (1 μ m) were prepared by the extrusion method in order to produce the consistent liposome vesicles. A single liposome was optically trapped with the 1070 nm laser and the Raman spectra was recorded at 488 nm laser. The region of interest for the study of the liposome structural changes is the C-H stretching region. The C-H stretching region is composed of symmetric and asymmetric methylene stretching (d^+ , d^-) and methyl stretching (rFR^+ , r^-). Previous studies have assigned peaks to different vibrations. The symmetric (d^+) and asymmetric (d^-) methylene stretching vibrations of POPC appear at 2851 cm^{-1} and 2900 cm^{-1} , respectively (Figure 5-7 A). The shoulder at 2925 cm^{-1} is assigned to the symmetric methyl stretch (rFR^+), and the peak around 2970 cm^{-1} to the asymmetric methyl stretch (r^-) of the fatty acid chain (Figure 5-7 A) (Snyder et al., 1978, Snyder et al., 1982, Aslanian et al., 1986). The Raman fingerprint of pure POPC and Chol were recorded separately to understand how they impact the Raman assignment peaks of liposome. Though the same C-H stretches shifted frequencies they are still identifiable as the d^+ , d^- , rFR^+ and r^- stretches respectively (Figure 5-7 B). This clearly shows that POPC is responsible for a significant fraction of the d^+ contribution and a broader d^- stretch vice versa d^+ is shifted and d^- is thinner in Chol. The rFR^+ and r^- are much stronger in Chol than the POPC peak.

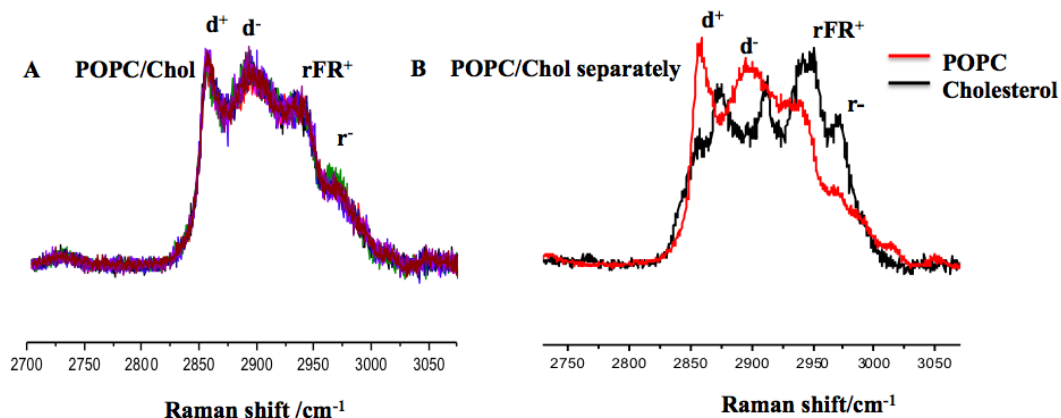


Figure 5-7: Representative Raman spectra of an-optically trapped POPC/Chol liposome and POPC/Chol separately.

Symbols on each peak represent different regions of the C-H stretching spectrum. Figure A (d^+) and (d^-) represent symmetric and asymmetric methylene (CH_2) stretching respectively and ($r\text{FR}^+$) (r^-) represents symmetric and asymmetric methyl (CH_3) stretching. Figure B shows the Raman peak of the POPC/Chol separately shown by the red and black lines.

5.10.2 Observing structural changes in a single liposome by wild-type Ply

The Y-shaped microfluidic device (Figure 5-3A) was used in order to study the interaction between a single POPC/Chol liposome and Ply. Movement of an optically trapped liposome across the laminar-flow boundary results in an immediate change in the environment enabling study of the structural changes in the lipid bilayer. The liposome was optically trapped with the red laser ($\lambda=1070$ nm) and moved into the flow of the toxin stream. The change in the Raman spectra of the liposome was recorded at 488 nm, every 30 sec. A control experiment was carried out in which the liposome was optically trapped in the same way but without the addition of Ply. The first spectrum, in black (Figure 5-8) was recorded whilst the liposome was stationary in PBS. The final spectrum in red (Figure 5-8) was recorded after 720 sec in the solution of Ply. A change in the Raman spectra is observed when Ply is present with a decrease in the CH_2 symmetric stretching mode (d^+) (Figure 5-8). Differences in the C-H stretching region of the liposome might be a sign of an increase in the diameter of the vesicle when Ply binds, with a decrease in short-range order of lipid molecules in the bilayer and an increase in membrane fluidity. The overall change in the Raman spectra of the liposome with Ply is similar to the change observed

by a temperature-induced transition from L_o into $L_o + L_d$. This change is characterized by a decrease in CH_2 symmetric stretching mode (d^+).

To confirm that Chol is necessary for the changes observed, Ply was mixed with pure POPC vesicles without Chol. Raman spectra were recorded for a series of liposomes (Figure 5-9 B). No changes were observed in the Raman spectra when exposed to the wild-type toxin indicating that Chol is essential for binding of Ply.

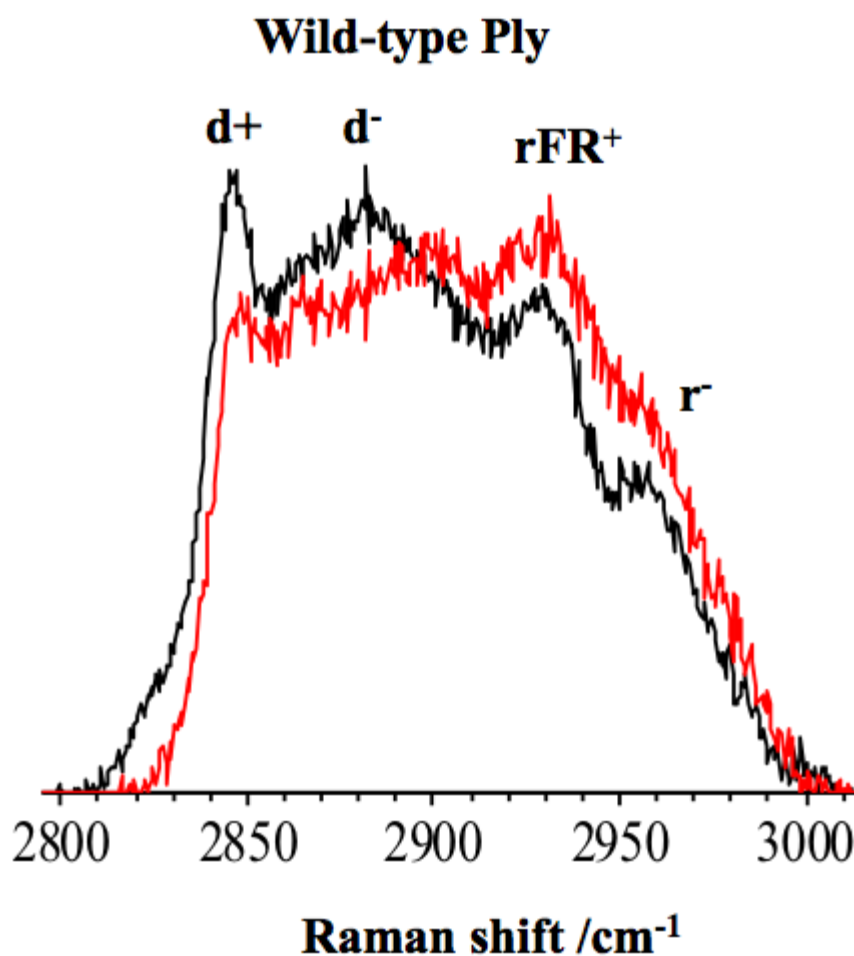


Figure 5-8: The Raman spectra profile of an-optimally trapped liposome (1:1 mole ratio POPC/Chol) with and without wild-type Ply.

Raman spectra of liposome was recorded in Y-shape microfluidic device. Then liposome transferred to the Ply site in Y-shaped device by OT. A sequence of experimental Raman spectra recorded at 30 sec intervals following exposure to Ply. Raman Spectra of liposome without (black) and with wild-type Ply (red after 720 sec).

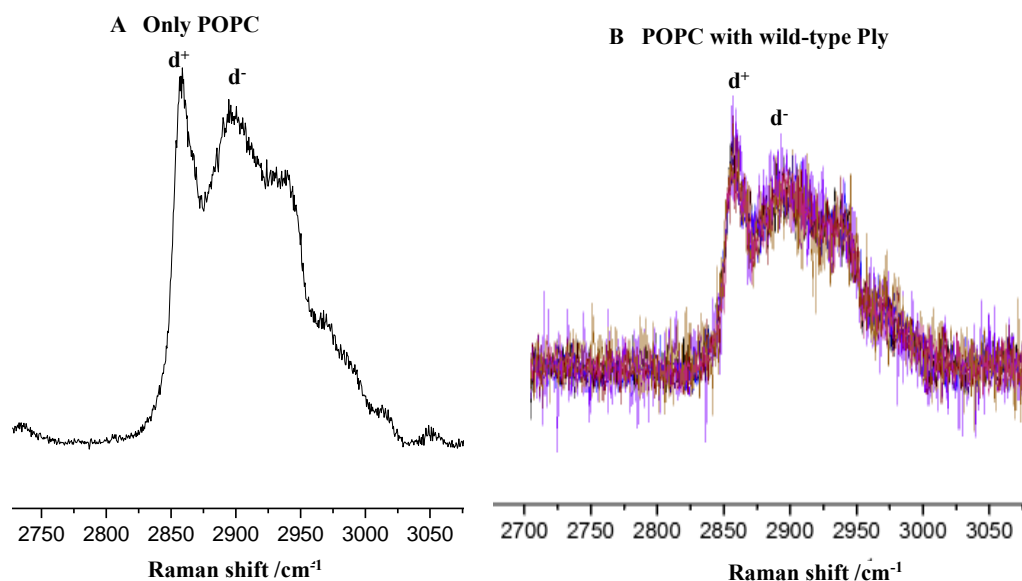


Figure 5-9: Raman spectra profile of an-optically trapped pure POPC liposome with and without wild-type Ply.

(A) Shows the pure POPC spectra. (B) Shows the Raman spectra of POPC with wild-type Ply, both spectra are identical indicating that Chol is essential for Ply binding. The d^+ and d^- bands are not changed in both figures A and B.

5.10.3 The influence of lipid composition on the changes observed in the bilayers following the addition of wild-type Ply

In this experiment liposomes were prepared with POPC/Chol ratios of 4:1 and 1:2. The latter ratio is the saturation limit of Chol in the POPC bilayers. This experiment was performed to observe how the Chol impacts the chemical and structural changes of the lipid in the liposome once incubated with Ply. Figure 5-10 A shows the Raman spectra of a single liposome with low Chol concentration. No change can be seen in the Raman spectra when the liposome is transferred to the wild-type Ply solution. However, a big change is observed with the high Chol concentration once exposure to Ply (Figure 5-10 B). The major change was in the d^+ symmetric CH_2 and rFR^+ CH_3 symmetric region, which decreased and increased respectively. Differences in the C-H stretching region was caused by sequestering of Chol by Ply. It has been suggested, that change in C-H stretching region on addition of Chol is caused by the Chol associating tightly with the acyl chain of the lipid in the membrane (Rojko and Anderluh, 2015). Taken together, the

results suggest that addition of Chol to the membrane causes the lipid acyl chains to become more packed and ordered. Addition of Ply changes the arrangement of the lipid acyl chains from packed ordered to disorder. Ply impact the membrane phase similar to the changes induced by temperature.

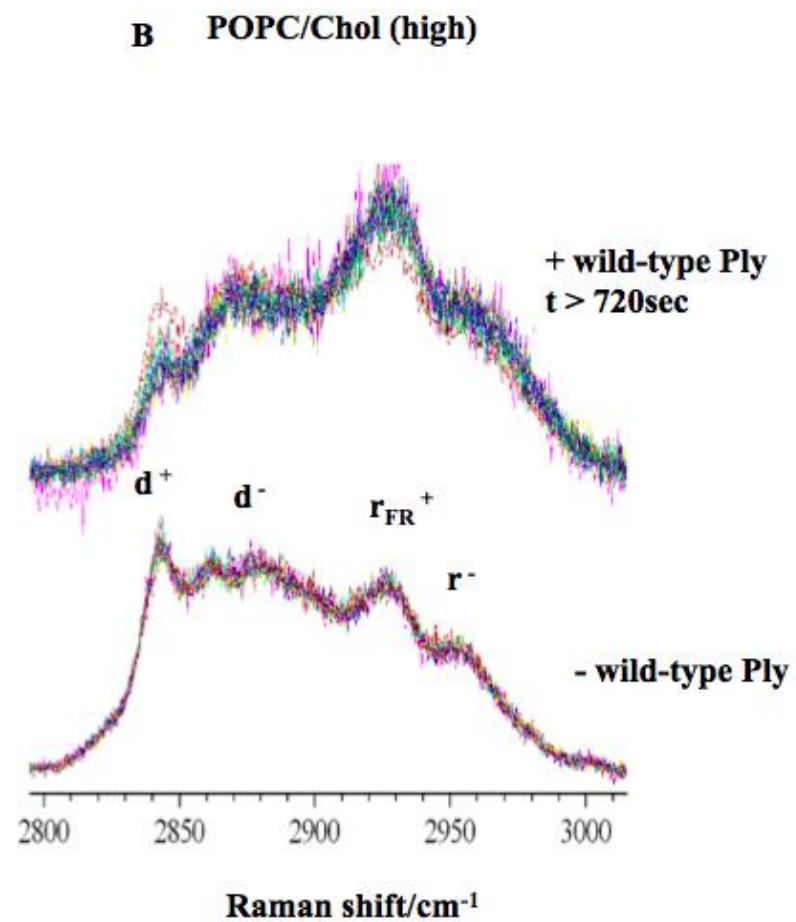
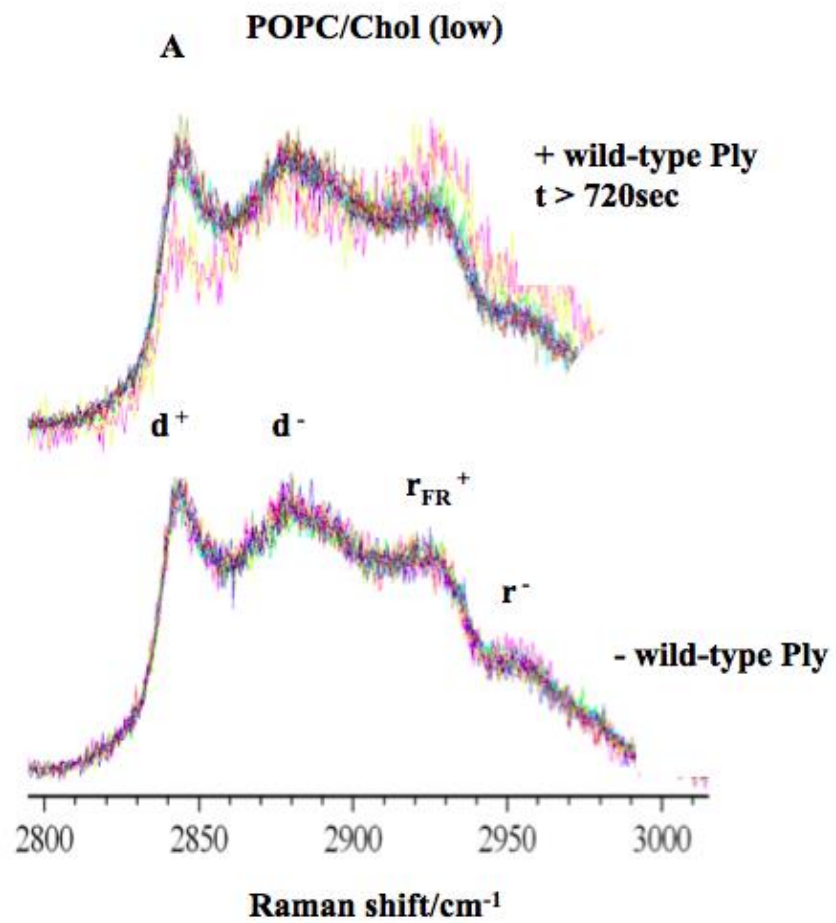


Figure 5-10: Comparison Raman spectra of an-optically trapped single liposome with and without wild-type Ply in low/high concentration of cholesterol.

A sequence of experimental Raman spectra recorded at 30 sec intervals following exposure to Ply. Top (A, B) images show Raman spectra of single liposome (containing low and high amounts of Chol) with Ply. Bottom images show the liposomes without Ply.

5.10.4 Raman spectra of liposome with the PlyD4

PlyD4 cannot lyse RBCs (Figure 4-10 B), however, it can bind to membrane Chol through the Trp-rich region (Gilbert et al., 1999, Baba et al., 2001). To measure the impact of PlyD4 on the chemical structure of the lipid a similar experiment was performed as described in section 5.10.2. When PlyD4 was incubated with the liposome no changes were observed with low or high Chol (Figure 5-11 A and B) indicating that the methylene and methyl C-H stretching is unaffected. This shows that binding alone does not cause spectral changes in the membrane structure that were observed for the full-length toxin. PlyD4 binds superficially to the membrane, but does not oligomerize and does not deeply embed into the membrane (Nollmann et al., 2004).

POPC/Chol (low) + PlyD4 $t > 720$ s

POPC/Chol (high) + PlyD4 $t > 720$ s

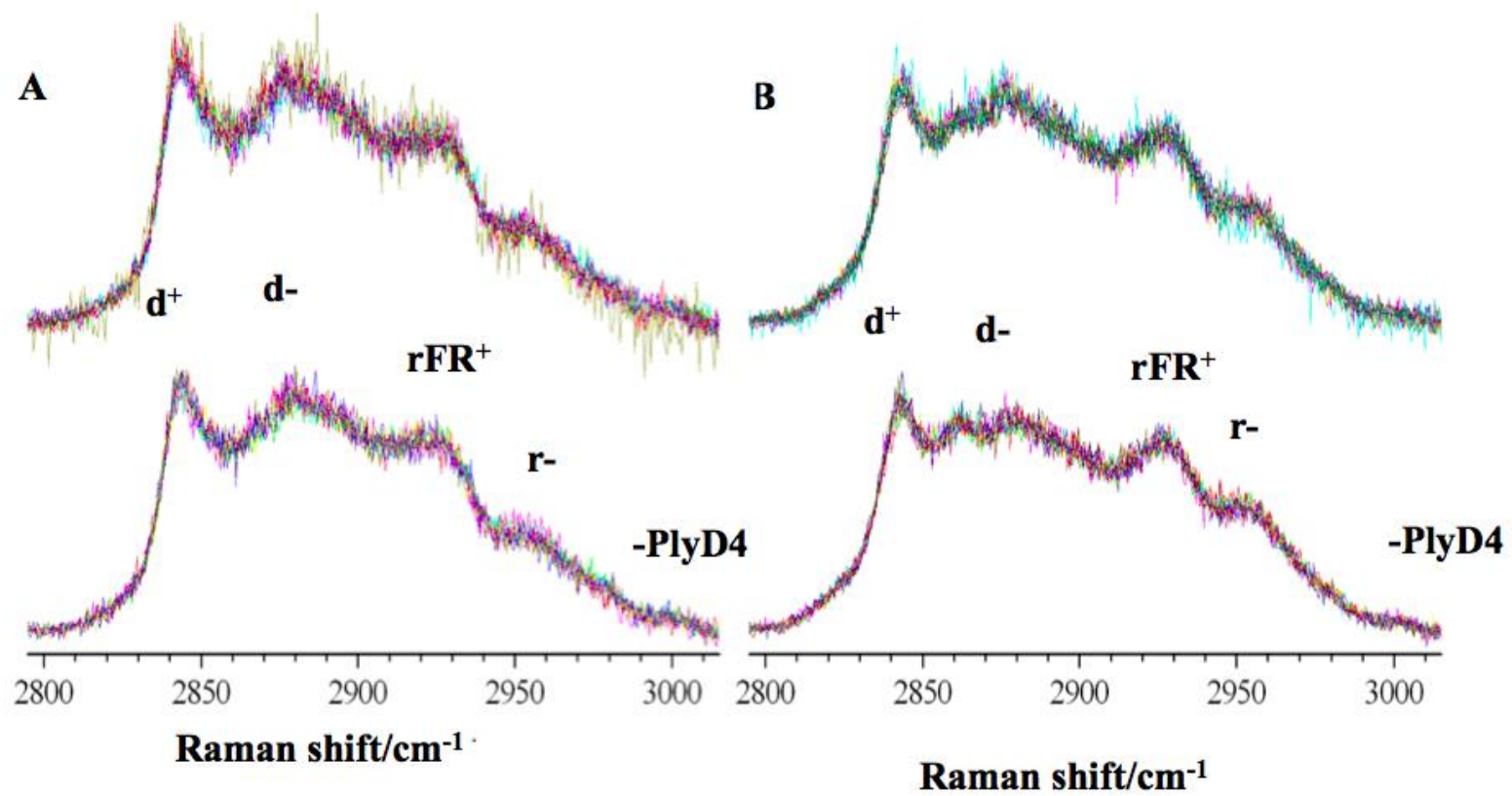


Figure 5-11: Comparison of Raman spectra of an-optically trapped liposome with and without PlyD4.

Top (A, B) images show Raman spectra of single liposome (containing low and high amounts of Chol) with PlyD4. Bottom images show the liposomes without PlyD4. A sequence of experimental Raman spectra recorded at 30 sec intervals following exposure to PlyD4. In both A and B images the four bands of CH₂ and CH₃ as labelled d⁺, d⁻, Rfr⁺, r⁻ respectively are not changed.

5.10.5 Monitoring membrane, structural change of the liposome with Ply Asp205Arg (D205R) and Asn339Arg (N339R)

The point mutations N339R and D205R abolished the haemolytic activity of Ply without affecting its overall structure or ability to interact with the membrane (Chapter 4). N339R does not oligomerise on liposomes whereas D205R can oligomerise but cannot form pores. Addition of the N339R mutant resulted in no change in the Raman spectra (Figure 5-12), indicating that the mutation prevents the structural changes in the membrane that were observed for wild-type toxin. Surprisingly, the D205R mutant (Figure 5-12) induced similar effects as wild-type toxin despite having no haemolytic activity. Thus the spectral changes observed are not caused by pore formation itself. Instead, it can be concluded that oligomerization of Ply monomers on the membrane surface causes the changes to the membrane.

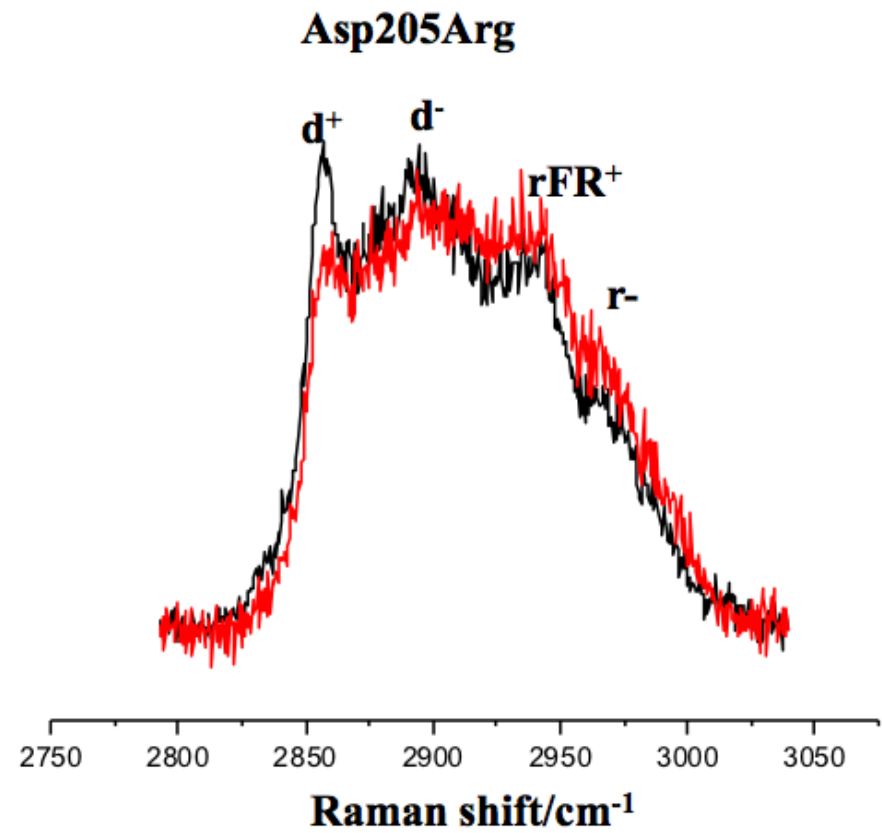
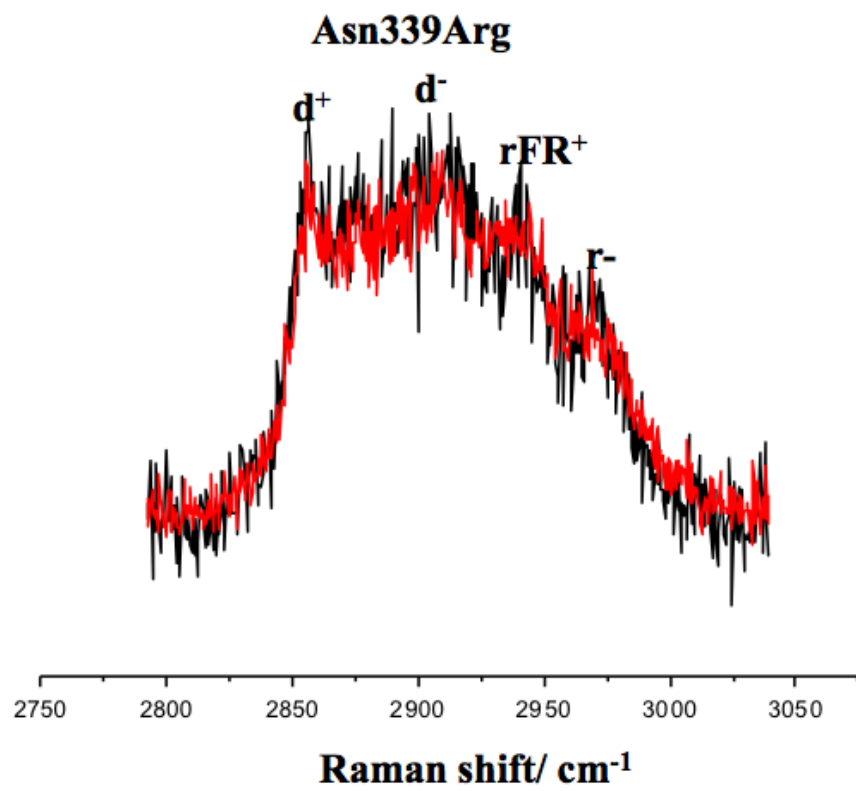


Figure 5-12: Raman spectra profile of an-optically trapped liposome (1:1 POPC/Chol) with mutant D205R and N339R.

A sequence of experimental Raman spectra recorded at 30 sec intervals following exposure to Ply D205R and N339R. Raman Spectra of liposome without (black) and with Ply D205R and N339R (red) recorded after 0 sec and 720 sec.

5.10.6 Monitoring membrane, structural change of the liposome with mutant Ply Thr304Arg, Arg226Ala, Thr88Glu, and Lys268Ala, Val341Arg and Leu11Arg

Spectral changes in a single liposome were also measured for a number of Ply point mutants including Thr304Arg, Arg226Ala, Thr88Glu, and Lys268Ala, Val341Arg and L11R. All showed similar changes to the wild-type toxin to varying degrees revealing similar structural changes to the membrane (Figure 5-13). Mutant Thr304Arg (Figure 5-14) caused large shifts in the C-H stretching spectrum and the d^+ band disappeared. This mutant reduced the haemolytic activity of Ply by ~300-fold (Chapter 4). At 1:1 ratio and low POPC/Chol ratio the d^+ band reduced significantly, (Figure 5-14A, B red line), however, no change was observed at a high Chol ratio (Figure 5-15). The reason for these differences is not clear.

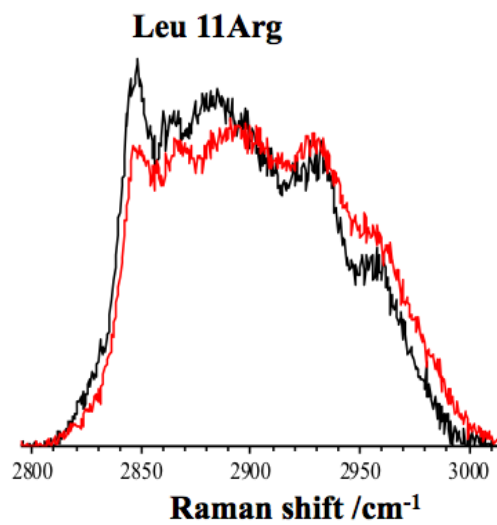
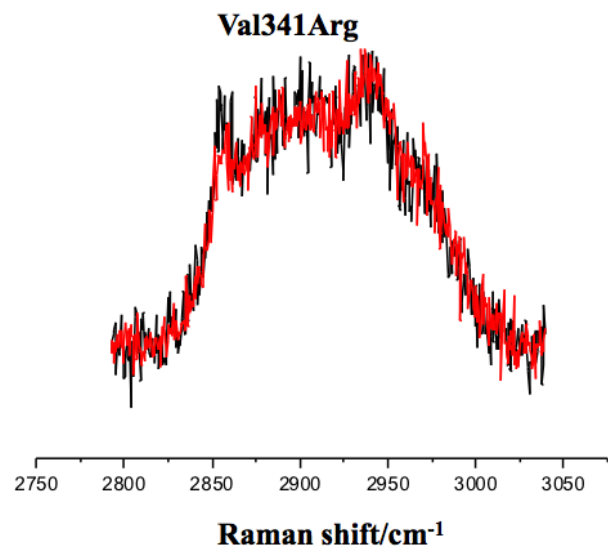
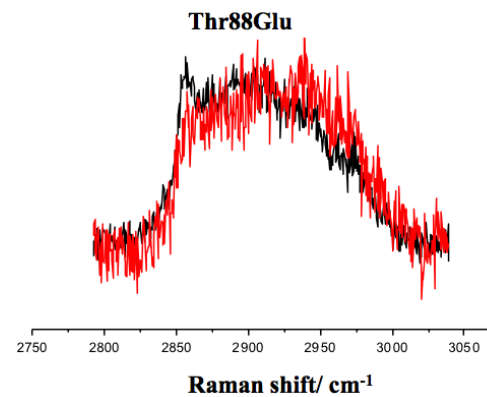
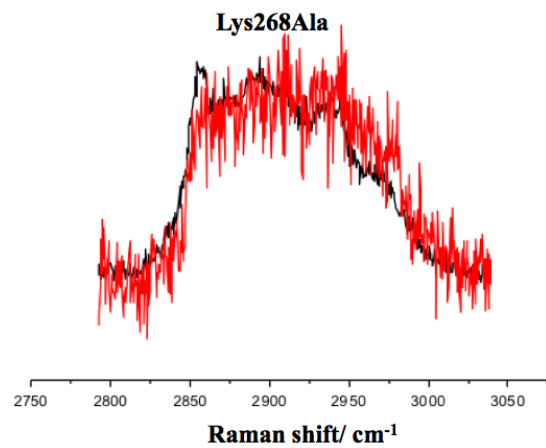
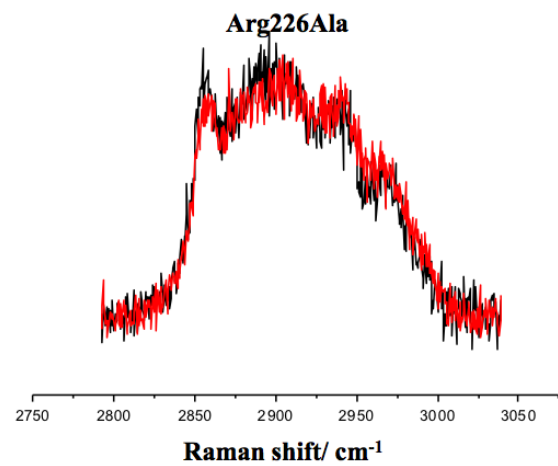


Figure 5-13: Raman spectra profile of-an optically trapped 1:1 POPC/Chol vesicle with mutant Lys268Ala, Arg226Ala, Val341Arg, Thr88Glu and Leu11Arg.

A sequence of experimental Raman spectra recorded at 30 sec intervals following exposure to all above mutants. Raman Spectra of liposome without (black) and with Ply mutants (red) recorded after 0 sec and 720 sec.

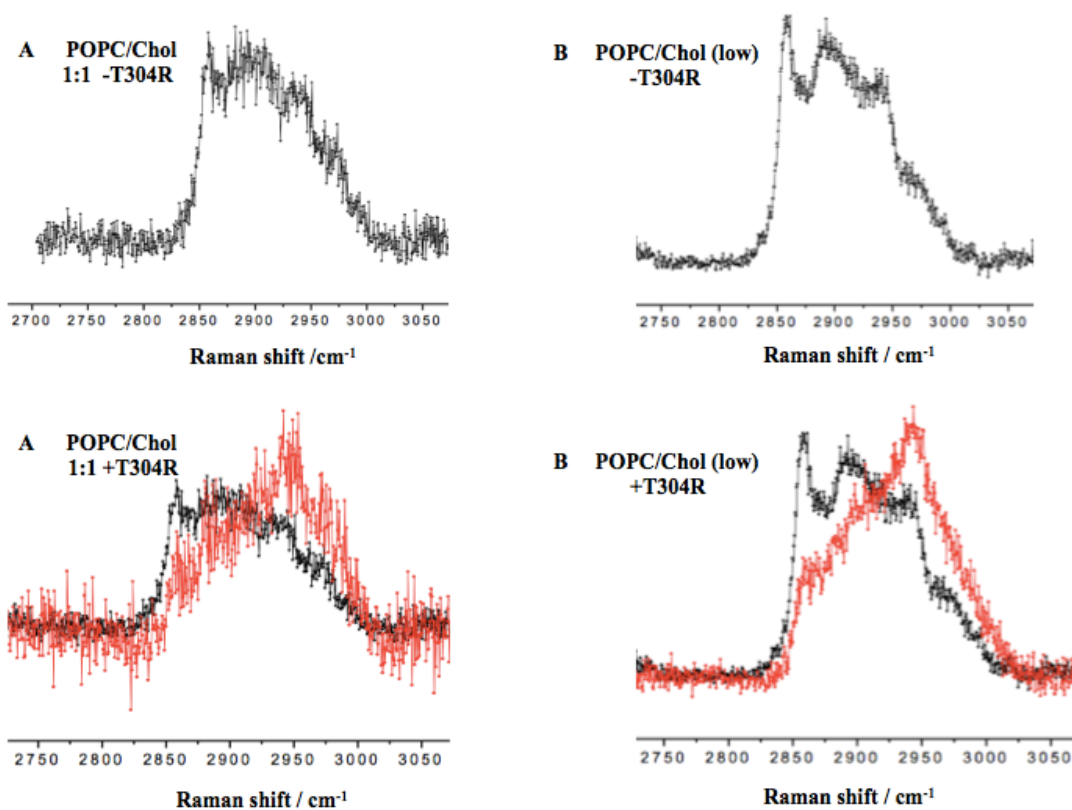


Figure 5-14: Comparison of Raman spectra for an-optically trapped liposome POPC/Chol 1:1 ratio and POPC/Chol low ratio with mutant Thr304Arg.

Top (A, B) images show Raman spectra of single liposome (containing 1:1 and low amounts of Chol) without PlyT304R. Bottom images show the liposomes with PlyT304R. Raman Spectra of liposome without (black) and with Ply T304R (red) recorded after 0 sec and 720 sec.

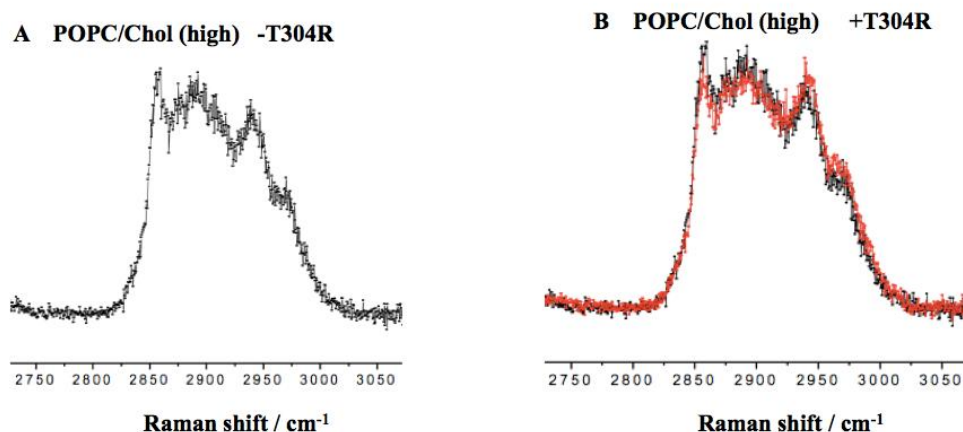


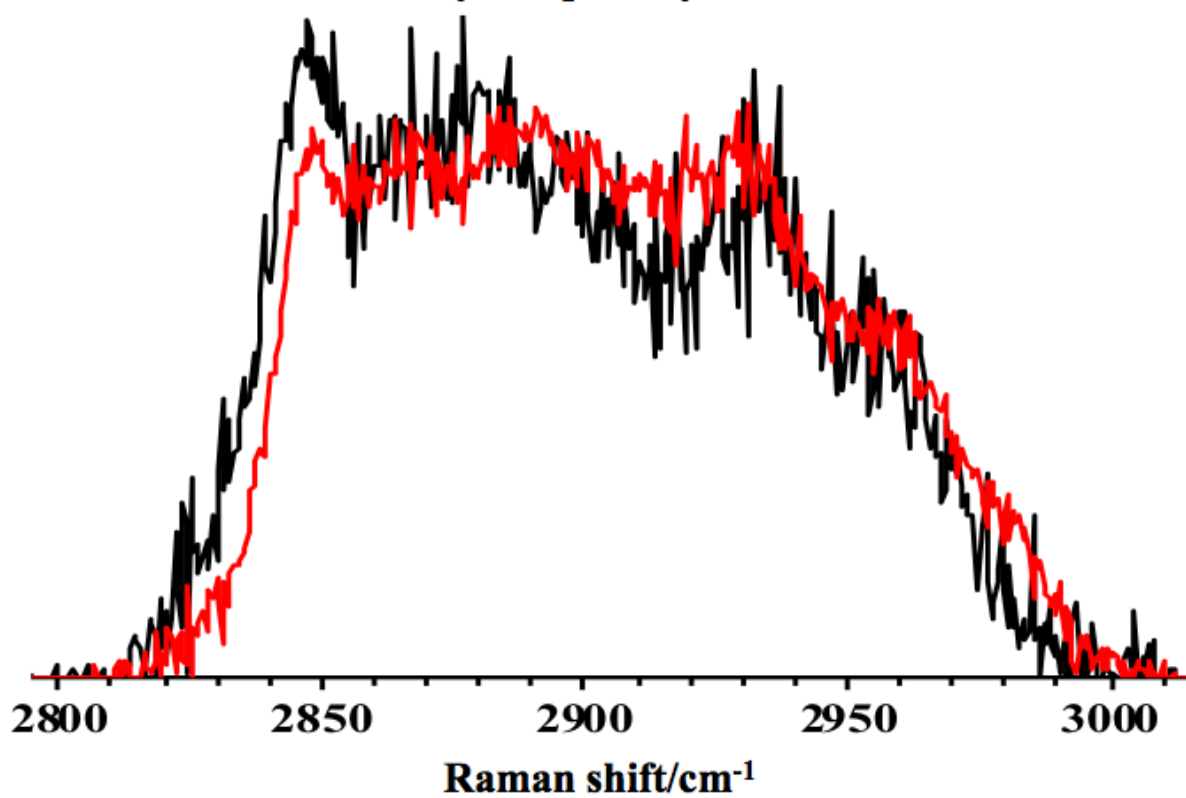
Figure 5-15: Comparison of Raman spectra for an-optically trapped liposome POPC/Chol high with and without Thr304Arg.

The A, spectra represent the liposome spectra without the Thr304Arg whereas; B, spectra represent the liposome spectra without (black) and with Thr304Arg (red) that result in no change.

5.10.7 Influence of locked mutant on the chemical structure of the membrane

The two locked mutants were also tested. Both mutants caused similar spectral changes as wild-type Ply (Figure 5-16), in which the d^+ peak disappeared. The locked mutants were designed to prevent pore insertion, but not Ply oligomerisation, so these results are consistent with the conclusion the changes to the membrane structure are not caused by pore formation itself. However, caution is needed because the locked mutants did retain some haemolytic as described in Chapter 4 (Figure 4-10 B) suggesting that a small proportion of the mutants were not disulphide trapped.

Ala262Cys+Trp278Cys



Thr55Cys+Val163Cys

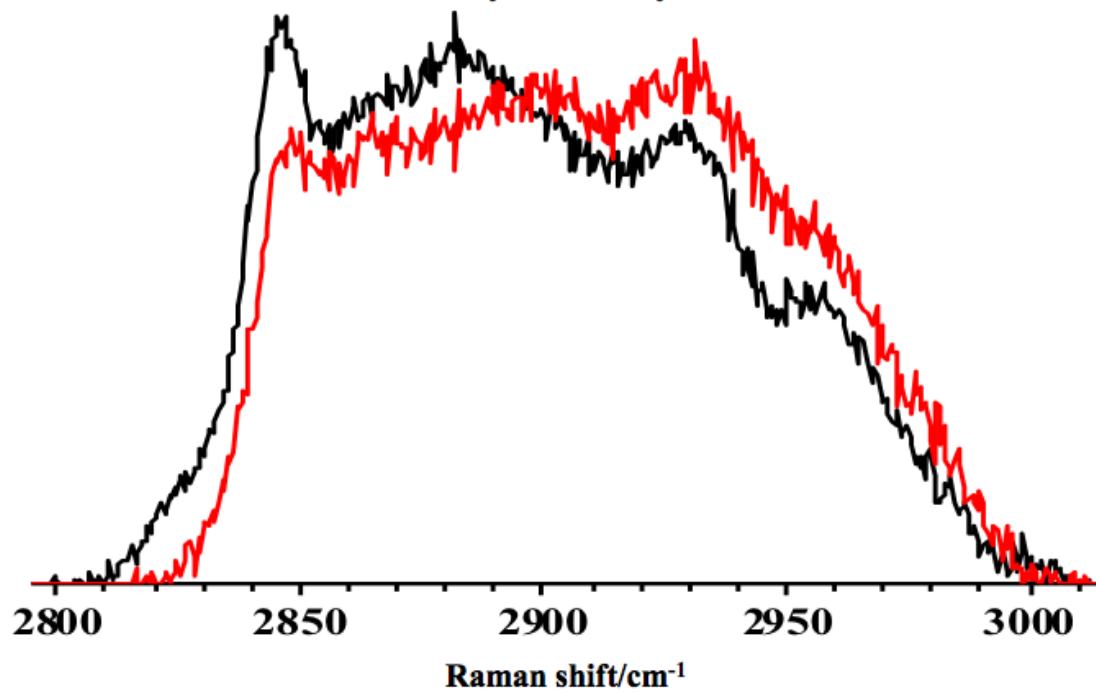


Figure 5-16: Raman spectra analysis of an-optically trapped liposome with Ply locked mutants (Thr55Cys+Val163Cys and Ala262Cys+Trp278Cys).

Raman spectra of POPC/Chol (1:1 mole ratio) was recorded for both mutants in the Y-shaped microfluidic device. A sequence of experimental Raman spectra recorded at 30 sec intervals following exposure to (Thr55Cys+Val163Cys and Ala262Cys+Trp278Cys). Ply. Raman Spectra of liposome without (black) and with mutants (red after 720 sec).

5.10.8 Monitoring change of the lipid layer of a liposome membrane composed of ternary mixture of POPC/Chol /SM (1:1:1)

To understand the interaction between lipid rafts and Ply toxins, spectra were recorded for liposomes containing 1:1:1 mixture of POPC/Chol/SM. SM is used to form lipid rafts in liposome preparations (Kai and Elina, 1997). No changes were detected on addition of wild-type Ply, PlyD4 or mutant T304R to POPC/Chol/SM liposomes (Figure 5-17). This result suggests that the presence of SM in a lipid membrane, causes the surrounding lipid to become more ordered, so that no Chol sequestering is required prior to pore insertion by Ply.

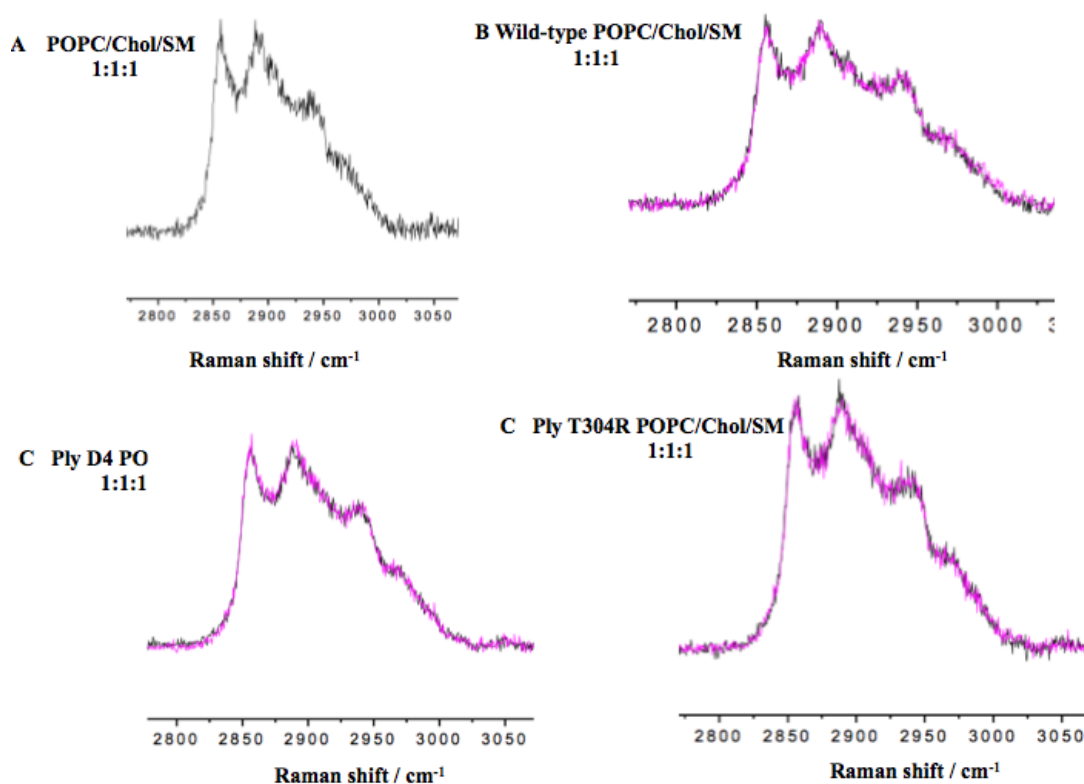


Figure 5-17: Raman spectra profile of 1:1:1 POPC/Chol/SM liposome with wild-type Ply, PlyD4 and Ply mutant T304R.

(A) Shows the pure Raman spectra of the POPC/Chol/SM alone; B, C, and D display Raman spectra profile of the liposome once exposed to the wild-type Ply, PlyD4 and the mutant Ply T304R consequently in a Y-shape microfluidic device.

5.11 Discussion

The present study observes changes in the membrane of single cell-sized liposome using Raman spectroscopy and optical tweezers. The process of pore formation by Ply is well established (Tilley et al., 2005, Gilbert et al., 1999) but how it impacts on the structure of the cell membrane is still poorly understood. The purpose of the work in this Chapter was to provide a greater understanding of the structural changes in the lipid membrane upon interaction with the Ply toxin. Raman spectroscopy is widely used to study membranes and gives a spectral fingerprint of a sample as a result of inelastic scattering of light (Rajan et al., 2017). Many studies have reported the characteristic changes in the chemical structure of the lipid in response to changes in temperature (Wu et al., 2016a, Lewis and McElhaney, 2013, Schaefer et al., 2012). According to the literature the Raman peaks of the lipid is divided into four overlapping bands due to symmetric and asymmetric stretching of the CH₂ and CH₃ bonds (Snyder et al., 1978). The Raman spectra of the liposome changes when Ply is added reflecting in an increase in the disorder of the membrane. The changes resemble those caused by heating in which the diameter of the vesicle is gradually increased and this leads to a decrease in a short-range order of lipid molecules in the lipid bilayer, and increase in membrane fluidity. The membrane phase changes from an ordered gel phase to a liquid-disordered phase. Comparison of the effects of wild-type Ply with the point mutants and truncated forms suggests that the observed changes to the membrane fluidity are caused by self-association of Ply monomers not by pore formation itself. Thus disulphide-locked mutants, which cannot form pores but can form pre-pore structures, showed similar changes to wild-type Ply confirming that the changes observed in the membrane are not caused by pore formation. By contrast, the Asn339Arg mutant binds to the membrane but cannot self-associate or form pores and caused no spectral changes (as did D4 alone). Asp205Arg self-associates on the membrane but cannot form pores, yet resembles wild-type Ply with respect to the changes in the Raman spectrum. This approach therefore provides a very useful way of

distinguishing pores from pre-pores, something that has not been possible previously using spectral methods. This in-turn can be used for characterising the molecular mechanism of Ply inhibitors.

The structural changes of the membrane were recorded for different Ply mutants include (Leu11Arg, Lys268Ala, Val341Arg, Arg226Ala, and Thr88Glu, Thr304Arg) through the Raman spectroscopy with highlighting on the C-H stretching region and specifically the d^+ band which represents the symmetric stretching of CH₂ region of lipid. All the mutants impact the structural changes with different degree, in all of them the d^+ band was reduced. Reducing of the d^+ band means that the membrane phase is changed from the L_o to L_d phase. Because the impact of Ply on the membrane structure some how similar to the impact of temperature on the membrane. Ply and Ply mutants once bind to the cholesterol in the membrane they sequester cholesterol from the membrane for the purpose of securing the most stable surface for pore formation. Sequestering of the cholesterol from the membrane by Ply and Ply mutants cause reduction of the d^+ band is then an indication of altering the phase of the membrane from the L_o to L_d (Figure 5-18).

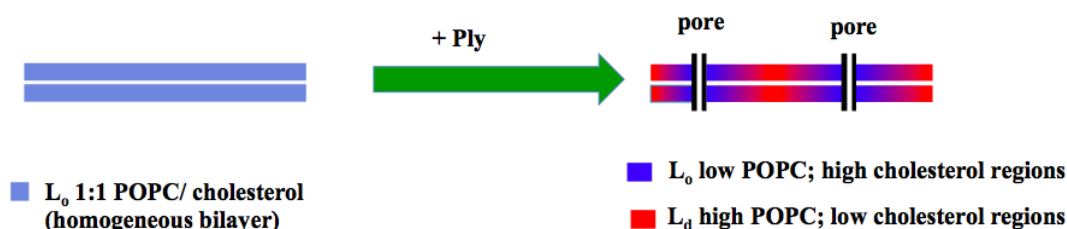


Figure 5-18: Schematic representation of impacting Ply on the the membrane phase.

When the membrane contains the equi-molar amounts of phosphocholine (POPC) and cholesterol (1:1), a liquid-ordered phase, L_o, exists (shown in blue in the figure). The L_o shares characteristics of the gel (L_β) and fluid (liquid-disordered, L_d) phases of a lipid membrane. While the intercalation of cholesterol with phosphocholine molecules disrupts the planar triangular lattice in the gel phase, a *trans* conformation of the hydrocarbon chains is more favoured in the fluid phase resulting in a higher degree of short-range order. After addition of the Ply and Ply mutants, we believe that the membrane transitions from a pure L_o phase into a state in which the L_o and L_d phases coexist (as shown in the figure in dark blue - L_o region with high cholesterol - and red L_d region with low cholesterol. The Ply sequesters cholesterol from the membrane.

5.12 General discussion

5.12.1 ELISA binding between Ply and human L-ficolin

Ply is a virulence factor of the pneumococcus, which is a pathogen of significant clinical importance; therefore, understanding the interaction of Ply with the immune system is critical. The work presented in (Chapter 3) revealed that Ply does not bind to human L-ficolin, contrary to a previous report (Ali et al., 2013). The inconsistency between the two studies is most likely to have been caused by contamination of Ply preparations. Because, Ply is produced in *E. coli*, a potential target of L-ficolin, any impurities (e.g. acetylated cell wall components) could lead to false positive results. I used highly pure preparations of Ply with an additional gel-filtration purification step. The resulting protein was successfully crystallized (Marshall et al., 2015).

5.12.2 ELISA binding between Ply and IgG isotypes

My data confirmed that Ply binds to IgG. However, the results were somewhat surprising regarding binding to IgG isotypes. Ply bound to IgG2, IgG3, and IgG4, but not to IgG1. The reason for these differences in binding is unclear. However, it is interesting to note that the length of the hinge regions in each IgG isotypes is different. Ali *et al* (2013) suggested that the long hinge region of IgG3 (62 amino acids) might facilitate its interaction with Ply. However, the hinge regions of IgG4 and IgG2 are shorter than IgG3 (12 amino acids), so this explanation is unlikely. More likely is that there is a binding site that is conserved in IgG2, IgG3 and IgG4 but not in IgG1 which is located in the CH1 region (Figure 3.22). Interestingly, IgG3 and IgG1 both activate the classical pathway, whereas IgG2 has lower activity and IgG4 fails to activate complement. Thus, most Ply-driven complement activation probably occurs through IgG3. The function of the interactions of Ply with IgG2 and IgG4 is less clear, although they would likely reduce the amount of functional IgG in serum, thereby impairing the immune response of the host.

5.12.3 Ply binds to the Fab region of IgG via domains 1-3

The results of this study indicate that the Ply-IgG interaction is mediated mainly through the Fab fragment of the IgG and the PlyD1-3 fragment of Ply. In contrast, to the findings of Mitchell *et al* (1991), Ply did not interact via IgG Fc. Binding of Ply to the Fab fragment of IgG would mean that the Fc portion is free to bind to C1q and activate CP.

5.12.4 Structural based mutation in Ply to block pore formation

Monomers of Ply pack side-by-side in the crystal structure of Ply (Marshall et al., 2015). We hypothesized that these packing interactions mimic the packing interactions that occur when Ply monomers come together on the cell-surface. To test this hypothesis, mutations were made to residues at the interface and the activities of the resulting Ply mutants were measured. The eight point mutations that were made all reduced the haemolytic activity of Ply, supporting our hypothesis. Two of the mutants completely abolished haemolysis by Ply. These affects were not caused by destabilization of Ply or by failure to bind to the membrane. Analysis by EM showed that the loss of activity was caused by distinct mechanisms. Asp205Arg mutants still formed oligomers but these oligomers were linear not curved, implying that the mutation prevents pore-formation. Pore formation would require flexibility in the packing to create the necessary curvature. Presumably the Asp205Arg mutation prevents this flexibility resulting in the linear arrays of molecules that were observed in electron micrographs rather than circular pores. The other mutant Asn339Arg appeared to block oligomerization completely, so that the mutant covered the membrane of liposomes but did not assemble to form pores, arcs or even linear arrays.

5.12.5 Raman spectral analysis of Ply on the lipid bilayer membrane

Analysis by Raman spectroscopy of single liposomes revealed that Ply impacts membrane chemical structure. Ply leads to a decrease in a short-range order of lipid molecules in the lipid bilayer. The changes observed were the result of oligomerization of Ply monomers on the membrane rather than pore formation itself leading to changes in the lipid vibrational mode (CH₂ and CH₃). Thus, the non-haemolytic mutant Asp205Arg caused changes in the lipid vibrational mode similar to the wild-type Ply. Asp205Arg mutant still oligomerized to form long chains, but could not form pores. Conversely, mutant Asn339Arg caused no changes to the lipid vibrational mode, despite binding to the membrane. Oligomerization of Ply was completely abolished by this mutation. Together, the data show that toxin oligomerization on the membrane is necessary to change the vibration mode of the CH₂ and CH₃ groups in the lipid molecule of the membrane.

5.13 Future work

5.13.1 Mutation in PlyD1-3 residues

Studies in this thesis revealed that the interaction between Ply and IgG occurs via the PlyD1-3 and Fab region of IgG. Thus it would be interesting to identify the residues that are responsible for this interaction by introducing point mutation into PlyD1-3 residues to identify the binding region on the toxin. The PlyD1-3/IgG Fab would also be a good target for crystallization/structural studies.

5.13.2 Disruption of Ply monomers

The chapter four results showed that disruption of packing interactions prevents pore formation by Ply. Therefore, a drug that blocks packing could potentially form the basis of a new treatment for pneumococcal disease. Ply activity could be prevented either by small molecules or antibodies. It would also be interesting to investigate the packing in other CDCs by introducing mutations at interface surface residues. This would confirm that interface is conserved in all CDCs and that they have a common mode of polymerization.

5.13.3 Raman spectroscopy and Ply

The structural changes in lipid membrane observed by the Raman spectroscopy caused by Ply provide a useful way of distinguishing pore from pre-pore formation. It would be interesting to investigate more Ply mutants to show the impact of residues on the chemical structure of the membrane. Additionally, it is important to investigate the impact of other CDCs on the chemical structure of the membrane to see if the observed changes are a common feature of CDCs.

Appendixes

Appendix 1- Blast DNA sequences of truncated Ply

Ply D1-3 forward primer blast

| | | | |
|-------|-----|--|-----|
| Query | 1 | ATGGCAAATAAAGCAGTAAATGACTTTATACTAGCTATGAATTACGATAAAAAAGAAACTC | 60 |
| Sbjct | 90 | ATGGCAAATAAAGCAGTAAATGACTTTATACTAGCTATGAATTACGATAAAAAAGAAACTC | 149 |
| Query | 61 | TTGACCCATCAGGGAGAAAGTATTGAAAATCGTTTCATCAAAGAGGGTAATCAGCTACCC | 120 |
| Sbjct | 150 | TTGACCCATCAGGGAGAAAGTATTGAAAATCGTTTCATCAAAGAGGGTAATCAGCTACCC | 209 |
| Query | 121 | GATGAGTTTGTGTTATCGAAAGAAAGAAGCGGAGCTTGTGACAAAATACAAGTGATAT | 180 |
| Sbjct | 210 | GATGAGTTTGTGTTATCGAAAGAAAGAAGCGGAGCTTGTGACAAAATACAAGTGATAT | 269 |
| Query | 181 | TCTGTAAACAGCTACCAACGACAGTCGCCCTCTATCCGAGCACTTCTCGTAGTGGATGAG | 240 |
| Sbjct | 270 | TCTGTAAACAGCTACCAACGACAGTCGCCCTCTATCCGAGCACTTCTCGTAGTGGATGAG | 329 |
| Query | 241 | ACCTTGTAGAGAAATAATCCCACTCTTCTTGGGGTCGATCGTGCCTCCGATGACTTATAGT | 300 |
| Sbjct | 330 | ACCTTGTAGAGAAATAATCCCACTCTTCTTGGGGTCGATCGTGCCTCCGATGACTTATAGT | 389 |
| Query | 301 | ATTGATTTGCCCTGGTTTGGCAAGTAGCGATAGCTTCTCCAAAGTGGAAAGACCCAGCAAT | 360 |
| Sbjct | 390 | ATTGATTTGCCCTGGTTTGGCAAGTAGCGATAGCTTCTCCAAAGTGGAAAGACCCAGCAAT | 449 |
| Query | 361 | TCAAGTGTTCGCGGAGCGGTAAACGATTTGTTGGCTAAGTGGCATCAAGATTATGGTCAG | 420 |
| Sbjct | 450 | TCAAGTGTTCGCGGAGCGGTAAACGATTTGTTGGCTAAGTGGCATCAAGATTATGGTCAG | 509 |
| Query | 421 | GTCAATAATGTCCAGCTAGAAATGCAGTATGAAAAAATCACGGCTCACAGCATGGAACAA | 480 |
| Sbjct | 510 | GTCAATAATGTCCAGCTAGAAATGCAGTATGAAAAAATCACGGCTCACAGCATGGAACAA | 569 |
| Query | 481 | CTCAAGGTCAAGTTTGGTTCTGACTTTGAAAAGACAGGGAATTCCTTGATATTGATTTT | 540 |
| Sbjct | 570 | CTCAAGGTCAAGTTTGGTTCTGACTTTGAAAAGACAGGGAATTCCTTGATATTGATTTT | 629 |
| Query | 541 | AACTCTGTCCATTCAGGGCAAAAGCAGATTCAGATTGTTAATTTTAAAGCAGATTTATTAT | 600 |
| Sbjct | 630 | AACTCTGTCCATTCAGGGCAAAAGCAGATTCAGATTGTTAATTTTAAAGCAGATTTATTAT | 689 |
| Query | 601 | ACAGTCAGCGTAGACGCTGTTAAAAATCCAGGAGATGTTTTCAGATACTGTAAACGGTA | 660 |
| Sbjct | 690 | ACAGTCAGCGTAGACGCTGTTAAAAATCCAGGAGATGTTTTCAGATACTGTAAACGGTA | 749 |
| Query | 661 | GAGGATTTAAAACAGAGAGGAATTTCTGCAGAGCGTCCCTTTGGTCTATATTTCCAGTGTT | 720 |
| Sbjct | 750 | GAGGATTTAAAACAGAGAGGAATTTCTGCAGAGCGTCCCTTTGGTCTATATTTCCAGTGNT | 809 |
| Query | 721 | GCTTATGGGGCCCAAGTCTATCTCAAGTTGGAAACCACGAGTAAGAGTGATGAAGTAGAG | 780 |
| Sbjct | 810 | GCTTATGGGGCCCAAGTCTATCTCAAGTTGGAAACCACGAGTAANAGTGATGAAGTAGAG | 869 |
| Query | 781 | GCTGCTTTTGAAGCTTTGATAAAAAGGAGTCAAGGTAGCTCCTCAGACAGAGTGGAAAGCAG | 840 |
| Sbjct | 870 | GCTGCTTTTGAAGCTTTGATAAAAAGGAGTCAAGGTAGCTCCTCNGACNGANTGGNAGCAN | 929 |
| Query | 841 | A-TTTTGGACAATACAGAAGTGAAGG-CGGTTATTTTAGGGGGCGACCCAAAGTTCGGGTG | 898 |
| Sbjct | 930 | ANTTTTGGACANNACAGAAGTGNANGNCGGTNATTTTNNNGGGCGACCCNAGTTCGGGTG | 989 |
| Query | 899 | CCC 901 | |
| Sbjct | 990 | CCC 992 | |

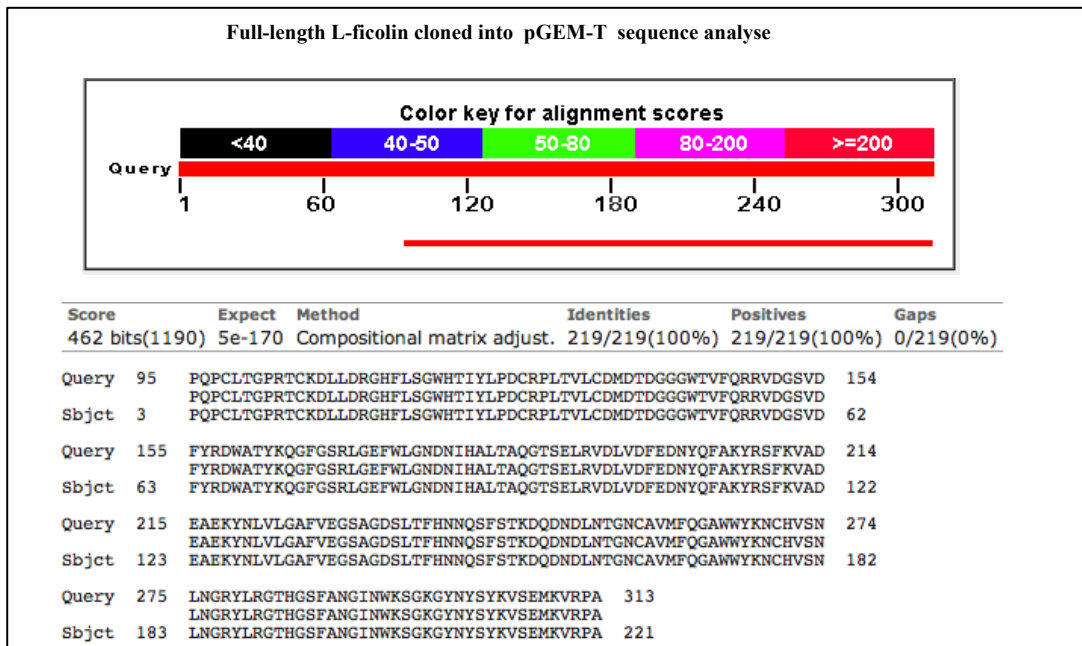
Ply D1-3 Reverse primer blast

| | | | |
|-------|------|---|------|
| Query | 199 | GACAGTCGCCCTCTATCCTGGAGCACTTCTCGTAGTGGATGAGACCTTGTAGAGAATAAT | 258 |
| Sbjct | 1024 | GACAGTNGCCTCTATNCTGGAGCACTNNTCGTAGTGGATGAGA-NNNGTTAGAGAATAAT | 966 |
| Query | 259 | CCCCTCTTCTTGGCGTTCGATCGTCTCCGATGACTTATAGTATGATTGCGCTGGTTTG | 318 |
| Sbjct | 965 | CCCANTNNT-NTGCGGTTGATCGTGNCTCCGATGACTTATAGTATGATTGCGCTGGTTTG | 907 |
| Query | 319 | GCAAGTAGCGATAGCTTTCTCCAAGTGGAAAGACCCAGCAATTC AAGTGTTCGCGGAGCG | 378 |
| Sbjct | 906 | GCAAGTAGCGATAGCTTTNCCAAAGTGGAAAGACCCAGCAATTC AAGTGTTCGCGGAGCG | 847 |
| Query | 379 | GTAAACGATTTGTTGGCTAAGTGGCATCAAGATTATGGTCAGGTC AATAATGTCCACGCT | 438 |
| Sbjct | 846 | GTAAACGATTTGTTGGCTAAGTGGCATCAAGATTATGGTCAGGTC AATAATGTCCACGCT | 787 |
| Query | 439 | AGAATGCAGTATGAAAAAATCACGGCTCACAGCATGGAACAAC TCAAGGTC AAGTTTGGT | 498 |
| Sbjct | 786 | AGAATGCAGTATGAAAAAATAACGGCTCACAGCATGGAACAAC TCAAGGTC AAGTTTGGT | 727 |
| Query | 499 | TCTGACTTTGAAAAGACAGGGAAATCTCTTGATATTGATTTTAA CTCTGTCCATTCAGGC | 558 |
| Sbjct | 726 | TCTGACTTTGAAAAGACAGGGAAATCTCTTGATATTGATTTTAA CTCTGTCCATTCAGGT | 667 |
| Query | 559 | GAAAAGCAGATTCAGATTGTTAATTTTAAAGCAGATTTATATA CAGTCAGCGTAGACGCT | 618 |
| Sbjct | 666 | GAAAAGCAGATTCAGATTGTTAATTTTAAAGCAGATTTATATA CAGTCAGCGTAGACGCT | 607 |
| Query | 619 | GTTAAAAATCCAGGAGATGTGTTTCAAGTACTGTAACGGTAGA GGATTTAAAACAGAGA | 678 |
| Sbjct | 606 | GTTAAAAATCCAGGAGATGTGTTTCAAGTACTGTAACGGTAGA GGATTTAAAACAGAGA | 547 |
| Query | 679 | GGAAATTTCTGCAGAGCGTCTCTTGGTCTATATTTGAGTGTG CTATATGGGCGCCAAGTC | 738 |
| Sbjct | 546 | GGAAATTTCTGCAGAGCGTCTCTTGGTCTATATTTGAGTGTG CTATATGGGCGCCAAGTC | 487 |
| Query | 739 | TATCTCAAGTTGGAAACCACGAGTAAGAGTGATGAAGTAGAGG CTGCTTTTGAAGCTTTG | 798 |
| Sbjct | 486 | TATCTCAAGTTGGAAACCACGAGTAAGAGTGATGAAGTAGAGG CTGCTTTTGAAGCTTTG | 427 |
| Query | 799 | ATAAAAGGAGTCAAGGTAGCTCCTCAGACAGAGTGGAAAGCAG ATTTGGACAATACAGAA | 858 |
| Sbjct | 426 | ATAAAAGGAGTCAAGGTAGCTCCTCAGACAGAGTGGAAAGCAG ATTTGGACAATACAGAA | 367 |
| Query | 859 | GTGAAGGCGGTTATTTTAGGGGGCGACCCAAAGTTCGGGTG CCGGAGTTGTAACAGGCAAG | 918 |
| Sbjct | 366 | GTGAAGGCGGTTATTTTAGGGGGCGACCCAAAGTTCGGGTG CCGGAGTTGTAACAGGCAAG | 307 |
| Query | 919 | GTGGATATGGTAGAGGACTTGATTCAAGAAGGCAGTCGCTTTA CAGCAGATCATCCAGGC | 978 |
| Sbjct | 306 | GTGGATATGGTAGAGGACTTGATTCAAGAAGGCAGTCGCTTTA CAGCAGATCATCCAGGC | 247 |
| Query | 979 | TTGCCGATTTCCCTATACAACCTCTCTTTTTTACGTGACAA TGTAGTTGCGACCTTTCAAAT | 1038 |
| Sbjct | 246 | TTGCCGATTTCCCTATACAACCTCTCTTTTTTACGTGACAA TGTAGTTGCGACCTTTCAAAC | 187 |
| Query | 1039 | AGTACAGACTATGTTGAGACTAAGGTTACAGCTTACAGAAACG GA | 1083 |
| Sbjct | 186 | AGTACAGACTATGTTGAGACTAAGGTTACAGCTTACAGAAACT GA | 142 |

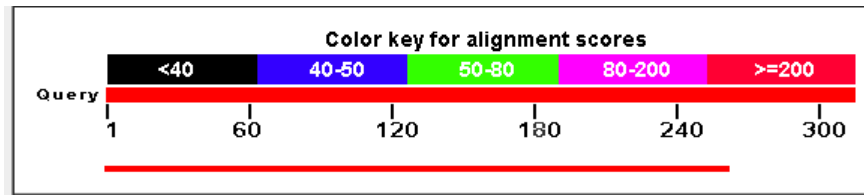
Ply D4 blast sequences

| | | | |
|-------|------|---|------|
| Query | 1074 | CAGAAACGGAGATTTACTGCTGGATCATAGTGGTGCCTATGTTGCCCAATATTATATTAC | 1133 |
| Sbjct | 828 | CAGAAACGGAGATTTACTGCTGGATCATAGTGGTGCCTATGTTGCCCAATATTATATTAC | 887 |
| Query | 1134 | TTGGAATGAATTATCCTATGATCATCAAGGTAAGGAAGTCTTGACTCCTAAGGCTTGGGA | 1193 |
| Sbjct | 888 | TTGGAATGAATTATCCTATGATCATCAAGGTAAGGAAGTCTTGACTCCTAAGGCTTGGGA | 947 |
| Query | 1194 | CAGAAATGGGCAGGATTTAACGGCTCACTTTACCACTAGTATTCCCTTTAAAAGGGAATGT | 1253 |
| Sbjct | 948 | CAGAAATGGGCAGGATTTAACGGCTCACTTTACCACTAGTATTCCCTTTAAAAGGGAATGT | 1007 |
| Query | 1254 | TCGTAATCTCTCTGTCAAAATTAGAGAGTGTACCGGGCTTGCCCTGGGAATGGTGGCGTAC | 1313 |
| Sbjct | 1008 | TCGTAATCTCTCTGTCAAAATTAGAGAGTGTACCGGGCTTGCCCTGGGAATGGTGGCGTAC | 1067 |
| Query | 1314 | GGTTTATGAAAAACCGATTTGCCACTAGTGCCTAAGCGGACGATTTCTATTTGGGGAAC | 1373 |
| Sbjct | 1068 | GGTTTATGAAAAACCGATTTGCCACTAGTGCCTAAGCGGACGATTTCTATTTGGGGAAC | 1127 |
| Query | 1374 | AACTCTCTATCCTCAGGTAGAAGATAAGGTAGAAAAATGACT | 1414 |
| Sbjct | 1128 | AACTCTCTATCCTCAGGTAGAAGATAAGGTAGAAAAATGACT | 1168 |

Appendix 2- L-ficolin and fibrinogen like domain blast sequences

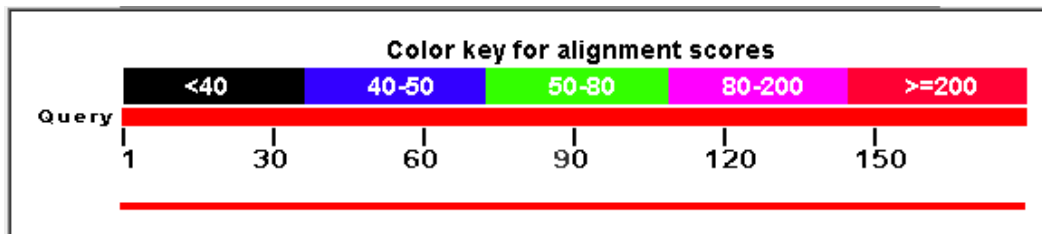


Full-length L-ficolin cloned into pED4 vector and the sequence analyse with the primer pED4 seq F



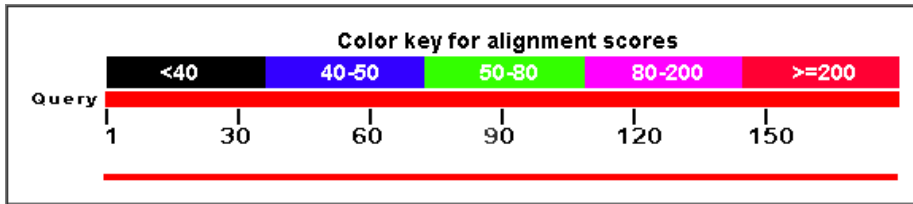
| Score | Expect | Method | Identities | Positives | Gaps |
|----------------|---|------------------------------|---------------|---------------|-----------|
| 538 bits(1387) | 0.0 | Compositional matrix adjust. | 261/261(100%) | 261/261(100%) | 0/261(0%) |
| Query 1 | MELDRAVGLGAATLLLSFLGMAWALQAADTCPEVKMVGLEGSCLKLTIIRGCPGLPGAPG | | | | 60 |
| Sbjct 1 | MELDRAVGLGAATLLLSFLGMAWALQAADTCPEVKMVGLEGSCLKLTIIRGCPGLPGAPG | | | | 60 |
| Query 61 | PKGEAGTNGKRGERGPPGPPGKAGPPGPNAPGEPQPCLTGPRTCKDLLDRGHFLSGWHT | | | | 120 |
| Sbjct 61 | PKGEAGTNGKRGERGPPGPPGKAGPPGPNAPGEPQPCLTGPRTCKDLLDRGHFLSGWHT | | | | 120 |
| Query 121 | IYLPDCRPLTVLCDMDTDGGGWTVFQRRVDGSVDFYRDWATYKQFGSRLGEFVLGNDNI | | | | 180 |
| Sbjct 121 | IYLPDCRPLTVLCDMDTDGGGWTVFQRRVDGSVDFYRDWATYKQFGSRLGEFVLGNDNI | | | | 180 |
| Query 181 | HALTAQGTSELRVLDLVDFEDNYQFAKYRSFKVADEAEKYNLVLGAFVEGSAGDSLTFHNN | | | | 240 |
| Sbjct 181 | HALTAQGTSELRVLDLVDFEDNYQFAKYRSFKVADEAEKYNLVLGAFVEGSAGDSLTFHNN | | | | 240 |
| Query 241 | QSFSTKDQDNDLNTGNCAVMF | | 261 | | |
| Sbjct 241 | QSFSTKDQDNDLNTGNCAVMF | | 261 | | |

Fibrinogen-like domain cloned into pGEM-T vector and the sequence analysed with T7-promoter prime



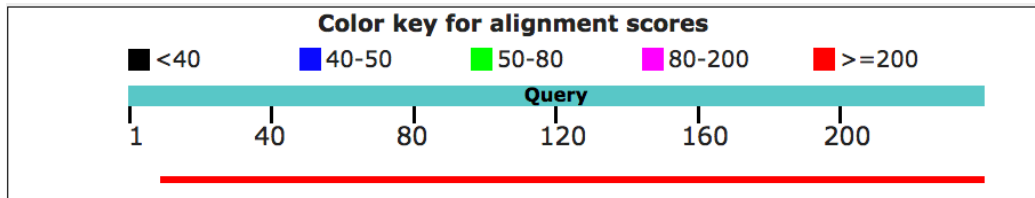
| Score | Expect | Method | Identities | Positives | Gaps |
|---------------|--|------------------------------|---------------|---------------|-----------|
| 371 bits(953) | 9e-136 | Compositional matrix adjust. | 179/179(100%) | 179/179(100%) | 0/179(0%) |
| Query 1 | MDTDGGGWTVFQRRVDGSVDFYRDWATYKQFGSRLGEFVLGNDNIHALTAQGTSELRVD | | | | 60 |
| Sbjct 43 | MDTDGGGWTVFQRRVDGSVDFYRDWATYKQFGSRLGEFVLGNDNIHALTAQGTSELRVD | | | | 102 |
| Query 61 | LVDFEDNYQFAKYRSFKVADEAEKYNLVLGAFVEGSAGDSLTFHNNQSFSTKDQDNDLNT | | | | 120 |
| Sbjct 103 | LVDFEDNYQFAKYRSFKVADEAEKYNLVLGAFVEGSAGDSLTFHNNQSFSTKDQDNDLNT | | | | 162 |
| Query 121 | GNCAMVFQGAWYKKNCHVSNLNGRYLRGTHGSFANGINWKS GKGYNYSYKVSEMVRPA | | | | 179 |
| Sbjct 163 | GNCAMVFQGAWYKKNCHVSNLNGRYLRGTHGSFANGINWKS GKGYNYSYKVSEMVRPA | | | | 221 |

Fibrinogen-like domain cloned into pGEM-T vector and the sequence analysed with SP6 prime



| Score | Expect | Method | Identities | Positives | Gaps |
|---------------|--|------------------------------|---------------|---------------|-----------|
| 373 bits(957) | 2e-135 | Compositional matrix adjust. | 179/179(100%) | 179/179(100%) | 0/179(0%) |
| Query 1 | MDTDGGGWTVFQRRVDGSVDFYRDWATYKQGFSGRLGEFVLGNDNIHALTAQGTSELRVD | | | | 60 |
| Sbjct 95 | MDTDGGGWTVFQRRVDGSVDFYRDWATYKQGFSGRLGEFVLGNDNIHALTAQGTSELRVD | | | | 154 |
| Query 61 | LVDFEDNYQFAKYRSFKVADEAEKYNLVLGAFVEGSAGDSLTFHNNQSFSTKDQDNDLNT | | | | 120 |
| Sbjct 155 | LVDFEDNYQFAKYRSFKVADEAEKYNLVLGAFVEGSAGDSLTFHNNQSFSTKDQDNDLNT | | | | 214 |
| Query 121 | GNCVAMFQGAWWYKNCHVSNLNGRYLRGTHGSFANGINWKSCKGYNYSYKVSEMVRPA | | | | 179 |
| Sbjct 215 | GNCVAMFQGAWWYKNCHVSNLNGRYLRGTHGSFANGINWKSCKGYNYSYKVSEMVRPA | | | | 273 |

Fibrinogen-like domain cloned into pET28 vector and the sequence analyse



| Score | Expect | Method | Identities | Positives | Gaps |
|----------------|--|------------------------------|--------------|--------------|-----------|
| 480 bits(1236) | 3e-178 | Compositional matrix adjust. | 228/230(99%) | 228/230(99%) | 0/230(0%) |
| Query 10 | HPQPCXTGPRCTCKDLLDRGHFLSGWHTIYLPDCRPLTVLCMETDTDGGGWTVFQRRVDG | | | | 69 |
| Sbjct 100 | EPQPCLTGPRTCKDLLDRGHFLSGWHTIYLPDCRPLTVLCMETDTDGGGWTVFQRRVDG | | | | 159 |
| Query 70 | SVDFYRDWATYKQGFSGRLGEFVLGNDNIHALTAQGTSELRVDLVDFEDNYQFAKYRSFK | | | | 129 |
| Sbjct 160 | SVDFYRDWATYKQGFSGRLGEFVLGNDNIHALTAQGTSELRVDLVDFEDNYQFAKYRSFK | | | | 219 |
| Query 130 | VADEAEKYNLVLGAFVEGSAGDSLTFHNNQSFSTKDQDNDLNTGNCVAMETFGAWWYKN | | | | 189 |
| Sbjct 220 | VADEAEKYNLVLGAFVEGSAGDSLTFHNNQSFSTKDQDNDLNTGNCVAMETFGAWWYKN | | | | 279 |
| Query 190 | CHVSNLNGRYLRGTHGSFANGINWKSCKGYNYSYKVSEMETKVRPASTOP | | | | 239 |
| Sbjct 280 | CHVSNLNGRYLRGTHGSFANGINWKSCKGYNYSYKVSEMETKVRPASTOP | | | | 329 |

Asn339Arg= N339R (Asn changed to Arg) **AAT D CGC**

```
Query 740 ATCTCAAGTTGGAACCACGAGTAAGAGTGATGAAGTAGAGGCTGCTTTTGAAGCTTTGA 799
          |||
Sbjct 374 ATCTCAAGTTGGAACCACGAGTAAGAGTGATGAAGTAGAGGCTGCTTTTGAAGCTTTGA 433
          |||
Query 800 TAAAAGGAGTCAAGGTAGCTCCTCAGACAGAGTGAAGCAGATTTTGGACAATACAGAAG 859
          |||
Sbjct 434 TAAAAGGAGTCAAGGTAGCTCCTCAGACAGAGTGAAGCAGATTTTGGACAATACAGAAG 493
          |||
Query 860 TGAAGGCGTTATTTTAGGGGGCACCAGTTCGGGTGCCCGAGTTGTAAACAGGCAAG 919
          |||
Sbjct 494 TGAAGGCGTTATTTTAGGGGGCACCAGTTCGGGTGCCCGAGTTGTAAACAGGCAAG 553
          |||
Query 920 TGGATATGGTAGAGGACTTGATTCAAGAAGCAGTCGCTTTACAGCAGATCATCCAGGCT 979
          |||
Sbjct 554 TGGATATGGTAGAGGACTTGATTCAAGAAGCAGTCGCTTTACAGCAGATCATCCAGGCT 613
          |||
Query 980 TGCCGATTTCTATACAACCTCTTTTTTACGTGCAATGAGTTGCGACCTTTCAAATA 1039
          |||
Sbjct 614 TGCCGATTTCTATACAACCTCTTTTTTACGTGCCGCTAGTTGCGACCTTTCAAACA 673
          |||
```

Thr304Arg=T304R (Thr changed to Arg) **ACA D CGT**

```
Query 602 CAGTCAGCGTAGACGCTGTTAAAAATCCAGGAGATGTGTTTCAAGATACTGTAACGGTAG 661
          |||
Sbjct 935 CAGTCAGCGTAGACGCTGTTAAAANNCCNGGAGATGNGTTTCAAGATACTGTAACGGTAG 876
          |||
Query 662 AGGATTTAAAACAGAGAGGAATTTCTGCAGAGCGTCTTTGGTCTATATTTGAGTGTG 721
          |||
Sbjct 875 AGGATTTAAAACAGAGAGGAATTTCTGCAGAGCGTCTTTGGTCTATATTTGAGTGTG 816
          |||
Query 722 CTTATGGGCGCCAAGTCTATCTCAAGTTGGAACCACGAGTAAGAGTGATGAAGTAGAGG 781
          |||
Sbjct 815 CTTATGGGCGCCAAGTCTATCTCAAGTTGGAACCACGAGTAAGAGTGATGAAGTAGAGG 756
          |||
Query 782 CTGCTTTTGAAGCTTTGATAAAAAGGAGTCAAGGTAGCTCCTCAGACAGAGTGAAGCAGA 841
          |||
Sbjct 755 CTGCTTTTGAAGCTTTGATAAAAAGGAGTCAAGGTAGCTCCTCAGACAGAGTGAAGCAGA 696
          |||
Query 842 TTTTGGACAATACAGAAGTGAAGGCGGTTATTTTAGGGGGCACCAGTTCGGGTGCC 901
          |||
Sbjct 695 TTTTGGACAATACAGAAGTGAAGGCGGTTATTTTAGGGGGCACCAGTTCGGGTGCC 636
          |||
Query 902 GAGTTGTACGTGCAAGGCAAGGTGGATATGGTAGAGGACTTGATTCAAGAAGCAGTCGCTTTA 961
          |||
Sbjct 635 GAGTTGTACGTGCAAGGCAAGGTGGATATGGTAGAGGACTTGATTCAAGAAGCAGTCGCTTTA 576
          |||
Query 962 CAGCAGATCATCCAGGCTTGCCGATTTCTATACAACCTCTTTTTTACGTGACAATGTAG 1021
          |||
Sbjct 575 CAGCAGATCATCCAGGCTTGCCGATTTCTATACAACCTCTTTTTTACGTGACAATGTAG 516
          |||
```

Leu11Arg= L11R (Leu changed to Arg) CTA Δ CGC

```
Query 1  ATGGCAAAATAAGCAGTAAATGACTTTATACTAGCTATGAATTACGATAAAAAAGAACTC 60
          |||
Sbjct 212 ATGGCAAAATAAGCAGTAAATGACTTTATACGCGCTATGAATTACGATAAAAAAGAACTC 271
          |||

Query 61  TTGACCCATCAGGGAGAAAAGTATTGAAAATCGTTTCATCAAAGAGGGTAATCAGCTACCC 120
          |||
Sbjct 272 TTGACCCATCAGGGAGAAAAGTATTGAAAATCGTTTCATCAAAGAGGGTAATCAGCTACCC 331
          |||

Query 121 GATGAGTTTGTGTTATCGAAAAGAAAAGCGGAGCTTGTGACAAAATACAAAGTATATT 180
          |||
Sbjct 332 GATGAGTTTGTGTTATCGAAAAGAAAAGCGGAGCTTGTGACAAAATACNANTGATATN 391
          |||
```

Asp205Arg= D205R (Asp changed to Arg) GAC D CGT

```
Query 361 TCAAGTGTTCGCGGAGCGGTAACGATTTGTTGGCTAAGTGGCATCAAGATTATGGTCAG 420
          |||
Sbjct 559 TCAAGTGTTCGCGGAGCGGTAACGATTTGTTGGCTAAGTGGCATCAAGATTATGGTCAG 618
          |||

Query 421 GTCAATAATGTCCAGCTAGAATGCAGTATGAAAAATCACGGCTCACAGCATGGAACAA 480
          |||
Sbjct 619 GTCAATAATGTCCAGCTAGAATGCAGTATGAAAAATAACGGCTCACAGCATGGAACAA 678
          |||

Query 481 CTCAAGTCAAGTTTGGTTCTGACTTTGAAAAGACAGGGAATCTCTTGATATTGATTTT 540
          |||
Sbjct 679 CTCAAGTCAAGTTTGGTTCTGACTTTGAAAAGACAGGGAATCTCTTGATATTGATTTT 738
          |||

Query 541 AACTCTGTCCATTCAGGCGAAAAGCAGATTCAGATTGTTAATTTAAGCAGATTTATTAT 600
          |||
Sbjct 739 AACTCTGTCCATTCAGGCGAAAAGCAGATTCAGATTGNTAATTTAAGCAGATTTATTAT 798
          |||

Query 601 ACAGTCAGCGTAGACCTGTTAAAAATCCAGGAGATGTGTTTCAAGATACTGTAACGGTA 660
          |||
Sbjct 799 ACAGTCAGCGTACGTGCTGTTAAAAATCCAGGAGATGTGTTTCAAGATACTGTAACGGTA 858
          |||
```

Lys268Ala = K268A (Lys changed to Ala) AAA ΔGCC

```
Query 679 GGAATTTCTGCAGAGCGTCCTTTGGTCTATATTTTCGAGTGTGCTTATGGGCGCCAAGTC 738
Sbjct 874 GGAATTTCTGCAGAGCGTCCTTTGGTCTATATTTTCGAGTGTGCTTATGGGCGCCAAGTC 815
Query 739 TATCTCAAGTTGGAACCACGAGTAAGAGTGATGAAGTAGAGGCTGCTTTTGAAGCTTTG 798
Sbjct 814 TATCTCAAGTTGGAACCACGAGTAAGAGTGATGAAGTAGAGGCTGCTTTTGAAGCTTTG 755
Query 799 ATAAAAAGAGTCAAGGTAGCTCCTCAGACAGAGTGAAGCAGATTTTGGACAATACAGAA 858
Sbjct 754 ATAGCCGAGTCAAGGTAGCTCCTCAGACAGAGTGAAGCAGATTTTGGACAATACAGAA 695
Query 859 GTGAAGGCGGTTATTTTAGGGGGCGACCCAAGTTCGGGTGCCCGAGTTGTAACAGGCAAG 918
Sbjct 694 GTGAAGGCGGTTATTTTAGGGGGCGACCCAAGTTCGGGTGCCCGAGTTGTAACAGGCAAG 635
```

Val341Arg= V341R (Val changed to Arg) GTT D CGT

```
Query 800 TAAAAGGAGTCAAGGTAGCTCCTCAGACAGAGTGAAGCAGATTTTGGACAATACAGAAG 859
Sbjct 752 TAAAAGGAGTCAAGGTAGCTCCTCAGACAGAGTGAAGCAGATTTTGGACAATACAGAAG 693
Query 860 TGAAGGCGGTTATTTTAGGGGGCGACCCAAGTTCGGGTGCCCGAGTTGTAACAGGCAAGG 919
Sbjct 692 TGAAGGCGGTTATTTTAGGGGGCGACCCAAGTTCGGGTGCCCGAGTTGTAACAGGCAAGG 633
Query 920 TGGATATGGTAGAGGACTTGATTCAAGAAGCAGTCGCTTTACAGCAGATCATCCAGGCT 979
Sbjct 632 TGGATATGGTAGAGGACTTGATTCAAGAAGCAGTCGCTTTACAGCAGATCATCCAGGCT 573
Query 980 TGCCGATTTTCCTATACAACCTCTTTTTTACGTGACAATGAGTTGCGACCTTTCAAATA 1039
Sbjct 572 TGCCGATTTTCCTATACAACCTCTTTTTTACGTGACAATGACGTGCGACCTTTCAAATA 513
Query 1040 GTACAGACTATGTTGAGACTAAGGTTACAGCTTACAGAAAACGGAGATTTACTGCTGGATC 1099
Sbjct 512 GTACAGACTATGTTGAGACTAAGGTTACAGCTTACAGAAAACGGAGATTTACTGCTGGATC 453
```

Tyr55Cys+Val163Cys= T55C+V163C (ACA changed into TGT and GTC changed into TGT)

```
-----  
Query 121 GATGAGTTTGGTTATCGAAAGAAAGCGGAGCTTGTGACAAATACAAGTGATATT 180  
Sbjct 305 GATGAGTTTGGTTATCGAAAGAAAGCGGAGCTTGTGCTGTAAATACAAGTGATATT 364  
Query 181 TCTGTAACAGCTACCAACGACAGTCGCCCTTATCCTGGAGCATTCTCGTAGTGGATGAG 240  
Sbjct 365 TCTGTAACAGCTACCAACGACAGTCGCCCTTATCCTGGAGCATTCTCGTAGTGGATGAG 424  
Query 241 ACCTGTTAGAGAATAATCCCACTCTTCTTGGCGTCGATCGTCCGATGACTTATAGT 300  
Sbjct 425 ACCTGTTAGAGAATAATCCCACTCTTCTTGGCGTTGATCGTCCGATGACTTATAGT 484  
Query 301 ATTGATTTGCCCTGGTTTGGCAAGTAGCGATAGCTTTCTCCAAGTGAAGACCCAGCAAT 360  
Sbjct 485 ATTGATTTGCCCTGGTTTGGCAAGTAGCGATAGCTTTCTCCAAGTGAAGACCCAGCAAT 544  
Query 361 TCAAGTGTTCGCGGAGCGGTAACGATTTGTTGGCTAAGTGGCATCAAGATTATGGTCAG 420  
Sbjct 545 TCAAGTGTTCGCGGAGCGGTAACGATTTGTTGGCTAAGTGGCATCAAGATTATGGTCAG 604  
Query 421 GTCATAATGTCCCAGCTAGAATGCAGTATGAAAAATACACGGCTCACAGCATGGAACAA 480  
Sbjct 605 GTCATAATGTCCCAGCTAGAATGCAGTATGAAAAATAACGGCTCACAGCATGGAACAA 664  
Query 481 CTC AAG-GTCAAGTTGGTCTGACTTTGAAAAGACAGGGAATTCTCTTGATATTGATT 539  
Sbjct 665 CTC AAGT-AGTTGGTCTGACTTTGAAAAGACAGGGAATTCTCTTGATATTGATT 723
```

Ala262Cys+Trp278Cys =A262C+W278C (GCT changed into TGT and TGG changed into TGT)

```
Query 722 CTTATGGGCGCAAGTCTATCTCAAGTTGAAACCACGAGTAAGAGTGATGAAGTAGAGG 781  
Sbjct 810 CTTATGGGCGCAAGTCTATCTCAAGTTGAAACCACGAGTAAGAGTGATGAAGTAGAGG 751  
Query 782 CTGCTTTGAAGCTTTGATAAAAAGGAGTCAAGGTAGCTCCTCAGACAGAGTGGAAAGCAGA 841  
Sbjct 750 CTTGTTTGAATCTTTGATAAAAAGGAGTCAAGGTAGCTCNTCAGACAGAGTGTAAAGCAGA 691  
Query 842 TTTTGGACAATAACAGAAGTGAAGGCGGTTATTTTAGGGGGCGACCAAGTTCGGGTGCCC 901  
Sbjct 690 TTTTG-ACAATAACAGAAGTGAAGGCGGTTATTTTAGGGGGCGACCAAGTTCGGGTGCCC 632  
Query 902 GAGTTGTAACAGGCAAGGTGGATATGGTAGAGGACTTGATTCAAGAAGGCAGTCGCTTTA 961  
Sbjct 631 GAGTTGTAACAGGCAAGGTGGATATGGTAGAGGACTTGATTCAAGAAGGCAGTCGCTTTA 572  
Query 962 CAGCAGATCATCCAGGCTTGCCGATTTCCCTATACAACCTCTTTTTTACGTGACAATGTAG 1021  
Sbjct 571 CAGCAGATCATCCAGGCTTGCCGATTTCCCTATACAACCTCTTTTTTACGTGACAATGTAG 512
```

Appendix 4- Raman data normalization

Raman data normalization equation and formula

Section 1 formula

$$y_b = \frac{y_a - \text{avg}(y_{c1}:y_{c10})}{\text{sum}(y_{d1}:y_{d465})}$$

Section 2 formula

$$y_d = y_c - \frac{(x \times \text{avg}(y_{e455}:y_{e465}) - \text{avg}(y_{c1}:y_{c10}))}{(x_{465} - x_1)} + \text{avg}(y_{c1}:y_{c10})$$

$$- (\text{avg}(y_{e455}:y_{e465}) - \text{avg}(y_{c1}:y_{c10})) \times \frac{x_1}{(x_{465} - x_1)}$$

$$y_e = \frac{y_d}{\text{sum}(y_{d1}:y_{d465})}$$

Section 3 formula

$$y_g = y_f - \frac{(x \times \text{avg}(y_{f61}:y_{f71}) - \text{avg}(y_{f1}:y_{f10}))}{(x_{71} - x_1)} + \text{avg}(y_{f1}:y_{f10})$$

$$- (\text{avg}(y_{f61}:y_{f71}) - \text{avg}(y_{f1}:y_{f10})) \times \frac{x_1}{(x_{71} - x_1)}$$

$$y_h = \frac{y_g}{\text{sum}(y_{d1}:y_{d465})}$$

Raman shift intensity correction formula

$$\left(\left(\frac{1}{488} \right) - \left(\frac{1}{x} \right) \right) \times 10^7$$

References

- AALBERSE, R. C. & SCHUURMAN, J. 2002. IgG4 breaking the rules. *Immunology*, 105, 9-19.
- AALBERSE, R. C., STAPEL, S. O., SCHUURMAN, J. & RISPENS, T. 2009. Immunoglobulin G4: an odd antibody. *Clin Exp Allergy*, 39, 469-77.
- ADAMS, P. D., AFONINE, P. V., BUNKOCZI, G., CHEN, V. B., DAVIS, I. W., ECHOLS, N., HEADD, J. J., HUNG, L. W., KAPRAL, G. J., GROSSEKUNSTLEVE, R. W., MCCOY, A. J., MORIARTY, N. W., OEFFNER, R., READ, R. J., RICHARDSON, D. C., RICHARDSON, J. S., TERWILLIGER, T. C. & ZWART, P. H. 2010. PHENIX: a comprehensive Python-based system for macromolecular structure solution. *Acta Crystallogr D Biol Crystallogr*, 66, 213-21.
- AGARWAL, V., AHL, J., RIESBECK, K. & BLOM, A. M. 2013. An alternative role of C1q in bacterial infections: facilitating *Streptococcus pneumoniae* adherence and invasion of host cells. *J Immunol*, 191, 4235-45.
- AGARWAL, V., HAMMERSCHMIDT, S., MALM, S., BERGMANN, S., RIESBECK, K., BLOM, A. M., FACULTY OF, M., MEDICINSK MIKROBIOLOGI, M., MEDICAL, M., INSTITUTIONEN FÖR LABORATORIEMEDICIN, M., LUNDS, U., PROTEIN, C., MEDICIN, DEPARTMENT OF LABORATORY MEDICINE, M., LUND, U. & PROTEINKEMI 2012. Enolase of *Streptococcus pneumoniae* binds human complement inhibitor C4b-binding protein and contributes to complement evasion. *J immuno (Baltimore, Md. : 1950)*, 189, 3575.
- AGARWAL, V., SROKA, M., FULDE, M., BERGMANN, S., RIESBECK, K. & BLOM, A. M. 2014. Binding of *Streptococcus pneumoniae* endopeptidase O (PepO) to complement component C1q modulates the complement attack and promotes host cell adherence. *J Biol Chem*, 289, 15833-44.
- AJITO, K. & TORIMITSU, K. 2002. Laser trapping and Raman spectroscopy of single cellular organelles in the nanometer range. *Lab Chip*, 2, 11-4.
- AKHTAR, M. S. & BHAKUNI, V. 2003. *Streptococcus pneumoniae* hyaluronate lyase contains two non-cooperative independent folding/unfolding structural domains: characterization of functional domain and inhibitors of enzyme. *J Biol Chem*, 278, 25509-16.
- ALHAMDI, Y., NEILL, D. R., ABRAMS, S. T., MALAK, H. A., YAHYA, R., BARRETT-JOLLEY, R., WANG, G., KADIOGLU, A. & TOH, C. H. 2015. Circulating Pneumolysin Is a Potent Inducer of Cardiac Injury during Pneumococcal Infection. *PLoS Pathog*, 11, e1004836.
- ALI, Y. M., KENAWY, H. I., MUHAMMAD, A., SIM, R. B., ANDREW, P. W. & SCHWAEBLE, W. J. 2013. Human L-ficolin, a recognition molecule of the lectin

activation pathway of complement, activates complement by binding to pneumolysin, the major toxin of *Streptococcus pneumoniae*. *PLoS One*, 8, e82583.

- ALI, Y. M., LYNCH, N. J., HALEEM, K. S., FUJITA, T., ENDO, Y., HANSEN, S., HOLMSKOV, U., TAKAHASHI, K., STAHL, G. L., DUDLER, T., GIRIJA, U. V., WALLIS, R., KADIOGLU, A., STOVER, C. M., ANDREW, P. W. & SCHWAEBLE, W. J. 2012. The lectin pathway of complement activation is a critical component of the innate immune response to pneumococcal infection. *PLoS pathogens*, 8, e1002793.
- ALONSODEVELASCO, E., VERHEUL, A. F., VERHOEF, J. & SNIPPE, H. 1995. *Streptococcus pneumoniae*: virulence factors, pathogenesis, and vaccines. *Microbiol Rev*, 59, 591-603.
- AMARASEKERA, M. 2011. Immunoglobulin E in health and disease. *Asia Pac Allergy*, 1, 12-5.
- AMMITZBOLL, C. G., THIEL, S., ELLINGSEN, T., DELEURAN, B., JORGENSEN, A., JENSENIUS, J. C. & STENGAARD-PEDERSEN, K. 2012. Levels of lectin pathway proteins in plasma and synovial fluid of rheumatoid arthritis and osteoarthritis. *Rheumatol Int*, 32, 1457-63.
- AN, Y., ZHANG, Y., MUELLER, H. M., SHAMEEM, M. & CHEN, X. 2014. A new tool for monoclonal antibody analysis: application of IdeS proteolysis in IgG domain-specific characterization. *MAbs*, 6, 879-93.
- AOYAGI, Y., ADDERSON, E. E., MIN, J. G., MATSUSHITA, M., FUJITA, T., TAKAHASHI, S., OKUWAKI, Y. & BOHNSACK, J. F. 2005. Role of L-ficolin/mannose-binding lectin-associated serine protease complexes in the opsonophagocytosis of type III group B streptococci. *J Immunol*, 174, 418-25.
- ASHKIN, A. 1970. Acceleration and Trapping of Particles by Radiation Pressure. *Phys. Rev. Lett.* 24, 156-159.
- ASHKIN, A. 1992. Forces of a single-beam gradient laser trap on a dielectric sphere in the ray optics regime. *Biophys J*, 61, 569-82.
- ASHKIN, A. & DZIEDZIC, J. 1971. Optical levitation by radiation pressure. *Appl. Phys. Lett*, 19, 283-285.
- ASLANIAN, D., NEGRERIE, M. & CHAMBERT, R. 1986. A Raman spectroscopic study on the interaction of an ion-channel protein with a phospholipid in a model membrane system (gramicidin A/L-alpha-lysophosphatidylcholine). *Eur J Biochem*, 160, 395-400.
- ASSAF, A., HOANG, T. V., FAIK, I., AEBISCHER, T., KREMSNER, P. G., KUN, J. F. & VELAVAN, T. P. 2012. Genetic evidence of functional ficolin-2 haplotype as susceptibility factor in cutaneous leishmaniasis. *PLoS One*, 7, e34113.

- AUCOUTURIER, P., DANON, F., DAVEAU, M., GUILLOU, B., SABBAH, A., BESSON, J. & PREUD'HOMME, J. L. 1984. Measurement of serum IgG4 levels by a competitive immunoenzymatic assay with monoclonal antibodies. *J Immunol Methods*, 74, 151-62.
- BABA, H., KAWAMURA, I., KOHDA, C., NOMURA, T., ITO, Y., KIMOTO, T., WATANABE, I., ICHIYAMA, S. & MITSUYAMA, M. 2001. Essential Role of Domain 4 of Pneumolysin from *Streptococcus pneumoniae* in Cytolytic Activity as Determined by Truncated Proteins. *Biochemical and Biophysical Research Communications*, 281, 37-44.
- BAI, X.-H., CHEN, H.-J., JIANG, Y.-L., WEN, Z., HUANG, Y., CHENG, W., LI, Q., QI, L., ZHANG, J.-R., CHEN, Y. & ZHOU, C.-Z. 2014. Structure of pneumococcal peptidoglycan hydrolase LytB reveals insights into the bacterial cell wall remodeling and pathogenesis. *J. Biol. Chem.*, 289, 23403-23416.
- BALACHANDRAN, P., BROOKS-WALTER, A., VIROLAINEN-JULKUNEN, A., HOLLINGSHEAD, S. K. & BRILES, D. E. 2002. Role of pneumococcal surface protein C in nasopharyngeal carriage and pneumonia and its ability to elicit protection against carriage of *Streptococcus pneumoniae*. *Infect Immun*, 70, 2526-34.
- BALACHANDRAN, P., HOLLINGSHEAD, S. K., PATON, J. C. & BRILES, D. E. 2001. The autolytic enzyme LytA of *Streptococcus pneumoniae* is not responsible for releasing pneumolysin. *J Bacteriol*, 183, 3108-16.
- BARKAI, G., GREENBERG, D., GIVON-LAVI, N., DREIFUSS, E., VARDY, D. & DAGAN, R. 2005. Community prescribing and resistant *Streptococcus pneumoniae*. *Emerg Infect Dis*, 11, 829-37.
- BASU, H., DHARMADHIKARI, A., DHARMADHIKARI, J., SHARMA, S. & MATHUR, D. A biophotonic study of live, flowing red blood cells in an optical trap. International Conference on Fiber Optics and Photonics, 2010. International Society for Optics and Photonics, 817309-817309-8.
- BELONGIA, E. A., SULLIVAN, B. J., CHYOU, P. H., MADAGAME, E., REED, K. D. & SCHWARTZ, B. 2001. A community intervention trial to promote judicious antibiotic use and reduce penicillin-resistant *Streptococcus pneumoniae* carriage in children. *Pediatrics*, 108, 575-83.
- BELTRAME, M. H., BOLDT, A. B., CATARINO, S. J., MENDES, H. C., BOSCHMANN, S. E., GOELDNER, I. & MESSIAS-REASON, I. 2015. MBL-associated serine proteases (MASPs) and infectious diseases. *Mol Immunol*, 67, 85-100.
- BERGMANN, S., ROHDE, M., CHHATWAL, G. S. & HAMMERSCHMIDT, S. 2001. alpha-Enolase of *Streptococcus pneumoniae* is a plasmin(ogen)-binding protein displayed on the bacterial cell surface. *Mol Microbiol*, 40, 1273-87.

- BERRY, A. M., YOTHER, J., BRILES, D. E., HANSMAN, D. & PATON, J. C. 1989. Reduced virulence of a defined pneumolysin-negative mutant of *Streptococcus pneumoniae*. *Infect Immun*, 57, 2037-42.
- BHAKDI, S., WELLER, U., WALEV, I., MARTIN, E., JONAS, D. & PALMER, M. 1993. A guide to the use of pore-forming toxins for controlled permeabilization of cell membranes. *Med Microbiol Immunol*, 182, 167-75.
- BIDULA, S., KENAWY, H., ALI, Y. M., SEXTON, D., SCHWAEBLE, W. J. & SCHELENZ, S. 2013. Role of ficolin-A and lectin complement pathway in the innate defense against pathogenic *Aspergillus* species. *Infect Immun*, 81, 1730-40.
- BIDULA, S., SEXTON, D. W., ABDOLRASOULI, A., SHAH, A., REED, A., ARMSTRONG-JAMES, D. & SCHELENZ, S. 2015. The serum opsonin L-ficolin is detected in lungs of human transplant recipients following fungal infections and modulates inflammation and killing of *aspergillus fumigatus*.(Report). 212, 234.
- BINDER, H., GUTBERLET, T., ANIKIN, A. & KLOSE, G. 1998. Hydration of the dienic lipid dioctadecadienoylphosphatidylcholine in the lamellar phase--an infrared linear dichroism and x-ray study on headgroup orientation, water ordering, and bilayer dimensions. *Biophys J*, 74, 1908-23.
- BINGEN, E., LEVY, C., VARON, E., DE LA ROCQUE, F., BOUCHERAT, M., D'ATHIS, P., AUJARD, Y. & COHEN, R. 2008. Pneumococcal meningitis in the era of pneumococcal conjugate vaccine implementation. *Eur J Clin Microbiol Infect Dis*, 27, 191-9.
- BOGAERT, D., SLUIJTER, M., DE GROOT, R. & HERMANS, P. W. M. 2004. Multiplex opsonophagocytosis assay (MOPA): a useful tool for the monitoring of the 7-valent pneumococcal conjugate vaccine. *Vaccine*, 22, 4014-4020.
- BOLDT, A. B., SANCHEZ, M. I., STAHLKE, E. R., STEFFENSEN, R., THIEL, S., JENSENIUS, J. C., PREVEDELLO, F. C., MIRA, M. T., KUN, J. F. & MESSIAS-REASON, I. J. 2013. Susceptibility to leprosy is associated with M-ficolin polymorphisms. *J Clin Immunol*, 33, 210-9.
- BORZA, D. B. 2016. Alternative Pathway Dysregulation and the Conundrum of Complement Activation by IgG4 Immune Complexes in Membranous Nephropathy. *Front Immunol*, 7, 157.
- BOULNOIS, G. J., PATON, J. C., MITCHELL, T. J. & ANDREW, P. W. 1991. Structure and function of pneumolysin, the multifunctional, thiol-activated toxin of *Streptococcus pneumoniae*. *Mol Microbiol*, 5, 2611-6.

- BOVIGNY, C., TAMO, G., LEMMIN, T., MAINO, N. & DAL PERARO, M. 2015. LipidBuilder: A Framework To Build Realistic Models for Biological Membranes. *J Chem Inf Model*, 55, 2491-9.
- BOZZUTO, G. & MOLINARI, A. 2015. Liposomes as nanomedical devices. *Int J Nanomedicine*, 10, 975-99.
- BRAUN, J. S., HOFFMANN, O., SCHICKHAUS, M., FREYER, D., DAGAND, E., BERMPOHL, D., MITCHELL, T. J., BECHMANN, I. & WEBER, J. R. 2007. Pneumolysin causes neuronal cell death through mitochondrial damage. *Infect Immun*, 75, 4245-54.
- BRIUGLIA, M. L., ROTELLA, C., MCFARLANE, A. & LAMPROU, D. A. 2015. Influence of cholesterol on liposome stability and on in vitro drug release. *Drug Deliv Transl Res*, 5, 231-42.
- BROWN, D. A. & LONDON, E. 2000. Structure and function of sphingolipid- and cholesterol-rich membrane rafts. *J Biol Chem*, 275, 17221-4.
- BROWN, J. S., GILLILAND, S. M., RUIZ-ALBERT, J. & HOLDEN, D. W. 2002a. Characterization of pit, a *Streptococcus pneumoniae* iron uptake ABC transporter. *Infect Immun*, 70, 4389-98.
- BROWN, J. S., HUSSELL, T., GILLILAND, S. M., HOLDEN, D. W., PATON, J. C., EHRENSTEIN, M. R., WALPORT, M. J. & BOTTO, M. 2002b. The classical pathway is the dominant complement pathway required for innate immunity to *Streptococcus pneumoniae* infection in mice. *Proc Natl Acad Sci U S A*, 99, 16969-74.
- BRUGGEMANN, M., WILLIAMS, G. T., BINDON, C. I., CLARK, M. R., WALKER, M. R., JEFFERIS, R., WALDMANN, H. & NEUBERGER, M. S. 1987. Comparison of the effector functions of human immunoglobulins using a matched set of chimeric antibodies. *J Exp Med*, 166, 1351-61.
- BUI, N. K., EBERHARDT, A., VOLLMER, D., KERN, T., BOUGAULT, C., TOMASZ, A., SIMORRE, J. P. & VOLLMER, W. 2012. Isolation and analysis of cell wall components from *Streptococcus pneumoniae*. *Anal Biochem*, 421, 657-66.
- BUNACIU, A. A., UDRISTIOIU, E. G. & ABOUL-ENEIN, H. Y. 2015. X-ray diffraction: instrumentation and applications. *Crit Rev Anal Chem*, 45, 289-99.
- BURTON, D. R., GREGORY, L. & JEFFERIS, R. 1986. Aspects of the molecular structure of IgG subclasses. *Monogr Allergy*, 19, 7-35.
- BURTON, D. R. & WOOF, J. M. 1992. Human antibody effector function. *Advances in immunology*, 51, 1-84.
- CABALLERO, J. & RELLO, J. 2011. Combination antibiotic therapy for community-acquired pneumonia. *Ann Intensive Care*, 1, 48.

- CANVIN, J. R., MARVIN, A. P., SIVAKUMARAN, M., PATON, J. C., BOULNOIS, G. J., ANDREW, P. W. & MITCHELL, T. J. 1995. The role of pneumolysin and autolysin in the pathology of pneumonia and septicemia in mice infected with a type 2 pneumococcus. *J Infect Dis*, 172, 119-23.
- CARLIER, F. M., SIBILLE, Y. & PILETTE, C. 2016. The epithelial barrier and immunoglobulin A system in allergy. *Clin Exp Allergy*, 46, 1372-1388.
- CASAL, H. L. & MANTSCH, H. H. 1984. Polymorphic phase behaviour of phospholipid membranes studied by infrared spectroscopy. *Biochim Biophys Acta*, 779, 381-401.
- CASSIDY, S. K. & O'RIORDAN, M. X. 2013. More than a pore: the cellular response to cholesterol-dependent cytolysins. *Toxins (Basel)*, 5, 618-36.
- CEDZYNSKI, M., NUYTINCK, L., ATKINSON, A. P., ST SWIERZKO, A., ZEMAN, K., SZEMRAJ, J., SZALA, A., TURNER, M. L. & KILPATRICK, D. C. 2007. Extremes of L-ficolin concentration in children with recurrent infections are associated with single nucleotide polymorphisms in the FCN2 gene. *Clin Exp Immunol*, 150, 99-104.
- CELIK, I., STOVER, C. M., BOTTO, M., THIEL, S., TZIMA, S., KÜNKEL, D., WALPORT, M., LORENZ, W. & SCHWAEBLE, W. J. 2001. Role of the classical pathway of complement activation in experimentally induced polymicrobial peritonitis.
- CELLIERS, P. M. & CONIA, J. 2000. Measurement of localized heating in the focus of an optical trap. *Appl Opt*, 39, 3396-407.
- CERUTTI, A. & RESCIGNO, M. 2008. The Biology of Intestinal Immunoglobulin A Responses. *Immunity*, 28, 740-750.
- CHAYEN, N. E. 2004. Turning protein crystallisation from an art into a science. *Curr Opin Struct Biol*, 14, 577-83.
- CHEN, T., HU, Y., DING, Q., YU, J., WANG, F., LUO, F. & ZHANG, X. L. 2015. Serum ficolin-2 concentrations are significantly changed in patients with hepatitis B virus infection and liver diseases. *Virol Sin*, 30, 249-60.
- CHENG, W., LI, Q., JIANG, Y. L., ZHOU, C. Z. & CHEN, Y. 2013. Structures of *Streptococcus pneumoniae* PiaA and its complex with ferrichrome reveal insights into the substrate binding and release of high affinity iron transporters. *PLoS One*, 8, e71451.
- CHERNEY, D. P. & HARRIS, J. M. 2010. Confocal Raman microscopy of optical-trapped particles in liquids. *Annu Rev Anal Chem (Palo Alto Calif)*, 3, 277-97.

- CHIOU, C. C. 2006. Does Penicillin Remain the Drug of Choice for Pneumococcal Pneumonia in View of Emerging in Vitro Resistance? *Clinical Infectious Diseases*, 42, 234-237.
- CHONGSIRIWATANA, N. P. & BARRON, A. E. 2010. Comparing bacterial membrane interactions of antimicrobial peptides and their mimics. *Methods Mol Biol*, 618, 171-82.
- CILLONIZ, C. & TORRES, A. 2014. Pneumococcal disease: Epidemiology and new vaccines.(Editorial). 1, 35.
- COCKERAN, R., ANDERSON, R. & FELDMAN, C. 2002. The role of pneumolysin in the pathogenesis of Streptococcus pneumoniae infection. *Curr Opin Infect Dis*, 15, 235-9.
- COCKERAN, R., THERON, A. J., STEEL, H. C., MATLOLA, N. M., MITCHELL, T. J., FELDMAN, C. & ANDERSON, R. 2001. Proinflammatory interactions of pneumolysin with human neutrophils. *J Infect Dis*, 183, 604-11.
- CORNICK, J. E., TASTAN BISHOP, O., YALCIN, F., KIRAN, A. M., KUMWENDA, B., CHAGUZA, C., GOVINDPERSHAD, S., OUSMANE, S., SENGHORE, M., DU PLESSIS, M., PLUSCHKE, G., EBRUKE, C., MCGEE, L., SIGAUQUE, B., COLLARD, J. M., BENTLEY, S. D., KADIOGLU, A., ANTONIO, M., VON GOTTBORG, A., FRENCH, N., KLUGMAN, K. P., HEYDERMAN, R. S., ALDERSON, M. & EVERETT, D. B. 2017. The global distribution and diversity of protein vaccine candidate antigens in the highly virulent Streptococcus pneumoniae serotype 1. *Vaccine*.
- COSTA, S., ALMEIDA, A., CASTRO, A. & DOMINGUES, L. 2014. Fusion tags for protein solubility, purification and immunogenicity in Escherichia coli: the novel Fh8 system. *Front Microbiol*, 5, 63.
- CSEH, S., VERA, L., MATSUSHITA, M., FUJITA, T., ARLAUD, G. J. & THIELENS, N. M. 2002. Characterization of the interaction between L-ficolin/p35 and mannan-binding lectin-associated serine proteases-1 and -2. *J Immunol*, 169, 5735-43.
- CZAJKOWSKY, D. M., HOTZE, E. M., SHAO, Z. & TWETEN, R. K. 2004. Vertical collapse of a cytolysin prepore moves its transmembrane beta-hairpins to the membrane. *Embo j*, 23, 3206-15.
- CZAJKOWSKY, D. M., SALANTI, A., DITLEV, S. B., SHAO, Z., GHUMRA, A., ROWE, J. A. & PLEASS, R. J. 2010. IgM, Fc mu Rs, and malarial immune evasion. *J Immunol*, 184, 4597-603.
- CZAJKOWSKY, D. M. & SHAO, Z. 2009. The human IgM pentamer is a mushroom-shaped molecule with a flexural bias. *Proc Natl Acad Sci U S A*, 106, 14960-5.

- CZAMARA, K., MAJZNER, K., PACIA, M. Z., KOCHAN, K., KACZOR, A. & BARANSKA, M. 2015. Raman spectroscopy of lipids: a review.(Report). *J Raman Spectrosc* 46, 4.
- DANG, T. X., HOTZE, E. M., ROUILLER, I., TWETEN, R. K. & WILSON-KUBALEK, E. M. 2005. Prepore to pore transition of a cholesterol-dependent cytolysin visualized by electron microscopy. *J Struct Biol*, 150, 100-8.
- DANIEL, M. 2013. Antibiotics for otitis media with effusion in children. *Clin Otolaryngol*, 38, 56-7.
- DAVIES, A. M. & SUTTON, B. J. 2015. Human IgG4: a structural perspective. *Immunol Rev*, 268, 139-59.
- DE LUCA, A. C., DHOLAKIA, K. & MAZILU, M. 2015. Modulated Raman Spectroscopy for Enhanced Cancer Diagnosis at the Cellular Level. *Sensors (Basel, Switzerland)*, 15, 13680-13704.
- DMITRIEV, A. A. & SUROVTSEV, N. V. 2015. Temperature-Dependent Hydrocarbon Chain Disorder in Phosphatidylcholine Bilayers Studied by Raman Spectroscopy. *J Phys Chem B*, 119, 15613-22.
- DOWD, K. J., FARRAND, A. J. & TWETEN, R. K. 2012. The cholesterol-dependent cytolysin signature motif: a critical element in the allosteric pathway that couples membrane binding to pore assembly. *PLoS pathogens*, 8, e1002787.
- DRIJKONINGEN, J. J. & ROHDE, G. G. 2014. Pneumococcal infection in adults: burden of disease. *Clin Microbiol Infect*, 20 Suppl 5, 45-51.
- DULLAERS, M., DE BRUYNE, R., RAMADANI, F., GOULD, H. J., GEVAERT, P. & LAMBRECHT, B. N. 2012. The who, where, and when of IgE in allergic airway disease. *J Allergy Clin Immunol*, 129, 635-45.
- DURBIN, S. D. & FEHER, G. 1996. Protein crystallization. *Annual review of physical chemistry*, 47, 171-204.
- EDGAR, P. F. 1995. Hucolin, a new corticosteroid-binding protein from human plasma with structural similarities to ficolins, transforming growth factor-beta 1-binding proteins. *FEBS Lett*, 375, 159-61.
- EHRENSTEIN, M. R. & NOTLEY, C. A. 2010. The importance of natural IgM: scavenger, protector and regulator. *Nat Rev Immunol*, 10, 778-86.
- ELDHOLM, V., JOHNSBORG, O., HAUGEN, K., OHNSTAD, H. S. & HAVARSTEIN, L. S. 2009. Fratricide in *Streptococcus pneumoniae*: contributions and role of the cell wall hydrolases CbpD, LytA and LytC. *Microbiology*, 155, 2223-34.

- ELEMRAID, M. A., RUSHTON, S. P., SHIRLEY, M. D., THOMAS, M. F., SPENCER, D. A., EASTHAM, K. M., HAMPTON, F., GORTON, R., POLLARD, K., GENNERLY, A. R. & CLARK, J. E. 2013. Impact of the 7-valent pneumococcal conjugate vaccine on the incidence of childhood pneumonia. *Epidemiol Infect*, 141, 1697-704.
- EMSLEY, P. & COWTAN, K. 2004. Coot: model-building tools for molecular graphics. *Acta Crystallogr D Biol Crystallogr*, 60, 2126-32.
- ENDO, Y., LIU, Y., KANNO, K., TAKAHASHI, M., MATSUSHITA, M. & FUJITA, T. 2004. Identification of the mouse H-ficolin gene as a pseudogene and orthology between mouse ficolins A/B and human L-/M-ficolins. *Genomics*, 84, 737-44.
- ENDO, Y., MATSUSHITA, M. & FUJITA, T. 2011. The role of ficolins in the lectin pathway of innate immunity. *Int J Biochem Cell Biol*, 43, 705-12.
- ENDO, Y., MATSUSHITA, M. & FUJITA, T. 2015. New insights into the role of ficolins in the lectin pathway of innate immunity. *Int Rev Cell Mol Biol*, 316, 49-110.
- ENDO, Y., NAKAZAWA, N., LIU, Y., IWAKI, D., TAKAHASHI, M., FUJITA, T., NAKATA, M. & MATSUSHITA, M. 2005. Carbohydrate-binding specificities of mouse ficolin A, a splicing variant of ficolin A and ficolin B and their complex formation with MASP-2 and sMAP. *Immunogenetics*, 57, 837-44.
- ENDO, Y., SATO, Y., MATSUSHITA, M. & FUJITA, T. 1996. Cloning and Characterization of the Human Lectin P35 Gene and Its Related Gene. *Genomics*, 36, 515-521.
- ENDO, Y., TAKAHASHI, M., IWAKI, D., ISHIDA, Y., NAKAZAWA, N., KODAMA, T., MATSUZAKA, T., KANNO, K., LIU, Y., TSUCHIYA, K., KAWAMURA, I., IKAWA, M., WAGURI, S., WADA, I., MATSUSHITA, M., SCHWAEBLE, W. J. & FUJITA, T. 2012. Mice deficient in ficolin, a lectin complement pathway recognition molecule, are susceptible to *Streptococcus pneumoniae* infection. *J Immunol*, 189, 5860-6.
- ERIKSSON, E., ENGER, J., NORDLANDER, B., ERJAVEC, N., RAMSER, K., GOKSOR, M., HOHMANN, S., NYSTROM, T. & HANSTORP, D. 2007. A microfluidic system in combination with optical tweezers for analyzing rapid and reversible cytological alterations in single cells upon environmental changes. *Lab Chip*, 7, 71-6.
- FAVIER, A. L., GOUT, E., REYNARD, O., FERRARIS, O., KLEMAN, J. P., VOLCHKOV, V., PEYREFITTE, C. & THIELENS, N. M. 2016. Enhancement of Ebola Virus Infection via Ficolin-1 Interaction with the Mucin Domain of GP Glycoprotein. *J Virol*, 90, 5256-69.
- FEIKIN, D. R. & KLUGMAN, K. P. 2002. Historical changes in pneumococcal serogroup distribution: implications for the era of pneumococcal conjugate vaccines. *Clin Infect Dis*, 35, 547-55.

- FELDMAN, C. & ANDERSON, R. 2016. Epidemiology, virulence factors and management of the pneumococcus. *F1000Res*, 5, 2320.
- FELDMAN, C., COCKERAN, R., JEDRZEJAS, M. J., MITCHELL, T. J. & ANDERSON, R. 2007. Hyaluronidase augments pneumolysin-mediated injury to human ciliated epithelium. *Int J Infect Dis*, 11, 11-5.
- FERNANDEZ-TORNERO, C., LOPEZ, R., GARCIA, E., GIMENEZ-GALLEGO, G. & ROMERO, A. 2001. A novel solenoid fold in the cell wall anchoring domain of the pneumococcal virulence factor LytA. *Nat Struct Biol*, 8, 1020-4.
- FILE, T. M. 2003. Community-acquired pneumonia. *Lancet*, 362, 1991-2001.
- FILE, T. M., GARAU, J., BLASI, F., CHIDIAC, C., KLUGMAN, K., LODE, H., LONKS, J. R., MANDELL, L., RAMIREZ, J. & YU, V. 2004. Guidelines for empiric antimicrobial prescribing in community-acquired pneumonia. *CHEST Journal*, 125, 1888-1901.
- FITZSIMMONS, C. M., FALCONE, F. H. & DUNNE, D. W. 2014. Helminth Allergens, Parasite-Specific IgE, and Its Protective Role in Human Immunity. *Front Immunol*, 5, 61.
- FLAUMENHAFT, E. & FLAUMENHAFT, C. 1993. Evolution of America's pioneer bacteriologist: George M. Sternberg's formative years. *Mil Med*, 158, 448-57.
- FORNERIS, F., WU, J. & GROS, P. 2012. The modular serine proteases of the complement cascade. *Curr Opin Struct Biol*, 22, 333-41.
- FOX, J. D. & WAUGH, D. S. 2003. Maltose-binding protein as a solubility enhancer. *Methods Mol Biol*, 205, 99-117.
- FREDERIKSEN, P. D., THIEL, S., LARSEN, C. B. & JENSENIUS, J. C. 2005. M-ficolin, an innate immune defence molecule, binds patterns of acetyl groups and activates complement. *Scand J Immunol*, 62, 462-73.
- FRIEND, J. & YEO, L. 2010. Fabrication of microfluidic devices using polydimethylsiloxane. *Biomicrofluidics*, 4.
- FUJIMORI, Y., HARUMIYA, S., FUKUMOTO, Y., MIURA, Y., YAGASAKI, K., TACHIKAWA, H. & FUJIMOTO, D. 1998. Molecular cloning and characterization of mouse ficolin-A. *Biochem Biophys Res Commun*, 244, 796-800.
- FUKUSUMI, M., CHANG, B., TANABE, Y., OSHIMA, K., MARUYAMA, T., WATANABE, H., KURONUMA, K., KASAHARA, K., TAKEDA, H., NISHI, J., FUJITA, J., KUBOTA, T., SUNAGAWA, T., MATSUI, T. & OISHI, K. 2017.

Invasive pneumococcal disease among adults in Japan, April 2013 to March 2015: disease characteristics and serotype distribution. *BMC Infect Dis*, 17, 2.

- GABORIAUD, C., THIELENS, N. M., GREGORY, L. A., ROSSI, V., FONTECILLA-CAMPS, J. C. & ARLAUD, G. J. 2004. Structure and activation of the C1 complex of complement: unraveling the puzzle. *Trends Immunol*, 25, 368-73.
- GARRED, P., GENSTER, N., PILELY, K., BAYARRI-OLMOS, R., ROSBJERG, A., MA, Y. J. & SKJOEDT, M. O. 2016. A journey through the lectin pathway of complement-MBL and beyond. *Immunol Rev*, 274, 74-97.
- GARRED, P., HONORE, C., MA, Y. J., RORVIG, S., COWLAND, J., BORREGAARD, N. & HUMMELSHOJ, T. 2010. The genetics of ficolins. *J Innate Immun*, 2, 3-16.
- GHISAIDOOBE, A. B. & CHUNG, S. J. 2014. Intrinsic tryptophan fluorescence in the detection and analysis of proteins: a focus on Forster resonance energy transfer techniques. *Int J Mol Sci*, 15, 22518-38.
- GILBERT, R. J. 2002. Pore-forming toxins. *Cell Mol Life Sci*, 59, 832-44.
- GILBERT, R. J., JIMENEZ, J. L., CHEN, S., TICKLE, I. J., ROSSJOHN, J., PARKER, M., ANDREW, P. W. & SAIBIL, H. R. 1999. Two structural transitions in membrane pore formation by pneumolysin, the pore-forming toxin of *Streptococcus pneumoniae*. *Cell*, 97, 647-55.
- GILBERT, R. J., ROSSJOHN, J., PARKER, M. W., TWETEN, R. K., MORGAN, P. J., MITCHELL, T. J., ERRINGTON, N., ROWE, A. J., ANDREW, P. W. & BYRON, O. 1998. Self-interaction of pneumolysin, the pore-forming protein toxin of *Streptococcus pneumoniae*. *J Mol Biol*, 284, 1223-37.
- GILBERT, R. J. & SONNEN, A. F. 2016. Measuring kinetic drivers of pneumolysin pore structure. *Eur Biophys J*, 45, 365-76.
- GINGRAS, A. R., GIRIJA, U. V., KEEBLE, A. H., PANCHAL, R., MITCHELL, D. A., MOODY, P. C. & WALLIS, R. 2011. Structural basis of mannan-binding lectin recognition by its associated serine protease MASP-1: implications for complement activation. *Structure*, 19, 1635-43.
- GIRIJA, U. V., MITCHELL, D. A., ROSCHER, S. & WALLIS, R. 2011. Carbohydrate recognition and complement activation by rat ficolin-B. *Eur J Immunol*, 41, 214-23.
- GLEICH, G. J., BIEGER, R. C. & STANKIEVIC, R. 1969. Antigen combining activity associated with immunoglobulin D. *Science*, 165, 606.

- GOLUSZKO, P. & NOWICKI, B. 2005. Membrane cholesterol: a crucial molecule affecting interactions of microbial pathogens with mammalian cells. *Infect Immun*, 73, 7791-6.
- GRAHAM, F. L. & VAN DER EB, A. J. 1973. A new technique for the assay of infectivity of human adenovirus 5 DNA. *Virology*, 52, 456-467.
- GRANIZO, J. J., AGUILAR, L., CASAL, J., GARCIA-REY, C., DAL-RE, R. & BAQUERO, F. 2000. Streptococcus pneumoniae resistance to erythromycin and penicillin in relation to macrolide and beta-lactam consumption in Spain (1979-1997). *J Antimicrob Chemother*, 46, 767-73.
- GREEN, R. & ROGERS, E. J. 2013. Transformation of chemically competent E. coli. *Methods Enzymol*, 529, 329-36.
- GRETER, M., HELFT, J., CHOW, A., HASHIMOTO, D., MORTHA, A., AGUDOCANTERERO, J., BOGUNOVIC, M., GAUTIER, E. L., MILLER, J., LEBOEUF, M., LU, G., ALOMAN, C., BROWN, B. D., POLLARD, J. W., XIONG, H., RANDOLPH, G. J., CHIPUK, J. E., FRENETTE, P. S. & MERAD, M. 2012. GM-CSF controls nonlymphoid tissue dendritic cell homeostasis but is dispensable for the differentiation of inflammatory dendritic cells. *Immunity*, 36, 1031-46.
- GUALDI, L., HAYRE, J. K., GERLINI, A., BIDOSSI, A., COLOMBA, L., TRAPPETTI, C., POZZI, G., DOCQUIER, J.-D., ANDREW, P., RICCI, S. & OGGIONI, M. R. 2012. Regulation of neuraminidase expression in Streptococcus pneumoniae.
- GUILLEMOT, D., VARON, E., BERNEDE, C., WEBER, P., HENRIET, L., SIMON, S., LAURENT, C., LECOEUR, H. & CARBON, C. 2005. Reduction of antibiotic use in the community reduces the rate of colonization with penicillin G-nonsusceptible Streptococcus pneumoniae. *Clin Infect Dis*, 41, 930-8.
- GUO, H. & LI, Z. 2013. Optical tweezers technique and its applications. *Science China Physics, Mechanics and Astronomy*, 56, 2351-2360.
- GUTZEIT, C., MAGRI, G. & CERUTTI, A. 2014. Intestinal IgA production and its role in host-microbe interaction. *Immunol Rev*, 260, 76-85.
- HAMED, M. R., BROWN, R. J., ZOTHNER, C., URBANOWICZ, R. A., MASON, C. P., KRARUP, A., MCCLURE, C. P., IRVING, W. L., BALL, J. K., HARRIS, M., HICKLING, T. P. & TARR, A. W. 2014. Recombinant human L-ficolin directly neutralizes hepatitis C virus entry. *J Innate Immun*, 6, 676-84.
- HAMILTON, R. G. 2010. Clinical laboratory assessment of immediate-type hypersensitivity. *J Allergy Clin Immunol*, 125, S284-96.

- HARRIS, J. R., LEWIS, R. J., BAIK, C., POKRAJAC, L., BILLINGTON, S. J. & PALMER, M. 2011. Cholesterol microcrystals and cochleate cylinders: attachment of pyolysin oligomers and domain 4. *J Struct Biol*, 173, 38-45.
- HARTZELL, J. D., OSTER, C. N. & GAYDOS, J. C. 2003. How contagious are common respiratory tract infections? *N Engl J Med*, 349, 95.
- HARUMIYA, S., OMORI, A., SUGIURA, T., FUKUMOTO, Y., TACHIKAWA, H. & FUJIMOTO, D. 1995. EBP-37, a new elastin-binding protein in human plasma: structural similarity to ficolins, transforming growth factor-beta 1-binding proteins. *J Biochem*, 117, 1029-35.
- HASHIMOTO, S., SUZUKI, T., DONG, H. Y., NAGAI, S., YAMAZAKI, N. & MATSUSHIMA, K. 1999. Serial analysis of gene expression in human monocyte-derived dendritic cells. *Blood*, 94, 845-52.
- HAUGHNEY, S. L., PETERSEN, L. K., SCHOOF, A. D., RAMER-TAIT, A. E., KING, J. D., BRILES, D. E., WANNEMUEHLER, M. J. & NARASIMHAN, B. 2013. Retention of structure, antigenicity, and biological function of pneumococcal surface protein A (PspA) released from polyanhydride nanoparticles. *Acta biomaterialia*, 9, 8262-8271.
- HAUSDORFF, W. P., BRYANT, J., PARADISO, P. R. & SIBER, G. R. 2000. Which pneumococcal serogroups cause the most invasive disease: implications for conjugate vaccine formulation and use, part I. *Clin Infect Dis*, 30, 100-21.
- HAZLEWOOD, M. A., KUMARARATNE, D. S., WEBSTER, A. D., GOODALL, M., BIRD, P. & DAHA, M. 1992. An association between homozygous C3 deficiency and low levels of anti-pneumococcal capsular polysaccharide antibodies. *Clin Exp Immunol*, 87, 404-9.
- HEIMBURG, T., WURZ, U. & MARSH, D. 1992. Binary phase diagram of hydrated dimyristoylglycerol-dimyristoylphosphatidylcholine mixtures. *Biophys J*, 63, 1369-78.
- HEJA, D., HARMAT, V., FODOR, K., WILMANN, M., DOBO, J., KEKESI, K. A., ZAVODSZKY, P., GAL, P. & PAL, G. 2012. Monospecific inhibitors show that both mannan-binding lectin-associated serine protease-1 (MASP-1) and -2 are essential for lectin pathway activation and reveal structural plasticity of MASP-2. *J Biol Chem*, 287, 20290-300.
- HELLER, I., HOEKSTRA, T. P., KING, G. A., PETERMAN, E. J. & WUITE, G. J. 2014. Optical tweezers analysis of DNA-protein complexes. *Chem Rev*, 114, 3087-119.
- HENRIQUES-NORMARK, B. & TUOMANEN, E. I. 2013. The pneumococcus: epidemiology, microbiology, and pathogenesis. *Cold Spring Harbor perspectives in medicine*, 3.

- HEUCK, A. P., TWETEN, R. K. & JOHNSON, A. E. 2003. Assembly and topography of the prepore complex in cholesterol-dependent cytolysins. *J Biol Chem*, 278, 31218-25.
- HIRST, R. A., GOSAI, B., RUTMAN, A., GUERIN, C. J., NICOTERA, P., ANDREW, P. W. & O'CALLAGHAN, C. 2008. Streptococcus pneumoniae deficient in pneumolysin or autolysin has reduced virulence in meningitis. *J Infect Dis*, 197, 744-51.
- HIRST, R. A., KADIOGLU, A., O'CALLAGHAN, C. & ANDREW, P. W. 2004. The role of pneumolysin in pneumococcal pneumonia and meningitis. *Clin Exp Immunol*, 138, 195-201.
- HOANG, T. V., TOAN, N. L., SONG LE, H., OUF, E. A., BOCK, C. T., KREMSNER, P. G., KUN, J. F. & VELAVAN, T. P. 2011. Ficolin-2 levels and FCN2 haplotypes influence hepatitis B infection outcome in Vietnamese patients. *PLoS One*, 6, e28113.
- HOHENESTER, E. 2011. Tackling the legs of mannan-binding lectin. *Structure*, 19, 1538-40.
- HOLMES, A. R., MCNAB, R., MILLSAP, K. W., ROHDE, M., HAMMERSCHMIDT, S., MAWDSLEY, J. L. & JENKINSON, H. F. 2001. The pavA gene of Streptococcus pneumoniae encodes a fibronectin-binding protein that is essential for virulence. *Mol Microbiol*, 41, 1395-408.
- HOMANN, C., VARMING, K., HOGASEN, K., MOLLNES, T. E., GRAUDAL, N., THOMSEN, A. C. & GARRED, P. 1997. Acquired C3 deficiency in patients with alcoholic cirrhosis predisposes to infection and increased mortality. *Gut*, 40, 544-9.
- HOTZE, E. M. & TWETEN, R. K. 2012. Membrane assembly of the cholesterol-dependent cytolysin pore complex. *Biochim Biophys Acta*, 1818, 1028-38.
- HOTZE, E. M., WILSON-KUBALEK, E., FARRAND, A. J., BENTSEN, L., PARKER, M. W., JOHNSON, A. E. & TWETEN, R. K. 2012. Monomer-monomer interactions propagate structural transitions necessary for pore formation by the cholesterol-dependent cytolysins. *J Biol Chem*, 287, 24534-43.
- HOULDSWORTH, S., ANDREW, P. W. & MITCHELL, T. J. 1994. Pneumolysin stimulates production of tumor necrosis factor alpha and interleukin-1 beta by human mononuclear phagocytes. *Infect Immun*, 62, 1501-3.
- HOURI, H., PORMOHAMMAD, A., RIAHI, S. M., NASIRI, M. J., FALLAH, F., DABIRI, H. & POURIRAN, R. 2017. Acute bacterial meningitis in Iran: Systematic review and meta-analysis. *PLoS One*, 12, e0169617.

- HSU, H. E., SHUTT, K. A., MOORE, M. R., BEALL, B. W., BENNETT, N. M., CRAIG, A. S., FARLEY, M. M., JORGENSEN, J. H., LEXAU, C. A., PETIT, S., REINGOLD, A., SCHAFFNER, W., THOMAS, A., WHITNEY, C. G. & HARRISON, L. H. 2009. Effect of pneumococcal conjugate vaccine on pneumococcal meningitis. *N Engl J Med*, 360, 244-56.
- HU, Y. L., LUO, F. L., FU, J. L., CHEN, T. L., WU, S. M., ZHOU, Y. D. & ZHANG, X. L. 2013. Early increased ficolin-2 concentrations are associated with severity of liver inflammation and efficacy of anti-viral therapy in chronic hepatitis C patients. *Scand J Immunol*, 77, 144-50.
- HUMMELL, D. S., SWIFT, A. J., TOMASZ, A. & WINKELSTEIN, J. A. 1985. Activation of the alternative complement pathway by pneumococcal lipoteichoic acid. *Infect Immun*, 47, 384-7.
- HUMMELSHOJ, T., MA, Y. J., MUNTHE-FOG, L., BJARNSHOLT, T., MOSER, C., SKJOEDT, M. O., ROMANI, L., FUJITA, T., ENDO, Y. & GARRED, P. 2012. The interaction pattern of murine serum ficolin-A with microorganisms. *PLoS One*, 7, e38196.
- HUMMELSHOJ, T., MUNTHE-FOG, L., MADSEN, H. O., FUJITA, T., MATSUSHITA, M. & GARRED, P. 2005. Polymorphisms in the FCN2 gene determine serum variation and function of Ficolin-2. *Hum Mol Genet*, 14, 1651-8.
- HUMMELSHOJ, T., THIELENS, N. M., MADSEN, H. O., ARLAUD, G. J., SIM, R. B. & GARRED, P. 2007. Molecular organization of human Ficolin-2. *Mol Immunol*, 44, 401-11.
- HUSSAIN, H. & CHONG, N. F. 2016. Combined Overlap Extension PCR Method for Improved Site Directed Mutagenesis. *Biomed Res Int*, 2016, 8041532.
- HUSSAIN, R., KIFAYET, A. & CHIANG, T. J. 1995. Immunoglobulin G1 (IgG1) and IgG3 antibodies are markers of progressive disease in leprosy. *Infect Immun*, 63, 410-5.
- HYAMS, C., CAMBERLEIN, E., COHEN, J. M., BAX, K. & BROWN, J. S. 2010. The *Streptococcus pneumoniae* capsule inhibits complement activity and neutrophil phagocytosis by multiple mechanisms. *Infect Immun*, 78, 704-15.
- HYAMS, C., TRZCINSKI, K., CAMBERLEIN, E., WEINBERGER, D. M., CHIMALAPATI, S., NOURSADEGHI, M., LIPSITCH, M. & BROWN, J. S. 2013. *Streptococcus pneumoniae* capsular serotype invasiveness correlates with the degree of factor H binding and opsonization with C3b/iC3b. *Infect Immun*, 81, 354-63.
- HYNES, W. L. & WALTON, S. L. 2000. Hyaluronidases of Gram-positive bacteria. *FEMS Microbiol Lett*, 183, 201-7.

- IANNELLI, F., CHIAVOLINI, D., RICCI, S., OGGIONI, M. R. & POZZI, G. 2004. Pneumococcal surface protein C contributes to sepsis caused by *Streptococcus pneumoniae* in mice. *Infect Immun*, 72, 3077-80.
- ICHIJO, H., HELLMAN, U., WERNSTEDT, C., GONEZ, L. J., CLAEISSON-WELSH, L., HELDIN, C. H. & MIYAZONO, K. 1993. Molecular cloning and characterization of ficolin, a multimeric protein with fibrinogen- and collagen-like domains. *J Biol Chem*, 268, 14505-13.
- ICHIJO, H., RONNSTRAND, L., MIYAGAWA, K., OHASHI, H., HELDIN, C. H. & MIYAZONO, K. 1991. Purification of transforming growth factor-beta 1 binding proteins from porcine uterus membranes. *J Biol Chem*, 266, 22459-64.
- IINUMA, Y., HIROSE, Y., TANAKA, T., KUMAGAI, K., MIYAJIMA, M., SEKIGUCHI, H., NOMOTO, Y., YABE, M., IMAI, Y. & YAMAZAKI, Y. 2007. Rapidly progressive fatal pneumococcal sepsis in adults: a report of two cases. *J Infect Chemother*, 13, 346-9.
- IMOHL, M., MOLLER, J., REINERT, R. R., PERNICIARO, S., VAN DER LINDEN, M. & AKTAS, O. 2015. Pneumococcal meningitis and vaccine effects in the era of conjugate vaccination: results of 20 years of nationwide surveillance in Germany. *BMC Infect Dis*, 15, 61.
- INGELS, H. A. 2015. Recurrent invasive pneumococcal disease in children host factors and vaccination response. *Dan Med J*, 62.
- IRANI, V., GUY, A. J., ANDREW, D., BEESON, J. G., RAMSLAND, P. A. & RICHARDS, J. S. 2015. Molecular properties of human IgG subclasses and their implications for designing therapeutic monoclonal antibodies against infectious diseases. *Mol Immunol*, 67, 171-82.
- ISENMAN, D., DORRINGTON, K. & PAINTER, R. 1975. The structure and function of immunoglobulin domains. *J Immunol*, 114, 1726-29.
- JACOBITZ, A. W., NAZIGA, E. B., YI, S. W., MCCONNELL, S. A., PETERSON, R., JUNG, M. E., CLUBB, R. T. & WERESZCZYNSKI, J. 2016. The "Lid" in the *Streptococcus pneumoniae* SrtC1 Sortase Adopts a Rigid Structure that Regulates Substrate Access to the Active Site. *J Phys Chem B*, 120, 8302-12.
- JANOFF, E. N. & RUBINS, J. B. 1997. Invasive pneumococcal disease in the immunocompromised host. *Microb Drug Resist*, 3, 215-32.
- JANOFF, E. N., RUBINS, J. B., FASCHING, C., CHARBONEAU, D., RAHKOLA, J. T., PLAUT, A. G. & WEISER, J. N. 2014. Pneumococcal IgA1 protease subverts specific protection by human IgA1. *Mucosal Immunol*, 7, 249-56.

- JANULCZYK, R., RICCI, S. & BJORCK, L. 2003. MtsABC is important for manganese and iron transport, oxidative stress resistance, and virulence of *Streptococcus pyogenes*. *Infect Immun*, 71, 2656-64.
- JASON, R. D. W.-C. S. 2010. Complement and its role in innate and adaptive immune responses. *细胞研究 : 英文版*, 20, 34-50.
- JEFFERIS, R. & KUMARARATNE, D. S. 1990. Selective IgG subclass deficiency: quantification and clinical relevance. *Clin Exp Immunol*, 81, 357-67.
- JENKINS, R. 2000. X-Ray Techniques: Overview. *Encyclopedia of analytical chemistry*.
- JIRAVANICHPAISAL, P., LEE, B. L. & SODERHALL, K. 2006. Cell-mediated immunity in arthropods: hematopoiesis, coagulation, melanization and opsonization. *Immunobiology*, 211, 213-36.
- JOHNSON, S., BROOKS, N. J., SMITH, R. A., LEA, S. M. & BUBECK, D. 2013. Structural basis for recognition of the pore-forming toxin intermedilysin by human complement receptor CD59. *Cell Rep*, 3, 1369-77.
- KADIOGLU, A., WEISER, J. N., PATON, J. C. & ANDREW, P. W. 2008. The role of *Streptococcus pneumoniae* virulence factors in host respiratory colonization and disease. *Nat Rev Microbiol*, 6, 288-301.
- KAI, S. & ELINA, I. 1997. Functional rafts in cell membranes. *Nature*, 387, 569.
- KALIA, V., SARKAR, S., GOURLEY, T. S., ROUSE, B. T. & AHMED, R. 2006. Differentiation of memory B and T cells. *Curr Opin Immunol*, 18, 255-64.
- KANG, H. J., COULIBALY, F., PROFT, T. & BAKER, E. N. 2011. Crystal Structure of Spy0129, a *Streptococcus pyogenes* Class B Sortase Involved in Pilus Assembly (Crystal Structure of a Pilin Polymerase). *PLoS ONE*, 6, e15969.
- KATO, N., ISHIJIMA, A., INABA, T., NOMURA, F., TAKEDA, S. & TAKIGUCHI, K. 2015. Effects of lipid composition and solution conditions on the mechanical properties of membrane vesicles. *Membranes (Basel)*, 5, 22-47.
- KAUFMAN, R. J., DAVIES, M. V., WASLEY, L. C. & MICHNICK, D. 1991. Improved vectors for stable expression of foreign genes in mammalian cells by use of the untranslated leader sequence from EMC virus. *Nucleic Acids Res*, 19, 4485-90.
- KAYHTY, H. & ESKOLA, J. 1996. New vaccines for the prevention of pneumococcal infections. *Emerg Infect Dis*, 2, 289-98.
- KEREPESI, L. A., HESS, J. A., NOLAN, T. J., SCHAD, G. A. & ABRAHAM, D. 2006. Complement component C3 is required for protective innate and adaptive immunity to larval *strongyloides stercoralis* in mice. *J Immunol*, 176, 4315-22.

- KIERNEY, P. C. & DORSHKIND, K. 1987. B lymphocyte precursors and myeloid progenitors survive in diffusion chamber cultures but B cell differentiation requires close association with stromal cells. *Blood*, 70, 1418-24.
- KILPATRICK, D. C. & CHALMERS, J. D. 2012. Human L-ficolin (ficolin-2) and its clinical significance. *J Biomed Biotechnol*, 2012, 138797.
- KING, S. J., HIPPE, K. R., GOULD, J. M., BAE, D., PETERSON, S., CLINE, R. T., FASCHING, C., JANOFF, E. N. & WEISER, J. N. 2004. Phase variable desialylation of host proteins that bind to *Streptococcus pneumoniae* in vivo and protect the airway. *Mol Microbiol*, 54, 159-71.
- KJAER, T. R., THIEL, S. & ANDERSEN, G. R. 2013. Toward a structure-based comprehension of the lectin pathway of complement. *Mol Immunol*, 56, 413-22.
- KLEGER, A., SEUFFERLEIN, T., WAGNER, M., TANNAPFEL, A., HOFFMANN, T. K. & MAYERLE, J. 2015. IgG4-related autoimmune diseases: Polymorphous presentation complicates diagnosis and treatment. *Dtsch Arztebl Int*, 112, 128-35.
- KOCHAN, K., MARZEC, K. M., CHRUSZCZ-LIPSKA, K., JASZTAL, A., MASLAK, E., MUSIOLIK, H., CHLOPICKI, S. & BARANSKA, M. 2013. Pathological changes in the biochemical profile of the liver in atherosclerosis and diabetes assessed by Raman spectroscopy. *Analyst*, 138, 3885-90.
- KODATI, V. R., EL-JASTIMI, R. & LAFLEUR, M. 1994. Contribution of the Intermolecular Coupling and Librotorsional Mobility in the Methylene Stretching Modes in the Infrared Spectra of Acyl Chains. *J. Phys. Chem.* 98, 12191-12197.
- KOLBERG, J., AASE, A., BERGMANN, S., HERSTAD, T. K., RODAL, G., FRANK, R., ROHDE, M. & HAMMERSCHMIDT, S. 2006. *Streptococcus pneumoniae* enolase is important for plasminogen binding despite low abundance of enolase protein on the bacterial cell surface. *Microbiology*, 152, 1307-17.
- KOLEV, M., LE FRIEC, G. & KEMPER, C. 2014. Complement--tapping into new sites and effector systems. *Nat Rev Immunol*, 14, 811-20.
- KOSTER, S., VAN PEE, K., HUDEL, M., LEUSTIK, M., RHINOW, D., KUHLBRANDT, W., CHAKRABORTY, T. & YILDIZ, O. 2014. Crystal structure of listeriolysin O reveals molecular details of oligomerization and pore formation. *Nat Commun*, 5, 3690.
- KRAPP, S., MIMURA, Y., JEFFERIS, R., HUBER, R. & SONDERMANN, P. 2003. Structural analysis of human IgG-Fc glycoforms reveals a correlation between glycosylation and structural integrity. *J Mol Biol*, 325, 979-89.
- KRARUP, A., THIEL, S., HANSEN, A., FUJITA, T. & JENSENIUS, J. C. 2004. L-ficolin is a pattern recognition molecule specific for acetyl groups. *J Biol Chem*, 279, 47513-9.

- KRARUP, A., SORENSEN, U. B., MATSUSHITA, M., JENSENIUS, J. C. & THIEL, S. 2005. Effect of capsulation of opportunistic pathogenic bacteria on binding of the pattern recognition molecules mannan-binding lectin, L-ficolin, and H-ficolin. *Infect Immun*, 73, 1052-60.
- KRISSINEL, E. 2015. CCP4 Software Suite: history, evolution, content, challenges and future developments. *Arbor: Ciencia*, 191, a220.
- KRISTO, A., UHARI, M., LUOTONEN, J., KOIVUNEN, P., ILKKO, E., TAPIAINEN, T. & ALHO, O.-P. 2003. Paranasal Sinus Findings in Children During Respiratory Infection Evaluated With Magnetic Resonance Imaging. *Pediatrics*, 111, e586-e589.
- KUNG, E., COWARD, W. R., NEILL, D. R., MALAK, H. A., MUHLEMANN, K., KADIOGLU, A., HILTY, M. & HATHAWAY, L. J. 2014. The pneumococcal polysaccharide capsule and pneumolysin differentially affect CXCL8 and IL-6 release from cells of the upper and lower respiratory tract. *PLoS One*, 9, e92355.
- KURAYA, M., MING, Z., LIU, X., MATSUSHITA, M. & FUJITA, T. 2005. Specific binding of L-ficolin and H-ficolin to apoptotic cells leads to complement activation. *Immunobiology*, 209, 689-97.
- KUROSAKA, D., LEBIEN, T. W. & PRIBYL, J. A. 1999. Comparative studies of different stromal cell microenvironments in support of human B-cell development. *Exp Hematol*, 27, 1271-81.
- LAFFLY, E., LACROIX, M., MARTIN, L., VASSAL-STERMANN, E., THIELENS, N. M. & GABORIAUD, C. 2014. Human ficolin-2 recognition versatility extended: an update on the binding of ficolin-2 to sulfated/phosphated carbohydrates. *FEBS Lett*, 588, 4694-700.
- LAGGNER, P. 2007. Life – As a Matter of Fat – The Emerging Science of Lipidomics edited by Ole G. Mouritsen. Weinheim.
- LAGOS, R., MUNOZ, A., VALENZUELA, M. T., HEITMANN, I. & LEVINE, M. M. 2002. Population-based surveillance for hospitalized and ambulatory pediatric invasive pneumococcal disease in Santiago, Chile. *Pediatr Infect Dis J*, 21, 1115-23.
- LAMBERT, P. J., WHITMAN, A. G., DYSON, O. F. & AKULA, S. M. 2006. Raman spectroscopy: the gateway into tomorrow's virology. *Viol J*, 3, 51.
- LAMBRIS, J. D., RICKLIN, D. & GEISBRECHT, B. V. 2008. Complement evasion by human pathogens. *Nat Rev Microbiol*, 6, 132-42.
- LATIFF, A. H. & KERR, M. A. 2007. The clinical significance of immunoglobulin A deficiency. *Ann Clin Biochem*, 44, 131-9.

- LAWRENCE, S. L., FEIL, S. C., MORTON, C. J., FARRAND, A. J., MULHERN, T. D., GORMAN, M. A., WADE, K. R., TWETEN, R. K. & PARKER, M. W. 2015. Crystal structure of *Streptococcus pneumoniae* pneumolysin provides key insights into early steps of pore formation. *Sci Rep*, 5, 14352.
- LAWTON, P. F., SAUNTER, C. D. & GIRKIN, J. M. Combining optical trapping in a microfluidic channel with simultaneous micro-Raman spectroscopy and motion detection. SPIE MOEMS-MEMS, 2014. International Society for Optics and Photonics, 89760V-89760V-9.
- LEFRANC, M. P. & LEFRANC, G. 2012. Human Gm, Km, and Am allotypes and their molecular characterization: a remarkable demonstration of polymorphism. *Methods Mol Biol*, 882, 635-80.
- LEI, X., LIU, C., AZADZOI, K., LI, C., LU, F., XIANG, A., SUN, J., GUO, Y., ZHAO, Q., YAN, Z. & YANG, J. 2015. A novel IgM-H-ficolin complement pathway to attack allogenic cancer cells in vitro. *Sci Rep*, 5, 7824.
- LEMIEUX, J., WOODY, S. & CAMILLI, A. 2008. Roles of the sortases of *Streptococcus pneumoniae* in assembly of the RlrA pilus. *J Bacteriol*, 190, 6002-13.
- LEUNG, C., DUDKINA, N. V., LUKOYANOVA, N., HODEL, A. W., FARABELLA, I., PANDURANGAN, A. P., JAHAN, N., PIRES DAMASO, M., OSMANOVIC, D., REBOUL, C. F., DUNSTONE, M. A., ANDREW, P. W., LONNEN, R., TOPF, M., SAIBIL, H. R. & HOOGENBOOM, B. W. 2014. Stepwise visualization of membrane pore formation by sullysin, a bacterial cholesterol-dependent cytolysin. *Elife*, 3, e04247.
- LEUSEN, J. H. 2015a. IgA as therapeutic antibody. *Mol Immunol*, 68, 35-9.
- LEVY, C., VARON, E., PICARD, C., BECHET, S., MARTINOT, A., BONACORSI, S. & COHEN, R. 2014. Trends of pneumococcal meningitis in children after introduction of the 13-valent pneumococcal conjugate vaccine in France. *Pediatr Infect Dis J*, 33, 1216-21.
- LEWIS, R. N. & MCELHANEY, R. N. 2013. Membrane lipid phase transitions and phase organization studied by Fourier transform infrared spectroscopy. *Biochim Biophys Acta*, 1828, 2347-58.
- LHERT, F., BLAUDEZ, D., HEYWANG, C. & TURLET, J. M. 2002. Free-Standing Black Films: An Alternative to Langmuir Monolayers for the Study by Raman Spectroscopy of Peptide-Phospholipid Interaction in Ultrathin Films. *Langmuir*, 18, 512-518.
- LI, C., WEN, A., SHEN, B., LU, J., HUANG, Y. & CHANG, Y. 2011. FastCloning: a highly simplified, purification-free, sequence- and ligation-independent PCR cloning method. *BMC Biotechnology*, 11, 92-92.

- LI, J., WANG, X., ZHANG, T., WANG, C., HUANG, Z., LUO, X. & DENG, Y. 2015. A review on phospholipids and their main applications in drug delivery systems. *Asian J. Pharm* 10, 81-98.
- LI, Q., LI, Y. X., DOUTHITT, K., STAHL, G. L., THURMAN, J. M. & TONG, H. H. 2012. Role of the alternative and classical complement activation pathway in complement mediated killing against *Streptococcus pneumoniae* colony opacity variants during acute pneumococcal otitis media in mice. *Microbes Infect*, 14, 1308-18.
- LI, Y., HILL, A., BEITELSHEES, M., SHAO, S. & LOVELL, J. F. 2016. Directed vaccination against pneumococcal disease. 113, 6898-903.
- LIN, H.-Y. & THOMAS, J. L. 2003. PEG-lipids and oligo (ethylene glycol) surfactants enhance the ultrasonic permeabilizability of liposomes. *Langmuir*, 19, 1098-1105.
- LIPMAN, N. S., JACKSON, L. R., TRUDEL, L. J. & WEIS-GARCIA, F. 2005. Monoclonal Versus Polyclonal Antibodies: Distinguishing Characteristics, Applications, and Information Resources. *ILAR Journal*, 46, 258-268.
- LITTMANN, M., ALBIGER, B., FRENTZEN, A., NORMARK, S., HENRIQUES-NORMARK, B. & PLANT, L. 2009. *Streptococcus pneumoniae* evades human dendritic cell surveillance by pneumolysin expression. *EMBO Mol Med*, 1, 211-22.
- LIU, H. & MAY, K. 2012. Disulfide bond structures of IgG molecules: structural variations, chemical modifications and possible impacts to stability and biological function. *MAbs*, 4, 17-23.
- LIU, J., ALI, M. A., SHI, Y., ZHAO, Y., LUO, F., YU, J., XIANG, T., TANG, J., LI, D., HU, Q., HO, W. & ZHANG, X. 2009. Specifically binding of L-ficolin to N-glycans of HCV envelope glycoproteins E1 and E2 leads to complement activation. *Cell Mol Immunol*, 6, 235-44.
- LIU, Y., ENDO, Y., IWAKI, D., NAKATA, M., MATSUSHITA, M., WADA, I., INOUE, K., MUNAKATA, M. & FUJITA, T. 2005. Human M-ficolin is a secretory protein that activates the lectin complement pathway. *J Immunol*, 175, 3150-6.
- LOMBARD, J. 2014. Once upon a time the cell membranes: 175 years of cell boundary research. *Biol Direct*, 9, 32.
- LOW, D. E. 2005. Changing trends in antimicrobial-resistant pneumococci: it's not all bad news. *Clin Infect Dis*, 41 Suppl 4, S228-33.
- LU, J., TAY, P. N., KON, O. L. & REID, K. B. 1996. Human ficolin: cDNA cloning, demonstration of peripheral blood leucocytes as the major site of synthesis and assignment of the gene to chromosome 9. *Biochem J*, 313 (Pt 2), 473-8.

- LUO, F., CHEN, T., LIU, J., SHEN, X., ZHAO, Y., YANG, R. & ZHANG, X. 2016. Ficolin-2 binds to HIV-1 gp120 and blocks viral infection. *Virology*, 31, 406-414.
- LUO, F., SUN, X., WANG, Y., WANG, Q., WU, Y., PAN, Q., FANG, C. & ZHANG, X. L. 2013. Ficolin-2 defends against virulent Mycobacteria tuberculosis infection in vivo, and its insufficiency is associated with infection in humans. *PLoS One*, 8, e73859.
- LUZ, P. R., BOLDT, A. B., GRISBACH, C., KUN, J. F., VELAVAN, T. P. & MESSIAS-REASON, I. J. 2013. Association of L-ficolin levels and FCN2 genotypes with chronic Chagas disease. *PLoS One*, 8, e60237.
- LYNCH, N. J., ROSCHER, S., HARTUNG, T., MORATH, S., MATSUSHITA, M., MAENNEL, D. N., KURAYA, M., FUJITA, T. & SCHWAEBLE, W. J. 2004. L-ficolin specifically binds to lipoteichoic acid, a cell wall constituent of Gram-positive bacteria, and activates the lectin pathway of complement. *J Immunol*, 172, 1198-202.
- MA, Y. G., CHO, M. Y., ZHAO, M., PARK, J. W., MATSUSHITA, M., FUJITA, T. & LEE, B. L. 2004. Human mannose-binding lectin and L-ficolin function as specific pattern recognition proteins in the lectin activation pathway of complement. *J Biol Chem*, 279, 25307-12.
- MAGARKAR, A., DHAWAN, V., KALLINTERI, P., VIITALA, T., ELMOWAFY, M., ROG, T. & BUNKER, A. 2014. Cholesterol level affects surface charge of lipid membranes in saline solution. *Sci Rep*, 4, 5005.
- MALHOTRA-KUMAR, S., LAMMENS, C., COENEN, S., VAN HERCK, K. & GOOSSENS, H. 2007. Effect of azithromycin and clarithromycin therapy on pharyngeal carriage of macrolide-resistant streptococci in healthy volunteers: a randomised, double-blind, placebo-controlled study. *Lancet*, 369, 482-90.
- MANDELL, L. A. 2015. Community-acquired pneumonia: An overview. *Postgrad Med*, 127, 607-15.
- MARSHALL, J. E., FARAJ, B. H., GINGRAS, A. R., LONNEN, R., SHEIKH, M. A., EL-MEZGUELDI, M., MOODY, P. C., ANDREW, P. W. & WALLIS, R. 2015. The Crystal Structure of Pneumolysin at 2.0 Å Resolution Reveals the Molecular Packing of the Pre-pore Complex. *Sci Rep*, 5, 13293.
- MARTNER, A., DAHLGREN, C., PATON, J. C. & WOLD, A. E. 2008. Pneumolysin released during Streptococcus pneumoniae autolysis is a potent activator of intracellular oxygen radical production in neutrophils. *Infect Immun*, 76, 4079-87.
- MARTNER, A., SKOVBJERG, S., PATON, J. C. & WOLD, A. E. 2009. Streptococcus pneumoniae autolysis prevents phagocytosis and production of phagocyte-activating cytokines. *Infect Immun*, 77, 3826-37.

- MASON, C. P. & TARR, A. W. 2015. Human lectins and their roles in viral infections. *Molecules*, 20, 2229-71.
- MATSUSHITA, M. 2010. Ficolins: complement-activating lectins involved in innate immunity. *J Innate Immun*, 2, 24-32.
- MATSUSHITA, M., ENDO, Y. & FUJITA, T. 2013. Structural and functional overview of the lectin complement pathway: its molecular basis and physiological implication. *Arch Immunol Ther Exp (Warsz)*, 61, 273-83.
- MATSUSHITA, M., ENDO, Y., TAIRA, S., SATO, Y., FUJITA, T., ICHIKAWA, N., NAKATA, M. & MIZUOCHI, T. 1996. A novel human serum lectin with collagen- and fibrinogen-like domains that functions as an opsonin. *J Biol Chem*, 271, 2448-54.
- MATSUSHITA, M. & FUJITA, T. 2001. Ficolins and the lectin complement pathway. *Immunol Rev*, 180, 78-85.
- MATSUSHITA, M., KURAYA, M., HAMASAKI, N., TSUJIMURA, M., SHIRAKI, H. & FUJITA, T. 2002. Activation of the lectin complement pathway by H-ficolin (Hakata antigen). *J Immunol*, 168, 3502-6.
- MCCOMBS, J. E. & KOHLER, J. J. 2016. Pneumococcal Neuraminidase Substrates Identified through Comparative Proteomics Enabled by Chemoselective Labeling. *Bioconjug Chem*, 27, 1013-22.
- MCGEE, L., MCDUGAL, L., ZHOU, J., SPRATT, B. G., TENOVER, F. C., GEORGE, R., HAKENBECK, R., HRYNIEWICZ, W., LEFEVRE, J. C., TOMASZ, A. & KLUGMAN, K. P. 2001. Nomenclature of major antimicrobial-resistant clones of *Streptococcus pneumoniae* defined by the pneumococcal molecular epidemiology network. *J Clin Microbiol*, 39, 2565-71.
- MCPHERSON, A. & GAVIRA, J. A. 2014. Introduction to protein crystallization. *Acta Crystallogr F Struct Biol Commun*, 70, 2-20.
- MELIS, J. P., STRUMANE, K., RUULS, S. R., BEURSKENS, F. J., SCHUURMAN, J. & PARREN, P. W. 2015. Complement in therapy and disease: Regulating the complement system with antibody-based therapeutics. *Mol Immunol*, 67, 117-30.
- MELLROTH, P., DANIELS, R., EBERHARDT, A., RONNLUND, D., BLOM, H., WIDENGREN, J., NORMARK, S. & HENRIQUES-NORMARK, B. 2012. LytA, major autolysin of *Streptococcus pneumoniae*, requires access to nascent peptidoglycan. *J Biol Chem*, 287, 11018-29.
- MENESTRINA, G. 1988. *Escherichia coli* hemolysin permeabilizes small unilamellar vesicles loaded with calcein by a single-hit mechanism. *FEBS letters*, 232, 217-220.

- MEYTS, I., BOSSUYT, X., PROESMANS, M. & DE, B. 2006. Isolated IgG3 deficiency in children: to treat or not to treat? Case presentation and review of the literature. *Pediatr Allergy Immunol*, 17, 544-50.
- MICHAELSEN, T. E., FRANGIONE, B. & FRANKLIN, E. C. 1977. Primary structure of the "hinge" region of human IgG3. Probable quadruplication of a 15-amino acid residue basic unit. *J Biol Chem*, 252, 883-9.
- MICHAELSEN, T. E., GARRED, P. & AASE, A. 1991. Human IgG subclass pattern of inducing complement-mediated cytolysis depends on antigen concentration and to a lesser extent on epitope patchiness, antibody affinity and complement concentration. *Eur J Immunol*, 21, 11-6.
- MICHAELSEN, T. E., SANDLIE, I., BRATLIE, D. B., SANDIN, R. H. & IHLE, O. 2009. Structural difference in the complement activation site of human IgG1 and IgG3. *Scand J Immunol*, 70, 553-64.
- MIMURA, Y., CHURCH, S., GHIRLANDO, R., ASHTON, P. R., DONG, S., GOODALL, M., LUND, J. & JEFFERIS, R. 2000. The influence of glycosylation on the thermal stability and effector function expression of human IgG1-Fc: properties of a series of truncated glycoforms. *Mol Immunol*, 37, 697-706.
- MIMURA, Y., SONDERMANN, P., GHIRLANDO, R., LUND, J., YOUNG, S. P., GOODALL, M. & JEFFERIS, R. 2001. Role of oligosaccharide residues of IgG1-Fc in Fc gamma RIIb binding. *J Biol Chem*, 276, 45539-47.
- MITCHELL, A. M. & MITCHELL, T. J. 2010. Streptococcus pneumoniae: virulence factors and variation. *Clin Microbiol Infect*, 16, 411-8.
- MITCHELL, T. J., ALEXANDER, J. E., MORGAN, P. J. & ANDREW, P. W. 1997. Molecular analysis of virulence factors of Streptococcus pneumoniae. *Soc Appl Bacteriol Symp Ser*, 26, 62s-71s.
- MITCHELL, T. J., ANDREW, P. W., SAUNDERS, F. K., SMITH, A. N. & BOULNOIS, G. J. 1991. Complement activation and antibody binding by pneumolysin via a region of the toxin homologous to a human acute-phase protein. *Mol Microbiol*, 5, 1883-8.
- MOGENSEN, T. H. 2009. Pathogen recognition and inflammatory signaling in innate immune defenses. *Clin Microbiol Rev*, 22, 240-73.
- MORGAN, P. J., HYMAN, S. C., BYRON, O., ANDREW, P. W., MITCHELL, T. J. & ROWE, A. J. 1994. Modeling the bacterial protein toxin, pneumolysin, in its monomeric and oligomeric form. *J Biol Chem*, 269, 25315-20.
- MORGAN, P. J., VARLEY, P. G., ROWE, A. J., ANDREW, P. W. & MITCHELL, T. J. 1993. Characterization of the solution properties and conformation of pneumolysin, the membrane-damaging toxin of Streptococcus pneumoniae. *Biochem J*, 296 (Pt 3), 671-4.

- MUKERJI, R., MIRZA, S., ROCHE, A. M., WIDENER, R. W., CRONEY, C. M., RHEE, D. K., WEISER, J. N., SZALAI, A. J. & BRILES, D. E. 2012. Pneumococcal surface protein A inhibits complement deposition on the pneumococcal surface by competing with the binding of C-reactive protein to cell-surface phosphocholine. *J Immunol*, 189, 5327-35.
- MUNISHKINA, L. A. & FINK, A. L. 2007. Fluorescence as a method to reveal structures and membrane-interactions of amyloidogenic proteins. *Biochim Biophys Acta*, 1768, 1862-85.
- MUNTHER-FOG, L., HUMMELSHOJ, T., HONORE, C., MOLLER, M. E., SKJOEDT, M. O., PALSGAARD, I., BORREGAARD, N., MADSEN, H. O. & GARRED, P. 2012. Variation in FCN1 affects biosynthesis of ficolin-1 and is associated with outcome of systemic inflammation. *Genes Immun*, 13, 515-22.
- NAGARAJAN, S., SCHULER, E. E., MA, K., KINDT, J. T. & DYER, R. B. 2012. Dynamics of the gel to fluid phase transformation in unilamellar DPPC vesicles. *J Phys Chem B*, 116, 13749-56.
- NALLAMSETTY, S., AUSTIN, B. P., PENROSE, K. J. & WAUGH, D. S. 2005. Gateway vectors for the production of combinatorially-tagged His6-MBP fusion proteins in the cytoplasm and periplasm of Escherichia coli. *Protein Sci*, 14, 2964-71.
- NAUMANN, C., BRUMM, T. & BAYERL, T. M. 1992. Phase transition behavior of single phosphatidylcholine bilayers on a solid spherical support studied by DSC, NMR and FT-IR. *Biophys J*, 63, 1314-9.
- NGO, C. C., MASSA, H. M., THORNTON, R. B. & CRIPPS, A. W. 2016. Predominant Bacteria Detected from the Middle Ear Fluid of Children Experiencing Otitis Media: A Systematic Review. *PLoS One*, 11, 0150949.
- NICOLSON, G. L. 2014. The Fluid-Mosaic Model of Membrane Structure: still relevant to understanding the structure, function and dynamics of biological membranes after more than 40 years. *Biochim Biophys Acta*, 1838, 1451-66.
- NILSSON, P. & LAURELL, M. H. 2001. Carriage of penicillin-resistant Streptococcus pneumoniae by children in day-care centers during an intervention program in Malmo, Sweden. *Pediatr Infect Dis J*, 20, 1144-9.
- NOLLMANN, M., GILBERT, R., MITCHELL, T., SFERRAZZA, M. & BYRON, O. 2004. The role of cholesterol in the activity of pneumolysin, a bacterial protein toxin. *Biophys J*, 86, 3141-51.
- NOTERMAN, H. & NURMIO, A. 2016. Infectious diseases in children and treatment at home: Guidebook for parents.

- NUORTI, J. P. & WHITNEY, C. G. 2010. Prevention of pneumococcal disease among infants and children - use of 13-valent pneumococcal conjugate vaccine and 23-valent pneumococcal polysaccharide vaccine - recommendations of the Advisory Committee on Immunization Practices (ACIP). *MMWR Recomm Rep*, 59, 1-18.
- O'BRIEN, K. L., WOLFSON, L. J., WATT, J. P., HENKLE, E., DELORIA-KNOLL, M., MCCALL, N., LEE, E., MULHOLLAND, K., LEVINE, O. S. & CHERIAN, T. 2009. Burden of disease caused by *Streptococcus pneumoniae* in children younger than 5 years: global estimates. *Lancet*, 374, 893-902.
- O'GRADY, K.-A. F., GRIMWOOD, K., CRIPPS, A., MULHOLLAND, E. K., MORRIS, P., TORZILLO, P. J., WOOD, N., SMITH-VAUGHAN, H., REVELL, A. & WILSON, A. 2013. Does a 10-valent pneumococcal-Haemophilus influenzae protein D conjugate vaccine prevent respiratory exacerbations in children with recurrent protracted bacterial bronchitis, chronic suppurative lung disease and bronchiectasis: protocol for a randomised controlled trial. *Trials*, 14, 1.
- OBARO, S. & ADEGBOLA, R. 2002. The pneumococcus: carriage, disease and conjugate vaccines. *J Med Microbiol*, 51, 98-104.
- OHASHI, T. & ERICKSON, H. P. 1998. Oligomeric structure and tissue distribution of ficolins from mouse, pig and human. *Arch Biochem Biophys*, 360, 223-32.
- OHNO-IWASHITA, Y., IWAMOTO, M., MITSUI, K., ANDO, S. & NAGAI, Y. 1988. Protease-nicked theta-toxin of *Clostridium perfringens*, a new membrane probe with no cytolytic effect, reveals two classes of cholesterol as toxin-binding sites on sheep erythrocytes. *Eur J Biochem*, 176, 95-101.
- PALMER, M., HARRIS, R., FREYTAG, C., KEHOE, M., TRANUM-JENSEN, J. & BHAKDI, S. 1998. Assembly mechanism of the oligomeric streptolysin O pore: the early membrane lesion is lined by a free edge of the lipid membrane and is extended gradually during oligomerization. *Embo j*, 17, 1598-605.
- PALMU, A. A., VERHO, J., JOKINEN, J., KARMA, P. & KILPI, T. M. 2004. The seven-valent pneumococcal conjugate vaccine reduces tympanostomy tube placement in children. *Pediatr Infect Dis J*, 23, 732-8.
- PAN, Q., CHEN, H., WANG, F., JEZA, V. T., HOU, W., ZHAO, Y., XIANG, T., ZHU, Y., ENDO, Y., FUJITA, T. & ZHANG, X. L. 2012. L-ficolin binds to the glycoproteins hemagglutinin and neuraminidase and inhibits influenza A virus infection both in vitro and in vivo. *J Innate Immun*, 4, 312-24.
- PANGBURN, M. K. & MULLER-EBERHARD, H. J. 1986. The C3 convertase of the alternative pathway of human complement. Enzymic properties of the bimolecular proteinase. *Biochem J*, 235, 723-30.

- PATERSON, G. K. & ORIHUELA, C. J. 2010. Pneumococci: immunology of the innate host response. *Respirology*, 15, 1057-63.
- PATON, J. C., LOCK, R. A. & HANSMAN, D. J. 1983. Effect of immunization with pneumolysin on survival time of mice challenged with *Streptococcus pneumoniae*. *Infect Immun*, 40, 548-52.
- PATON, J. C., ROWAN-KELLY, B. & FERRANTE, A. 1984. Activation of human complement by the pneumococcal toxin pneumolysin. *Infect Immun*, 43, 1085-7.
- PILISHVILI, T. & BENNETT, N. M. 2015. Pneumococcal disease prevention among adults: Strategies for the use of pneumococcal vaccines. *Vaccine*, 33, D60-D65.
- PLEASS, R. J., MOORE, S. C., STEVENSON, L. & HVIID, L. 2016. Immunoglobulin M: Restrainer of Inflammation and Mediator of Immune Evasion by *Plasmodium falciparum* Malaria. *Trends Parasitol*, 32, 108-19.
- POLLARD, A. J., NADEL, S., NINIS, N., FAUST, S. N. & LEVIN, M. 2007. Emergency management of meningococcal disease: eight years on. *Arch Dis Child*, 92, 283-6.
- POOLE, J. A. & ROSENWASSER, L. J. 2005. The role of immunoglobulin E and immune inflammation: implications in allergic rhinitis. *Curr Allergy Asthma Rep*, 5, 252-8.
- POUGET, J. P., LAUNOIS, H., D'HAENENS, J. P., MERENDA, P. & RICE, T. M. 1975. Electron Localization Induced by Uniaxial Stress in Pure V O 2. *Physical Review Letters*, 35, 873-875.
- PRACHT, D., ELM, C., GERBER, J., BERGMANN, S., ROHDE, M., SEILER, M., KIM, K. S., JENKINSON, H. F., NAU, R. & HAMMERSCHMIDT, S. 2005. PavA of *Streptococcus pneumoniae* modulates adherence, invasion, and meningeal inflammation. *Infect Immun*, 73, 2680-9.
- PRICE, K. E. & CAMILLI, A. 2009. Pneumolysin localizes to the cell wall of *Streptococcus pneumoniae*. *J Bacteriol*, 191, 2163-8.
- PRICE, K. E., GREENE, N. G. & CAMILLI, A. 2012. Export requirements of pneumolysin in *Streptococcus pneumoniae*. *J Bacteriol*, 194, 3651-60.
- PRINCIPI, N. & ESPOSITO, S. 2016. Prevention of Community-Acquired Pneumonia with Available Pneumococcal Vaccines. *Int J Mol Sci*, 18.
- PRINCIPI, N. & ESPOSITO, S. 2016. Prevention of Community-Acquired Pneumonia with Available Pneumococcal Vaccines. *Int J Mol Sci*, 18.30.
- QORONFLEH, M. W., HESTERBERG, L. K. & SEEFELDT, M. B. 2007. Confronting high-throughput protein refolding using high pressure and solution screens. *Protein Expr Purif*, 55, 209-24.

- QUREISHI, A., LEE, Y., BELFIELD, K., BIRCHALL, J. P. & DANIEL, M. 2014. Update on otitis media - prevention and treatment. *Infect Drug Resist*, 7, 15-24.
- RACINE, R. & WINSLOW, G. M. 2009. IgM in microbial infections: taken for granted? *Immunol Lett*, 125, 79-85.
- RAI, P., HE, F., KWANG, J., ENGELWARD, B. P. & CHOW, V. T. 2016. Pneumococcal Pneumolysin Induces DNA Damage and Cell Cycle Arrest. *Sci Rep*, 6, 22972.
- RAJAN, S., GAZZALI, P. M. & CHANDRASEKARAN, G. 2017. Impact of Fe on structural modification and room temperature magnetic ordering in BaTiO₃. *Spectrochim Acta A Mol Biomol Spectrosc*, 171, 80-89.
- RAMACHANDRAN, R., HEUCK, A. P., TWETEN, R. K. & JOHNSON, A. E. 2002. Structural insights into the membrane-anchoring mechanism of a cholesterol-dependent cytolysin. *Nat Struct Biol*, 9, 823-7.
- RANDLE, E., NINIS, N. & INWALD, D. 2011. Invasive pneumococcal disease. *Archives of disease in childhood - Education & practice edition*, 96, 183.
- RASHID, F., SHARMA, S. & BANO, B. 2005. Comparison of guanidine hydrochloride (GdnHCl) and urea denaturation on inactivation and unfolding of human placental cystatin (HPC). *Protein J*, 24, 283-292.
- REDDING, B., SCHWAB, M. & PAN, Y.-L. 2015. Raman Spectroscopy of Optically Trapped Single Biological Micro-Particles. *Sensors (Basel, Switzerland)*, 15, 19021-19046.
- REDPATH, S., MICHAELSEN, T., SANDLIE, I. & CLARK, M. R. 1998. Activation of complement by human IgG1 and human IgG3 antibodies against the human leucocyte antigen CD52. *Immunol*, 93, 595-600.
- REYNOLDS, C. A., FINKELSTEIN, J. A., RAY, G. T., MOORE, M. R. & HUANG, S. S. 2014. Attributable healthcare utilization and cost of pneumonia due to drug-resistant streptococcus pneumonia: a cost analysis. *Antimicrob Resist Infect Control*, 3, 16.
- RICHARD, L. M. 2001. Raman spectroscopy for chemical analysis. *Meas. Sci. Technol.* 12, 653-654.
- RICKLIN, D., HAJISHENGALLIS, G., YANG, K. & LAMBRIS, J. D. 2010. Complement: a key system for immune surveillance and homeostasis. *Nat Immunol*, 11, 785-97.
- ROGERS, K. A., RICHARDSON, J. P., SCINICARIELLO, F. & ATTANASIO, R. 2006. Molecular characterization of immunoglobulin D in mammals:

- immunoglobulin heavy constant delta genes in dogs, chimpanzees and four old world monkey species. *Immunol*, 118, 88-100.
- ROJKO, N. & ANDERLUH, G. 2015. How Lipid Membranes Affect Pore Forming Toxin Activity. *Acc Chem Res*, 48, 3073-9.
- ROOS, A., BOUWMAN, L. H., VAN GIJLSWIJK-JANSSEN, D. J., FABER-KROL, M. C., STAHL, G. L. & DAHA, M. R. 2001. Human IgA activates the complement system via the mannan-binding lectin pathway. *Journal of immunology (Baltimore, Md. : 1950)*, 167, 2861.
- ROSBJERG, A., MUNTHE-FOG, L., GARRED, P. & SKJOEDT, M. O. 2014. Heterocomplex formation between MBL/ficolin/CL-11-associated serine protease-1 and -3 and MBL/ficolin/CL-11-associated protein-1. *J Immunol*, 192, 4352-60.
- ROSSJOHN, J., FEIL, S. C., MCKINSTY, W. J., TWETEN, R. K. & PARKER, M. W. 1997. Structure of a cholesterol-binding, thiol-activated cytolysin and a model of its membrane form. *Cell*, 89, 685-92.
- ROSSJOHN, J., GILBERT, R. J., CRANE, D., MORGAN, P. J., MITCHELL, T. J., ROWE, A. J., ANDREW, P. W., PATON, J. C., TWETEN, R. K. & PARKER, M. W. 1998. The molecular mechanism of pneumolysin, a virulence factor from *Streptococcus pneumoniae*. *J Mol Biol*, 284, 449-61.
- ROSTENBERG, I. & PENALOZA, R. 1978. Serum IgG and IgD and levels in some infectious and noninfectious diseases. *Clin Chim Acta*, 85, 319-21.
- RUDAN, I., BOSCHI-PINTO, C., BILOGLAV, Z., MULHOLLAND, K. & CAMPBELL, H. 2008. Epidemiology and etiology of childhood pneumonia. *Bull World Health Organ*, 86, 408-16.
- RUNZA, V. L., HEHLGANS, T., ECHTENACHER, B., ZAHRINGER, U., SCHWAEBLE, W. J. & MANNEL, D. N. 2006. Localization of the mouse defense lectin ficolin B in lysosomes of activated macrophages. *J Endotoxin Res*, 12, 120-6.
- RUSKAMP, J. M., HOEKSTRA, M. O., POSTMA, D. S., KERKHOF, M., BOTTEMA, R. W., KOPPELMAN, G. H., ROVERS, M. M., WIJGA, A. H., DE JONGSTE, J. C., BRUNEKREEF, B. & SANDERS, E. A. 2009. Exploring the role of polymorphisms in ficolin genes in respiratory tract infections in children. *Clin Exp Immunol*, 155, 433-40.
- SAHU, A., KOZEL, T. R. & PANGBURN, M. K. 1994. Specificity of the thioester-containing reactive site of human C3 and its significance to complement activation. *Biochem J*, 302 (Pt 2), 429-336.

- SAINT-MICHEL, B., DUBRULLE, B., MARIÉ, L., RAVELET, F. & DAVIAUD, F. 2014. Influence of reynolds number and forcing type in a turbulent von kármán flow. *New J. Phys*, 16, 063037.
- SAMBROOK, J. & RUSSELL, D. W. 2001. *Molecular cloning: a laboratory manual*, Cold Spring Harbor, N.Y, Cold Spring Harbor Laboratory Press.
- SANDERSON, J. M. & WARD, A. D. 2004. Analysis of liposomal membrane composition using Raman tweezers. *Chem Commun (Camb)*, 1120-1.
- SANDGREN, A., SJOSTROM, K., OLSSON-LILJEQUIST, B., CHRISTENSSON, B., SAMUELSSON, A., KRONVALL, G. & HENRIQUES NORMARK, B. 2004. Effect of clonal and serotype-specific properties on the invasive capacity of *Streptococcus pneumoniae*. *J Infect Dis*, 189, 785-96.
- SASSI, P., CAPONI, S., RICCI, M., MORRESI, A., OLDENHOF, H., WOLKERS, W. F. & FIORETTO, D. 2015. Infrared versus light scattering techniques to monitor the gel to liquid crystal phase transition in lipid membranes. *J. Raman Spectrosc*, 46, 644-51.
- SCHAEFER, J. J., MA, C. & HARRIS, J. M. 2012. Confocal Raman microscopy probing of temperature-controlled release from individual, optically-trapped phospholipid vesicles. *Anal Chem*, 84, 9505-12.
- SCHAFFER, T., FLOGERZI, B., SCHOEPFER, A. M., SEIBOLD, F. & MULLER, S. 2013. Increased titers of anti-*Saccharomyces cerevisiae* antibodies in Crohn's disease patients with reduced H-ficolin levels but normal MASP-2 activity. *J Crohns Colitis*, 7, e1-10.
- SCHECK, F. 2013. *Quantum physics*, Berlin, Springer.
- SCHMIDT, K. & MUELLER-ECKHARDT, C. 1973. Antinuclear autoantibodies of IgD class. An analysis of 82 patients. *Z Immunitätsforsch Exp Klin Immunol*, 145, 385-91.
- SCHROEDER JR, H. W. 2010. Structure and function of immunoglobulins. *J Allergy Clin Immunol*, 125, S41-S52.
- SCHROEDER, M. R. & STEPHENS, D. S. 2016. Macrolide Resistance in *Streptococcus pneumoniae*. *Front Cell Infect Microbiol*, 6.
- SELMAN, L. & HANSEN, S. 2012. Structure and function of collectin liver 1 (CL-L1) and collectin 11 (CL-11, CL-K1). *Immunobiology*, 217, 851-863.
- SERCOMBE, L., VEERATI, T., MOHEIMANI, F., WU, S. Y., SOOD, A. K. & HUA, S. 2015. Advances and Challenges of Liposome Assisted Drug Delivery. *Front Pharmacol*, 6, 286.

- SHATURSKY, O., HEUCK, A. P., SHEPARD, L. A., ROSSJOHN, J., PARKER, M. W., JOHNSON, A. E. & TWETEN, R. K. 1999. The mechanism of membrane insertion for a cholesterol-dependent cytolysin: a novel paradigm for pore-forming toxins. *Cell*, 99, 293-9.
- SHENOY, A. T. & ORIHUELA, C. J. 2016. Anatomical site-specific contributions of pneumococcal virulence determinants. *Pneumonia (Nathan)*, 8.
- SHEPARD, L. A., HEUCK, A. P., HAMMAN, B. D., ROSSJOHN, J., PARKER, M. W., RYAN, K. R., JOHNSON, A. E. & TWETEN, R. K. 1998. Identification of a membrane-spanning domain of the thiol-activated pore-forming toxin *Clostridium perfringens* perfringolysin O: an alpha-helical to beta-sheet transition identified by fluorescence spectroscopy. *Biochemistry*, 37, 14563.
- SHEPARD, L. A., SHATURSKY, O., JOHNSON, A. E. & TWETEN, R. K. 2000. The mechanism of pore assembly for a cholesterol-dependent cytolysin: formation of a large prepore complex precedes the insertion of the transmembrane beta-hairpins. *Biochemistry*, 39, 10284-93.
- SHEWELL, L. K., HARVEY, R. M., HIGGINS, M. A., DAY, C. J., HARTLEY-TASSELL, L. E., CHEN, A. Y., GILLEN, C. M., JAMES, D. B., ALONZO, F., 3RD, TORRES, V. J., WALKER, M. J., PATON, A. W., PATON, J. C. & JENNINGS, M. P. 2014. The cholesterol-dependent cytolysins pneumolysin and streptolysin O require binding to red blood cell glycans for hemolytic activity. *Proc Natl Acad Sci U S A*, 111, E5312-20.
- SHOMA, S., TSUCHIYA, K., KAWAMURA, I., NOMURA, T., HARA, H., UCHIYAMA, R., DAIM, S. & MITSUYAMA, M. 2008. Critical involvement of pneumolysin in production of interleukin-1alpha and caspase-1-dependent cytokines in infection with *Streptococcus pneumoniae* in vitro: a novel function of pneumolysin in caspase-1 activation. *Infect Immun*, 76, 1547-57.
- SIEMIENIUK, R. A., MEADE, M. O., ALONSO-COELLO, P., BRIEL, M., EVANIEW, N., PRASAD, M., ALEXANDER, P. E., FEI, Y., VANDVIK, P. O., LOEB, M. & GUYATT, G. H. 2015. Corticosteroid Therapy for Patients Hospitalized With Community-Acquired Pneumonia: A Systematic Review and Meta-analysis. *Ann Intern Med*, 163, 519-28.
- SIMONSEN, L., TAYLOR, R. J., YOUNG-XU, Y., HABER, M., MAY, L. & KLUGMAN, K. P. 2011. Impact of pneumococcal conjugate vaccination of infants on pneumonia and influenza hospitalization and mortality in all age groups in the United States. *MBio*, 2, e00309-10.
- SIRE, J., AUFRAY, C. & JORDAN, B. R. 1982. Rat immunoglobulin delta heavy chain gene: nucleotide sequence derived from cloned cDNA. *Gene*, 20, 377-86.
- SKOV SORENSEN, U. B., YAO, K., YANG, Y., TETTELIN, H. & KILIAN, M. 2016. Capsular Polysaccharide Expression in Commensal *Streptococcus* Species: Genetic and Antigenic Similarities to *Streptococcus pneumoniae*. 7.

- SMATHERS, R. L., CHIANG, D. J., MCMULLEN, M. R., FELDSTEIN, A. E., ROYCHOWDHURY, S. & NAGY, L. E. 2016. Soluble IgM links apoptosis to complement activation in early alcoholic liver disease in mice. *Mol Immunol*, 72, 9-18.
- SMITH, A., JOHNSTON, C., INVERARITY, D., SLACK, M., PATERSON, G. K., DIGGLE, M. & MITCHELL, T. 2013. Investigating the role of pneumococcal neuraminidase A activity in isolates from pneumococcal haemolytic uraemic syndrome. *J Med Microbiol*, 62, 1735-42.
- SNYDER, R., STRAUSS, H. & ELLIGER, C. 1982. Carbon-hydrogen stretching modes and the structure of n-alkyl chains. 1. Long, disordered chains. *J. Phys. Chem*, 86, 5145-5150.
- SNYDER, R. G., HSU, S. L. & KRIMM, S. 1978. Vibrational spectra in the CH stretching region and the structure of the polymethylene chain. *Spectrochimica Acta Part A: Molecular Spectroscopy*, 34, 395-406.
- SOLOVYOVA, A. S., NOLLMANN, M., MITCHELL, T. J. & BYRON, O. 2004. The solution structure and oligomerization behavior of two bacterial toxins: pneumolysin and perfringolysin O. *Biophys J*, 87, 540-52.
- SONG, J. Y., EUN, B. W. & NAHM, M. H. 2013. Diagnosis of Pneumococcal Pneumonia: Current Pitfalls and the Way Forward. *Infect Chemother*, 45, 351-366.
- SONNEN, A. F., PLITZKO, J. M. & GILBERT, R. J. 2014. Incomplete pneumolysin oligomers form membrane pores. *Open Biol*, 4, 140044.
- SOSONIUK, E., VALLEJOS, G., KENAWY, H., GABORIAUD, C., THIELENS, N., FUJITA, T., SCHWAEBLE, W., FERREIRA, A. & VALCK, C. 2014. Trypanosoma cruzi calreticulin inhibits the complement lectin pathway activation by direct interaction with L-Ficolin. *Mol Immunol*, 60, 80-5.
- SQUIRES, T. & QUAKE, S. 2005. Microfluidics: Fluid physics at the nanoliter scale. *Reviews of Modern Physics*, 77, 977-1026.
- SRIVASTAVA, A., HENNEKE, P., VISINTIN, A., MORSE, S. C., MARTIN, V., WATKINS, C., PATON, J. C., WESSELS, M. R., GOLENBOCK, D. T. & MALLEY, R. 2005. The apoptotic response to pneumolysin is Toll-like receptor 4 dependent and protects against pneumococcal disease. *Infect Immun*, 73, 6479-87.
- STEVENS, D. L. & KAPLAN, E. L. 2000. Streptococcal infections: clinical aspects, microbiology, and molecular pathogenesis, Oxford University Press, USA.

- STOCKMANN, C., AMPOFO, K., BYINGTON, C. L., FILLOUX, F., HERSH, A. L., BLASCHKE, A. J., COWAN, P., KORGENSKI, K., MASON, E. O. & PAVIA, A. T. 2013. Pneumococcal meningitis in children: epidemiology, serotypes, and outcomes from 1997-2010 in Utah. *Pediatrics*, 132, 421-8.
- STONE, K. D., PRUSSIN, C. & METCALFE, D. D. 2010. IgE, mast cells, basophils, and eosinophils. *J Allergy Clin Immunol*, 125, S73-80.
- STOOP, J. W., ZEGERS, B. J., SANDER, P. C. & BALLIEUX, R. E. 1969. Serum immunoglobulin levels in healthy children and adults. *Clin Exp Immunol*, 4, 101-12.
- SUN, T., HOU, H., LU, J., XU, M., GU, T., WANG, D., DONG, Y., JIANG, C., KONG, W. & WU, Y. 2015. Detection and comparison of structure and function of wild-type pneumolysin and its novel mutant PlyM2. *Chem Res Chin Univ*, 31, 553-557.
- SUROVTSEV, N. V. & DZUBA, S. A. 2014. Flexibility of phospholipids with saturated and unsaturated chains studied by Raman scattering: The effect of cholesterol on dynamical and phase transitions. *J. Chem. Phys.* 140.
- TANIO, M., KONDO, S., SUGIO, S. & KOHNO, T. 2007. Trivalent recognition unit of innate immunity system: crystal structure of trimeric human M-ficolin fibrinogen-like domain. *J Biol Chem*, 282, 3889-95.
- TAO, M. H., SMITH, R. I. & MORRISON, S. L. 1993. Structural features of human immunoglobulin G that determine isotype-specific differences in complement activation. *J Exp Med*, 178, 661-7.
- TEH, C., LE, Y., LEE, S. H. & LU, J. 2000. M-ficolin is expressed on monocytes and is a lectin binding to N-acetyl-D-glucosamine and mediates monocyte adhesion and phagocytosis of Escherichia coli. *Immunology*, 101, 225-32.
- TEHRANIROKH, M., KOUZANI, A. Z., FRANCIS, P. S. & KANWAR, J. R. 2013. Microfluidic devices for cell cultivation and proliferation. *Biomicrofluidics*, 7, 51502.
- THIELENS, N. M., CSEH, S., THIEL, S., VORUP-JENSEN, T., ROSSI, V., JENSENIUS, J. C. & ARLAUD, G. J. 2001. Interaction properties of human mannan-binding lectin (MBL)-associated serine proteases-1 and -2, MBL-associated protein 19, and MBL. *J. Immunol*, 166, 5068-77.
- TIAN, X., LANGKILDE, A. E., THOROLFSSON, M., RASMUSSEN, H. B. & VESTERGAARD, B. 2014. Small-angle x-ray scattering screening complements conventional biophysical analysis: comparative structural and biophysical analysis of monoclonal antibodies IgG1, IgG2, and IgG4. *J Pharm Sci*, 103, 1701-10.

- TILLEY, S. J., ORLOVA, E. V., GILBERT, R. J. C., ANDREW, P. W. & SAIBIL, H. R. 2005. Structural Basis of Pore Formation by the Bacterial Toxin Pneumolysin. *Cell*, 121, 247-256.
- TOMASZ, A. & SAUKKONEN, K. 1989. The nature of cell wall-derived inflammatory components of pneumococci. *Pediatr Infect Dis J*, 8, 902-3.
- TON-THAT, H., LIU, G., MAZMANIAN, S. K., FAULL, K. F. & SCHNEEWIND, O. 1999. Purification and characterization of sortase, the transpeptidase that cleaves surface proteins of *Staphylococcus aureus* at the LPXTG motif. *Proc Natl Acad Sci U S A*, 96, 12424-9.
- TSAI, Y. H., HSIEH, M. J., CHANG, C. J., WEN, Y. W., HU, H. C., CHAO, Y. N., HUANG, Y. C., YANG, C. T. & HUANG, C. C. 2015. The 23-valent pneumococcal polysaccharide vaccine is effective in elderly adults over 75 years old--Taiwan's PPV vaccination program. *Vaccine*, 33, 2897-902.
- TU, A.-H. T., FULGHAM, R. L., MCCRORY, M. A., BRILES, D. E. & SZALAI, A. J. 1999. Pneumococcal Surface Protein A Inhibits Complement Activation by *Streptococcus pneumoniae*. *Infect Immun*, 67, 4720-24.
- TURKYILMAZ, S., ALMEIDA, P. F. & REGEN, S. L. 2011. Effects of isoflurane, halothane, and chloroform on the interactions and lateral organization of lipids in the liquid-ordered phase. *Langmuir*, 27, 14380-5.
- TWETEN, R. K. 2005. Cholesterol-dependent cytolysins, a family of versatile pore-forming toxins. *Infect Immun*, 73, 6199-209.
- TWETEN, R. K., HOTZE, E. M. & WADE, K. R. 2015. The Unique Molecular Choreography of Giant Pore Formation by the Cholesterol-Dependent Cytolysins of Gram-Positive Bacteria. *Annu Rev Microbiol*, 69, 323-40.
- UBELHART, R., HUG, E., BACH, M. P., WOSSNING, T., DUHREN-VON MINDEN, M., HORN, A. H., TSIANTOULAS, D., KOMETANI, K., KUROSAKI, T., BINDER, C. J., STICHT, H., NITSCHKE, L., RETH, M. & JUMAA, H. 2015. Responsiveness of B cells is regulated by the hinge region of IgD. *Nat Immunol*, 16, 534-43.
- URLAUB, G. & CHASIN, L. A. 1980. Isolation of Chinese hamster cell mutants deficient in dihydrofolate reductase activity. *Proc Natl Acad Sci U S A*, 77, 4216-20.
- VALCK, C., RAMIREZ, G., LOPEZ, N., RIBEIRO, C. H., MALDONADO, I., SANCHEZ, G., FERREIRA, V. P., SCHWAEBLE, W. & FERREIRA, A. 2010. Molecular mechanisms involved in the inactivation of the first component of human complement by *Trypanosoma cruzi* calreticulin. *Mol Immunol*, 47, 1516-21.

- VAN DE BEEK, D., DE GANS, J., MCINTYRE, P. & PRASAD, K. 2007. Corticosteroids for acute bacterial meningitis. *Cochrane Database Syst Rev*, Cd004405.
- VAN DER FLIER, M., CHHUN, N., WIZEMANN, T. M., MIN, J., MCCARTHY, J. B. & TUOMANEN, E. I. 1995. Adherence of *Streptococcus pneumoniae* to immobilized fibronectin. *Infect Immun*, 63, 4317-22.
- VAN DER LINDEN, M., WINKEL, N., KUNTZEL, S., FARKAS, A., PERNICIARO, S. R., REINERT, R. R. & IMOHL, M. 2013. Epidemiology of *Streptococcus pneumoniae* serogroup 6 isolates from IPD in children and adults in Germany. *PLoS One*, 8, e60848.
- VAN DER POLL, T. & OPAL, S. M. 2009. Pathogenesis, treatment, and prevention of pneumococcal pneumonia. *The Lancet*, 374, 1543-1556.
- VAN PEE, K., MULVIHILL, E., MULLER, D. J. & YILDIZ, O. 2016. Unraveling the Pore-Forming Steps of Pneumolysin from *Streptococcus pneumoniae*. *Nano Lett*, 16, 7915-7924.
- VAN PEE, K., NEUHAUS, A., D'IMPRIMA, E., MILLS, D. J. & KUHLBRANDT, W. 2017. CryoEM structures of membrane pore and prepore complex reveal cytolytic mechanism of Pneumolysin. 6.
- VEATCH, S. L. & KELLER, S. L. 2005. Seeing spots: complex phase behavior in simple membranes. *Biochim Biophys Acta*, 1746, 172-85.
- VELVE-CASQUILLAS, G., LE BERRE, M., PIEL, M. & TRAN, P. T. 2010. Microfluidic tools for cell biological research. *Nano Today*, 5, 28-47.
- VERMA, A., WHITE, M., VATHIPADIEKAL, V., TRIPATHI, S., MBIANDA, J., IEONG, M., QI, L., TAUBENBERGER, J. K., TAKAHASHI, K., JENSENIUS, J. C., THIEL, S. & HARTSHORN, K. L. 2012. Human H-ficolin inhibits replication of seasonal and pandemic influenza A viruses. *J Immunol*, 189, 2478-87.
- VESTRHEIM, A. C., MOEN, A., EGGE-JACOBSEN, W., REUBSAET, L., HALVORSEN, T. G., BRATLIE, D. B., PAULSEN, B. S. & MICHAELSEN, T. E. 2014. A pilot study showing differences in glycosylation patterns of IgG subclasses induced by pneumococcal, meningococcal, and two types of influenza vaccines. *Immun Inflamm Dis*, 2, 76-91.
- VIDARSSON, G., DEKKERS, G. & RISPENS, T. 2014. IgG subclasses and allotypes: from structure to effector functions. *Front Immunol*, 5, 520.
- VISITSUNTHORN, N., HENGRAWIT, W., JIRAPONGSANANURUK, O. & LUANGWEDCHAKAM, V. 2011. Immunoglobulin G (IgG) subclass deficiency in Thai children. *Asian Pac J Allergy Immunol*, 29, 332-7.

- VLADUTIU, A. O. 2000. Immunoglobulin D: properties, measurement, and clinical relevance. *Clin Diagn Lab Immunol*, 7, 131-40.
- WALKER, J. A., ALLEN, R. L., FALMAGNE, P., JOHNSON, M. K. & BOULNOIS, G. J. 1987. Molecular cloning, characterization, and complete nucleotide sequence of the gene for pneumolysin, the sulfhydryl-activated toxin of *Streptococcus pneumoniae*. *Infect and Immun*, 55, 1184-1189.
- WALLIS, R. & DRICKAMER, K. 1999. Molecular determinants of oligomer formation and complement fixation in mannose-binding proteins. *J Biol Chem*, 274, 3580-9.
- WALLIS, R., MITCHELL, D. A., SCHMID, R., SCHWAEBLE, W. J. & KEEBLE, A. H. 2010. Paths reunited: Initiation of the classical and lectin pathways of complement activation. *Immunobiology*, 215, 1-11.
- WALTHER, E., RICHTER, M., XU, Z., KRAMER, C., VON GRAFENSTEIN, S., KIRCHMAIR, J., GRIENKE, U., ROLLINGER, J. M., LIEDL, K. R., SLEVOGT, H., SAUERBREI, A., SALUZ, H. P., PFISTER, W. & SCHMIDTKE, M. 2015. Antipneumococcal activity of neuraminidase inhibiting artocarpin. *Int J Med Microbiol*, 305, 289-97.
- WANG, W., SINGH, S., ZENG, D. L., KING, K. & NEMA, S. 2007. Antibody structure, instability, and formulation. Hoboken.
- WANI, J. H., GILBERT, J. V., PLAUT, A. G. & WEISER, J. N. 1996. Identification, cloning, and sequencing of the immunoglobulin A1 protease gene of *Streptococcus pneumoniae*. *Infect Immun*, 64, 3967-74.
- WATSON, H. 2015. Biological membranes. *Essays Biochem*, 59, 43-69.
- WATT, J. P., WOLFSON, L. J., O'BRIEN, K. L., HENKLE, E., DELORIA-KNOLL, M., MCCALL, N., LEE, E., LEVINE, O. S., HAJJEH, R., MULHOLLAND, K. & CHERIAN, T. 2009. Burden of disease caused by *Haemophilus influenzae* type b in children younger than 5 years: global estimates. *Lancet*, 374, 903-11.
- WEIS, S. & PALMER, M. 2001. Streptolysin O: the C-terminal, tryptophan-rich domain carries functional sites for both membrane binding and self-interaction but not for stable oligomerization. *Biochim Biophys Acta*, 1510, 292-9.
- WEISER, J. N., BAE, D., FASCHING, C., SCAMURRA, R. W., RATNER, A. J. & JANOFF, E. N. 2003. Antibody-enhanced pneumococcal adherence requires IgA1 protease. *Proc Natl Acad Sci U S A*, 100, 4215-20.
- WELLMER, A., ZYSK, G., GERBER, J., KUNST, T., VON MERING, M., BUNKOWSKI, S., EIFFERT, H. & NAU, R. 2002. Decreased virulence of a pneumolysin-deficient strain of *Streptococcus pneumoniae* in murine meningitis. *Infect Immun*, 70, 6504-8.

- WHALAN, R. H., FUNNELL, S. G., BOWLER, L. D., HUDSON, M. J., ROBINSON, A. & DOWSON, C. G. 2005. PiuA and PiaA, iron uptake lipoproteins of *Streptococcus pneumoniae*, elicit serotype independent antibody responses following human pneumococcal septicaemia. *FEMS Immunol Med Microbiol*, 43, 73-80.
- WOLKERS, W. F., OLDENHOF, H. & GLASMACHER, B. 2010. Dehydrating phospholipid vesicles measured in real-time using ATR Fourier transform infrared spectroscopy. *Cryobiology*, 61, 108-14.
- WOOF, J. M. & BURTON, D. R. 2004. Human antibody-Fc receptor interactions illuminated by crystal structures. *Nat Rev Immunol*, 4, 89-99.
- WOOF, J. M. & KERR, M. A. 2006. The function of immunoglobulin A in immunity. *J. Pathol*, 208, 270-82.
- WU, H. L., TONG, Y., PENG, Q., LI, N. & YE, S. 2016a. Phase transition behaviors of the supported DPPC bilayer investigated by sum frequency generation (SFG) vibrational spectroscopy and atomic force microscopy (AFM). *Phys Chem Chem Phys*, 18, 1411-21.
- WU, L., SU, S., LIU, F., XU, T., WANG, X., HUANG, Y., SUN, X., GE, X., CHEN, T., LIU, H., WANG, C., CHOREV, M., XU, T. & QIN, X. 2012. Removal of the tag from His-tagged ILYd4, a human CD59 inhibitor, significantly improves its physical properties and its activity. *Curr Pharm Des*, 18, 4187-96.
- WU, L. C. & ZARRIN, A. A. 2014. The production and regulation of IgE by the immune system. *Nat Rev Immunol*, 14, 247-259.
- WU, Y., CHEN, W., CHEN, H., ZHANG, L., CHANG, Y., YAN, S., DAI, X., MA, Y., HUANG, Q. & WEI, W. 2016b. The Elevated Secreted Immunoglobulin D Enhanced the Activation of Peripheral Blood Mononuclear Cells in Rheumatoid Arthritis. *PLoS One*, 11, e0147788.
- XU, D. D., WANG, C., JIANG, F., WEI, L. L., SHI, L. Y., YU, X. M., LIU, C. M., LIU, X. H., FENG, X. M., PING, Z. P., JIANG, T. T., CHEN, Z. L., LI, Z. J. & LI, J. C. 2015. Association of the FCN2 Gene Single Nucleotide Polymorphisms with Susceptibility to Pulmonary Tuberculosis. *PLoS One*, 10, e0138356.
- XU, G., KIEFEL, M. J., WILSON, J. C., ANDREW, P. W., OGGIONI, M. R. & TAYLOR, G. L. 2011. Three *Streptococcus pneumoniae* sialidases: three different products. *J Am Chem Soc*, 133, 1718-21.
- YAE, Y., INABA, S., SATO, H., OKOCHI, K., TOKUNAGA, F. & IWANAGA, S. 1991. Isolation and characterization of a thermolabile beta-2 macroglycoprotein ('thermolabile substance' or 'Hakata antigen') detected by precipitating (auto) antibody in sera of patients with systemic lupus erythematosus. *Biochim Biophys Acta*, 1078, 369-76.

- YANG, J., MARTI, J. & CALERO, C. 2016. Pair interactions among ternary DPPC/POPC/cholesterol mixtures in liquid-ordered and liquid-disordered phases. *Soft Matter*, 12, 4557-61.
- YOTHER, J. & BRILES, D. E. 1992. Structural properties and evolutionary relationships of PspA, a surface protein of *Streptococcus pneumoniae*, as revealed by sequence analysis. *J. Bacterio*, 174, 601-609.
- YOUNG, E., LOCK, E., WARD, D. G., COOK, A., HARDING, S. & WALLIS, G. L. 2014. Estimation of polyclonal IgG4 hybrids in normal human serum. *Immunology*, 142, 406-13.
- YU, B., LEE, R. J. & LEE, L. J. 2009. *Microfluidic Methods for Production of Liposomes*. United States: Elsevier Science & Technology.
- YUSTE, J., SEN, A., TRUEDSSON, L., JONSSON, G., TAY, L. S., HYAMS, C., BAXENDALE, H. E., GOLDBLATT, F., BOTTO, M. & BROWN, J. S. 2008. Impaired opsonization with C3b and phagocytosis of *Streptococcus pneumoniae* in sera from subjects with defects in the classical complement pathway. *Infect Immun*, 76, 3761-70.
- ZACHO, R. M., JENSEN, L., TERP, R., JENSENIUS, J. C. & THIEL, S. 2012. Studies of the pattern recognition molecule H-ficolin: specificity and purification. *J Biol Chem*, 287, 8071-81.
- ZAKIR, S., SMITH, R. N. & JAMES, R. S. 2015. An elevated IgG4 response in chronic infectious aortitis is associated with aortic atherosclerosis. *Mod Pathol*, 28, 1428-34.
- ZARTLER, E. R., PORAMBO, R. J., ANDERSON, C. L., CHEN, L. H., YU, J. & NAHM, M. H. 2009. Structure of the capsular polysaccharide of pneumococcal serotype 11A reveals a novel acetylglycerol that is the structural basis for 11A subtypes. *J Biol Chem*, 284, 7318-29.
- ZHANG, C., GAO, C., MU, J., QIU, Z. & LI, L. 2013. Spectroscopic studies on unfolding processes of apo-neuroglobin induced by guanidine hydrochloride and urea. *Biomed Res Int*, 2013, 349542.
- ZHANG, H., LI, P., WU, D., XU, D., HOU, Y., WANG, Q., LI, M., LI, Y., ZENG, X., ZHANG, F. & SHI, Q. 2015. Serum IgG subclasses in autoimmune diseases. *Medicine (Baltimore)*, 94, e387.
- ZHANG, H. & LIU, K.-K. 2008. Optical tweezers for single cells. *J R Soc Interface*, 5, 671-90.
- ZHANG, X. L. & ALI, M. A. 2008. Ficolins: structure, function and associated diseases. *Adv Exp Med Biol*, 632, 105-15.

- ZHAO, H., JUNG, J. A., BRILES, D. E., KITA, H., TSIGRELIS, C. & JUHN, Y. J. 2013. Asthma and antibodies to pneumococcal virulence proteins. *Infection*, 41, 927-934.
- ZHAO, Y., REN, Y., ZHANG, X., ZHAO, P., TAO, W., ZHONG, J., LI, Q. & ZHANG, X. L. 2014. Ficolin-2 inhibits hepatitis C virus infection, whereas apolipoprotein E3 mediates viral immune escape. *J Immunol*, 193, 783-96.
- ZIELNIK-JURKIEWICZ, B. & BIELICKA, A. 2015. Antibiotic resistance of *Streptococcus pneumoniae* in children with acute otitis media treatment failure. *Int J Pediatr Otorhinolaryngol*, 79, 2129-33.
- ZWART, B., CIURANA, C., RENSINK, I., MANOE, R., HACK, C. E. & AARDEN, L. A. 2004. Complement activation by apoptotic cells occurs predominantly via IgM and is limited to late apoptotic (secondary necrotic) cells. *Autoimmunity*, 37, 95-102.
- ZWIJNENBURG, P. J., VAN DER POLL, T., FLORQUIN, S., VAN DEVENTER, S. J., ROORD, J. J. & VAN FURTH, A. M. 2001. Experimental pneumococcal meningitis in mice: a model of intranasal infection. *J Infect Dis*, 183, 1143-6.